Performance Analysis of Modernized GNSS Signal Acquisition

Myriam Foucras

THÈSE

En vue de l'obtention du

DOCTORAT DE L'UNIVERSITÉ DE TOULOUSE

Délivré par : *l'Institut National Polytechnique de Toulouse (INP Toulouse)*

Présentée et soutenue le *06/02/2015* **par :**

Myriam FOUCRAS

Analyse des Performances de l'Acquisition des Nouveaux Signaux GNSS

Performance Analysis of Modernized GNSS Signal Acquisition

JURY

Jari NURMI	Professeur *Université de Tampere*	Président du jury
Mark PETOVELLO	Professeur *Université de Calgary*	Rapporteur
Giovanni CORAZZA	Professeur *Université de Bologne*	Rapporteur
Damien KUBRAK	Ingénieur *Thalès Alenia Space*	Examinateur
Olivier JULIEN	Enseignant-Chercheur *ENAC*	Directeur de thèse
Christophe MACABIAU	Enseignant-Chercheur *ENAC*	Co-Directeur de thèse
Bertrand EKAMBI	Ingénieur *ABBIA GNSS Technologies*	Invité

École doctorale et spécialité :
MITT : Domaine SIAO : Signal, Image, Acoustique et Optimisation
Unité de Recherche :
École Nationale de l'Aviation Civile (TELECOM Lab/SIGNAV Group)
Directeur(s) de Thèse :
Olivier JULIEN et *Christophe MACABIAU*
Rapporteurs :
Mark PETOVELLO et *Giovanni CORAZZA*

FOURNISSEUR DE MOBILITÉ

abbia

GNSS TECHNOLOGIES

www.abbia.fr

Votre fournisseur de mobilité

Myriam FOUCRAS
Tél : 05 34 61 25 44
Mobile : 06 79 87 44 12
myriam.foucras@abbia.fr

www.abbia.fr

A ma famille

Savoir qu'aucun jour n'est semblable à un autre,
et que chaque matin comporte son miracle particulier,
son moment magique, où de vieux univers s'écroulent
et de nouvelles étoiles apparaissent.

Paulo Coelho

Aknowledgements

C'est avec nostalgie que j'écris ces derniers mots, consacrés à mes remerciements… J'ai vécu une belle aventure humaine, grâce à vous tous, que j'ai eu la chance de rencontrer, et qui avez été mes étoiles, le temps d'un marché de Noël Munichois, d'une croisière au large de San Diego, d'une pomme d'Amour à Nashville, d'un coucher de soleil sur le Pacifique, de dégustations de bubble tea et d'une (ou plusieurs) glace à Vienne, d'une soirée bowling à Monterey, de parties de billard à Berchtesgaden, d'une virée à pédalo parmi les cygnes Danubiens… le temps d'une thèse à Toulouse…

J'adresse mes premiers remerciements et ma reconnaissance à Bertrand Ekambi, avec qui l'aventure a commencé. Au cours de notre première rencontre, tu m'as donné cet abbia, en gage de porte-bonheur. Grâce à toi, à tes grandes qualités humaines et techniques, j'ai eu la chance de pouvoir me réaliser et m'épanouir professionnellement.

Sur le chemin de la thèse, j'ai eu la chance de rencontrer, dans un deuxième temps, Olivier Julien et Christophe Macabiau, mes directeurs de thèse ! Vous m'avez accueilli au sein du laboratoire SIGNAV et nous avons construit ensemble mon projet de thèse. Je vous remercie tous les deux pour votre encadrement de qualité. Ma thèse a été grandement enrichie grâce à votre expertise technique, vos connaissances et conseils, votre exigence mais aussi patience!

I would like to express my thanks to the jury of this thesis and in particular Prof. Mark Petovello and Prof. Giovanni Corazza, who kindly accepted to review my work! Your comments and remarks permit me to improve the quality of the thesis. Many thanks are also due to Prof. Jari Nurmi who accepts to be the president of my jury. Je voudrais aussi remercier Damien Kubrak, examinateur de ma thèse, pour son analyse mais aussi nos divers échanges et discussions. Enfin, je remercie toutes les personnes qui ont participé à ma soutenance, famille, amis, collègues, connaissances, votre présence m'a beaucoup touchée.

Je ne peux continuer mes remerciements sans avoir une pensée pour les 2 équipes avec lesquelles j'ai travaillé ! J'aimerais donc remercier l'équipe ABBIA, avec qui je poursuis l'aventure, Laurence, Jérémy, Eduardo et puis mes deux anciens «petits stagiaires » Fayaz et Ulrich. Ils ont fait partie de l'aventure et ont apporté leur pierre à cet édifice qu'est cette thèse. J'en profite pour remercier aussi mes amis doctorants (ou docteurs !) avec qui j'ai partagé les bureaux, Sébastien, Leslie, Amani, Philippe, Jérémy et Lina, sans oublier mes voisins de bureaux, les chefs de département Robert et Mathy et les secrétaires, Coco et Cathy. Et plus généralement, je remercie le labo SIGNAV du groupe de recherche TELECOM de l'ENAC.

Pour votre présence et votre amitié, je remercie, Fabien, Florence, Ludovic et Pascal. Je tiens à vous remercier pour mon intégration aux différentes équipes pédagogiques de l'ENAC et de l'ENSICA. Grâce à vous, j'ai découvert les joies de l'enseignement et j'ai eu beaucoup de plaisir à transmettre mon savoir mais aussi à échanger sur nos expériences. J'ai une pensée pour tous les étudiants que j'ai pu croiser, aussi bien, les jeunes ingénieurs IENAC ou de l'ENSICA mais aussi les TSA avec des profils variés et enrichissants.

Les remerciements ne seraient pas complets sans une pensée pour tous mes amis, collègues de longue date ou rencontrés au cours de ces dernières années. Among them, I would like to thank the « NaviWordPark » team, as to know, Cookie, Michael, Antonios, Daniel and Khurram that I had the pleasure to meet at the ESA summer school 2011 and also Luciano and Claudia. It was always a pleasure to meet you again in Toulouse or in conference around the world… Parce que les conférences sont des lieux d'échanges privilégiés, j'ai eu la joie de rencontrer, entre autres, Boubeker, Emilien. Que de bons moments, de discussions, d'échanges, extra-ordinaires, partagés ensemble sous le soleil californien…

Parce qu'il faut traverser l'Atlantique pour se rencontrer, je voudrais remercier les docteurs toulousains pour tous les bons moments passés ensemble ; je pense bien entendu à Sébastien, Paulo, et Sébastien ! Il y a un remerciement particulier que j'aimerais adresser à Jérôme. Malgré les frontières, nous avons saisi notre chance de pouvoir échanger et débattre autour de la corrélation, du GNSS et des choses de la vie... Je te remercie pour tous tes « trucs et astuces » et Angus mais aussi pour toutes tes relectures pointilleuses ! Notre article est le bel aboutissement de ce travail et de notre amitié ! Je tiens à remercier mes amis et compagnons d'acquisition, Jérôme, François-Xavier et Paulo, qui ont eu la gentillesse de relire minutieusement mon manuscrit. A nous 4, nous avons redonné un souffle nouveau au DBZP…

Je profite de l'occasion pour exprimer mon affection à mes amis. Je pense à Valérie, avec qui j'ai « partagé » la thèse mais aussi à Claire, Aurélie, Julien, Michou, Gary, Guillaume et Isabelle. J'ai une pensée aussi pour mes anciens collègues de la SODIT et en particulier Alexandre et Yvan, qui m'a tant accompagné et fait voyager en musique.

Je termine par ceux qui veillent sur moi, jour après jour, depuis de nombreuses années. Je pense, bien sûr, à mes parents et à Jean-Hubert, mon conjoint, et plus généralement ma famille, la famille de Jean-Hubert et mes proches. Je vous remercie pour votre soutien au quotidien, votre compréhension et surtout votre amour…

Abstract

Since the development of the GPS, the Global Navigation Satellite Systems (GNSS) have been widely diversified: maintenance and modernization of GPS and GLONASS, and deployment of new systems such as Galileo and BeiDou. While originally a military project, GPS and other GNSS are, now, considered as a dual-use technology, meaning they have significant military and civilian applications. The number of GNSS applications increases constantly, based on the computation of absolute location (the most known and used by people, for positioning and by extension, computation of itinerary, track of vehicles…), relative movement (displacement of glacier, for example) and time computation (time transfer, traffic signal timing, synchronization of cell phone base stations…).

The traditional implementation of GNSS receivers (equipping our vehicles, smartphones…) is hardware-based, conceived as a dedicated chip (Application Specific Integrated Circuit (ASIC), Field Programmable Gate Array (FPGA), for example) with the only purpose of being a GNSS receiver. However, to meet these new challenges and integrate GNSS evolutions, GNSS receivers should constantly evolve. An innovative trend is a software implementation; in this case, the GNSS receiver is designed as a software running on a Digital Signal Processor (DSP) or on a computer. The software technology is more flexible because to implement new algorithms or track new GNSS signals, the hardware equipment does not need to be changed. Furthermore, the GNSS software receiver is not a black box as the hardware ones and it is possible to have access to data or functions in the core of the signal processing.

This PhD thesis is part of a common project between a laboratory (research group TELECOM/SIGNAV at ENAC) and a company (ABBIA GNSS Technologies), consisting in the development of a software receiver tracking the GPS L1 C/A and Galileo E1 OS signals. The more specific aim of the thesis is to study and design, in details, the acquisition part of the receiver, the first signal processing stage, which provides a rough estimation of the incoming signal parameters. This work focuses particularly on relatively low power signals; an acquisition threshold has been set to 27 dB-Hz with an associated acquisition success rate that should be at least 9 times out of 10, without any aid or knowledge of almanac or ephemeris.

Among the main sources of acquisition performance degradation, can be cited:

- The residual code Doppler,
- The uncertainty on the acquisition grid,
- The bit sign transitions: due to the presence of the navigation message and the secondary code on the pilot component of the modernized GNSS signals.

For each one, the probability of detection when considering the source of degradation is compared to the probability of detection when the source of degradation is not considered and then the impact on the acquisition performance can be shown. In addition, the average probability of detection when considering one or two sources of degradations seems to be a more relevant and representative figure. For example, for the data bit sign transition, the average is taken on the bit sign transition location and on the number of bit sign transition occurring in a given time interval.

This comprehensive theoretical study permits to prove the need of a transition insensitive acquisition method for the acquisition of the modernized GNSS signals, which present bit transitions at each spreading code period. It is why an innovative method, the Double-Block Zero-Padding Transition-Insensitive (DBZPTI) is developed to permit the efficient acquisition of the Galileo E1 OS signal. It takes part in the development of the global acquisition strategy, which should provide an estimate of the Doppler frequency and code delay, fine and reliable, for a satisfactory signal tracking.

Résumé

Depuis le développement du GPS, les systèmes de navigation par satellites (GNSS) se sont largement diversifiés : maintenance et modernisation du GPS et de GLONASS et déploiement de nouveaux systèmes, comme Galileo ou BeiDou. Alors que le GPS fut, à l'origine, mis en place pour des besoins militaires, le GPS et les autres systèmes sont, considérés comme une technologie duale, c'est-à-dire qu'ils ont des applications aussi bien militaires que civiles. Le nombre d'applications du GNSS ne cesse d'augmenter, visant le calcul d'une position absolue (la plus connue et utilisée, pour le positionnement et par extension, le calcul d'itinéraire, suivi de véhicules…), position relative (déplacement de glacier par exemple) et calcul de temps (transfert, synchronisation du réseau cellulaire, …). Les récepteurs GNSS, éventuellement intégrés dans des smartphones ou des ordinateurs, peuvent être utilisés à bord de voitures, navires, avions, satellites… En plus d'une utilisation autonome, des récepteurs GNSS peuvent être couplés à des équipements comme des caméras, des centrales inertielles, des accéléromètres, pour améliorer la qualité et fiabilité du positionnement.

L'implémentation traditionnelle du récepteur GNSS (équipant nos véhicules, smartphones,…) est matérielle, conçue sur une puce dédiée (ASIC ou FPGA par exemple) avec l'unique but d'être un récepteur GNSS. Cependant, pour répondre à ces nouveaux défis, les nouvelles exigences, et pour utiliser les futurs et diversifiés signaux GNSS, les récepteurs GNSS doivent constamment évoluer. Une nouvelle tendance est l'implémentation logicielle ; dans ce cas, le récepteur GNSS est conçu comme un logiciel s'exécutant sur un ordinateur ou sur DSP. La technologie logicielle est plus flexible car pour implémenter de nouveaux algorithmes, traiter de nouveaux signaux, l'équipement matériel ne nécessite pas d'être changé. De plus, le récepteur logiciel n'est pas une boite noire comme le récepteur matériel et il est possible d'accéder aux données et fonctions au cœur du traitement du signal.

Cette thèse de doctorat s'inscrit dans le projet commun d'un laboratoire (groupe de recherche TELECOM/SIGNAV de l'ENAC) et d'une entreprise (ABBIA GNSS Technologies) consistant au développement d'un récepteur logiciel utilisant les signaux GPS L1 C/A et Galileo E1 OS. L'objectif plus spécifique de la thèse est d'étudier l'acquisition, première étape du traitement du signal GNSS qui doit fournir une estimation grossière des paramètres du signal entrant. Ce travail vise particulièrement les signaux à faible puissance ; un seuil d'acquisition a été fixé à 27 dB-Hz pouvant s'apparenter à l'acquisition en milieu urbain ou dégradé. Il est important de noter qu'une des contraintes est de réussir l'acquisition de tels signaux au moins 9 fois sur 10, sans aucune aide extérieure ou connaissance des almanachs ou éphémérides.

Parmi les principales sources de dégradations de l'acquisition, peuvent être citées

- La fréquence de code reçue, impactée par la fréquence Doppler,
- L'incertitude sur la grille d'acquisition,
- Les transitions de bits dues à la présence du message de navigation et du code secondaire sur la voie pilote des nouveaux signaux.

Pour chaque source de dégradations, la probabilité de détection en l'absence de la source de dégradation est comparée à la probabilité en présence de la source. C'est alors que la probabilité de détection moyenne est calculée apparaissant comme une valeur plus significative et représentative des cas réels. Par exemple, concernant les transitions de bit, la moyenne est prise sur la position de la transition et sur le nombre de transitions de signe intervenant dans un intervalle de temps donné.

La transition de bit est synonyme d'inversion de signe et donc de dégradation sur l'opération de corrélation. Est ainsi mis en lumière la nécessité d'avoir recours à une méthode d'acquisition insensible aux inversions de signe du message de navigation. C'est pourquoi une méthode innovante, le Double-Block Zero-Padding Transition-Insensitive (DBZPTI), est donc développée pour permettre l'acquisition du signal Galileo E1 OS de façon efficiente. Elle prend part au développement de la stratégie globale d'acquisition dont l'objectif est d'avoir en sortie une estimation de la fréquence Doppler et du retard de code du signal entrant, assez fine et fiable pour une poursuite du signal satisfaisante.

Table of Contents

Aknowledgements v
Abstract vii
Résumé ix
Table of Contents xi
List of Figures xv
List of Tables xxi
List of Symbols xxv
List of Acronyms xxxi

Chapter 1 **Introduction 1**
1.1 Thesis background and motivations 1
1.2 Thesis objectives 3
1.3 Thesis outline 6
1.4 Personal Publications and Thesis contributions 8

Chapter 2 **GPS L1 C/A and the Modernized GNSS Signals 11**
2.1 Satellite-based navigation 12
2.2 GNSS signals 13
2.2.1 GNSS signals structure 13
2.2.2 Considered GNSS signals 19
2.3 Reception of the GNSS signal 20
2.4 Discussion 22

Chapter 3 **GNSS Signal Acquisition Principle 25**
3.1 Correlation operation 26
3.1.1 Correlation concept 26
3.1.2 Correlator output in absence of data 27
3.2 Serial-search classical acquisition method 31
3.2.1 Acquisition grid uncertainties 31
3.2.2 Review of accumulation techniques 33
3.2.3 GNSS signal detection 34

3.3 Acquisition methods 45
3.3.1 Optimized acquisition methods 45
3.3.2 Multi-trial and verification strategies 48
3.3.3 Modernized GNSS signal acquisition 54
3.4 Discussion 62

Chapter 4 Investigation of Acquisition Degradation Sources 65
4.1 Introduction 66
4.2 Acquisition grid uncertainties 66
4.3 Effect of code Doppler 68
4.3.1 Generalities on code Doppler effect 70
4.3.2 Mathematical model of the distorted correlation function 72
4.3.3 Acquisition performance when considering uncompensated code Doppler . 74
4.4 Effect of data message 80
4.4.1 GNSS signal detection statistical model in presence of bit sign transition . 81
4.4.2 Application to the acquisition of GNSS signals 86
4.4.3 Comparison of modernized GNSS signals with GPS L1 C/A 98
4.5 Discussion 101

Chapter 5 Acquisition Method based on DBZP 105
5.1 Double-Block Zero-Padding (DBZP) method 106
5.1.1 DBZP method algorithm 106
5.1.2 DBZP performance study 113
5.2 Proposed DBZP improvements 118
5.2.1 Data transition insensitivity 119
5.2.2 Dependence on the incoming Doppler frequency 120
5.2.3 Sub-sampling 124
5.3 Software implementation and results 125
5.3.1 Matlab implementation 125
5.3.2 Computation efficiency 126
5.4 Discussion 130

Chapter 6 Global Acquisition Strategy 133
6.1 Discussion on the acquisition steps 134
6.1.1 Preliminary discussion 134
6.1.2 Search step 134
6.1.3 Step of verification 138
6.2 Discussion on the acquisition parameters at 27 dB-Hz 141
6.2.1 Wide Doppler frequency uncertainty space 141
6.2.2 Restricted Doppler frequency uncertainty space 144
6.2.3 Acquisition of the GPS L1 C/A signal 145
6.3 Acquisition of signals not at 27 dB-Hz 146
6.4 Discussion 148

Chapter 7 Acquisition-to-Tracking Transition 149
7.1 FLL frequency refinement 150
7.1.1 FLL and frequency discriminators 150
7.1.2 Discriminator combination techniques 157
7.1.3 Simulation scheme 161
7.1.4 Simulation results 162
7.2 Pilot secondary code acquisition 174
7.2.1 Pilot secondary code features 175
7.2.2 Pilot secondary code acquisition methods 177
7.2.3 Simulation results 180
7.3 Discussion 185

Chapter 8 Conclusions and Recommendations for Future Work 187
8.1 Thesis achievements 187
8.2 Recommendations for future work 192

Bibliography 195
Appendix A Receiver Survey 205
Appendix B Mathematical identities 209
B.1 Trigonometric identities 209
B.2 Complex identities 209
B.3 Summations identities 210
Appendix C GPS L1 C/A and Galileo E1 OS code correlation properties 211
C.1 Autocorrelation 212
C.2 Cross-correlation 218
Appendix D Correlator output expression 225
Appendix E Signals Effects on the Acquisition 227
E.1 Effect of the code Doppler 227
E.2 Correlator output in presence of data modulation 230
Appendix F Double-Block Zero-Padding 235
F.1 DBZP outputs 235
F.2 DBZP output with zero-padding (Step 4') 237

List of Figures

Figure 1.1 General view of a GNSS receiver 2
Figure 1.2 General view of the signal processing block 5
Figure 1.3 Structure of the thesis and interdependence of the different chapters 6
Figure 2.1 GPS, GLONASS and Galileo navigational frequency bands 12
Figure 2.2 GPS L1 C/A signal structure (figure is not to scale) 14
Figure 2.3 Galileo E1 OS CBOC(6,1,1/11) subcarriers modulating one PRN chip 15
Figure 2.4 Power Spectral Densities functions of GPS L1 C/A and Galileo E1 OS signals 16
Figure 2.5 Normalized correlation function shapes of Galileo and GPS L1 C/A spreading codes (as a function of the modulation) 17
Figure 2.6 Illustration of an RF front-end 21
Figure 3.1 GPS L1 C/A autocorrelation function (PRN 2) 26
Figure 3.2 Block diagram of the correlation 27
Figure 3.3 Representation of the equations (3.5) and (3.6) 29
Figure 3.4 Representation of the absolute difference between equations (3.5) and (3.6) 29
Figure 3.5 Comparison of the CAF of PRN 1 when $|\varepsilon\tau|<1$ chip 30
Figure 3.6 Comparison of the CAF of PRN 1 when $|\varepsilon_{fD}|$ is relatively small 30
Figure 3.7 Matrix acquisition based on an acquisition grid 32
Figure 3.8 Coherent scheme 33
Figure 3.9 Non-coherent summations scheme 34
Figure 3.10 Illustration of the acquisition characterization 35
Figure 3.11 Probability of detection of the strategy among the N_M maximums as a function of N_M (Galileo E1 OS, $N_C = 50\ 000$ cells) 45
Figure 3.12 PFS method implementation description 46
Figure 3.13 Block diagram of the PCPS 47
Figure 3.14 Parallel Code Search acquisition method with "1 + 1 ms" technique 47
Figure 3.15 Illustration of the "1+1 ms" acquisition method output 48
Figure 3.16 Probabilities per cell at the output of the acquisition step 49
Figure 3.17 Immediate rejection verification techniques 51
Figure 3.18 Non-immediate rejection verification techniques 51
Figure 3.19 Probabilities of detection obtained for different implementations of Tong detector (Galileo E1 OS, $T_C = 4$ ms, $K = 20$, $P_{FA} = 10^{-1}$) 53
Figure 3.20 Probabilities of detection obtained for different implementations of M of N detector (Galileo E1 OS, $T_C = 4$ ms, $K = 20$, $P_{FA} = 10^{-1}$) 54

Figure 3.21 Non-coherent combining acquisition method scheme (red: data, blue: pilot, solid line: in-phase, dashed line: quadrature-phase) 56
Figure 3.22 Coherent combining with sign recovery (purple: data+pilot, orange: data-pilot, solid line: in-phase, dashed line: quadrature-phase) 57
Figure 3.23 Experimental probability to correctly determines the optimal spreading code sequence between data+ pilot and data-pilot (Galileo E1 OS, $K = 1$, $T_C = 4$ ms) 58
Figure 3.24 Differentially coherent combining acquisition method scheme (red: data, blue: pilot, solid line: in-phase, dashed line: quadrature-phase) 60
Figure 4.1 Probability of detection on the right cell in frequency and time domains 67
Figure 4.2 Probability of detection in the right cell (GPS L1 C/A, $T_C = 1$ ms and $C/N_0 = 27$ dB-Hz) 68
Figure 4.3 Code Doppler effect on the spreading code period 69
Figure 4.4 Sampling of 2 chips of the Galileo E1 OS spreading code PRN B/1 for an incoming Doppler frequency of 10 kHz and a sampling frequency of 40.96 MHz 71
Figure 4.5 Autocorrelation process: same spreading code but with different length due to code Doppler 73
Figure 4.6 Non-coherent summation scheme when considering code Doppler on the received signal 74
Figure 4.7 Normalized squared autocorrelation function when considering code Doppler (GPS L1 C/A) 75
Figure 4.8 Normalized squared autocorrelation function when considering code Doppler (Galileo E1 OS, $T_I = 80$ ms, $K = 20$) 76
Figure 4.9 Normalized squared autocorrelation function when considering code Doppler 76
Figure 4.10 Description of the peak (amplitude and argmax) of the autocorrelation function 77
Figure 4.11 Losses on the autocorrelation function due to code Doppler 78
Figure 4.12 Probability of detection when considering code Doppler (no Doppler frequency error) 78
Figure 4.13 Coherent summation scheme when considering code Doppler on the received signal 79
Figure 4.14 Normalized squared autocorrelation function when considering code Doppler (coherent summation – GPS L1 C/A and Galileo E1 OS) 79
Figure 4.15 Normalized squared autocorrelation function when considering code Doppler (coherent summation – GPS L1C and L5) 80
Figure 4.16 Bit sign transition scheme 82
Figure 4.17 Non-centrality parameter in presence of a bit sign transition 83
Figure 4.18 Illustration of different parameters related to bit sign transition 85
Figure 4.19 Scheme to determine the probability of detection (GPS L1 C/A) with $T_I = 20$ ms 87
Figure 4.20 Probabilities of detection for different coherent integration times when not considering bit sign transition (GPS L1 C/A) 88

Figure 4.21 Probabilities of detection for different coherent integration times and different location of the transition when considering bit sign transition (GPS L1 C/A) 89
Figure 4.22 Illustration of a bit sign transition for a total integration time of 40 ms 90
Figure 4.23 Average probabilities of detection on t_0 for different coherent integration times when considering bit sign transition (GPS L1 C/A) 91
Figure 4.24 Secondary code on the Galileo E1 OS pilot component 93
Figure 4.25 Probabilities of detection P_{Dj} and $P_D(t_0)$ for one integration ($K = 1$) on 4 ms on both components and considering a bit sign transition in the middle of the integration interval (Galileo E1 OS) 94
Figure 4.26 Probabilities of detection on $T_I = 20$ ms when considering or not bit sign transitions (Galileo E1 OS) 94
Figure 4.27 Product of data sequence and secondary code on the GPS L5 data component 95
Figure 4.28 Secondary code on the GPS L5 pilot component 96
Figure 4.29 Probabilities of detection when considering or not bit sign transitions (GPS L5) 97
Figure 4.30 Probabilities of detection on $T_I = 20$ ms when considering or not bit sign transitions (GPS L1C) 98
Figure 4.31 Probabilities of detection for $T_I = 20$ ms when considering or not bit sign transitions (modernized GNSS signals) 99
Figure 4.32 Probabilities of detection when considering or not bit sign transitions on T_I =20 ms and $T_C = 1$ ms for GPS L1 C/A and GPS L5 99
Figure 4.33 Probabilities of detection when considering or not bit sign transitions on $T_I = 20$ ms and $T_C = 4$ ms for GPS L1 C/A and Galileo E1 OS 100
Figure 4.34 Probabilities of detection when considering or not bit sign transitions on $T_I = 20$ ms and $T_C = 10$ ms for GPS L1 C/A and GPS L1C 101
Figure 5.1 Pre-processing of the incoming signal 107
Figure 5.2 Pre-processing of the local code 108
Figure 5.3 Full and partial GPS L1 C/A and Galileo E1 OS autocorrelations 108
Figure 5.4 Illustration of the use of the zero-padding for the partial correlation 109
Figure 5.5 DBZP output in frequency domain 111
Figure 5.6 Double-Block Zero-Padding (DBZP) method block diagram 112
Figure 5.7 Degradations of the criterion due to incoming Doppler frequency 116
Figure 5.8 Representation of (5.25) for different incoming Doppler frequencies 117
Figure 5.9 Losses due to the incoming Doppler frequency 117
Figure 5.10 Probability of detection as a function of the incoming Doppler frequency for the DBZP acquisition method (no code delay error) 118
Figure 5.11 Difference DBZP/DBZPTI 119
Figure 5.12 Transition insensitivity of the DBZPTI 120
Figure 5.13 Losses reduction due to high Doppler frequencies 120
Figure 5.14 Losses reduction at intermediate incoming Doppler frequencies 122
Figure 5.15 Losses due to the incoming Doppler frequency after improvements 122

Figure 5.16 DBZPTI method block diagram 123
Figure 5.17 Implementation of Step1/1'-5/5' 126
Figure 6.1 Probability of detection as a function of the incoming Doppler frequency (Galileo E1 OS, $T_C = 4$ ms, $K = 40$, $C/N_0 = 27$ dB-Hz, $P_{FA} = 10^{-3}$, $\varepsilon\tau = 0$) 135
Figure 6.2 Required number of non-coherent summations for the Approach 1 (C/N_0= 27 dB-Hz) 136
Figure 6.3 Required number of non-coherent summations for the Approach 2 ($C/N_0 = 27$ dB-Hz) 137
Figure 6.4 Examples of acquisition performance for 2 choices of probabilities of false alarm for Approach 3 ($C/N_0 = 27$ dB-Hz) 137
Figure 6.5 Required number of non-coherent summations for Approach 3 138
Figure 6.6 Probability of detection for different values of C/N_0 with the DBZPTI acquisition parameters given in Table 6.4 146
Figure 6.7 Required number of non-coherent summations as a function of the C/N_0 (DBZPTI method, no errors, null incoming Doppler frequency) 147
Figure 7.1 Block diagram of a typical frequency lock loop 150
Figure 7.2 Average CP discriminator response to frequency error for a noise-free signal and different C/N_0 cases 152
Figure 7.3 DDCP discriminator response to frequency error for a noise-free signal and different C/N_0 cases 153
Figure 7.4 Atan discriminator response to frequency error for a noise-free signal and different C/N_0 cases 154
Figure 7.5 Atan2 discriminator response to frequency error for a noise-free signal and different C/N_0 cases 155
Figure 7.6 Theoretical and estimated discriminator gains 156
Figure 7.7 Frequency error standard deviation due to thermal noise (theoretical and simulated results) (Galileo E1 OS, $T_C = 4$ ms, $B_L = 10$ Hz) 157
Figure 7.8 Classical FLL technique 158
Figure 7.9 GPS L1 C/A FLL technique based on a frequency update every 20 ms 158
Figure 7.10 Illustration of the impact of bit sign transition for different discriminator combination technique (GPS L1 C/A) 159
Figure 7.11 Classical FLL technique applied to data/pilot GNSS signals 159
Figure 7.12 Galileo E1 OS FLL technique based on a frequency update every 20 ms 160
Figure 7.13 FLL technique applied to data/pilot GNSS signals using partial correlations 160
Figure 7.14 Illustration of the impact of bit sign transition for different discriminator combination technique (Galileo E1 OS) 161
Figure 7.15 Convergence scheme 162
Figure 7.16 Probability to get locked in function of the FLL loop bandwidth (GPS L1 C/A, $C/N_0 = 27$ dB-Hz, frequency update every 20 ms) 163
Figure 7.17 Probability to get locked in function of the FLL loop bandwidth (Galileo E1 OS (both components), $C/N_0 = 27$ dB-Hz, frequency update every 20 ms and full correlations on 4 ms) 164
Figure 7.18 Results for FLL schemes for GPS L1 C/A 164

Figure 7.19 Results for FLL schemes for GPS L1 C/A (low C/N_0) 165
Figure 7.20 Results for FLL schemes for Galileo E1 OS with a frequency update every 8 ms ($C/N_0 = 27$ dB-Hz, $T_C = 4$ ms) 166
Figure 7.21 Results for FLL schemes for Galileo E1 OS with a frequency update every 20 ms ($C/N_0 = 27$ dB-Hz, $T_C = 4$ ms) 167
Figure 7.22 Results for FLL schemes for Galileo E1 OS with a frequency update every 8 ms (both components) 168
Figure 7.23 Results for FLL schemes for Galileo E1 OS with a frequency update every 20 ms (both components) 169
Figure 7.24 Results for FLL schemes for Galileo E1 OS with a frequency update every 20 ms (both components) (low C/N_0) 169
Figure 7.25 Results for FLL schemes for Galileo E1 OS with a frequency update every 20 ms at 27 dB-Hz (both components) 170
Figure 7.26 Results for FLL schemes for GPS L1C with a frequency update every 20 ms ($T_C = 10$ ms) 171
Figure 7.27 Results for FLL schemes for GPS L1C with a frequency update every 20 ms ($T_C = 5$ ms) 172
Figure 7.28 Results for FLL schemes for GPS L1C with a frequency update every 20 ms at 27 dB-Hz (both components) 172
Figure 7.29 Results for FLL schemes for Galileo E5 with a frequency update every 2 ms ($T_C = 1$ ms) 173
Figure 7.30 Results for FLL schemes for Galileo E5 with a frequency update every 20 ms ($T_C = 1$ ms) 173
Figure 7.31 Results for FLL schemes for Galileo E5 with a frequency update every 20 ms at 27 dB-Hz (both components) 174
Figure 7.32 Galileo E1 OS secondary code autocorrelation function description 176
Figure 7.33 GPS L1C secondary codes autocorrelation function description 176
Figure 7.34 GPS L5 secondary code autocorrelation function description 176
Figure 7.35 Galileo E5 a/b secondary codes autocorrelation function description 177
Figure 7.36 Acquisition of secondary code using both correlator outputs 178
Figure 7.37 Probability that the sign of the in-phase correlator output is the sign of the secondary code (all secondary code bits) 181
Figure 7.38 Probability of correct main peak secondary code autocorrelation function detection for both techniques (applied to Galileo E1 OS for $K = 1$) 182
Figure 7.39 Comparison of the secondary code acquisition methods for three signals ($K = 1$) 183
Figure 7.40 Pilot secondary code correlation properties in presence of residual Doppler frequency error 184
Figure 7.41 Probability of Galileo E1 OS secondary code acquisition when considering or not frequency and phase errors (Technique 1 – 5000 simulations) 185

Figure C.1 Maximum of the autocorrelation function versus the Doppler frequency (excluding the correct code delay alignment) 213

Figure C.2 Maximum per C/A code of the autocorrelation function (excluding the correct code delay alignment) 213
Figure C.3 Maximum of the autocorrelation function per Doppler frequency for different coherent integration times (excluding the correct code delay alignments) 215
Figure C.4 Experimental CDF of the autocorrelation function values for different coherent integration times (for a Doppler frequency between 0 and 10 kHz) 215
Figure C.5 Maximum of the autocorrelation function per PRN code (excluding the correct code delay alignment and no Doppler) 216
Figure C.6 Distribution of the maximum Galileo PRN codes autocorrelation function per PRN code (excluding the correct code delay alignment) 217
Figure C.7 Distribution of the GPS C/A codes cross-correlation function values per C/A code (Doppler frequency between 0 and 1 kHz) 219
Figure C.8 Distribution of the maximum of the cross-correlation function per GPS C/A codes couple (Doppler frequency between 0 and 10 kHz) 220
Figure C.9 Experimental CDF of the Galileo E1 OS PRN codes cross-correlation (no Doppler) 221
Figure C.10 Maximum of the autocorrelation and cross-correlation functions per Doppler frequency for all codes and couples of codes 222
Figure E.1 Product of the chip "u" of the local spreading code by the received spreading code 228
Figure E.2 Illustration of the potential integration intervals (GPS L1 C/A) 232

List of Tables

Table 1.1 Performance objectives of the developed GNSS software receiver 4
Table 2.1 Main features of the modernized GNSS signals 17
Table 2.2 Characteristic figures of the secondary peaks maximums of the correlation function for the GPS L1 C/A and Galileo E1 OS signals (considering CBOC modulation) 18
Table 2.3 Signal features of the modernized GNSS signal components 19
Table 2.4 Values of the parameters in the generic signal expression for each GNSS signal 20
Table 3.1 Comparison of two acquisition detector performances ($T_C = 1$ ms, $K = 1$, $C/N_0 = 40$ dB-Hz, $P_{FA} = 10^{-3}$, $\lambda = 20$) 37
Table 3.2 Probabilities describing the serial strategy 39
Table 3.3 Probabilities describing the maximum strategy 41
Table 3.4 Probabilities describing the hybrid strategy ([Borio, 2008]) 41
Table 3.5 Experimental probability of detection for characteristic values of q 44
Table 3.6 Probabilities describing the strategy among the N_M maximums 44
Table 3.7 Performance study for the acquisition of the pilot component 55
Table 3.8 Performance study for non-coherent combining acquisition method 56
Table 3.9 Choice of α as a function of the data and secondary code bit signs 58
Table 3.10 Performance study for coherent combining with sign recovery acquisition method 59
Table 3.11 Performance study for differentially coherent combining acquisition method 61
Table 3.12 Exhaustive sign search acquisition method 62
Table 4.1 Time to get an offset of 1 chip depending on the incoming Doppler frequency 70
Table 4.2 Required dwell time to acquire signal with a C/N_0 of 27 dB-Hz for a desired probability of detection (obtained from theoretical study 3.2.3.1) 74
Table 4.3 Probability of detection for an integration time of 20 ms (GPS L1 C/A) 88
Table 4.4 Optimal coherent integration time T_C (in ms) for $T_I = 20$ ms (GPS L1 C/A) 91
Table 4.5 Probability of detection for the optimal coherent integration time (Table 4.4) for $T_I = 20$ ms (GPS L1 C/A) 92
Table 4.6 Average probabilities of detection for different integration times and considering potential sources of acquisition degradations at 27 dB-Hz (GPS L1 C/A) 102
Table 4.7 Average probabilities of detection for different integration times and considering potential sources of acquisition degradations at 27 dB-Hz (Galileo E1 OS) 103

Table 5.1 Impact of the code Doppler on the partial autocorrelation terms 115
Table 5.2 Number of required operations for the execution of the DBZP acquisition method 127
Table 5.3 Number of required operations for the execution of the PCPS with 1+1 ms acquisition method (reference acquisition method) 127
Table 5.4 Number of required operations for the execution of the DBZPTI acquisition method 128
Table 5.5 Comparison of the number of operations for the different acquisition methods and for GPS L1 C/A and Galileo E1 OS signals 129
Table 5.6 Comparison of the gain on the number of operations for the different acquisitions methods and for Galileo E1 OS 130
Table 6.1 Acquisition parameters for the Tong detector technique 140
Table 6.2 Acquisition parameters for the M of N detector technique 140
Table 6.3 Acquisition parameters with a correct estimation of the incoming signal parameters (DBZPTI/Reference) 141
Table 6.4 Acquisition parameters with a rough estimation of the incoming signal parameters (DBZPTI/Reference) 142
Table 6.5 Acquisition parameters with a rough estimation of the incoming signal parameters (comparison DBZPTI/DBZP) 143
Table 6.6 Acquisition parameters with a rough estimation of the incoming signal parameters (restricted Doppler frequency uncertainty space) 144
Table 6.7 Acquisition parameters for the acquisition of the GPS L1 C/A signal ($T_C = 1$ ms) 145
Table 6.8 Search step integration time for different value of C/N_0 146
Table 7.1 Average probability to get locked at 27 dB-Hz in presence/absence of data (GPS L1 C/A) 165
Table 7.2 Average probability to get locked at 27 dB-Hz in presence/absence of data and secondary code (Galileo E1 OS) 167
Table 7.3 Pilot secondary code features 175
Table 7.4 Performance study for the acquisition of the secondary based on the pilot correlator output pair 179
Table 7.5 Performance study for the acquisition of the secondary based on the pilot in-phase correlator output 180
Table 7.6 Galileo E1 OS and GPS L5 secondary code autocorrelation function (not normalized by Nc_2) properties in presence of wrong secondary code bit sign estimation 181

Table A.1 Repartition of the GNSS constellations 206
Table A.2 Repartition of the multi-constellation GNSS receivers 206
Table A.3 Absolute repartition of each constellation (GPS, Galileo, GLONASS) 206
Table A.4 Absolute repartition of each constellation (QZSS, BeiDou) 207
Table A.5 For each constellation, relative repartition of the association with 1, 2, 3 or 4 GNSS (GPS, Galileo, GLONASS) 207

Table A.6 For each constellation, relative repartition of the association with 1, 2, 3 or 4 GNSS (QZSS, BeiDou) 207
Table C.1 Theoretical and experimental C/A code autocorrelation properties (no Doppler) 212
Table C.2 Distribution of the GPS L1 C/A codes autocorrelation function values (excluding the correct code delay alignment and all Doppler) 214
Table C.3 Distribution of the Galileo PRN codes autocorrelation function values (excluding the correct code delay alignment) 217
Table C.4 Theoretical and experimental C/A code cross-correlation properties (no Doppler) 218
Table C.5 Maximum of the GPS L1 C/A code couples cross-correlation function 219
Table C.6 Distribution of the Galileo PRN codes cross-correlation function values (data and pilot codes for the same satellite) 220
Table C.7 Maximum of the Galileo PRN codes cross-correlation function values 221
Table C.8 Characteristic figures of the correlation for the GPS L1 C/A and Galileo E1 OS signals (considering CBOC modulation) 222
Table C.9 Distribution of the GPS and Galileo PRN codes (no Doppler) 223

List of Symbols

This thesis contains many symbols, mathematical functions and acronyms. There follows a brief description of the notations used, followed by a reference to the page on which they are first introduced. Some symbols are re-used, through it should be clear from the context which meaning is intended.

All important results will be indicated by a simple surrounding box, the novel results will be indicated by a double surrounding box.

Roman letters		
A	Parameter of the Tong detector (maximum value of the counter)	52
A_d	Signal amplitude on the data component	20
A_p	Signal amplitude on the pilot component	20
B	Parameter of the Tong detector (initialization of the counter)	52
B_l^c	l-th block of the local code	152
B_l^s	l-th block of the incoming signal	151
B_L	Loop bandwidth	153
C	Total signal power	20
c_1	Spreading code (PRN code)	13
$c_{1,d}$	Spreading code used for the data component	18
$c_{1,p}$	Spreading code used for the pilot component	18
c_2	Secondary code	18
$c_{2,d}$	Secondary code on the data component	18
$c_{2,p}$	Secondary code on the pilot component	18
C_i	Cell in the acquisition grid	38
d	Navigation message (data)	13
e_{Atan}	Atan discriminator output	145
e_{Atan2}	Atan2 discriminator output	145
e_{CP}	CP discriminator output	143
e_{DDCP}	DDCP discriminator output	144
F	Parameter for the FLL tracking error variance expression	148
f_0	Common frequency ($f_0 = 1.023$ MHz)	14
f_{c_1}	Chipping rate (Spreading code frequency)	13
$f_{c_1,D}$	Chipping rate affected by code Doppler	72
f_D	Incoming Doppler frequency	18

$\hat{f}_D$	Local estimate of the received Doppler frequency	27
$f_{D,Max}$	Maximum received Doppler frequency	105
$f_{D,Med}$	Central frequency of the Doppler frequency range	105
$f_{D,Min}$	Minimum received Doppler frequency	105
f_{IF}	Intermediate frequency	3
f_L	Carrier frequency in the L-band	13
f_s	Sampling frequency	3
H_0	Null hypothesis	34
H_1	Alternative hypothesis	34
$I(k)$	k-th in-phase correlator output	28
$\tilde{I}_l(k)$	l-th partial in-phase correlator output on the k-th spreading code period	104
$I_d(k)$	k-th in-phase correlator output computed on data component	57
$I_p(k)$	k-th in-phase correlator output computed on pilot component	55
$I(t_0, k)$	k-th in-phase correlator output with a bit sign transition at t_0	82
j	Index to refer to the number bit sign transitions	82
j_d	Index to refer to the number of bit sign transitions on the data component	92
K	Number of non-coherent summations	33
K_D	Discriminator gain	147
M	Parameter of the M of N detector (minimum number of success)	53
N	Parameter of the M of N detector (number of detectors)	53
N_0	Single sided noise power spectral density	21
N_b	Number of code delay blocks	106
N_c	Number of cells in the acquisition grid	31
N_{c_1}	Spreading code length (number of chips)	13
N_{c_2}	Secondary code length (number of bits)	18
n_d	Number of bit sign transitions on the data component	96
N_d	Number of bit transitions	85
N_f	Number of Doppler frequency cells in the acquisition grid	31
N_{FA}	Number of false alarms at the output of the acquisition process	50
N_M	Number of maximums	38
N_r	Number of circular permutation (DBZP) or incoming signal blocks shift (DBZPTI)	106
N_s	Number of samples per spreading code period	21
N_{spb}	Number of samples per block	106
N_{t_0}	Maximum number of bit sign transitions	85
N_v	Number verified cells by the step of verification	50
N_τ	Number of code delay cells in the acquisition grid	31
p_d	Probability that a bit sign transition on the data component	87

P_D	Probability of detection	35
$P_{D,acq}$	Probability of detection of the acquisition process	50
$P_{D,MofN}$	Probability of detection of the M of N detector	54
$P_{D,search}$	Probability of detection of the search step	50
$P_{D,Tong}$	Probability of detection of the Tong detector	53
$P_{D,verif}$	Probability of detection of the step of verification	50
$P_{D,(x_i)}$	Average probability of detection on the variables x_i	70
$P_{D,(x_i)}(y_j)$	Average probability of detection on the variables x_i for a particular values of y_j	101
$P_D(t_0)$	Average probability of detection on the number of bit sign transitions occurring in T_I ms	86
P_{D,t_0}	Average probability of detection	83
$P_{D_j}(t_0)$	Probability of detection knowing that $j$bit sign transitions occur at t_0	83
P_{FA}	Probability of false alarm	35
$P_{FA,acq}$	Probability of false alarm of the acquisition process	50
$P_{FA,MofN}$	Probability of false alarm of the M of N detector	54
$P_{FA,search}$	Probability of false alarm of the search step	50
$P_{FA,Tong}$	Probability of false alarm of the Tong detector	53
$P_{FA,verif}$	Probability of false alarm of the step of verification	50
$P_{H_0}(T > \gamma)$	Probability of the event $\{T > \gamma\}$ under the hypothesis H_0	36
$P_{H_1}(T > \gamma)$	Probability of the event $\{T > \gamma\}$ under the hypothesis H_1	37
$P_{j/K}$	Probability of occurrence of j bit sign transitions (over K bit transitions)	86
P_{j,j_d}	Probability of occurrence of j bit sign transitions knowing that j_d bit sign transitions occur on the data component	96
P_l	Probability to get locked	152
P_{MD}	Probability of miss detection	35
p_p	Probability of a bit sign transition on the pilot component	87
$\overline{p_p}$	Probability of a bit transition without sign transition on the pilot component	94
P_s	Power of the useful signal at the DBZP output	108
P_{η_ι}	Power of the noise at the DBZP output	108
$Q(k)$	k-th quadrature-phase correlator output	27
$\tilde{Q}_l(k)$	l-th partial quadrature-phase correlator output on the k-th spreading code period	104
$Q_d(k)$	k-th quadrature-phase correlator output computed on data component	57
$Q_p(k)$	k-th in-quadrature correlator output computed on pilot component	55
$Q(t_0, k)$	k-th quadrature-phase correlator output with a bit sign transition at t_0	82
R_{c_1}	Autocorrelation function of the PRN code	26

$R_{c_{1,d}}$	Autocorrelation function of the data PRN code	53
$R_{c_1,d/p}$	Cross-correlation function of the PRN codes from the same satellite	58
$R_{c_1,D}$	Autocorrelation function affected by a code Doppler	121
$R_{c_{1,p}}$	Autocorrelation function of the pilot PRN code	53
R_{c_2}	Autocorrelation function of the pilot secondary code	167
$sc_{BOC}(y)$	BOC(y,1) subcarrier	15
$sc_{CBOC(6,1,1/11)}$	CBOC(6,1,1/11) subcarrier	16
sc_d	Subcarrier modulating the spreading code on the data component	20
sc_p	Subcarrier modulating the spreading code on the pilot component	20
$sc_{TMBOC(6,1,1/11)}$	TMBOC(6,1,1/11) subcarrier	16
T	Normalized acquisition detector	31
$T(t_0)$	Normalized acquisition transition with one bit sign transition at t_0	83
t_b	Duration of one block	106
t_0	Instant of the bit sign transition	82
T_0	Beginning of the integration interval	27
T_C	Coherent integration time	27
t_{c_1}	Spreading code chip duration	13
T_{c_1}	Spreading code period	13
$t_{c_1,D}$	Spreading code chip duration affected by code Doppler	117
t_{c_2}	Secondary code bit duration	20
T_d	Data bit duration	13
T_I	Integration time (dwell-time)	33
T_s	Sampling period	21
X_A	Random variable associated to the right cell	38
X_i	Random variable associated to the acquisition grid cells	38
$X_{(i)}$	i-th random variable ascending ordered	42
Greek letters		
α_{N_d}	Probability of occurrence of the event $\{N_{t_0} = N_d\}$	86
β	Number of zero-padded blocks (DBZPTI)	115
γ	Normalized detection threshold	35
Δ	Received secondary code delay	167
$\widehat{\Delta}$	Local secondary code delay	167
$\delta_{f_{c_1,D}}$	Code Doppler shift	66
δ_{f_D}	Residual Doppler frequency error	69
Δ_f	Width of an acquisition grid cell in the frequency domain	32

$\delta_{t_{c_1,D}}$	Spreading code chip duration difference between local and received code	76
δ_τ	Residual code delay error	68
$\delta_\tau(f_D)$	Induced code delay by code Doppler	72
Δ_τ	Width of an acquisition grid cell in the time domain	32
ε_{f_D}	Doppler frequency error	27
ε_Δ	Secondary code delay error	179
ε_{ϕ_0}	Phase error at the beginning of the integration interval	28
ε_τ	PRN code delay error	27
η_I	Noise at the in-phase correlator output	28
η_Q	Noise at the quadrature-phase correlator output	28
$\iota(m)$	DBZP in-phase output	105
$\lambda(t_0)$	Non-centrality parameter of a non-central χ^2 distribution with 2 DOF and a bit sign transition at t_0	83
$\lambda(t_0, \varepsilon_{f_D})$	Non-centrality parameter of a non-central χ^2 distribution with 2 DOF and a bit sign transition at t_0 for a specific value of ε_{f_D}	84
λ_0	Non-centrality parameter of a non-central χ^2 distribution with 2 DOF	70
$\lambda_{0,d}$	Non-centrality parameter of a non-central χ^2 distribution with 1 DOF (data component)	87
$\lambda_{0,p}$	Non-centrality parameter of a non-central χ^2 distribution with 1 DOF (pilot component)	87
$\lambda_d(t_0)$	Non-centrality parameter of a non-central χ^2 distribution with 1 DOF and a bit sign transition at t_0 (data component)	87
$\lambda_p(t_0)$	Non-centrality parameter of a non-central χ^2 distribution with 1 DOF and a bit sign transition at t_0 (pilot component)	87
Λ	Non-centrality parameter of a non-central χ^2 distribution with $2K$ DOF	36
$\rho(m)$	DBZP quadrature output	105
σ_{FLL}	Standard deviation of the tracking error	148
σ_η^2	Variance of the noise of the correlator output	28
$\sigma_{\eta_{DBZP}}^2$	Variance of the complex noise at the DBZP output	105
τ	Received PRN code delay	22
$\hat{\tau}$	Local estimate of the received PRN code delay	27
ϕ_0	Initial phase of the incoming signal	20
$\hat{\phi}_0$	Local initial phase	20
$\phi_0(k,l)$	Initial phase for the k-th integration and the l-th block	154
$\phi_{0,d}$	Initial phase of the incoming data component	20
$\phi_{0,p}$	Initial phase of the incoming pilot component	20

Mathematical functions

atan	Arctangent function with 1 parameter	153
atan2	Arctangent function with 2 parameters	154

$\mathcal{B}(N,p)$	Binomial distribution with parameters N (number of trial) and p (probability of success)	53
$E_{(x_i)}(X)$	Expectation operator of the random variable X, on the variables x_i	36
$\mathcal{E}(\theta)$	Exponential distribution with parameter θ (rate)	62
f_X	Probability density function of the random variable X	42
F_X	Cumulative distribution function of the random variable X	38
F_X^{-1}	Inverse cumulative distribution function of the random variable X	36
$\mathcal{F}$	Fast Fourier transform operator	47
$\mathcal{F}^{-1}$	Inverse fast Fourier transform operator	47
i	Imaginary number, equal to $\sqrt{-1}$	28
Im	Imaginary part of a complex number	224
$a \bmod b$	Remainder of the Euclidean division of a by b	110
$\text{Laplace}(\mu, b)$	Laplace distribution of parameters μ (location) and b (scale)	58
$\mathcal{N}(\mu, \sigma^2)$	Gaussian distribution with parameters μ (mean) and σ^2 (variance)	35
Re	Real part of a complex number	109
rect	Rectangular function	75
sign	Sign function	144
UW	Phase-unwrapping function	145
$\lceil x \rceil$	Ceiling function (smallest following integer)	82
δ_0	Dirac function	110
$\chi^2(DOF)$	χ^2 distribution with DOF degrees of freedom	36
$\chi^2(DOF, \Lambda)$	Non-central χ^2 distribution with DOF degrees of freedom and a non-centrality parameter equal to Λ	36
$1_{[a,b]}$	Indicator function (not null on the interval $[a, b]$)	76

List of Acronyms

ADC	Analog-to-Digital Converter	21
AGC	Automatic Gain Control	21
AltBOC	Alternative Binary Offset Carrier	15
ASIC	Application Specific Integrated Circuit	vii
ASPeCT	Autocorrelation Side-Peak Correlation Technique	193
AWGN	Additive White Gaussian Noise	22
BOC	Binary Offset Carrier	4
BPSK	Binary Phase Shift Keying	14
C/A	Coarse Acquisition	vii
CBOC	Composite Binary Offset Carrier	15
CDF	Cumulative Distribution Function	37
CDMA	Code Division Multiple Access	12
C/N_0	Carrier-to-Noise Ratio	5
CP	Cross Product	151
CPU	Central Processing Unit	3
DBZP	Double-Block Zero-Padding	7
DBZPTI	Double-Block Zero-Padding Transition-Insensitive	viii
DDCP	Decision Directed Cross Product	152
DFT	Discrete Fourier Transform	46
DOF	Degree Of Freedom	36
DOP	Dilution Of Precision	xxxi
DSP	Digital Signal Processor	vii
DS-SS	Direct Sequence Spread Spectrum	12
EGNOS	European Geostationary Navigation Overlay Service	1
FFT	Fast Fourier Transform	106
FLL	Frequency Lock Loop	9

FOC	Full Operational Capability	12
FPGA	Field Programmable Gate Array	vii
GNSS	Global Navigation Satellite System	vii
GPS	Global Positioning System	vii
GPU	Graphics Processing Unit	3
ICD	Interface Control Document	13
IF	Intermediate Frequency	3
IOV	In-Orbit Validation	12
IRNSS	Indian Regional Navigational Satellite System	1
LFSR	Linear Feedback Shift Register	14
LNA	Low Noise Amplifier	21
MDBZP	Modified Double-Block Zero-Padding	115
NCO	Numerically Controlled Oscillator	150
OS	Galileo Open Service	vii
PCPS	Parallel Code-Phase Search	46
PDF	Probability Distribution Function	42
PFS	Parallel Frequency Search	45
PLL	Phase Lock Loop	149
PPM	Part Per Million	22
PRN	Pseudo-Random Noise	14
PSD	Power Spectral Density	16
PVT	Position, Velocity, Time	1
QZSS	Quasi-Zenith Satellite System	1
RF	Radio Frequency	1
SNR	Signal-to-Noise Ratio	114
TMBOC	Time Modulated Binary Offset Carrier	15
UTC	Coordinated Universal Time	13
VCO	Voltage Controlled Oscillator	21

Chapter 1
Introduction

1.1 Thesis background and motivations

The focus of this research is on Global Navigation Satellite Systems (GNSS) and in particular on the signal processing done in GNSS receivers. Although, the first GNSS was developed in 1970s –GPS (USA) and GLONASS (Russia)-, GNSS receiver technology needs to constantly evolve due to GNSS modernization and applications evolutions. Indeed, new global coverage capabilities have been offered: Galileo (European Union (EU)) and BeiDou (China) are being deployed, GPS and GLONASS are being maintained and modernized and regional GNSS enhancement systems such as QZSS (Quasi-Zenith Satellite System - Japan), IRNSS (Indian Regional Navigation Satellite System - India) or EGNOS (European Geostationary Navigation Overlay Service - Europe) are emerging.

As it can be observed in the annual GPS World Receiver Survey, which provides the longest running, most comprehensive database of GPS and GNSS equipment available, the number of tracked signals constantly increases and diversifies and more and more multi-constellation and multi-frequency GNSS receivers are available every year. In *Appendix A*, a recap is provided for the last four years ([Hamilton, 2011], [Hamilton, 2012], [Hamilton, 2013] and [Hamilton, 2014]). The signals, transmitted on new frequencies with new signal structures and targeting new applications and needs, require new signal processing methods to be performed within a GNSS receiver.

GNSS receiver operations can be decomposed in 3 blocks, as presented in Figure 1.1. The first one deals with the reception of the signal by the antenna and the Radio Frequency (RF) front-end processing (selection and amplification of the useful signal, down-conversion to an intermediate frequency, sampling and quantization). The second block concerns the actual digital signal processing. It consists in firstly estimating in a coarse way the incoming signal parameters, like timing and frequency information in the acquisition stage and later in refining these estimates by tracking the code delay and the carrier phase in the tracking circuit. Finally, in the last block, the navigation message is demodulated in order to have access to key information and to be able to compute the pseudo-range and the Position, Velocity, Time (PVT) solution.

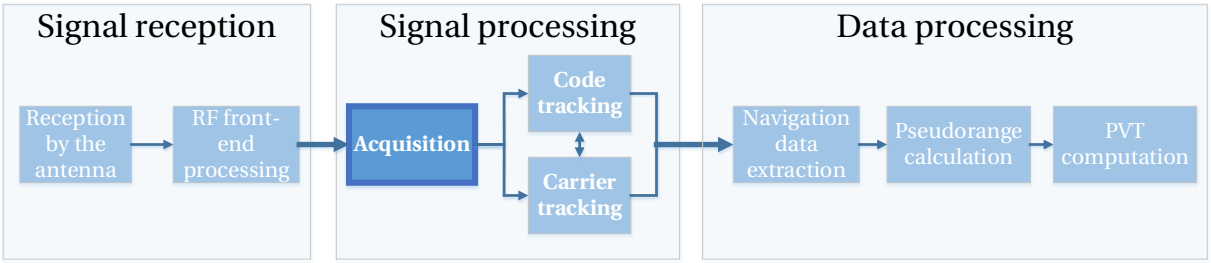

Figure 1.1 General view of a GNSS receiver

Mass-market GNSS receivers are produced in very high volumes and sold at a limited price: in fact, 60 millions of smartphones and tablets are equipped and sold every year, and in-car GNSS receivers represent a market of more than 45 millions of units per year [Mattos & Petovello, 2013], [Van Diggelen, 2014]. The hardware GNSS receivers market is clearly present in our daily life. The new GNSS receiver technology is now based on the software approach. Since the signal processing can be heavy, it is usually performed on a FPGA or ASIC but nowadays, in GNSS software receivers, it is done in a software way (computer or DSP). For the first time, this kind of GNSS receiver is addressing domains such as research and education. Indeed, software implementations are becoming more and more attractive due to their numerous advantages. Among them, their flexibility and re-configurability can be cited. Indeed, without (or very limited) changes in hardware equipment, they can answer the implementation needs of different signal processing methods required for the processing of modernized GNSS signals or by the comparison of algorithms performance [Ramachandran *et al.*, 2011]. For some years, GNSS software receivers have been developed by:

- Companies:
  - In Europe: IFEN [IFEN GmbH, 2014], Fastrax ([u-blox, 2014a]) Nottingham Scientific Ltd [NSL, 2014], Thales Avionics Division [Thales Group, 2014], Istituto Superiori Mario Boella [ISMB, 2014],
  - In America: Spirit DSP [Spirit DSP, 2014], NavSys Corporation [NAVSYS, 2014]…
- Universities:
  - In Europe: University of Westminster [University of Westminster, 2014], University of Aalborg (open-source) [Aalborg University, 2014], [Borre *et al.*, 2007], GNSS-SDR (open-source) [GNSS-SDR, 2014],
  - In America: University of Texas [University of Texas, 2014], Cornell university [Cornell University, 2014], Stanford university [Stanford University, 2014], University of Colorado [University of Colorado Boulder, 2014], University of Calgary [University of Calgary, 2014],
  - In Australia and Asia: University of New South Wales [UNSW, 2014], Tsinghua University [Tsinghua University, 2014]…

1.2 Thesis objectives

This thesis is part of a common project between a laboratory (TELECOM/SIGNAV) and a company (ABBIA GNSS Technologies), consisting of the development of a GNSS software receiver. In particular, this thesis deals with the acquisition of the modernized GNSS signals, studying the acquisition performance and the potential source of degradation, and developing an innovative acquisition method, efficient for the modernized GNSS signals.

The developed GNSS software receiver targets research, pedagogic and educational activities. Among them, implementations and tests of new algorithms, integration of new GNSS signal processing algorithms, comparison of performance, manipulations by researchers, teachers and students. Even from the industrial point of view, the software GNSS receiver answers the need of adaptation without having to modify the hardware.

From the point of view of the software implementations on a laptop, two strategies can be considered: either based on the Graphics Processing Unit (GPU) or based on Central Processing Unit (CPU). For example, [Humphreys *et al.*, 2009] and [Knežević *et al.*, 2010] present the different architectures and determine their advantages and drawbacks for a GNSS software receiver. It results that:

- The GPU is well adapted for the execution in parallel of simple operations on a large block of data but the execution of a program on a GPU needs to be dedicated, the data transfer to the GPU and the scheduling of the data before the execution to have a maximal gain of performance,
- The implementation on the CPU should manage the cores. This implies the repartition and synchronization of the tasks through threads.

It is difficult to compare the performance on both architectures since they depend on the algorithm and implementation. However, the multi-cores architecture seems more flexible and suitable for the objectives of this work and the aimed hardware equipment.

At this time, real-time is not an objective for the developed GNSS software receiver. However, the signal processing is based on real conditions and it is assumed that the sampled signal entering the signal processing block is the output of the RF front-end NavPort Multiband High-Speed USB sampling described in [IFEN GmbH, 2013] such as:

- The intermediate frequency (IF) $f_{IF} = 5.5$ MHz,
- The sampling frequency $f_s = 40.96$ MHz,
- Quantization on 2 bits,
- Bandwidth: 15 MHz

The goal of this thesis is to develop a GNSS software receiver that tracks (at least) two types of signal in order to improve the PVT computation. The choice of tracking the GPS L1 C/A signal is obvious because it is the reference civil signal that is available everywhere and it is well known. A multi-constellation is preferred to a multi-frequency receiver for many reasons. Even if two time and space references are used, the multi-

constellation single-frequency presents the advantages of not being dependent on one GNSS, with the additional benefits of using only one band for the RF front-end and having a better Dilution Of Precision (DOP). Naturally, the choice of the second constellation was Galileo since it is the European GNSS, even if it is not yet complete and operational. Compared to GLONASS, Galileo E1 OS signals have a modulation based on Binary Offset Carrier (BOC) which is the typical structure of future signals in the L1 band thus providing greater potential for innovation. However, it should be noted as presented in *Appendix A* that since GLONASS is already operational, it is the main trend for second constellation in a GNSS receiver at the moment (around 50% of the 366 GNSS receivers available in 2013 can track GLONASS signals), but at least 1/3 are designed to be able to track Galileo E1 OS.

As it is the first step of the GNSS signal processing block, this thesis focuses on the development of the acquisition process. It is one of the most challenging step, in particular when dealing with the modernized GNSS signals. One objective is that the acquisition of Galileo E1 OS should be done independently from GPS L1 C/A. Indeed, the typical acquisition technique used in mass-market GPS/Galileo L1 receivers signals tends to first acquire the GPS L1 C/A signals, and then, with the information provided by the acquisition of GPS L1 C/A signals, to acquire the Galileo E1 OS signal. Because relying on GPS L1 C/A as a first step to acquire efficiently Galileo E1 OS signals does not appear satisfactory, this thesis investigates an acquisition strategy to efficiently and independently acquire Galileo E1 OS. Based on the performance of mass-markets GNSS receivers, the performance requirements of the developed GNSS software receiver were established and presented in Table 1.1.

		Novatel OEM4-G2L [NovAtel, 2006]	IFEN SX-NSR [IFEN GmbH, 2013]	u-blox LEA-M8F [u-blox, 2014b]	Expected performance of the developed GNSS software receiver
Acquisition	Hot start(1)	30 s	1s	1 s	30 s
	Warm start(1)	40 s	10 s	26 s	40 s
	Cold start(1)	50 s	55 s	26 s	60(2)(3) s
	Reacquisition	0.5 s			2 s
Sensitivity	Acquisition		19 dB-Hz	-155 dBm (GPS)	27 dB-Hz (4) (GPS and Galileo)
	Tracking & Navigation		10 dB-Hz	-167 dBm (GPS)	20 dB-Hz(4) -(5) (GPS) 15 dB-Hz(4) -(5) (Galileo)

Table 1.1 Performance objectives of the developed GNSS software receiver

(1) *Hot start: almanac and recent ephemerides saved and approximate position and time entered*
Warm start: almanac saved and approximate position and time entered, no recent ephemerides
Cold start: no almanac or ephemerides and no approximate position or time

(2) The cold start (first position) is decided at 60 seconds, whatever is the sensitivity but a probability of 90% of time is associated.

(3) The GPS navigation message is divided in 5 subframes. The 3 first subframes contain information about the satellite clock, health data and satellite ephemeris data and are needed to compute a satellite position and so the receiver position. Each subframe has a length of 300 bits and the transmission of a subframe lasts 6 seconds. Let consider that the acquisition lasts 15 seconds and the reading of the 3 subframes lasts 18 seconds. If the read of the navigation message begins at the first subframe (the best case), the total time before the first position is 33 (=15+18) seconds but in the worst case (the reading begins at the 4th subframe), the first position is given in 45 seconds. If a second reading of the 3 firsts subframes is needed, the first position is given between 62 seconds and 75 seconds. So if the cold start is fixed at 60 seconds, the number of reading is minimized. Previous details justify the short cold start fixed at 60 seconds.

(4) Based on [Joseph & Petovello, 2010]*, 27 dB-Hz is equivalent to -147 dBm, 20 dB-Hz to -154 dBm and 15 dB-Hz to -159 dBm.*

(5) A probability of tracking of 90% is associated.

It is important to note that the acquisition threshold is fixed to a Carrier-to-Noise Ratio (C/N_0) of 27 dB-Hz but with a very high probability (90% of the time). This acquisition threshold can be considered as representative of urban or degraded environment. The acquisition of Galileo E1 OS, independently from GPS L1 C/A, and with a probability of detection equal or above 90% for signals at 27 dB-Hz thus constitutes a challenge. Note that the sensitivity given by receiver manufacturers is rarely associated with a given probability of detection or loss of lock, thus they are difficult to interpret and compare.

As previously explained, this thesis deals with the acquisition of GNSS signals. Before delving into the details of the technical points, it is appropriate to define the acquisition as it will be used in this thesis. As presented in Figure 1.2, the broad definition of the acquisition covers:

- A *search step*, which should provide a reduced set of potential couples corresponding to a rough estimation of the incoming signal parameters,
- A *verification step*, which consists in eliminating false alarms and confirming the right estimation of the incoming signal parameters,
- A *refinement step*, which refines the Doppler frequency error and allows the acquisition of the pilot secondary code for the modernized GNSS signals and the carrier tracking. This step is required in the context of the development of a complete GNSS receiver, for pedagogic and research purposes, in which tracking and data demodulation are necessary, contrarily to a snap-shot receiver [Carrasco-Martos *et al.*, 2010].

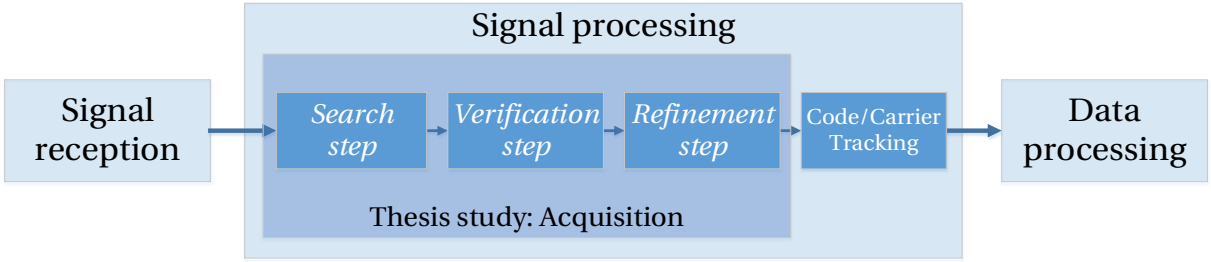

Figure 1.2 General view of the signal processing block

When dealing with the acquisition, two aspects are important: the sensitivity and the mean acquisition time. The sensitivity is defined as the minimum signal power required for a specifed reliability of correct acquisition [Weill & Petovello, 2011] and the mean acquisition time is the average time to detect the signal [Pany, 2010], meaning to reach successful acquisition. This thesis focuses on the sensitivity, that means the success of the acquisition of Galileo E1 OS signals at 27 dB-Hz, 90% of the time but with the constraint of an efficient acquisition. Even if it is not the main objective, the acquisition process is developed with a constraint of reasonable mean acquisition time. In the literature, this process, as a random variable, can be described by using the method of flow graphs as developed in [Holmes, 2007]. It takes into account the penalty of time when veirfying all false alarms and also the penalty of time when tracking a false alarm (tracking until detection of false alarm and reacquisition).

1.3 Thesis outline

Two PhD objectives were then defined. The first deals with a deep and complete study on the acquisition of the modernized GNSS signals. This theoretical part permits to identify the main acquisition degradation sources and evaluate their effect on the acquisition performance. The second, more practical, concerns the design of the global acquisition strategy, adapted to the acquisition of Galileo E1 OS signals and meeting the platform requirements.

In order to provide a comprehensive view of the performed research, the thesis outline is provided below.

Figure 1.3 depicts the structure of the thesis and the dependencies between the different chapters. It can be observed that the first chapters deal with the principles of the acquisition of GNSS signals (GPS L1 C/A and the new generation), while the last chapters present a global acquisition strategy dedicated to the acquisition of Galileo E1 OS –from the search acquisition to the step just before the tracking, through a verification step, a frequency refinement and the acquisition of the secondary code on the pilot component.

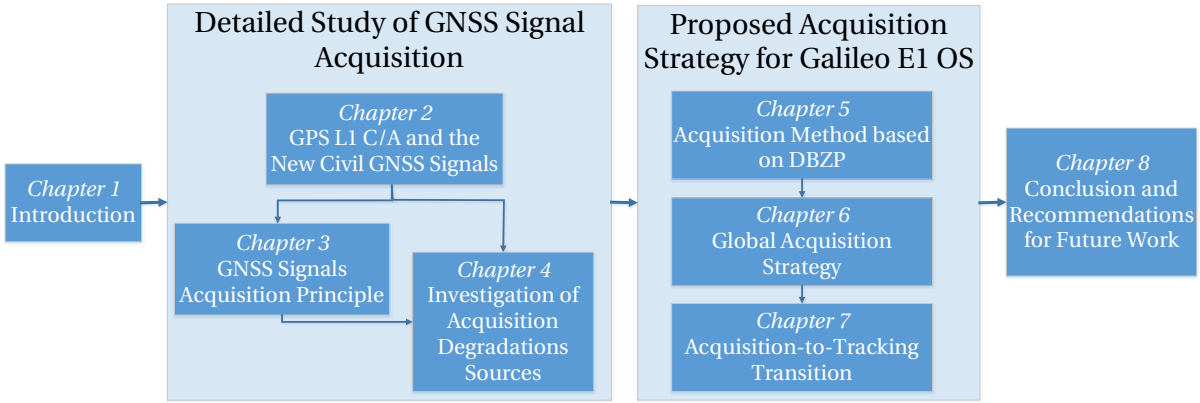

Figure 1.3 Structure of the thesis and interdependence of the different chapters

Going further, the thesis is organized as follows:

*Chapter 2 p*rovides an overview of the new GNSS signals and the legacy GPS L1 C/A, describing the signal structure choices which were made for the new generation of GNSS signals, such as the introduction of the pilot component, the presence of secondary codes, the use of longer spreading code periods, the BOC modulation, etc. Furthermore, a section is dedicated to the study of the correlation properties of the GNSS signals in the L1 band.

Chapter 3 describes the GNSS signal acquisition principle. Firstly, the basic operation of the acquisition, the correlation, is introduced. The current state-of-the-art of the common acquisition methods is provided. Then, the verification step is detailed by presenting the multi-trial techniques.

Chapter 4 deals with the signals effect on the acquisition performance, in particular for the new generation of GNSS signals. The code Doppler, impacting the spreading code period is discussed first. A comprehensive analysis of the impact of the bit sign transition on the acquisition is then presented.

Chapter 5 is devoted to the development of an efficient search acquisition method based on the Double-Block Zero-Padding (DBZP), which is an acquisition method well-known for its computationally efficient properties.

Chapter 6 proposes a global acquisition strategy to reach the acquisition objectives, the acquisition of Galileo E1 OS at 27 dB-Hz, with a high probability of success. A discussion on the choice of parameters of each step of the acquisition steps is carried.

Chapter 7 considers the transition step between the end of the acquisition providing a rough estimation of the incoming signal parameters and the start of the tracking, which needs a refinement on the frequency estimation and longer coherent integrations (possible if the secondary code on the pilot component is demodulated).

Chapter 8 draws conclusions from this dissertation, discussing the achievements and results of the thesis and proposals for future works are made.

All the results derived in the theoretical study (presented in *Chapters 3, 4, 5, 7*) have been verified by Monte-Carlo simulations.

It is worth noting that these simulations operated under a simplified signal model and did not take into account the effects of quantization and front-end filtering.

1.4 Personal Publications and Thesis contributions

Publications in International Conference:

P1 M. Foucras, O. Julien, C. Macabiau and B. Ekambi, *A Novel Computationally Efficient Galileo E1 OS Acquisition Method for GNSS Software Receiver*, in Proceedings of the 25th International Technical Meeting of The Satellite Division of the Institute of Navigation (ION GNSS 2012). Nashville, TN (USA), pp. 365 – 383, September 2012.

P2 M. Foucras, O. Julien, C. Macabiau and B. Ekambi, *An Efficient Strategy for the Acquisition of Weak Galileo E1 OS Signals*, in Proceedings of the European Navigation Conference 2013 (ENC 2013). Vienna (Austria), April 2013.

P3 M. Foucras, O. Julien, C. Macabiau and B. Ekambi, *Probability of Secondary Code Acquisition for Multi-Component GNSS Signals*, in Proceedings of the 6th European Workshop on GNSS Signals and Signal Processing (SIGNALS 2013). Neubiberg (Germany), December 2013.

P4 M. Foucras, O. Julien, C. Macabiau and B. Ekambi, *Detailed Analysis of the Impact of the Code Doppler on the Acquisition Performance of New GNSS Signals*, in Proceedings of the 2014 International Technical Meeting of The Institute of Navigation (ION ITM 2014). San Diego, CA (USA), pp. 513 – 524, January 2014.

P5 M. Foucras, O. Julien, C. Macabiau, B. Ekambi and F. Bacardi, *Optimal GNSS Acquisition Parameters when Considering Bit Transitions*, in Proceedings of IEEE/ION PLANS 2014. Monterey, CA (USA), pp. 804 – 817, May 2014.

P6 M. Foucras, U. Ngayap, J.Y. Li, O. Julien, C. Macabiau and B. Ekambi, *Performance Study of FLL Schemes for a Successful Acquisition-to-Tracking Transition*, in Proceedings of IEEE/ION PLANS 2014. Monterey, CA (USA), pp. 529 – 540, May 2014.

Publications in International Journals/Magazines

P7 M. Foucras, O. Julien, C. Macabiau, B. Ekambi and F. Bacard, *Assessing the Performance of GNSS Signal Acquisition*. Inside GNSS, vol. 9, no. 4, pp. 68 –79, August 2014.

P8 M. Foucras, O. Julien, C. Macabiau, B. Ekambi and F. Bacard, *Probability of Detection for GNSS Signals with Sign Transitions*. IEEE Transactions on Aerospace and Electronic Systems, Submitted in August 2014, in second revision.

P9 M. Foucras, J. Leclère, C. Botteron, O. Julien, C. Macabiau, P.-A. Farine, B. Ekambi, *Study on the cross-correlation of GNSS signals and usual approximations*. GPS Solutions, Submitted in July 2015.

The original contributions of this thesis are (brief insight in Publication *P7*):

- One of the major contributions of this thesis is the comprehensive study on the impact of bit sign transitions on the acquisition performance and in particular the probability of detection. This source of performance degradations of the GNSS acquisition process is generally overlooked in the literature but the presence of a binary sequence reflects the realistic case. Different publications deal with this phenomenon from the theoretical and practical point of view (*P2, P5, and P8*). Based on the expression of the correlator outputs considering the realistic assumption of one bit sign transition, these publications and *Chapter 4* and *Chapter 5* discuss the need of a Transition-Insensitive acquisition method for the new generation of GNSS signals and the optimal acquisition parameters such as the coherent integration time for GPS L1 C/A.
- One contribution of this thesis is the development of a global acquisition strategy for the acquisition of Galileo E1 OS. This includes the development of an innovative efficient Transition-Insensitive acquisition method, presented in *P1*, *P2* and *Chapter 5*, and the study on the tradeoff between the search initial acquisition and the verification step regarding the probabilities of detection and false alarm and the computation load (*P2* and *Chapter 6*).
- A detailed analysis of the impact of the code Doppler on the acquisition. As it is explained in *P4* and in *Chapter 4*, for the new challenges (low C/N_0 environments, new GNSS signal structures, new applications, etc.), the degradations on the acquisition performance are considerable and for the new GNSS signals it can hardly be overlooked as it was generally the case for GPS L1 C/A.
- A study on the correlation function looking at the approximations usually introduced and characteristics of the GPS L1 C/A and Galileo E1 OS autocorrelation and cross-correlation in the presence of Doppler. As published in *P9* and presented in *Chapter 3*, the points of interest are the isolation considering several ranges of Doppler frequencies, and the cumulative distribution of the maximum cross-correlation values.
- A performance study for various Frequency Lock Loop (FLL) schemes in order to achieve frequency refinement and then carrier tracking. This is a critical stage in GNSS signal processing because if this transition is not well calibrated, even a successful acquisition can lead to unsuccessful tracking. The optimal choice of the FLL scheme parameters is not presented clearly in the literature and is presented in *Chapter 7* and *P6*.
- A last contribution concerns the acquisition of the secondary code on the pilot component. The theoretical probability of correct acquisition is presented in *Chapter 7* and *P3* and applied for weak GNSS signals.

Chapter 2
GPS L1 C/A and the Modernized GNSS Signals

This chapter provides a brief description of the concept of the GNSS: how, with satellites, the position of a user on Earth can be determined? The GNSS signal design is presented; it is constituted by a navigation message, a spreading code and a carrier. The new generation of the GNSS signals differs from the GPS L1 C/A signal since they are also composed of a pilot component. For each signal, the spreading codes are different, for example, the Galileo E1 OS spreading codes are 4 times longer than the GPS L1 C/A codes.

It is then interesting to study the correlation properties of the spreading codes when considering Doppler frequencies. Indeed, due to the transmission by satellites, the crossing of the atmosphere, the reception by the antenna and the RF front-end processing, the original signal is delayed, affected by a Doppler frequency and potentially attenuated and deformed.

Contents

2.1 Satellite-based navigation 12
2.2 GNSS signals 13
2.2.1 GNSS signals structure 13
2.2.2 Considered GNSS signals 19
2.3 Reception of the GNSS signal 20
2.4 Discussion 22

2.1 Satellite-based navigation

In 2014, only the American (GPS) and Russian (GLONASS) systems are offering a fully operational global coverage with respectively 31 satellites [U.S. Naval Observatory, 2014] and 24 satellites [Federal Space Agency, 2014]; the European system (Galileo) is under development with 4 In-Orbit Validation (IOV) and 4 Full Operational Capability (FOC) satellites [European Commission, 2015] and [European GNSS Service Centre, 2015]; the Chinese system (BeiDou) contains 14 in-service satellites [SpaceFlight, 2014]. This work focuses on GPS and Galileo signals only.

GPS and Galileo satellites transmit signals in the L-band, which is divided in 4 sub-bands, as described in Figure 2.1:

- L5/E5, which can be sub-divided into E5a (centered at 1176.45 MHz) and E5b (centered at 1207.14 MHz),
- L2, centered at 1227.60 MHz,
- L1, centered at 1575.42 MHz.
-

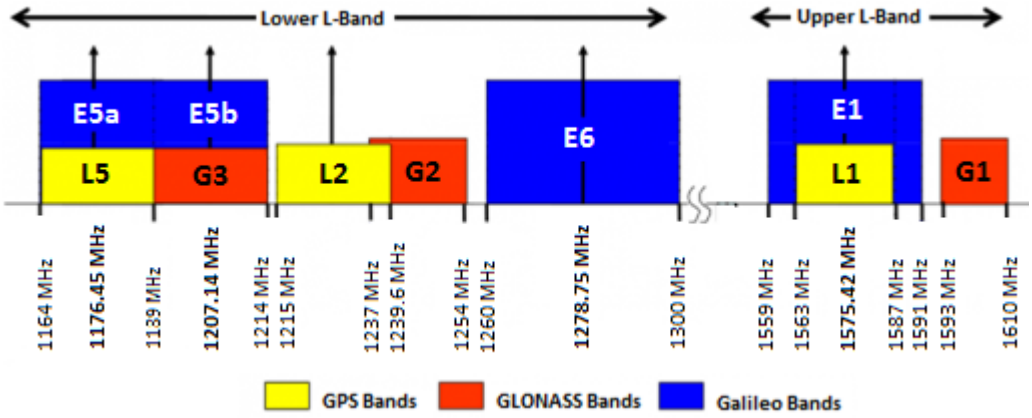

Figure 2.1 GPS, GLONASS and Galileo navigational frequency bands

GPS and Galileo signals are based on the Direct Sequence Spread Spectrum (DS-SS) technique. In particular, GPS and Galileo systems use Code Division Multiple Access (CDMA), allowing that satellites to transmit signals simultaneously, over a single communication band, with only very limited interference between them. The current and future civil GPS and Galileo signals are:

- In the L1 band: the GPS L1 C/A [Navstar, 2012a] and GPS L1C [Navstar, 2012b] signals, the Galileo E1 OS signal [European Union, 2014],
- In the L2 band: the GPS L2C signal [Navstar, 2012a],
- In the L5/E5 band: the GPS L5 signal [Navstar, 2012c] and the Galileo E5a and E5b signals [European Union, 2014].

In this work, only the GPS and Galileo signals in the L1 and L5 bands are studied.

2.2 GNSS signals

2.2.1 GNSS signals structure

In this section, a brief summary of the GNSS signal structure is given. For more details, refer to [Avila-Rodriguez, 2008] or Interface Control Documents (ICD).

2.2.1.1 Carrier and navigation message

The carrier is a continuous radio frequency sinusoidal signal, whose frequency is the central L-band frequency of interest, denoted f_L.

The navigation message, or data denoted d, with a low bit rate (the data bit duration is denoted T_d), contains useful information regarding, at least:

- Satellite clock information (bias, drift and acceleration parameters),
- Satellite health status,
- Satellite ephemeris data (satellite orbit, …),
- Almanac (with a reduced accuracy ephemeris data set of the other constellation satellites),
- Ionospheric information,
- Coordinated Universal Time (UTC) conversion.

The structure and content of the GPS and Galileo navigation message is described in the ICDs. For example, the GPS L1 C/A navigation message is a 37 500-bit long sequence and one entire navigation message lasts 12.5 minutes.

The demodulation of the GNSS navigation message is necessary to be able to compute the user position and time. However, from the point of view of the acquisition, which is the first of the signal processing step, the navigation message is assimilated to a random binary sequence of 1 and -1. Consequently, during the acquisition process, the data bit sign transitions will be one of the points of interest.

2.2.1.2 Spreading code and modulation

A spreading code, denoted c_1, is a finite known sequence of 1 and -1, with a high frequency rate f_{c_1} with respect to the data rate, which permits the receiver to determine:

- The transmitting satellite (identification),
- The travel time of the signal from the satellite to the receiver (synchronization).

A spreading code bit is called “chip” to emphasize that it does not hold any information. The spreading codes are periodically repeated (the spreading code period is denoted T_{c_1} and contains N_{c_1} chips of length t_{c_1}) and each transmitted signal is using a unique spreading code that is as orthogonal as possible to the other spreading codes.

Spreading codes are also referred to as Pseudo-Random Noise (PRN) codes due to their noise-like properties that are characterized by:

- Very low cross-correlation with other signals,
- A high autocorrelation only in 0 delay and very low elsewhere.

It is important to note that the beginning of a useful data bits is always synchronized with the beginning of the spreading code period. However, there can be several repetitions of the PRN code with one data bit.

Spreading codes can be generated by a generating algorithm, for instance of Linear Feedback Shift Register (LFSR) or not. For instance,

- The spreading codes used for GPS L1 C/A belong to the family of Gold codes. They are deterministic sequences and are generated by shift registers. 37 different Gold codes [Gold, 1967] of length 1023 chips are assigned to the GPS L1 C/A satellites [Navstar, 2012a].
- Galileo E1 OS signals use memory codes, which means that they cannot be obtained from a code generator algorithm and have to be stored in receiver memory. A family of 100 codes of length 4092 has been defined for Galileo E1 OS.

The modulation of the GNSS signal usually refers to the modulation of the PRN code. In the case of GPS L1 C/A, the modulation of the signal is referred to as Binary Phase Shift Keying (BPSK) since the PRN code chip are represented as rectangles with a length equal to the PRN code chip. In this case, the transmitted signal is represented in Figure 2.2.

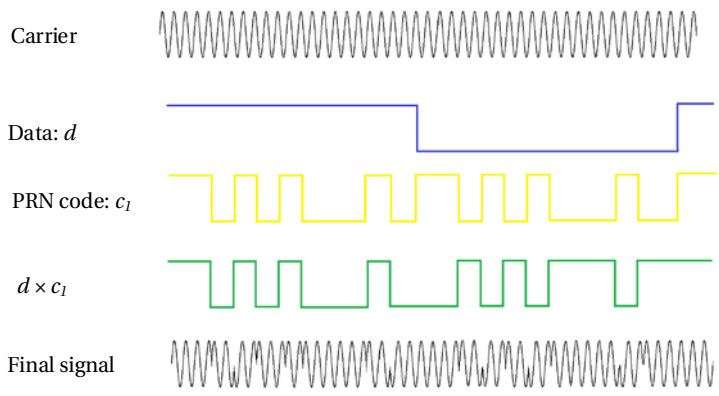

Figure 2.2 GPS L1 C/A signal structure (figure is not to scale)

Unlike the GPS L1 C/A, some of the modernized GNSS signals can use a different modulation. The main one is referred to as BOC modulation. It is the result of the multiplication of the PRN code with a square wave sub-carrier denoted $sc_{BOC(y)}$ which is mathematically obtained by taking the sign of a sine waveform of frequency yf_0 where $f_0 = 1.023$ MHz:

$$sc_{BOC(y)}(t) = \text{sign}(\sin(2\pi y f_0 t)) \tag{2.1}$$

As defined in [Betz, 2001], the BOC signals are commonly referred to BOC(m, n). The first parameter m defines the subcarrier frequency ($m \times f_0$) and the second parameter n defines the spreading code rate ($n \times f_0$).

The rough effect of the BOC modulation is to split the spectrum of the spreading code and to create 2 main side-lobes located at $\pm m f_0$. As a consequence, the minimum front-end bandwidth to receive a BOC signal is generally $2(m+n)f_0$ thus much wider than for a BPSK modulation which requires at least a front-end bandwidth of $2nf_0$.

Different modulations, based on one or several BOC modulations, are implemented in the modernized GNSS signals such as:

- Composite BOC (CBOC) modulations: CBOC(6,1,1/11,'+') and CBOC(6,1,1/11,'-') and for the Galileo E1 OS signal which are linear combinations of BOC(1,1) and BOC(6,1) modulations (both modulating the same PRN code). It is illustrated in Figure 2.3. Their expressions are:

$$\begin{aligned} sc_{CBOC\left(6,1,\frac{1}{11},'+'\right)}(t) &= \sqrt{\frac{10}{11}}p_{BOC(1)}(t) + \sqrt{\frac{1}{11}}p_{BOC(6)}(t) \\ sc_{CBOC\left(6,1,\frac{1}{11},'-'\right)}(t) &= \sqrt{\frac{10}{11}}p_{BOC(1)}(t) - \sqrt{\frac{1}{11}}p_{BOC(6)}(t) \end{aligned} \tag{2.2}$$

- Time Multiplexed BOC (TMBOC) modulation: TMBOC(6,1,1/11) for the GPS L1C signal which is a time-multiplexed combinations of BOC(1,1) and BOC(6,1) modulations (both modulating the same PRN code). Its expression is:

$$sc_{TMBOC\left(6,1,\frac{1}{11}\right)}(t) = \begin{cases} sc_{BOC(6)}, & \text{for 4 chips every 33 chips (at index } 0, 4, 6, 29) \\ sc_{BOC(1)}, & \text{otherwise} \end{cases} \tag{2.3}$$

- Alternative BOC (AltBOC) modulation: AltBOC(15,10) for the Galileo E5 signals.
-

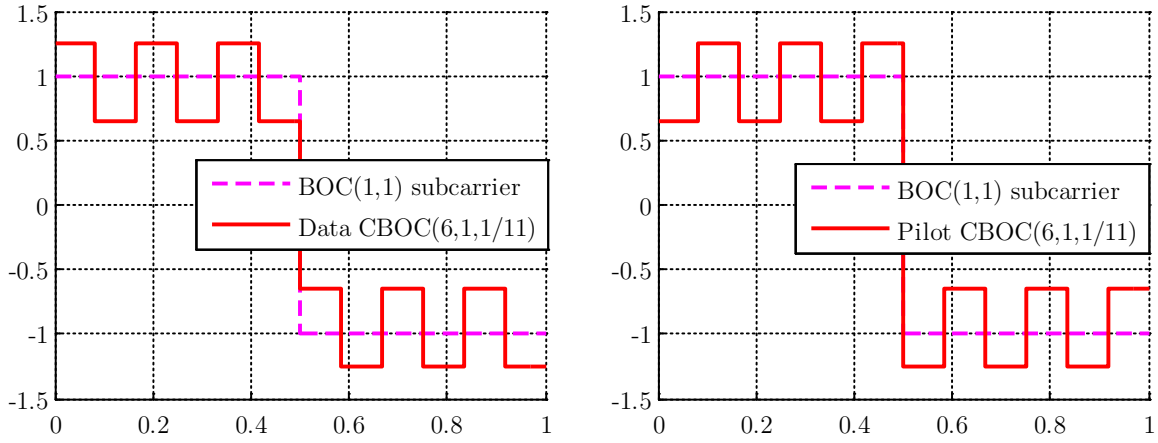

(a) CBOC(6,1,1/11,'+') (b) CBOC(6,1,1/11,'-')

Figure 2.3 Galileo E1 OS CBOC(6,1,1/11) subcarriers modulating one PRN chip

Because most of the signal power is put on the BOC(1,1) component for the BOC and TMBOC modulations, it means that the receiver manufacturer can decide to process these signals as themselves, or as a BOC(1,1). The latter will obviously result in a slight loss of power.

Figure 2.4 provides an illustration of the Power Spectral Densities (PSD) of different BPSK and BOC signals (expressions can be found in [Avila-Rodriguez, 2008]). It can be observed that a minimum bandwidth of 4 MHz is needed to include the BOC(1,1) main lobes. Consequently, for the Galileo E1 OS, the receiver designer has the choice to have a large bandwidth (at least 15 MHz) to collect all the signal power (meaning the BOC(6,1) lobes) or a bandwidth of 4 MHz that implies the loss of 1/11 of the power signal, induced by the lobes of the BOC(6,1).

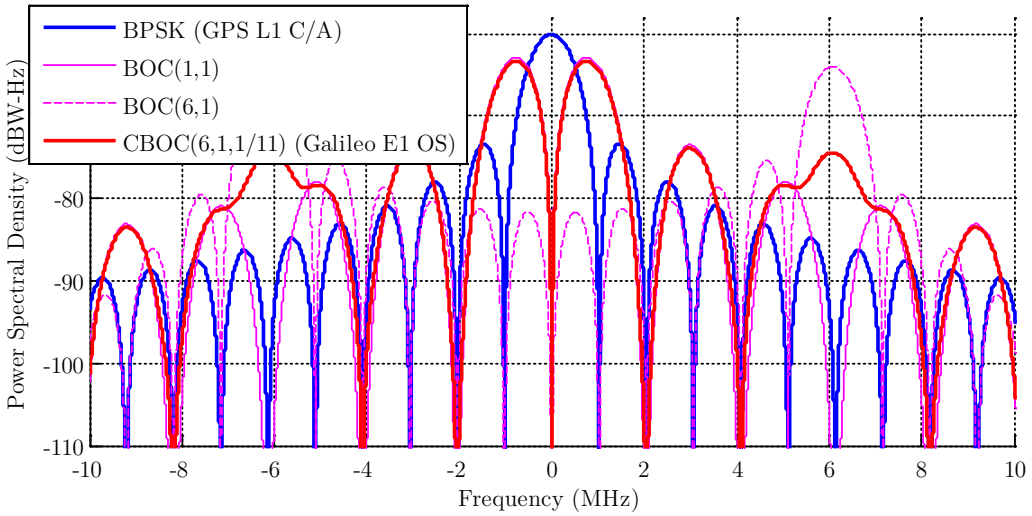

Figure 2.4 Power Spectral Densities functions of GPS L1 C/A and Galileo E1 OS signals

In Figure 2.5, the associated normalized autocorrelation functions are represented and compared to the GPS L1 C/A signal autocorrelation function. It can be seen that the use of the BOC sub-carrier affects significantly the shape of the autocorrelation function. In particular, the main peak of the autocorrelation function is much steeper. A negative peak also appears at 0.5 chip. The use of a CBOC sub-carrier creates also small local peaks.

The case of the correlation between a CBOC and a BOC(1,1) signal is also shown. The resulting correlation function looks like the autocorrelation function of the BOC(1,1), but with a slight reduction of the maximum amplitude equivalent to a loss of 0.41 dB in power due to the loss of the BOC(6,1) component. The expression of the autocorrelation functions are given in [Julien *et al.*, 2007].

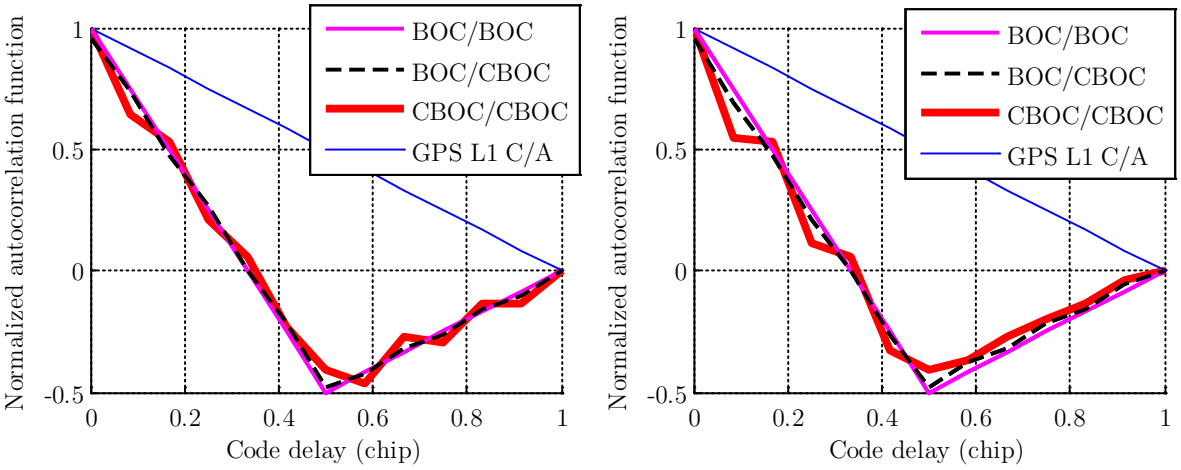

(a) Data correlation function (b) Pilot correlation function

Figure 2.5 Normalized correlation function shapes of Galileo and GPS L1 C/A spreading codes (as a function of the modulation)

2.2.1.3 Modernized GNSS signals

Due to the modernization of GPS and GLONASS and the development of Galileo, a number of new GNSS signals have been proposed in the recent years (Table 2.1).

			f_L (MHz)	Modulation	Spreading code			
					Family	Rate wrt f_0	N_{c_1} (chip)	T_{c_1} (ms)
GPS	L1	L1 C/A	1575.42	BPSK(1)	Gold code	f_0	1023	1
		L1C	1575.42	TMBOC	Weil code	f_0	10 230	10
	L5	L5	1176.45	BPSK	Combination and short-cycling of M-sequence	$10f_0$	10 230	1
Galileo	L1	E1 OS	1575.42	CBOC	Memory code	f_0	4092	4
	L5	E5a	1176.45	AltBOC(15,10)	M-sequence	$10f_0$	10 230	1
		E5b	1207.14		M-sequence	$10f_0$	10 230	1

Table 2.1 Main features of the modernized GNSS signals

The different point of design features compared to the GPS 1 C/A signal are:

- The spreading code: generally longer in terms of number of chips, but with a spreading code period of 1 ms or a few ms, due to a higher chipping rate; the spreading code on the pilot component, denoted $c_{1,p}$, is different from the spreading code present on the data component $c_{1,d}$,
- The data rate: higher, which leads to data bit duration of a few ms and generally equal to the spreading code period,
- The use of a pilot component which is dataless. Such a dataless component is known to offer improved tracking capabilities. As a consequence, the receiver can track the pilot component while demodulating the data on the traditional data component. This pilot component is thus sent in a synchronous way with the traditional data component. Its structure is very similar to that of the data component (PRN code modulating a carrier). The PRN code used to modulate the pilot component is however as orthogonal as possible to that of the data component in order to minimize the cross-correlation. The modernized civil GPS and Galileo signals have a structure in two components (data/pilot), with a split of the total signal power between both,
- The use of secondary codes on the pilot component c_2 of N_{c_2} bits (or $c_{2,p}$ if precision is required) and sometimes on the data component, denoted $c_{2,d}$. The presence of secondary code on the pilot component mainly results in:
    - Better autocorrelation properties of the pilot spreading code by making the overall period much longer,
    - Minimization of the cross-correlation and improvement of narrowband interferences suppression through decreasing spectral lines [Rushanan, 2007],
    - Providing of a data message synchronization [Stansell *et al.*, 2010].

In *Appendix C*, the significant values of autocorrelation and cross-correlation for the GPS L1 C/A and Galileo E1 OS signals are provided. They are computed for all the PRN codes (or all the couple of PRN codes) and for received Doppler frequencies f_D between -10 kHz and 10 kHz. Table 2.2 provides the significant values.

	Autocorrelation		Cross-correlation		
				Galileo E1 OS	
	GPS L1 C/A	Galileo E1 OS	GPS L1 C/A	Same satellite	Diff. satellite
$f_D = 0$ Hz	-23.94 dB	-25.39 dB	-23.94 dB	-26.66 dB	-24.49 dB
$f_D \in [0, 10]$ kHz	-19.18 dB	-23.44 dB	-19.08 dB	-25.16 dB	-22.82 dB

Table 2.2 Characteristic figures of the secondary peaks maximums of the correlation function for the GPS L1 C/A and Galileo E1 OS signals (considering CBOC modulation)

2.2.2 Considered GNSS signals

In this work, several modernized GNSS signals are considered in order to study the impact of their features on some specific points of the acquisition.

		Signal power	Modulation	Data		Secondary code		
				Bit rate (bit/s)	T_d (ms)	N_{c_2} (bit)	T_{c_2} (ms)	t_{c_2} (ms)
GPS L1 C/A		100%	BPSK(1)	50	20	None		
GPS L1C	Data	25%	BOC(1,1)	50/100	10	None		
	Pilot	75%	TMBOC(6,1,1/11)	None		18 000	1800	10
GPS L5	Data	50%	BPSK(10)	50/100	10	10	10	1
	Pilot	50%	BPSK(10)	None		20	20	1
Galileo E1 OS	Data	50%	CBOC(6,1,1/11,'+')	250	4	None		
	Pilot	50%	CBOC(6,1,1/11,'-')	None		25	100	4
Galileo E5a	Data	50%	BPSK(10)	50	1	20	20	1
	Pilot	50%	BPSK(10)	None		100	100	1
Galileo E5b	Data	50%	BPSK(10)	250	1	4	4	1
	Pilot	50%	BPSK(10)	None		100	100	1

Table 2.3 Signal features of the modernized GNSS signal components

Table 2.3 provides a global overview of the features of the civil GPS and Galileo signals, differencing the data and pilot components of the modernized GNSS signals when appropriate. It can be seen that the features presented in the previous section are all used by the new civil GPS and Galileo signals in the L1 and L5 bands.

GPS L1 C/A has the smallest spreading code in terms of number of chips. For the modernized GNSS signals, they are 10230-chip length, except for Galileo E1 OS, which is 4092-chip length. Signals in the L5 band use high chipping rates that allow better tracking performance. For the new GPS and Galileo civil signals, the data bit duration is lower than the GPS L1 C/A bit duration: 4 ms for Galileo E1 OS signal and 10 ms for GPS L1C and GPS L5. Let us note that, on the data component of GPS L5, there is the presence of a secondary code of 10 bit which fits exactly within one data bit.

For the modernized GPS and Galileo civil signals, the secondary code bit duration, denoted T_{c_2}, is always equal to the spreading code period.

The emitted composite GNSS signal can be generically represented as follows:

$$s(t) = A_d c_{2,d}(t) c_{1,d}(t) sc_d(t) d(t) \cos\left(2\pi f_L t + \phi_{0,d}\right) + A_p c_{2,p}(t) c_{1,p}(t) sc_p(t) \sin\left(2\pi f_L t + \phi_{0,p}\right) \quad (2.4)$$

where

- x stands for "d" for the data component and "p" for the pilot component,
- A_x is the signal amplitude on the component and depends upon the total signal power C,
- sc_x is the subcarrier modulating the spreading codes,
  $\phi_{0,x}$ is the initial phase on each component depending on ϕ_0 the initial phase of the incoming signal.

For each GNSS signal, Table 2.4 provides the value of the parameters, previously described.

	Data component				Pilot component		
	A_d	$c_{2,d}$	sc_d	$\phi_{0,d}$	A_p	sc_p	$\phi_{0,p}$
GPS L1 C/A	$\sqrt{2C}$	1	1	ϕ_0	0	None	None
GPS L1C	$\frac{\sqrt{C}}{\sqrt{2}}$	1	$sc_{BOC(1)}(t)$	ϕ_0	$\frac{\sqrt{3C}}{\sqrt{2}}$	$sc_{TMBOC\left(6,1,\frac{1}{11}\right)}(t)$	$\phi_0 + \frac{\pi}{2}$
GPS L5	$\sqrt{C}$	NH_{10}	1	ϕ_0	$\sqrt{C}$	1	ϕ_0
Galileo E1 OS	$\sqrt{C}$	1	$sc_{CBOC\left(6,1,\frac{1}{11},'+'\right)}(t)$	ϕ_0	$\sqrt{C}$	$sc_{CBOC\left(6,1,\frac{1}{11},'-'\right)}(t)$	$\phi_0 - \frac{\pi}{2}$
Galileo E5a	$\sqrt{C}$	$c_{2,d}$	1	ϕ_0	$\sqrt{C}$	1	ϕ_0
Galileo E5b	$\sqrt{C}$	$c_{2,d}$	1	ϕ_0	$\sqrt{C}$	1	ϕ_0

Table 2.4 Values of the parameters in the generic signal expression for each GNSS signal

2.3 Reception of the GNSS signal

The antenna of the GNSS receiver receives the signal emitted by GNSS satellites, with different delays and different signal power due to attenuations. Indeed, due to the receiver environment, interferences and propagation losses [Leclère, 2014], the power of the received signal can be strongly attenuated and the acquisition of these signals is a challenge, as it will be described.

As illustrated in Figure 1.1, the goal of the RF front-end is to provide a sampled signal as clean as possible to the signal processing block, to permit a successful signal processing. As depicted in Figure 2.6, the different missions of the RF front-end are:

- Selection of the useful signal,
- Mitigation of out-of-band interference,
- Amplification of the signal,
- Down-conversion of the signal to an intermediate frequency,
- Sampling of the signal.

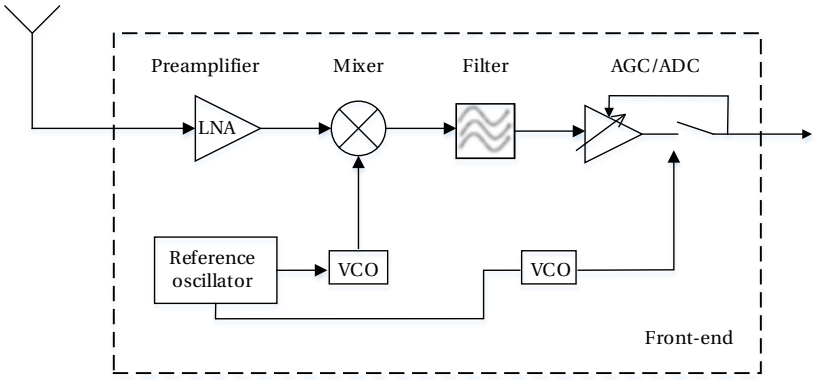

Figure 2.6 Illustration of an RF front-end

After the reception of the signal by the antenna, a preamplifier intends to limit the noise bandwidth and to reject the out-of-band interference to protect the electronics located in the receiver chain. Furthermore, because the received signal is very weak, one or several cascaded Low Noise Amplifier (LNA) are used to amplify the received signal. An LNA is mainly characterized by its gain and its noise figure ([Van Diggelen, 2009]). The PSD of the noise is denoted N_0.

To evaluate the incoming signal parameters, the receiver generates reference signals, which are compared to the incoming signal. To do so, a local reference oscillator is used to generate a local carrier. The receiver performance is highly dependent on the local oscillator, characterized by the short and long-term stabilities and the sensitivity to vibrations. The Voltage Controlled Oscillator (VCO) generates a tone, whose frequency depends upon the input control voltage. Then, the incoming signal is mixed with the local sine wave and filtered to remove all the unwanted signal generated by the mixer and provide a good rejection of out-of-band interference. The signal is amplified by an amplifier with an Automatic Gain Control (AGC).

The choice of the sampling frequency is dictated by the Nyquist theorem: the sampling frequency should be at least twice the useful signal bandwidth. Consequently, the wider the signal bandwidth, the higher the sampling frequency is. In general, the signal is down-converted to an intermediate frequency of several MHz (compared to the received frequency that is higher than 1 GHz) to use filters with a high frequency selectivity [Kaplan & Hegarty, 2005]. By means of an Analog-to-Digital Converter (ADC), the sampling process transforms the received continuous signal in a discrete digital signal, with a sampling period T_s. Then, to map the infinite set of the sampled signal values to a small set (less than 20 values), the ADC quantizes the signal. The number of samples per spreading code is denoted N_s (it can vary from a spreading period to another).

2.4 Discussion

The received signal is affected by a code delay and a Doppler frequency, which both should be estimated in the acquisition process. Due to the periodicity of spreading code, the code delay uncertainty is the spreading code period. As detailed in [Kubrak, 2007], the Doppler frequency affecting the received signal, results in the contributions of:

- The user's Doppler,
- The satellite's Doppler,
- The local oscillator's Doppler-like effect.

As also explained in [Tsui, 2005], the maximum Doppler frequency shift for GPS L1 C/A is about 4.9 kHz caused by the satellite motion. In addition, if a vehicle carrying a GPS receiver moves at a velocity of 150 km/h, the maximum Doppler frequency shift introduced by the user motion is equal to 219 Hz. The overall Doppler affecting the received signal at the user antenna is then the combination of the satellite and user Doppler, plus an extra contribution due to the receiver local oscillator drift. That contribution, for a 1 Part Per Million (PPM) local oscillator is around 1575 Hz for the L1 and E1 signals [Chibout, 2008]. At the end, taking into account the previously described contributions, the maximum Doppler frequency is approximately 6.7 kHz. In this work, the Doppler frequency range uncertainty is rounded to $[-10, 10]$ kHz.

Clearly, the received carrier frequency is affected by the Doppler frequency but the chipping rate also suffers from the Doppler effect and implies a change in the received spreading code period; *Chapter 4* thoroughly studies its impact on the acquisition performance.

At the end, the down-converted and filtered composite GNSS signal entering the correlation block of the receiver can be generically represented as follows:

$$\begin{aligned} r(t) = {} & A_d d(t-\tau) c_{2,d}(t-\tau) c_{1,d}(t-\tau) sc_d(t-\tau) \cos\left(2\pi(f_{IF} + f_D)t + \phi_{0,d}\right) \\ & + A_p c_{2,p}(t-\tau) c_{1,p}(t-\tau) sc_p(t-\tau) \sin\left(2\pi(f_{IF} + f_D)t + \phi_{0,p}\right) + \eta(t) \end{aligned} \tag{2.5}$$

where

- τ is the received code delay,
- η is the incoming noise which is assumed to be an Additive White Gaussian Noise (AWGN) with centered Gaussian distribution with a constant two-sided power spectral density equal to $N_0/2$ dBW/Hz.

As discussed in this chapter and in [Van Dierendonck, 2014], the modernized GNSS signals have adopted a variety of features not used for the GPS L1 C/A signal. The next chapters try to evaluate the benefits or at least the effect of these improvements on the acquisition performance.

The main points of the modernized GNSS signal designs are reminded:

- Due to the use of longer spreading codes, the correlation properties are improved and in particular the autocorrelation isolation. As an example on Galileo E1 OS, it was shown that for a Doppler frequency between 0 and 10 kHz, the maximum autocorrelation value is -23.41 dB, which is more than 4 dB better than the GPS L1 C/A autocorrelation isolation (-19.18 dB).
- For most of the modernized GNSS signals, due to higher data rate, the data bit duration (or the resulting binary sequence on the data component for signals in the L5 band) is equal to the spreading code period (and also the pilot secondary code bit duration) and since both sequences are synchronized (a data bit transition occurs at the beginning of a spreading code period), this implies potential bit sign transition at each spreading code period.
- A pilot component is commonly used in communication systems to improve the signal tracking. But this implies that the power of the signal is split between the data and the pilot component. Furthermore, since the pilot component does not have the same spreading code as the data component, the acquisition and tracking can be completely independent.
- The multiplexed BOC(6,1) signal is added to the BOC(1,1) signal of the Galileo E1 OS and GPS L1C signals. Receiver designers can ignore the part of the signal spectrum of the BOC(6,1).

Chapter 3
GNSS Signal Acquisition Principle

In GNSS receivers, the first stage of the signal processing is the acquisition. It consists in assessing the presence of GNSS signals, identifying all satellites visible to the user and giving a rough estimation of the incoming signal parameters.

This chapter provides a global description of the acquisition of GNSS signals (GPS L1 C/A and the new generation of signals). A section is dedicated to the correlation operation. Then, a classical acquisition method, the serial-search, is presented as well as the mathematical approach considering the acquisition as a detection problem. This chapter permits to understand the acquisition principle by presenting its performance, parameters and requirements.

Contents

3.1 Correlation operation 26
3.1.1 Correlation concept 26
3.1.2 Correlator output in absence of data 27
3.2 Serial-search classical acquisition method 31
3.2.1 Acquisition grid uncertainties 31
3.2.2 Review of accumulation techniques 33
3.2.3 GNSS signal detection 34
3.3 Acquisition methods 45
3.3.1 Optimized acquisition methods 45
3.3.2 Multi-trial and verification strategies 48
3.3.3 Modernized GNSS signal acquisition 54
3.4 Discussion 62

3.1 Correlation operation

As previously said the acquisition aims at deciding either the presence or the absence of the GNSS signal and provides a rough estimation of the code delay and Doppler frequency of the incoming signal. To do so, a replica is locally generated (depending on an estimation of the incoming code delay and Doppler frequency) and correlated with the incoming signal.

3.1.1 Correlation concept

The correlation operation is the basic operation performed in the signal processing part of a GNSS software receiver and is dependent upon the GNSS signals properties, particularly the spreading code properties. Indeed, these codes have been carefully chosen to have very good pseudo-randomness properties. This means that they have properties that are close to those of a white noise (this is why they are called Pseudo-Random Noise (PRN) codes). In other words, when the spreading code is correlated with itself, the correlation function result is equal to 1 for a perfect alignment and close to being null for a misalignment or when two different spreading codes are correlated. Figure 3.1 shows the autocorrelation function between the local and incoming spreading code of the GPS L1 C/A spreading code number 2. The correlation operation is denoted R_{c_1} and defined by:

$$\begin{aligned} R_{c_1}(\tau) &= \frac{1}{N_s}\sum_{n=0}^{N_s-1} c_1(n)c_1(n-\tau) \text{ (discrete form)} \\ &= \frac{1}{T_{c_1}}\int_0^{T_{c_1}} c_1(t)c_1(t-\tau)dt \text{ (continuous form)} \end{aligned} \tag{3.1}$$

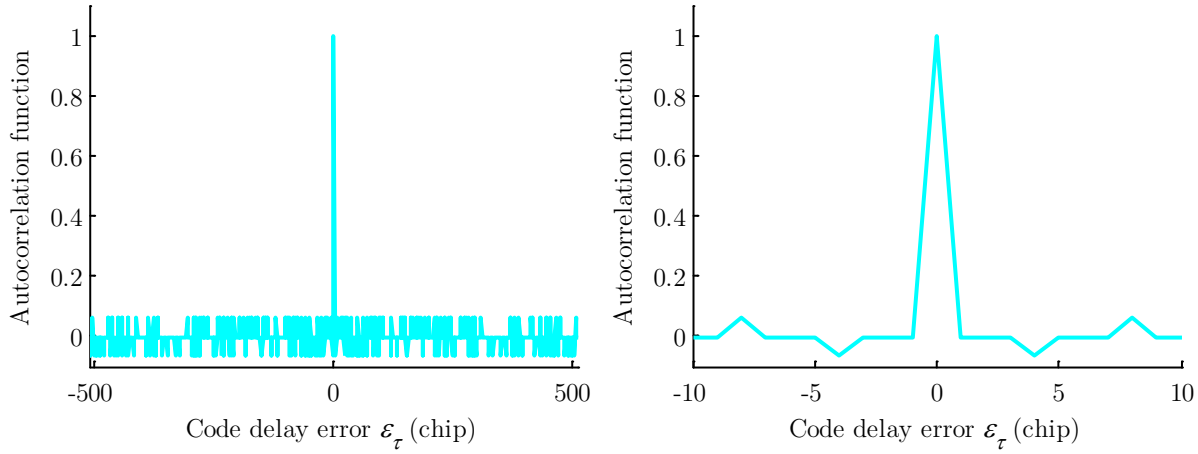

(a) Full function (b) Zoom around $\tau = 0$

Figure 3.1 GPS L1 C/A autocorrelation function (PRN 2)

In a GNSS receiver, the correlation operation consists in correlating the received signal with a local replica of the carrier and spreading code of the received signal. To do so, the received signal is multiplied by a sinusoid and a local spreading code. The resulting signal is

then integrated, generating the in-phase correlator output I. As illustrated in Figure 3.2, the same process is also performed with a shifted sinusoid of $\pi/2$. This provides the quadrature-phase correlator output Q. The acquisition of GNSS signals described in literature [Ward *et al.*, 2005b], [Tsui, 2005], [Holmes, 2007] is based on the evaluation and processing of the correlator outputs.

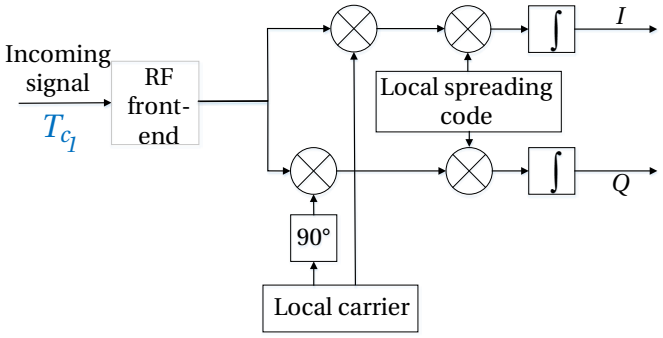

Figure 3.2 Block diagram of the correlation

3.1.2 Correlator output in absence of data

3.1.2.1 Assumptions

In this section, the expression of the correlator output will be described. To do so, some assumptions are taken. Firstly, in the literature, it is generally assumed that the data bit value is constant during the correlation interval. It can be assimilated to the absence of data [O'Driscoll, 2007]. In the next chapter, the correlator output expressions are presented in a more realistic case assuming data bit transitions during the correlation operation.

The slice of time corresponding to the considered signal for the accumulation and for evaluating the correlator outputs defines the coherent integration time, denoted T_C. It is chosen as a multiple of the spreading code period T_{c_1} and shorter usually than a data bit duration. Then, the k-th integration interval is defined as $[T_0 + (k-1)T_C, T_0 + kT_C]$ where T_0 is the beginning of the first correlation interval. The incoming signal depends on the parameters $\tau(k)$ and $f_D(k)$ which are the instantaneous code delay and the Doppler frequency and the local replica $\cos\left(2\pi\left(f_{IF} + \hat{f}_D\right)t\right) c_1(t - \hat{\tau})$ depends on the estimates $\hat{\tau}$ and $\hat{f}_D$ of these parameters made by the receiver. Based on the correlation operation, the acquisition process consists in determining the received Doppler frequency and code delay. The Doppler frequency error ε_{f_D} and code delay error ε_τ are denoted by:

$$\begin{aligned} \varepsilon_\tau(k) &= \tau(k) - \hat{\tau} \\ \varepsilon_{f_D}(k) &= f_D(k) - \hat{f}_D \end{aligned} \tag{3.2}$$

It is generally assumed that the incoming Doppler frequency and the code delay error are constant on the correlation interval and also the amplitude of the signal. In addition, the phase is assumed to linearly vary. It is important to note that the effect of oscillator errors and multipath are ignored in this thesis even though they are paramount in real-world data.

3.1.2.2 Correlator output expression (continuous case)

In this case, it is assumed that the signals are continuous and not sampled. As developed in *Appendix D*, the in-phase and quadrature correlator output expression is as follows:

$$\begin{aligned} I(k) &= \frac{A}{2} d(k) R_{c_1}\left(\varepsilon_\tau(k)\right) \cos\left(\pi \varepsilon_{f_D}(k) T_C + \varepsilon_{\phi_0}(k)\right) \operatorname{sinc}\left(\pi \varepsilon_{f_D}(k) T_C\right) + \eta_I(k) \\ Q(k) &= \frac{A}{2} d(k) R_{c_1}\left(\varepsilon_\tau(k)\right) \sin\left(\pi \varepsilon_{f_D}(k) T_C + \varepsilon_{\phi_0}(k)\right) \operatorname{sinc}\left(\pi \varepsilon_{f_D}(k) T_C\right) + \eta_Q(k) \end{aligned} \tag{3.3}$$

where

- $\varepsilon_{\phi_0}(k) = \phi_0 - \hat{\phi}_0$ represents the phase error at the beginning of the integration interval $[T_0 + (k-1)T_C, T_0 + kT_C]$,
- $d(k)$ is the data bit value on the correlation interval,
- η_I and η_Q represent the noise at the in-phase and quadrature correlation output which is assumed to follow a centered Gaussian distribution which variance is [Julien, 2005]:

$$\sigma_\eta^2 = \frac{N_0}{4T_C} \tag{3.4}$$

In GNSS receivers, the received signal is discretized and then in a discretized case, the term $\operatorname{sinc}\left(\pi \varepsilon_{f_D} T_C\right)$ becomes $\frac{\operatorname{sinc}\left(\pi \varepsilon_{f_D} T_C\right)}{\operatorname{sinc}\left(\pi \varepsilon_{f_D} T_s\right)}$, named a Dirichlet kernel as the ratio of two sinus terms. Both terms are equivalent for high sampling frequency because T_s would be very close to 0.

3.1.2.3 Validity region

The previously presented expression of the correlator outputs is often presented in literature but almost never computed. In particular, there is a critical step that transforms one integral into the product of two integrals (see *Appendix D*) that is never clearly justified. Some arguments are exposed but it necessitates more details and precisions. On one hand, [Holmes, 2007] explains that the autocorrelation function can be factored out of the integral as an approximation assuming that the Doppler frequency error is small compared to the chip rate. On the other hand, [Van Dierendonck, 1996] explains that the correlated signals can still be considered pseudorandom and the accumulation serving as a time average, the correlator output expression result as an expected value. It is legitimate that one wonders what the limits of the approximation are. This work intends to evaluate this assumptions to complete the study proposed in [Motella *et al.*, 2010].

The objective is thus to compare what is actually done in a GNSS software receiver with the theoretical approximation given in (3.3). The phase uncertainty of the phase correlator outputs is eliminated by taking the modulus. The received signal is also assumed normalized. Thus, the modulus of the correlator output value considered as "true" corresponds to the discrete software implementation and is given by:

$$\left| \sum_{n=0}^{N_s - 1} c_1(nT_s - \tau) c_1(nT_s - \hat{\tau}) e^{i(2\pi(f_d - \hat{f}_D) n T_s)} \right| \tag{3.5}$$

It is compared with its approximation provided by:

$$\left|R_{c_1}(\varepsilon_\tau)\,\mathrm{sinc}\left(\pi\varepsilon_{f_D}T_C\right)\right| \tag{3.6}$$

Based on Matlab simulations on GPS L1 C/A with a correlation integration duration $T_C = 1$ ms, it is possible to evaluate the adequacy between both expressions (3.5) and (3.6) for different values of code delay and Doppler frequency errors in order to provide a region of validity of the taken approximation to obtain (3.3).

As expected, both representations appear to have the same shape and relatively close from of global point of view (Figure 3.3). The differences appear for the small values.

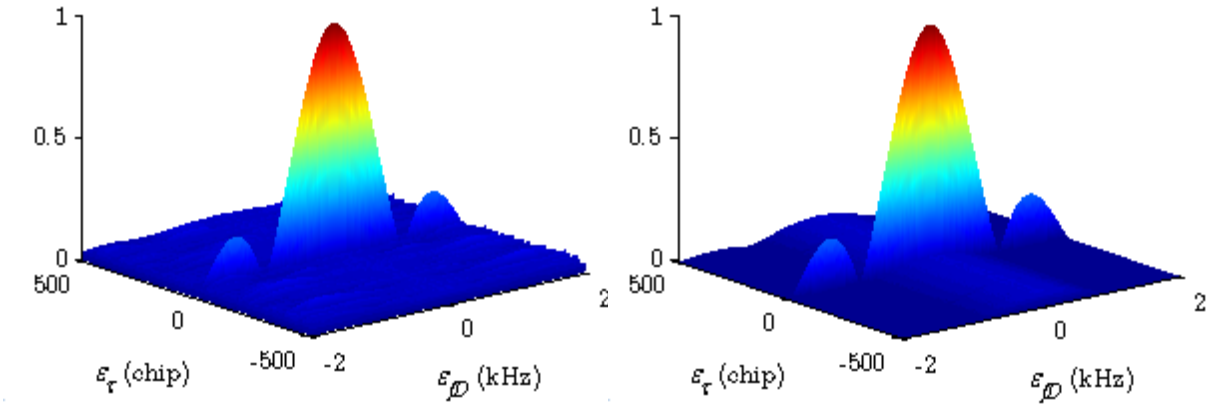

(a) True (3.5) (b) Approximation (3.6)

Figure 3.3 Representation of the equations (3.5) and (3.6)

When one looks at absolute difference $|(3.5) - (3.6)|$ between the truth and its approximation, some disparities in yellow (difference around 0.05) and red (difference around 0.075) appear in Figure 3.4. Obviously, when the code delay or the Doppler frequency is correctly estimated, the approximation is excellent (in line with Holmes approximation).

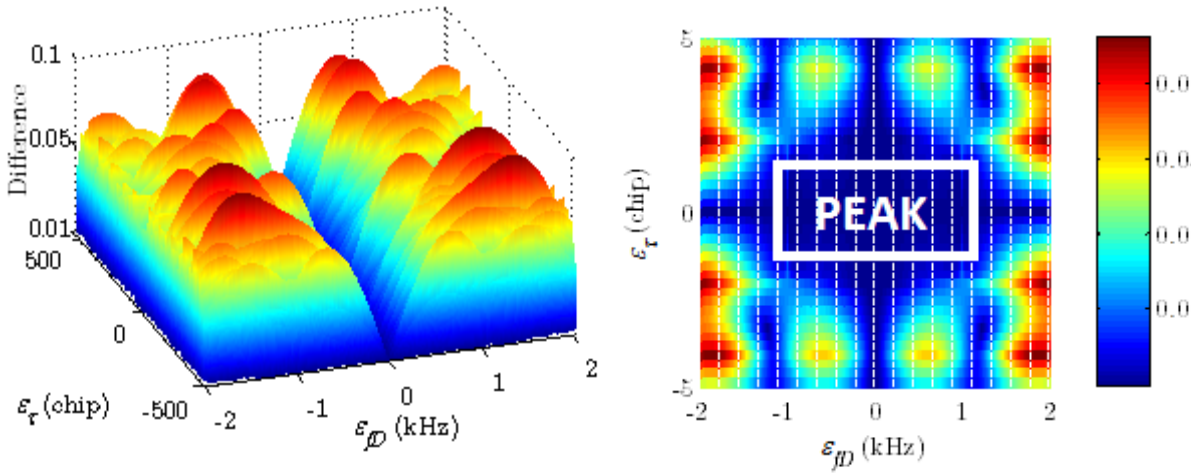

(a) Whole space (b) Zoom around (0,0)

Figure 3.4 Representation of the absolute difference between equations (3.5) and (3.6)

As depicted in dark blue, the difference is close to 0 for a small Doppler frequency error (Figure 3.4(a)), or very small Doppler frequency and code delay errors corresponding to the main peak (Figure 3.4(b)). To complete these results and quantify the order of errors, Figure 3.5 and Figure 3.6 present the approximation and true values in dB and their difference in the frequency and time domains (equivalent loss of incoming signal power).

When the code delay error $|\varepsilon_\tau|$ is relatively small, typically lower than 1 chip (for example $|\varepsilon_\tau| = 0.3$ and $|\varepsilon_\tau| = 0.9$ in Figure 3.5), the approximation is very close to the exact value mainly for the main lobe of the sinc ($|\varepsilon_{f_D}| < 1$ kHz). Outside the main lobe, the approximation differs from the exact value, the higher ε_τ is, the higher the difference is.

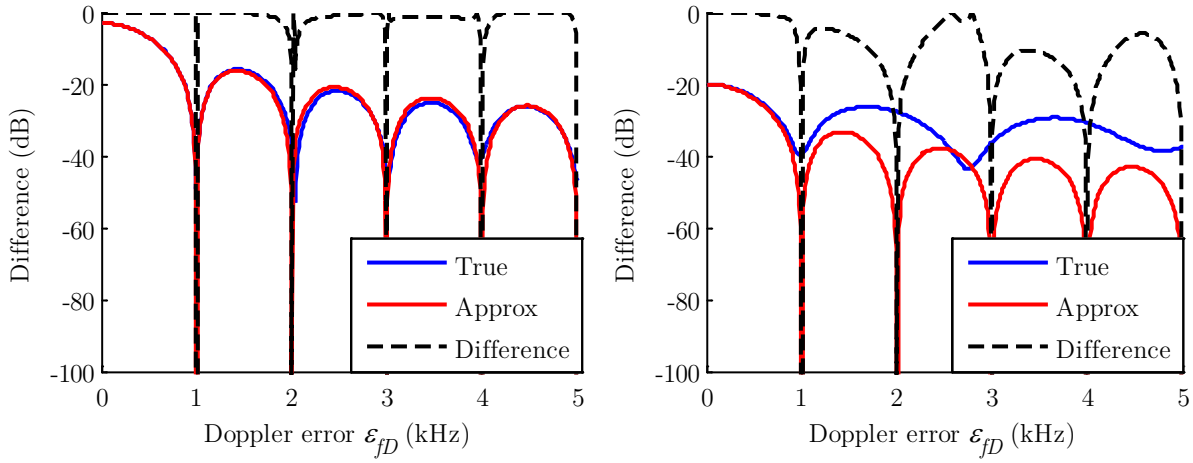

(a) $|\varepsilon_\tau| = 0.3$ chip (b) $|\varepsilon_\tau| = 0.9$ chip

Figure 3.5 Comparison of the CAF of PRN 1 when $|\varepsilon_\tau|$<1 chip

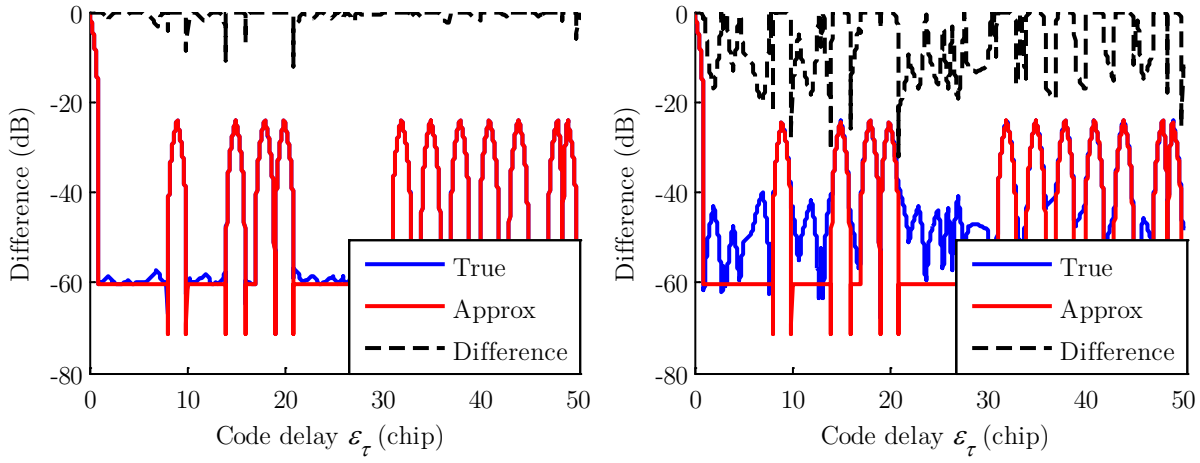

(a) $|\varepsilon_{f_D}| = 10$ Hz (b) $|\varepsilon_{f_D}| = 100$ Hz

Figure 3.6 Comparison of the CAF of PRN 1 when $|\varepsilon_{fD}|$ is relatively small

However, even for small Doppler frequency errors, the approximation does not exactly match the exact value (Figure 3.6) but it is very close for Doppler frequency errors in the order of a few tens Hz.

When the code delay error exceeds 1 chip or the Doppler frequency error is high, the expression (3.6) is not valid to approximate the exact correlation operation (3.5). In the same way, concerning the cross-correlation (correlation between two different spreading codes), the approximation can only be used when the Doppler frequency error is close to null. The cross-correlation value depends then on the code delay and Doppler frequency errors.

In conclusion, it has been observed that, for GPS L1 C/A, the approximation of the correlator outputs systematically used in theoretical analysis:

- Provides an exact result for a correct estimation of the code delay ($\varepsilon_\tau = 0$ chip) or Doppler frequency ($\varepsilon_{f_D} = 0$ Hz), or quite exact for a code delay error less than 1 chip and for a frequency error less than a few hundreds of hertz ($|\varepsilon_\tau| < 1$ chip and $|\varepsilon_{f_D}| < 1$ kHz). Then, in this region (main peak), the difference between the approximation and the true value is less than 0.0058 (for a maximum amplitude of 1, that means less than 1%).
- Is not valid for a code delay error higher than 1 chip ($|\varepsilon_\tau| > 1$ chip) or a Doppler frequency error greater than a 1 kHz and the difference can reach 0.095, this corresponds to a case in which the approximation value is close to 0 and the true value close to 0.1 (more than 90%).

3.2 Serial-search classical acquisition method

The most challenging step in the GNSS receiver signal processing module is the initial acquisition, whose objective is the coarse alignment between the received incoming signal and its locally generated replica. To do so, a set of local replicas taking all possible values for the couple $(\hat{f}_D, \hat{\tau})$ (referred to as uncertainty space) is used to generate correlator outputs that are used to compute values of the normalized acquisition detector T which expression is:

$$T = \left(\frac{I(k)}{\sigma_\eta}\right)^2 + \left(\frac{Q(k)}{\sigma_\eta}\right)^2 \tag{3.7}$$

A classic acquisition method is the serial-search acquisition method based on a discretization of the uncertainty time and frequency domain into an acquisition grid.

3.2.1 Acquisition grid uncertainties

The uncertainty space corresponds to all possible values that the incoming Doppler frequency and the code delay can take. This 2D-space (frequency and time) is discretized into an acquisition grid as presented in Figure 3.7. In this figure, N_f refers to the number of Doppler frequency cells and N_τ refers to the number of code delay cells forming the acquisition grid. N_c

refers to the total number of cells in the acquisition grid, it is the product of N_f and N_τ. Furthermore, Δ_f and Δ_τ are the widths of the frequency and code delay cells, referred to as cell size.

A cell in the acquisition grid is thus represented by a couple $(\hat{f}_l, \hat{\tau}_j)$ where $l = 1, \ldots, N_f$ and $j = 1, \ldots, N_\tau$ and $\hat{f}_l$ and $\hat{\tau}_j$ are the central values of the cell. To each cell in the acquisition grid, is associated an acquisition detector value. Regarding Figure 3.7, it can be seen that the incoming signal has a Doppler frequency close to 2600 Hz and a code delay of approximately 766 chips.

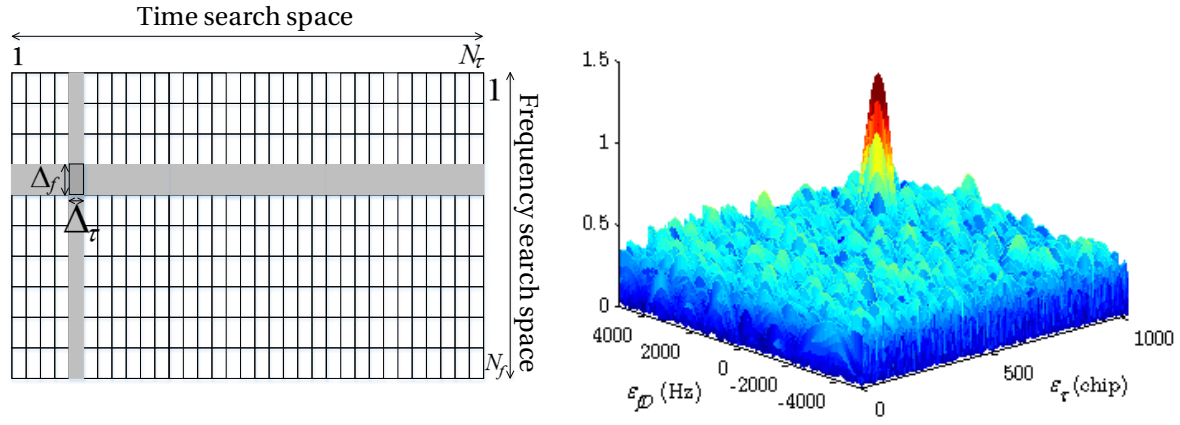

(a) Acquisition grid (b) Acquisition matrix

Figure 3.7 Matrix acquisition based on an acquisition grid

Clearly, it is irrelevant to assume that the acquisition cell size is infinitely small. Indeed, a trade-off should be chosen between the acquisition cell size and then loss and the acquisition duration: a large bin size leads to degradation of the acquisition performance (the error between the tested value and the true value can be significant), while a narrow cell size means that a significant number of cells has to be potentially visited, thus increasing the mean time to acquire the signal. In general the acquisition grid is defined as a function of the maximum acceptable degradation on the detector. Following the example used in [RTCA, Inc, 2008], it has been chosen:

- A Doppler cell size of $\Delta_f = \frac{1}{2T_C}$ Hz, corresponding to an equivalent degradation of the received signal C/N_0 of 0.9 dB, in the worst case, and which corresponds to a maximum Doppler frequency error $|\varepsilon_{f_D}| \leq \frac{1}{4T_C}$ Hz,
- A cell size in the code delay domain sufficient to generate a maximum equivalent degradation of the received C/N_0 of 2.5 dB in the worst case. The code delay cell size, thus, depends on the autocorrelation function shape (and in fact on the RF front-end filter as well). For example, it corresponds to a cell size $|\Delta_\tau| = \frac{1}{2}$ chip for an unfiltered BPSK signal, such as the GPS L1 C/A or GPS L5 signals (such as $R_{c_1}(\varepsilon_\tau) \geq 0.75$).

In the next chapter, a study on the effect of the acquisition cell size on the acquisition performance is proposed.

3.2.2 Review of accumulation techniques

When the signal is too weak and does not allow obtaining desired acquisition performance, some techniques can be applied to reduce the noise and accumulate the signal energy. They are well described in [Esteves, 2014] and [O'Driscoll, 2007].

3.2.2.1 Coherent summation

The first one, called long coherent integration and presented in Figure 3.8, consists in accumulating signal over T_C ms with $T_C > T_{c_1}$ (correlation over more than one spreading code period, for example, the total accumulation time $T_I = T_C = 100$ ms). This kind of integration provides the best performance in terms of noise variance reduction since the noise power at the output of a correlator is inversely proportional to T_C as presented in (3.4).

When considering a coherent integration time longer than the data bit duration, the sign of the data bits can change over the considered slice of incoming signal. As developed in *Chapter 4*, data bit sign transition during the correlation process degrades the performance. The second drawback is the performance losses due to the frequency error. Indeed, the sinc term in (3.3) depends on the coherent integration time T_C. Then for example, for a Doppler frequency error of $\varepsilon_{f_D} = 50$ Hz (which is relatively small), if $T_C = 1$ ms (GPS L1 C/A spreading code period), then the degradation due to the term $\mathrm{sinc}(\pi \varepsilon_{f_D} T_C)$ equals 0.03 dB but become equal to 3.92 dB for $T_C = 10$ ms.

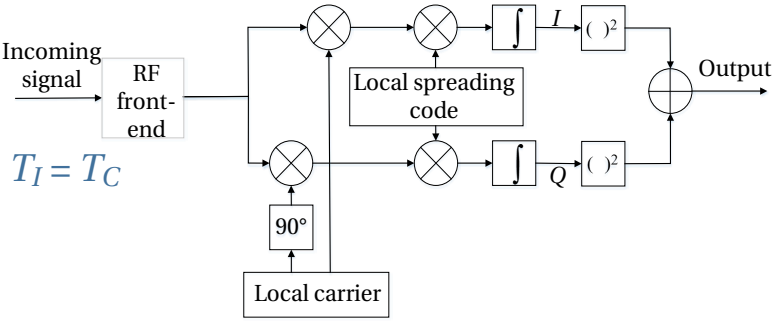

Figure 3.8 Coherent scheme

The acquisition grid discretization is linked to the coherent time in the frequency domain, for example, $\Delta_f = \frac{1}{2T_C}$. This implies that the higher T_C is, the smaller Δ_f should be but and thus the higher N_f will be. Increasing the coherent time increases the number of cells in the acquisition grid and then the exploration time.

3.2.2.2 Non-coherent summation

The non-coherent integration, presented in Figure 3.9, widely used in the acquisition of GPS signals [Van Dierendonck, 1996], [Ward *et al.*, 2005b] and fully analyzed in [Borio & Akos, 2009], consists in accumulating a number, denoted K, of squared correlator outputs computed over T_C (in general $T_C = T_{c_1}$). In the end, the total accumulation time, called the dwell time, is $T_I = KT_C$ (for example $T_I = K \times T_C = 25 \times 4$ ms).

In terms of acquisition sensitivity, for the same dwell time T_I, when not considering bit sign transitions, it is preferable to use long coherent summation ($T_I = T_C$) rather than non-coherent summation ($T_I = KT_C$), as entitled [Pany *et al.*, 2009], "the coherent integration time: the longer, the better…"

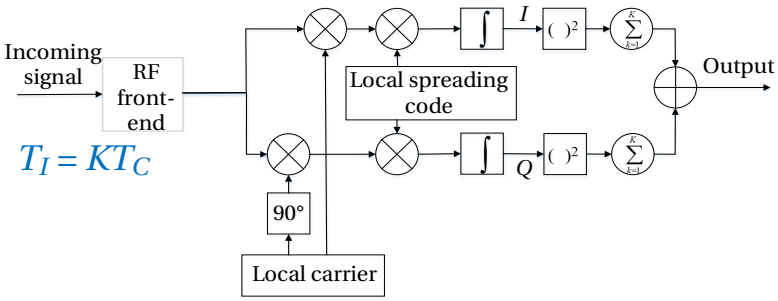

Figure 3.9 Non-coherent summations scheme

Other integration techniques can be used such as differential integration initially proposed by [Coenen & Van Nee, 1992] and [Zarrabizadeh & Sousa, 1997].

3.2.3 GNSS signal detection

In a more general case, considering that several correlator outputs are computed and coherently or non-coherently combined, the chosen normalized acquisition detector T is (3.8). It is the sum of the squared normalized correlator outputs to eliminate the phase dependency:

$$T = \sum_{k=1}^{K} \left(\left(\frac{I(k)}{\sigma_\eta} \right)^2 + \left(\frac{Q(k)}{\sigma_\eta} \right)^2 \right) \tag{3.8}$$

To simplify the theoretical analysis, the acquisition detector is expressed on its normalized version; in GNSS receiver, in general, its not-normalized version is used since the variance is unknown and estimated.

3.2.3.1 Statistical model

Several acquisition strategies are developed to determine the cell in the acquisition grid corresponding to a right estimation of the parameters. For example, the acquisition detector is computed for all the cells and only the maximum is retained. In this work, it was chosen that the acquisition detector is compared to an acquisition threshold. The objective is then to make a decision regarding the presence of the signal transmitted by a specific satellite. In this sense, a hypothesis test is used, comparing the metric to a threshold. In the GNSS signal theory detection, the two conditions of signal presence and absence correspond to the two following hypotheses:

- The null hypothesis H_0: the desired signal is not present or the local replica is not correctly synchronized (in time and/or in frequency),
- The alternative hypothesis H_1: the desired signal is present and the local replica is correctly synchronized in time and frequency.

Mathematically, both hypotheses can be modelled as:

$$H_0: \left\{ (\hat{f}_D, \hat{\tau}) \text{ such that } |\varepsilon_{f_D}| > \frac{\Delta_f}{2} \text{ or } |\varepsilon_\tau| > \frac{\Delta_\tau}{2} \text{ if correct PRN code used; or wrong PRN code is used} \right\}$$
$$H_1: \left\{ (\hat{f}_D, \hat{\tau}) \text{ such that } |\varepsilon_{f_D}| \leq \frac{\Delta_f}{2} \text{ and } |\varepsilon_\tau| \leq \frac{\Delta_\tau}{2} \text{ if correct PRN code used} \right\} \quad (3.9)$$

Knowing the distributions of the acquisition detector under H_0 and H_1, as shown in Figure 3.10, it is then possible to determine the normalized detection threshold γ for a desired probability of false alarm P_{FA} and evaluate the probability of detection P_D, which corresponds to correctly assess the signal presence when it is effectively present.

The hypothesis test becomes:

$$H_0: T < \gamma \text{ against } H_1: T \geq \gamma \quad (3.10)$$

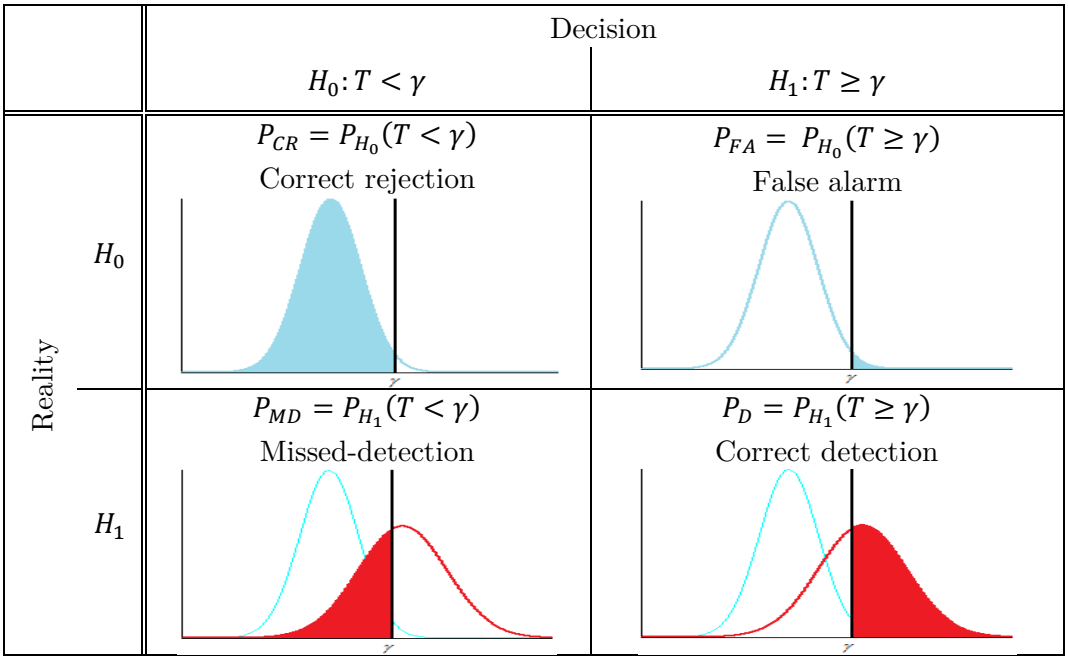

Figure 3.10 Illustration of the acquisition characterization

Two errors can be made:

- Declare the signal present whereas it is absent (or not correctly aligned with the local replica): this error corresponds to a false alarm. It is obvious that, not to penalize the receiver acquisition time, this probability P_{FA} should be low. It is generally set by the receiver manufacturer as a function of the acquisition settings. It is the value of P_{FA} that will determine the detector threshold.
- Declare the signal absent whereas it is present and correctly aligned with the local replica: this error corresponds to a missed-detection. The probability of miss detection P_{MD} should be as small as possible.

Let us now study the distribution of the acquisition detector, according to both hypothesis.

Under H_0 (the correlator outputs are dominated by noise):

$$T = \sum_{k=1}^{K} \left(\frac{I(k)}{\sigma_\eta}\right)^2 + \left(\frac{Q(k)}{\sigma_\eta}\right)^2 =_{H_0} \sum_{k=1}^{K} \left(\frac{\eta_I(k)}{\sigma_\eta}\right)^2 + \left(\frac{\eta_Q(k)}{\sigma_\eta}\right)^2 \sim_{H_0} \chi^2(2K) \tag{3.11}$$

The correlation sidelobes are neglected as a first approximation since their level is very low. However, they are sometimes considered as in [Van Dierendonck, 1996]. In addition, since in this thesis, the effects of front-end filtering are neglected, the noise components $\eta_I(k)$ and $\eta_I(k+1)$ (and in the same way $\eta_Q(k)$ and $\eta_Q(k+1)$) are assumed statistically independent, which is roughly true in a real-data world thanks to the use of filters. Then, the acquisition detector T can be seen as the sum of K square absolute of two independent unit Gaussian random variables and then T is a χ^2 distribution with $2K$ Degrees Of Freedom (DOF). For a desired probability of false alarm P_{FA}, the acquisition threshold is then:

$$\begin{aligned} P_{FA} &= P_{H_0}(T > \gamma) = 1 - F_{\chi^2(2K)}(\gamma) \\ \gamma &= F^{-1}_{\chi^2(2K)}(1 - P_{FA}) \end{aligned} \tag{3.12}$$

where $F_{\chi^2(2K)}$ is the inverse cumulative distribution function of a χ^2 with $2K$ degrees of freedom.

Under H_1 (presence of signal): it can be assumed that $\varepsilon_{f_D}(k)$ and $\varepsilon_\tau(k)$ are small since the investigated cell of the acquisition grid is the correct one and then the correlator outputs are non-centered Gaussian distributions. Thus,

$$\begin{aligned} E\big(I(k)\big) &= \frac{A}{2} R_{c_1}\big(\varepsilon_\tau(k)\big) \cos\Big(\pi \varepsilon_{f_D}(k) T_C + \varepsilon_{\phi_0}(k)\Big) \operatorname{sinc}\big(\pi \varepsilon_{f_D}(k) T_C\big) \\ E\big(Q(k)\big) &= \frac{A}{2} R_{c_1}\big(\varepsilon_\tau(k)\big) \sin\Big(\pi \varepsilon_{f_D}(k) T_C + \varepsilon_{\phi_0}(k)\Big) \operatorname{sinc}\big(\pi \varepsilon_{f_D}(k) T_C\big) \end{aligned} \tag{3.13}$$

The sum of the square of $2K$ non-zero mean independent Gaussian random variables has a non-central χ^2 distribution with $2K$ degrees of freedom [Proakis, 2007] and a non-centrality parameter Λ:

$$T \sim_{H_1} \chi^2(2K, \Lambda) \tag{3.14}$$

where, assuming that the key parameters of the incoming signal and local replica do not change:

$$\begin{aligned} \Lambda &= \sum_{k=1}^{K} E^2\left(\frac{I(k)}{\sigma_\eta}\right) + E^2\left(\frac{Q(k)}{\sigma_\eta}\right) \approx K\left(E^2\left(\frac{I(k)}{\sigma_\eta}\right) + E^2\left(\frac{Q(k)}{\sigma_\eta}\right)\right) \approx K\lambda_0 \\ \lambda_0 &= E^2\left(\frac{I(k)}{\sigma_\eta}\right) + E^2\left(\frac{Q(k)}{\sigma_\eta}\right) \approx \frac{A^2}{4\sigma_\eta^2} R_{c_1}^2(\varepsilon_\tau) \operatorname{sinc}^2\big(\pi \varepsilon_{f_D} T_C\big) \\ &\approx \frac{A^2}{N_0} T_C R_{c_1}^2(\varepsilon_\tau) \operatorname{sinc}^2\big(\pi \varepsilon_{f_D} T_C\big) \end{aligned} \tag{3.15}$$

The probability of detection is thus given by:

$$P_D = P_{H_1}(T > \gamma) = 1 - F_{\chi^2(2K,\Lambda)}(\gamma) \tag{3.16}$$

where $F_{\chi^2(2K,\Lambda)}$ is the cumulative distribution function (CDF) of a non-central χ^2 distribution with $2K$ degrees of freedom. The cumulative distribution function for non-central chi-squared distribution can be expressed in terms of the generalized Marcum's Q-function [Proakis, 2007].

In the same way, in literature ([O'Driscoll, 2007] for example), the normalized acquisition detector is expressed as $\sqrt{T}$. Under H_0, if T follows a $\chi^2(2)$ distrubution, then $\sqrt{T}$ follows a Rayleigh distribution of parameter 1 (equivalent to a Ricean distribution $\mathcal{R}(0,1)$). Under H_1, T follows a $\chi^2(2,\lambda)$ and $\sqrt{T}$ follows a Ricean distribution $\mathcal{R}\left(1,\sqrt{\lambda}\right)$. In this case, the cumulative distribution function is a Marcum Q-function of order 1 [Proakis, 2007].

	$T = \left(\frac{I(k)}{\sigma_\eta}\right)^2 + \left(\frac{Q(k)}{\sigma_\eta}\right)^2$	$R = \sqrt{T} = \sqrt{\left(\frac{I(k)}{\sigma_\eta}\right)^2 + \left(\frac{Q(k)}{\sigma_\eta}\right)^2}$
Under H_0	$\gamma_T = F^{-1}_{\chi^2(2)}(1 - P_{FA}) \approx 13.82$	$\gamma_R = F^{-1}_{\mathcal{R}(0,1)}(1 - P_{FA}) \approx 3.72 = \sqrt{13.82} = \sqrt{\gamma_T}$
Under H_1	$P_D = 1 - F_{\chi^2(2,\lambda)}(\gamma_T) = Q_1\left(\sqrt{\Lambda}, \sqrt{\gamma_T}\right) \approx 81.03\%$	$P_D = 1 - F_{\mathcal{R}(1,\sqrt{\lambda})}(\gamma_R) = Q_1\left(\sqrt{\Lambda}, \gamma_R\right) \approx 81.03\%$

Table 3.1 Comparison of two acquisition detector performances ($T_C = 1$ ms, $K = 1$, $C/N_0 = 40$ dB-Hz, $P_{FA} = 10^{-3}$, $\lambda = 20$)

As it can be observed with Table 3.1, for one integration, the probabilities of detection obtained when the acquisition detector is T or $\sqrt{T}$ are equivalent. From the point of view of the implementation, the computation of $\sqrt{T}$ requires one more operation (the square root) and the Rice and Rayleigh distributions functions (such as CDF, PDF…) are not necessarily implemented (in Matlab for example, the $F_{\mathcal{R}(1,\sqrt{\lambda})}(\gamma)$ should be evaluated with the Marcum Q-function) where the χ^2 distributions functions are available, then the acquisition detector is chosen to be T.

3.2.3.2 Searching strategies

Several strategies can be considered when dealing with the comparison of the acquisition detector amplitude computed for a cell in the acquisition grid to the threshold. Indeed, for example, only the variable on the whole acquisition grid which provides the maximum amplitude is compared to the threshold and the GNSS detection signal is function of this unique variable, or all the variables can be compared to the threshold until the first crossing. Based on [Borio, 2008], for each presented searching strategy, the associated probabilities of false alarm $P_{FA,search}$, of detection $P_{D,search}$ and of missed-detection $P_{MD,search}$ are reported with an illustration. They are expressed as a function of the probability of detection P_D, missed-detection P_{MD} and false alarm P_{FA} for one cell and presented in section 3.2.3.1.

In the illustrations given in Table 3.2 and Table 3.6, the red triangle represents the amplitude of the acquisition detector for the right cell whereas the blue points are the amplitude of the acquisition detector for an erroneous cell. The threshold γ is materialized by a blue line. For the last strategy, the dashed line refers to the amplitude of the N_M highest points. Indeed, this study introduces a new searching strategy accepting that the acquisition detector amplitude associated to the correct cell is not necessarily the maximum but should be part of the N_M highest ones.

The major part of the following results are taken from [Borio, 2008], they are validated on a simplified scenario; the innovative results are theoretically verified.

The objective of the searching strategy is to determine if the signal is present (and the parameters are correctly estimated). In this case, the null hypothesis corresponds to the absence of the signal, meaning that the local PRN code is not one of the received codes. The alternative hypothesis stays unchanged and assumes the presence of the signal and that the parameters are well estimated:

$$\begin{aligned} &H_0': \{\text{wrong PRN code is used}\} \\ &H_1: \left\{\text{correct PRN code used and } \left(\hat{f}_D, \hat{\tau}\right) \text{ such that } \left|\varepsilon_{f_D}\right| \leq \frac{\Delta_f}{2} \text{ and } \left|\varepsilon_\tau\right| \leq \frac{\Delta_\tau}{2}\right\} \end{aligned} \tag{3.17}$$

For simplicity, it is assumed that only one cell satisfies the hypotheses H_1. [Borio, 2008] and [Corazza *et al.*, 2004] differentiate the errors that can be made under H_1 by talking of a missed-detection or a "false alarm in the H_1 sector". When the signal is present, the acquisition detector for parameter couples which do not correspond to the incoming signal parameter couple can produce false alarms as defined in section 3.2.3.1. In this work, the term missed-detection corresponds to the event of no-detection under H_1 and is the union of all the events leading to a detection failure.

Since the search space is evaluated over a finite and discrete set of code delays and Doppler frequencies, it can be represented as a matrix of random cells X_i with $i = 1, 2, \ldots, N_c$. The random cell verifying H_1 is denoted X_A. If C_i denotes the cell i, X_A can be inside C_i following a uniform distribution and then $P(X_A \in C_i) = 1/N_c$. Let us assume that $X_1, \ldots, X_{N_c-1}$ are independent and identically distributed (since they represent the false alarms – under H_0, signal present but wrong estimation- and then follow white Gaussian noise) and let us note F_X their cumulative distributive function.

- Serial strategy

The serial search, the simplest one, consists in sequentially evaluating the acquisition detector cell by cell and immediately comparing it against the acquisition threshold. Once the acquisition detector crosses the threshold, the acquisition process goes to the next step. The estimated Doppler frequency and code delay are those corresponding to the parameters for the acquisition detector computation.

The performance study is synthetized in Table 3.2.

Under H_0'	Probability of correct rejection 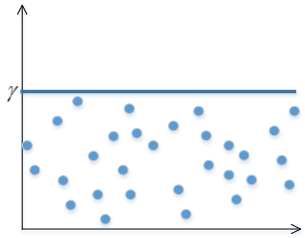 $P_{CR,Serial} = (1 - P_{FA})^{N_c}$	Probability of false alarm 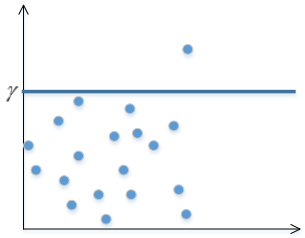 $P_{FA,Serial} = 1 - (1 - P_{FA})^{N_c}$
Under H_1	Probability of detection 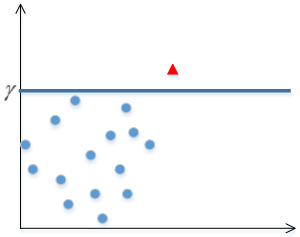 $P_{D,Serial} = \frac{1}{N_c} P_D \frac{1 - (1 - P_{FA})^{N_c}}{P_{FA}}$	Probability of missed-detection 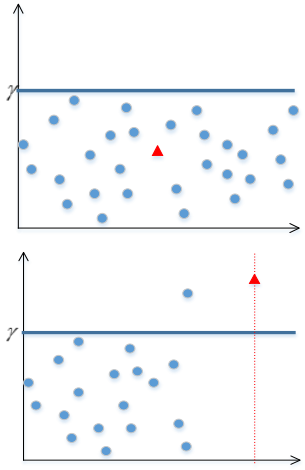 $P_{MD,Serial} = 1 - P_{D,Serial}$

Table 3.2 Probabilities describing the serial strategy

Under H_0': absence of the signal

In a serial strategy, a false alarm occurs when a variable crosses the threshold whereas all the previous ones are below the threshold. All the cases should be taken into account: the first cell crosses the threshold, the second cell crosses the threshold whereas the first does not, etc.

$$\begin{aligned} P_{FA,Serial} &= P(X_1 > \gamma) + P(X_2 > \gamma)P(X_1 < \gamma) + P(X_3 > \gamma)P(X_2 < \gamma)P(X_3 < \gamma) \\ &\quad + \cdots \\ &= P_{FA} + P_{FA}(1 - P_{FA}) + P_{FA}(1 - P_{FA})^2 + \cdots \\ &= P_{FA} \sum_{n=0}^{N_c} (1 - P_{FA})^n = P_{FA} \times \frac{1 - (1 - P_{FA})^{N_c}}{1 - (1 - P_{FA})} \\ &= 1 - (1 - P_{FA})^{N_c} \end{aligned} \tag{3.18}$$

Under H_1: presence of the signal

Three cases should be considered:

- The first one is the detection of the signal, which means the right cell crosses the threshold whereas the previous ones do not,
- There can be a missed-detection when:
    - no cell exceeds the threshold,
    - a cell, corresponding to a false alarm (under H_0, erroneous estimation of the signal parameters) exceeds the threshold before the right cell.

$$\begin{aligned} P_{D,Serial} &= P\left(\bigcup_{i=1}^{N_c}\left((X_A \in C_i) \cap (X_i > \gamma) \cap \left(\bigcap_{j=1}^{i-1} X_j < \gamma\right)\right)\right) \\ &= \sum_{i=1}^{N_c} P(X_A \in C_i) P(X_i > \gamma) P\left(\bigcap_{j=1}^{i-1} X_j < \gamma\right) \\ &= \frac{1}{N_c} P_D \sum_{i=1}^{N_c} (1 - P_{FA})^{i-1} = \frac{1}{N_c} P_D \frac{1 - (1 - P_{FA})^{N_c}}{P_{FA}} \end{aligned} \tag{3.19}$$

When the search step stops because the threshold is exceeded, the cell is verified. If the step of verification rejects the detection of the cell, the search step continues where it was stopped to test the other cell of the acquisition grid. If the whole acquisition grid is explored, the exploration begins again at the beginning of the acquisition grid.

- Maximum strategy

For all of the cells of the acquisition grid, the acquisition detector is evaluated. Only the maximum of them is retained and compared against the threshold. If it is greater than the threshold, the signal is acquired and the estimated Doppler frequency and code delay are those corresponding to the maximum variable. It is an extreme case of the developed strategy.

Under H_0': absence of the signal

In the maximum strategy, a false alarm occurs when the cell with the maximum amplitude exceeds the threshold. It is equivalent to the false alarm of the serial strategy.

Under H_1: presence of the signal

The correct detection of the signal occurs when the right cell crosses the threshold and is the maximum of the variable.

The missed-detection occurs when the amplitude of the right cell is not the maximum (crossing or not the threshold). If the cell with the maximum amplitude exceeds the threshold, it corresponds to a false alarm (under H_0, erroneous estimation of the signal parameters).

In the end, the performance study is given in Table 3.3 as given in [Corazza, 1996] and [Borio, 2008].

Under H_0'	Probability of correct rejection	$P_{CR,Max} = (1 - P_{FA})^{N_c}$
	Probability of false alarm	$P_{FA,Max} = 1 - (1 - P_{FA})^{N_c}$
Under H_1	Probability of detection	$P_{D,Max} = \int_{\gamma}^{+\infty} \left(F_X(x)\right)^{N_c - 1} f_{X_A}(x) dx$
	Probability of missed-detection	$P_{MD,Max} = 1 - P_{D,Max}$

Table 3.3 Probabilities describing the maximum strategy

- Hybrid strategy

The acquisition detector is evaluated on a set of cells (for example a row or a column of the acquisition grid) and the decision is taken on the maximum in the current set. The performance study is reported in Table 3.4 and developments can be found in [Borio, 2008].

Under H_0'	Probability of correct rejection	$P_{CR,Hybrid} = (1 - P_{FA})^{N_c}$
	Probability of false alarm	$P_{FA,Hybrid} = 1 - (1 - P_{FA})^{N_c}$
Under H_1	Probability of detection	$P_{D,Hybrid} \approx \frac{1}{N_\tau} \frac{1 - (1 - P_{FA})^{N_c}}{1 - (1 - P_{FA})^{N_f}} (1 - P_{FA})^{N_f - 1} P_D$
	Probability of missed-detection	$P_{MD,Hybrid} = 1 - P_{D,Hybrid}$

Table 3.4 Probabilities describing the hybrid strategy ([Borio, 2008])

- Among the N_M maximums

In this work, a new searching strategy is proposed. It is a mix between the maximum and hybrid strategies. Instead of constraining the right cell to be the highest one, it is tolerated that it is among the N_M highest ones, with N_M to define.

Under H_0': absence of the signal

A false alarm occurs when at least one cell exceeds the threshold. For all the presented searching strategies, the probability of false alarm is the probability of the same event and then it is equal.

Under H_1: presence of the signal

The correct detection of the signal occurs when the right cell crosses the threshold and is among cells with the N_M highest amplitudes. The missed-detection occurs when the right cell is not among the N_M highest (crossing or not the threshold), that means that the acquisition detector amplitude of, at least, N_M false alarms (under H_0, erroneous estimation of the signal parameters) are higher than the amplitude of the right cell.

Let us evaluate the probability of detection for this strategy, it will permit to determine $N_c - N_M$, defined by the minimum number of cells with an amplitude lower than the right cell amplitude.

The k-th order statistic of a statistical sample is equal to its k-th smallest value. Given the $N_c - 1$ random variables $X_1, \dots, X_{N_c-1}$, the order statistics $X_{(1)}, \dots, X_{(N_c-1)}$ are also random variables, defined by sorting the values of $X_1, \dots, X_{N_c-1}$ in increasing order. Then, the first order is the minimum of the sample and the $N_c - 1$-th order is the maximum:

$$\begin{aligned} X_{(1)} &= \min_{i=1,\dots,N_c-1}(X_i) \\ X_{(N_c-1)} &= \max_{i=1,\dots,N_c-1}(X_i) \end{aligned} \tag{3.20}$$

As given in [Lecoutre & Tassi, 1987], the cumulative distribution $F_{X_{(q)}}$ of $X_{(q)}$ is:

$$F_{X_{(q)}}(x) = P\big(X_{(q)} \le x\big) = \sum_{i=q}^{N_c-1} \binom{N_c - 1}{i} \big(F_X(x)\big)^i \big(1 - F_X(x)\big)^{N_c-1-i} \tag{3.21}$$

As illustrated in Table 3.6 with $N_M = 3$, a detection can occur when the right cell (materialized by a red triangle) is above the threshold γ (solid line) and it is among the N_M highest points above the threshold (materialized by a dashed line at the N_M-th point). For a fixed number of cells N_c, being among the N_M highest values is equivalent to be higher than at least $N_c - N_M$ variables.

Following the same development as [Borio, 2008], the probability of detection $P_{D,Max(q)}$ can be written as :

$$P_{D,Max(q)} = P\Big(\big(X_{(q)} \le X_A\big) \cap \big(X_A > \gamma\big)\Big) \tag{3.22}$$

Knowing the cumulative distribution function of X_A denoted F_{X_A} which is absolutely continuous, the probability density function (PDF) is such that $f_{X_A}(x)dx = dF_{X_A}(x)$. By using the theorem of the total probability in the case of continuous random variables, $P_{D,Max(q)}$ can be expressed as:

$$\begin{aligned} P_{D,Max(q)} &= \int_{\gamma}^{+\infty} P\Big(\big(X_{(q)} \le x\big) \cap \big(X_A = x\big)\Big)\, dx = \int_{\gamma}^{+\infty} P\big(X_{(q)} \le x | X_A = x\big) f_{X_A}(x) dx \\ &\approx \int_{\gamma}^{+\infty} P\big(X_{(q)} \le x\big)\, f_{X_A}(x) dx \end{aligned} \tag{3.23}$$

The term $P\big(X_{(q)} \le x | X_A = x\big)$ is equal to $P\big(X_{(q)} \le x\big)$ because the variables $X_{(q)}$ and X_A are independent. The term $P\big(X_{(q)} \le x\big)$ in (3.23) corresponds to the cumulative distribution $F_{X(q)}$ of the order statistic which expression is given by (3.21).

$$\begin{aligned} P_{D,Max(q)} &= \int_{\gamma}^{+\infty} F_{X_{(q)}}(x)\, f_{X_A}(x)dx \\ &= \int_{\gamma}^{+\infty} \sum_{i=q}^{N_c-1} \binom{N_c-1}{i} \big(F_X(x)\big)^i \big(1-F_X(x)\big)^{N_c-1-i} f_{X_A}(x)dx \\ &= \sum_{i=q}^{N_c-1} \binom{N_c-1}{i} \int_{\gamma}^{+\infty} \big(F_X(x)\big)^i \big(1-F_X(x)\big)^{N_c-1-i} f_{X_A}(x)dx \end{aligned} \tag{3.24}$$

For $x = \gamma$, $1 - F_X(\gamma)$ corresponds to the probability of false alarm P_{FA}. When x is big, $F_X(x)$ is close to 1 (property of cumulative distribution function) and then $\big(1 - F_X(x)\big)$ tends to 0.

If $q = N_c - N_M$, that means X_A is among the N_M maximas, the probability of detection is:

$$P_{D,Max(N_c-N_M)} = \sum_{i=N_c-N_M}^{N_c-1} \binom{N_c-1}{i} \int_{\gamma}^{+\infty} \big(F_X(x)\big)^i \big(1-F_X(x)\big)^{N_c-1-i} f_{X_A}(x)dx \tag{3.25}$$

Let us note that if $N_M = 1$, $(q = N_c - 1)$, that means X_A is the maximum, the probability of detection is:

$$P_{D,Max(N_c-1)} = \int_{\gamma}^{+\infty} \big(F_X(x)\big)^{N_c-1} f_{X_A}(x)dx \tag{3.26}$$

If $N_M = N_c \times P_{FA}$, $(q = N_c(1 - P_{FA}))$, the probability that $\big((X_A > \gamma) \cap \big(X_A > X_{(q)}\big)\big)$ is equivalent to $(X_A > \gamma)$ and then $P_{D,Max(q)}$ is close to P_D.

This theoretical result is confirmed by simulations, based on the acquisition of GPS L1 C/A, with parameters:

- $N_c = 50\,000$ cells,
- $K = 40$, $T_c = 1$ ms,
- $C/N_0 = 27$ dB-Hz,
- $X \sim \chi^2\,(2K)$, $X_A \sim \chi^2(2K, \Lambda)$ with $\Lambda \approx 2\frac{C}{N_0}KT_C \approx 40.095$.

The results are presented in Table 3.5 for two extreme values of N_M. Firstly, if $N_M = N_c \times P_{FA}$ (second column), the experimental probability of detection given by (3.25) is close to the probability of detection P_D which corresponds to the probability that X_A is higher than the threshold. Secondly, if X_A is the maximum, the probability $P_{D,Max(q)}$ is obviously lower than the probability of detection P_D. To check the result, the probability of false alarm such that $P_D = 0.092$ is searched and is $P_{FA} = 1.37 \times 10^{-5}$. As it can be seen, in this case, $N_c \times P_{FA} = 0.685$ which means that there is rarely false alarm and then X_A is the maximum since it is the only one under the threshold.

	$q = N_c(1 - P_{FA}) = 50$	$q = N_c - 1$	
	$P_{FA} = 10^{-3}$	$P_{FA} = 10^{-3}$	$P_{FA} = 1.37 \times 10^{-5}$
P_D	37.90%	37.90%	9.21%
(3.25)	37.53%	9.20%	

Table 3.5 Experimental probability of detection for characteristic values of q

At the end, the performance study of the strategy among the N_M maximums is described by Table 3.6. Figure 3.11 provides the resulting probability of detection for different acquisition parameters.

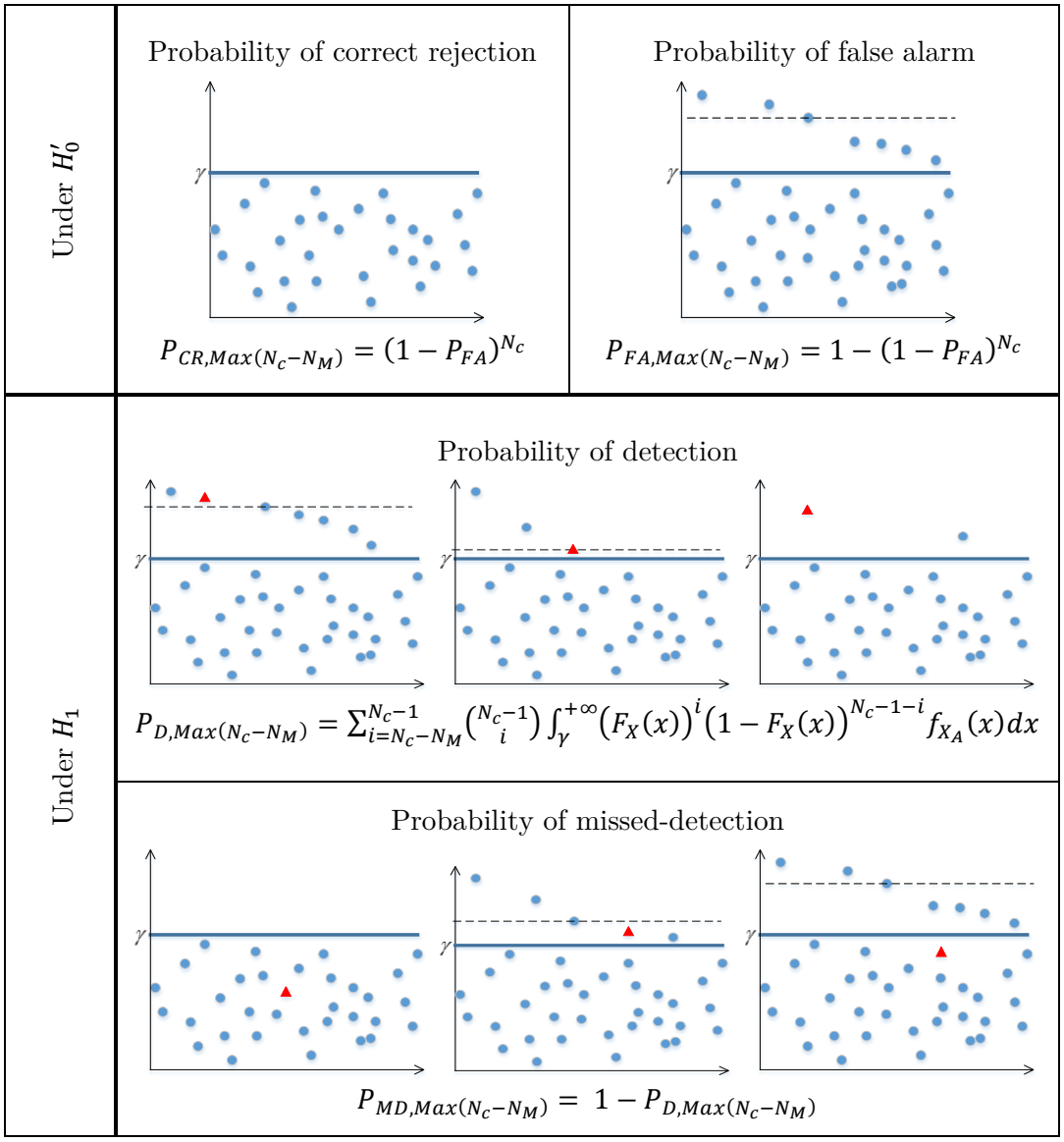

Table 3.6 Probabilities describing the strategy among the N_M maximums

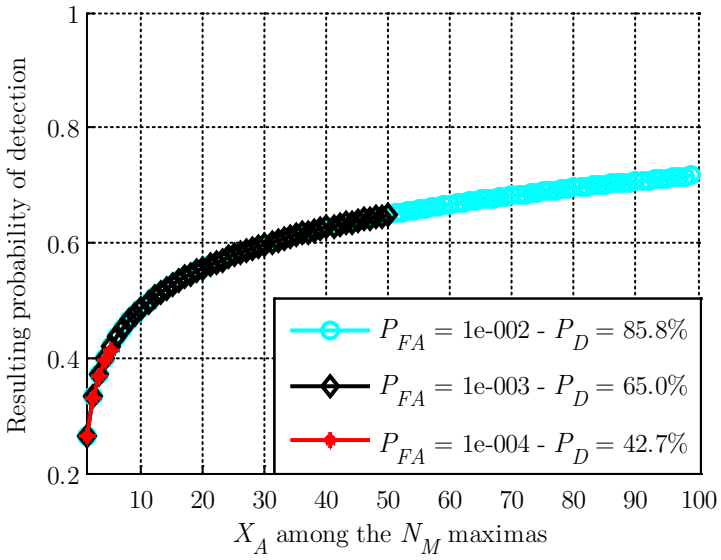

Figure 3.11 Probability of detection of the strategy among the N_M maximums as a function of N_M (Galileo E1 OS, $N_C = 50\ 000$ cells)

3.3 Acquisition methods

The computation of the acquisition detector for all the potential signal parameters couples (and then for all the cells of the acquisition grid) can be very long. Some acquisition methods based on a parallelization, for one or both parameters, relying on Discrete Fourier Transform and in general Fast Fourier Transform (FFT) were proposed and are briefly presented here. To go further, [Borre *et al.*, 2007], [Leclère, 2014] can be consulted.

3.3.1 Optimized acquisition methods

3.3.1.1 Parallel acquisition in the frequency domain

The Parallel Frequency Search (PFS) performs the search in the frequency dimension in a parallel way and in a serial way in the time domain. Figure 3.12 is a block diagram of the PFS and as it can be observed, the incoming signal is multiplied by a locally generated spreading code sequence depending on a code delay estimate $\hat{\tau}$. The resulting signal is transformed into the frequency domain by a Fourier transform (implemented as a Discrete Fourier Transform or a Fast Fourier Transform which is computationally efficient). For a perfectly aligned locally generated spreading code sequence, the squared output will show a distinct peak located at the frequency index corresponding to the frequency of the incoming signal.

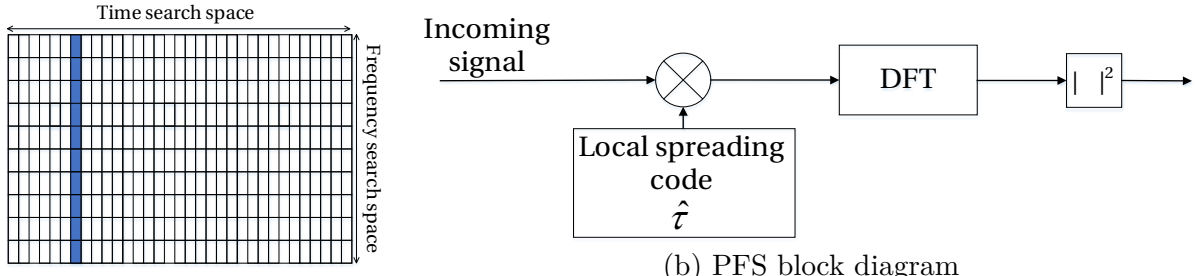

(a) PFS acquisition grid

(b) PFS block diagram

Figure 3.12 PFS method implementation description

From the mathematical point of view, the output for the j_f-th row and a code delay estimate $\hat{\tau}$ is:

$$\frac{1}{N_s}\left|\sum_{n=0}^{N_s-1} r(n)c_1(n-\hat{\tau})\exp\left(-\frac{2i\pi j_f n}{N_s}\right)\right|^2 \tag{3.27}$$

From the implementation point of view, there are as many local spreading code replicas as estimate of code delay $\hat{\tau}$. The process is repeated for each code delay estimate, therefore the gain compared to the serial search depends on the number of Doppler frequency estimates $\hat{f}_D$. The drawback is the high number of insignificant and unused computed points. Indeed, due to the definition of the Fourier Transform, the Discrete Fourier Transform (DFT) output describes the frequency space $\left[-\frac{f_s}{2},\frac{f_s}{2}\right]$, which is for example, $[-20{,}20]$ MHz whereas the searched Doppler frequency is at the maximum 10 kHz. To reduce the size of the DFT (in the order of 10^5), it can be proposed to average (or down-sample) the sampled incoming signal, as suggested in [Starzyk & Zhu, 2001].

3.3.1.2 Parallel acquisition in time domain

Knowing that the number of code delay cells N_τ is generally larger than the number of Doppler frequency cells N_f, the motivation behind this idea is to parallelize the correlation in the time domain. This method, called, the Parallel Code-Phase Search (PCPS) acquisition method and illustrated in Figure 3.13, is widely used. The incoming signal is multiplied by a locally generated carrier signal which depends on the estimate of the incoming Doppler frequency $\hat{f}_D$. The locally generated spreading code is transformed into the frequency domain and the result is complex conjugated. Then, the Fourier transform of the input multiplied by the Fourier transform of the local spreading code is transformed into the time domain by an inverse Fourier transform. By taking the absolute value, the correlation between the incoming signal and the spreading code is retrieved. If the correlation presents a peak, it indicates the incoming code delay τ.

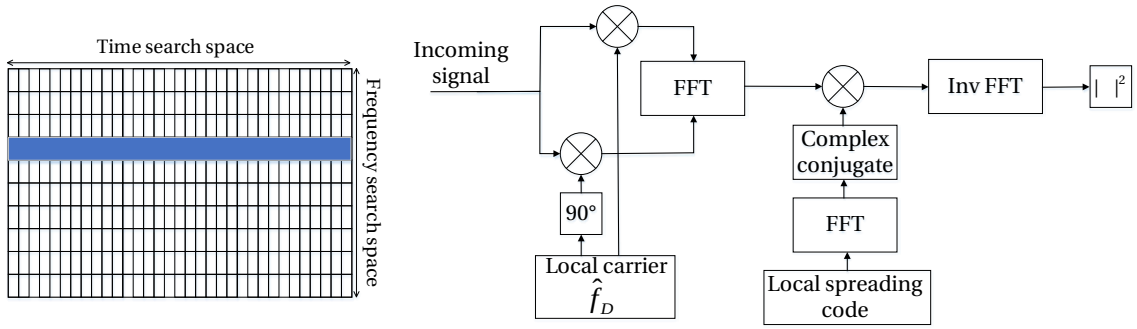

(a) PCPS acquisition grid

(b) PCPS block diagram

Figure 3.13 Block diagram of the PCPS

The mathematical model of the PCPS output is as follows:

$$\left|\frac{1}{N_s}\mathcal{F}^{-1}\left(\mathcal{F}\left(r(n)\exp\left(2i\pi\left(f_{IF}+\hat{f}_D\right)n\right)\right)\times\bar{\mathcal{F}}\left(c_1(n)\right)\right)\right|^2 \tag{3.28}$$

where $\mathcal{F}$ and $\mathcal{F}^{-1}$ stand for the Discrete Fourier Transform and the Inverse Discrete Fourier Transform.

The number of repetitions of the process corresponds to the number of Doppler frequency estimates N_f. Thus, the PCPS performance depends on the implementation of the Fourier and inverse Fourier transforms.

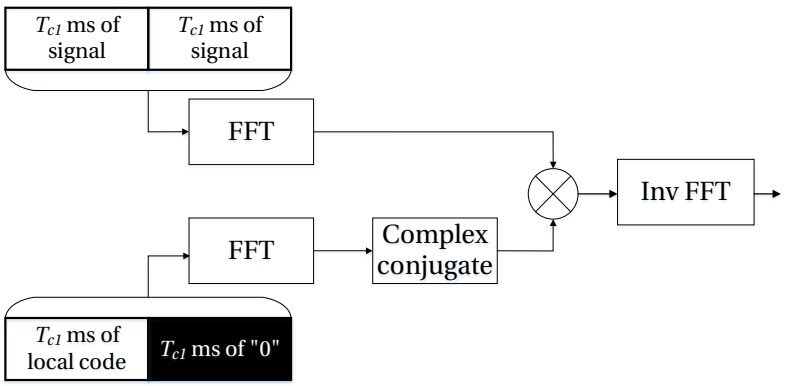

Figure 3.14 Parallel Code Search acquisition method with “1 + 1 ms” technique

To avoid the degradations due to potential bit sign transition (developed in *Chapter 4*), a variant of the PCPS is proposed. It is based on the known “1+1 ms” acquisition method presented in [Chibout, 2008] and [Yang *et al.*, 2004] and is illustrated in Figure 3.14.

Then, in $2T_{c_1}$ ms of signal, at least T_{c_1} ms is insured to be free of data bit transition and then the circular correlation with the local spreading code is not degraded. The resulting correlation function presents two peaks at $\hat{\tau}=\tau$ and $\hat{\tau}=\tau+T_{c_1}$ but only the first one is kept.

Indeed, as explained in [Leclère *et al.*, 2013], the amplitude of the second peak can be affected by a data bit sign transition as illustrated in Figure 3.15.

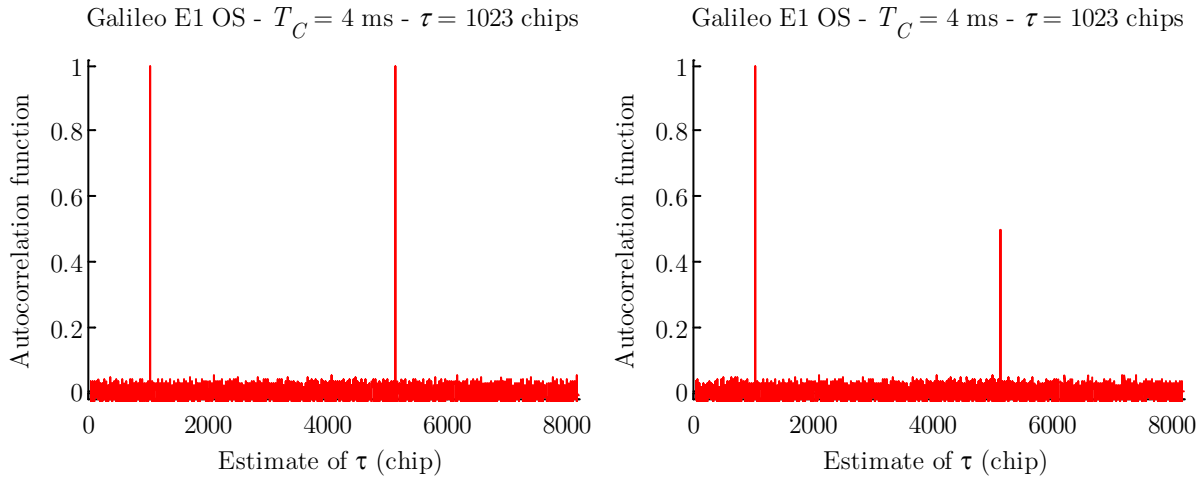

(a) Without bit sign transition (Same amplitude for both peaks)

(b) With a bit sign transition (The second peak is attenuated)

Figure 3.15 Illustration of the "1+1 ms" acquisition method output

This technique will be considered as the "reference acquisition method" in this work since it is commonly used for the acquisition of modernized GNSS signals and the developed acquisition method will be compared to this acquisition method in terms of acquisition performance and computation needs.

3.3.1.3 Double-Block Zero-Padding

The Double-Block Zero-Padding is an acquisition method which takes profit of a double parallelization in the time and frequency domain. It is based on the use of DFT over fractions of code period. *Chapter 5* is dedicated to this method, which is known as one of the most efficient acquisition methods. Furthermore, an acquisition method based on the DBZP is developed.

3.3.2 Multi-trial and verification strategies

After a first decision about the presence or absence of the desired signal and thus one or several estimations of the Doppler frequency and code delay, a step of verification can be performed. This permits to confirm detection (cell in the H_1 sector) and eliminate false alarms (cells in the H_0 sector, erroneous estimation of the signal parameters) and avoid tracking the signal with an erroneous estimation of the incoming signal parameters. Mainly, three techniques are used and presented in this section. The main lack in literature is the choice of the step of verification parameters and how to combine it with the first step (search step).

3.3.2.1 Performance study of the acquisition process

The search step investigates the whole search acquisition domain (in time and frequency) whereas only a few cells are under investigation in the step of verification. Indeed, only the set provided by the search step is verified. Then, for the serial and maximum search strategies, the set has only one cell whereas for the other search strategies, it can be larger. The set size cannot exceed the number of false alarm plus one, since only the variables having crossed the threshold are verified.

At the output of the step of verification, there is only a reduced set of size N_v, that in theory should contains the variable associated to the right cell (it can be empty if variables detected at the search step are not confirmed at the verification step) and then the probabilities of detection/missed-detection and false alarm are re-evaluated.

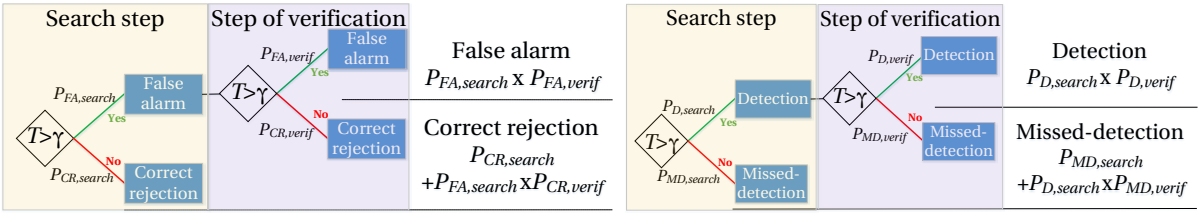

(a) Under H_0' (b) Under H_1

Figure 3.16 Probabilities per cell at the output of the acquisition step

Under H_0': bad estimation

As depicted in Figure 3.16(a), a false alarm is declared when the variable (which can be seen as noise only) satisfies the double detection. The resulting probability of false alarm $P_{FA,cell}$ per cell is then the product of the respective probabilities of false alarm (probability of false alarm of the search step $P_{FA,search}$ and probability of false alarm of the verification step $P_{FA,verif}$):

$$P_{FA,cell} = P_{FA,search} \times P_{FA,verif} \tag{3.29}$$

Some assumptions are taken when expressing the probability of false alarm of the acquisition process. It is assumed that the noise at the output of consecutive correlators are not correlated (in space and in time). In real-world data, if the same slice of incoming signal is used to compute the correlation function for all cells, then the noise components for two adjacent cells in the acquisition grid are correlated (the correlation value corresponds to the autocorrelation function taken in the absolute difference between the cell center values in time domain). Since in this study, effects of RF front-end are ignored, it is assumed that noises are independent. In addition, the step of verification uses different slices of time, the independence in time is thus assumed. Then, it is possible to express the probability of false alarm of the acquisition process, it is equal to the probability of false alarm of a cell.

$$P_{FA,acq} \approx P_{FA,cell} \tag{3.30}$$

Knowing that:

- The number of potential alarm at the output of the acquisition process is N_{FA}, the probability of false alarm $P_{FA,acq}$ is wanted to be $P_{FA,acq} \approx \frac{N_{FA}}{N_c}$,
- The number of potential false alarms at the search step is N_v, the probability of false alarm of the search step is $P_{FA,search} \approx \frac{N_v}{N_c}$,

The probability of false alarm of the step of verification is: $P_{FA,search} \approx \frac{N_{FA}}{N_v}$.

Under H_1: presence of the signals

The declaration of the presence of the signal occurs when the variable corresponding to the right cell satisfies the search and verification criteria (Figure 3.16(a)). The probability of detection of the acquisition process $P_{D,acq}$ is the product of the probabilities of detection of the search $P_{D,search}$ and verification $P_{D,verif}$ steps.

$$P_{D,acq} = P_{D,cell} = P_{D,search} \times P_{D,verif} \tag{3.31}$$

3.3.2.2 Step of verification techniques

Only a few number of verification techniques have been suggested in the literature, which can be classed as immediate rejection or non-immediate rejection. For each presented verification techniques, it is assumed that N detectors are used. Since the parameters of the incoming signal are roughly estimated, the acquisition method generally used is the classical one which consists in locally generating a replica of the incoming signal.

- Immediate rejection

The principle of the immediate rejection technique is to use N different detectors. To do so, the detectors are numbered and the tests are run sequentially in numerical order (as illustrated in Figure 3.17).

The step of verification stops when a detector rejects the detection decision. With this technique, it can be hoped that false alarms are eliminated with the first detectors. The detectors are characterized by a dwell time (T_C and K) and by the decision threshold. It can be imagined that the decision threshold decreases when the numerical order of the detector increases. As described in [Dicarlo & Weber, 1983] and [Pan *et al.*, 1990], the probabilities of detection and false alarm of the step of verification are the product of the probabilities of detection and false alarm associated to each test. The total dwell time to satisfy the step of verification is fixed (it is the sum of the dwell time for each detector) whereas the time to reject is a random variable.

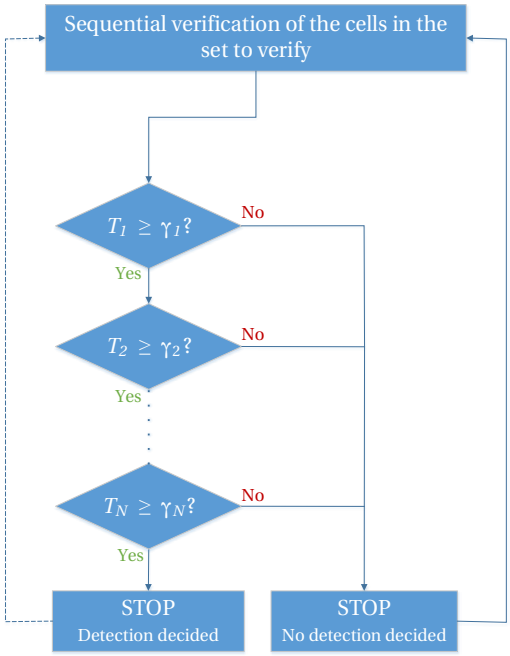

Figure 3.17 Immediate rejection verification techniques

- Non-immediate rejection

Unlike the immediate rejection, the non-immediate rejection techniques need several runs to decide to reject or to confirm the detection. In this case, all detectors are identical. Among them, two techniques emerge, the Tong detector and the M of N detector (described in Figure 3.18).

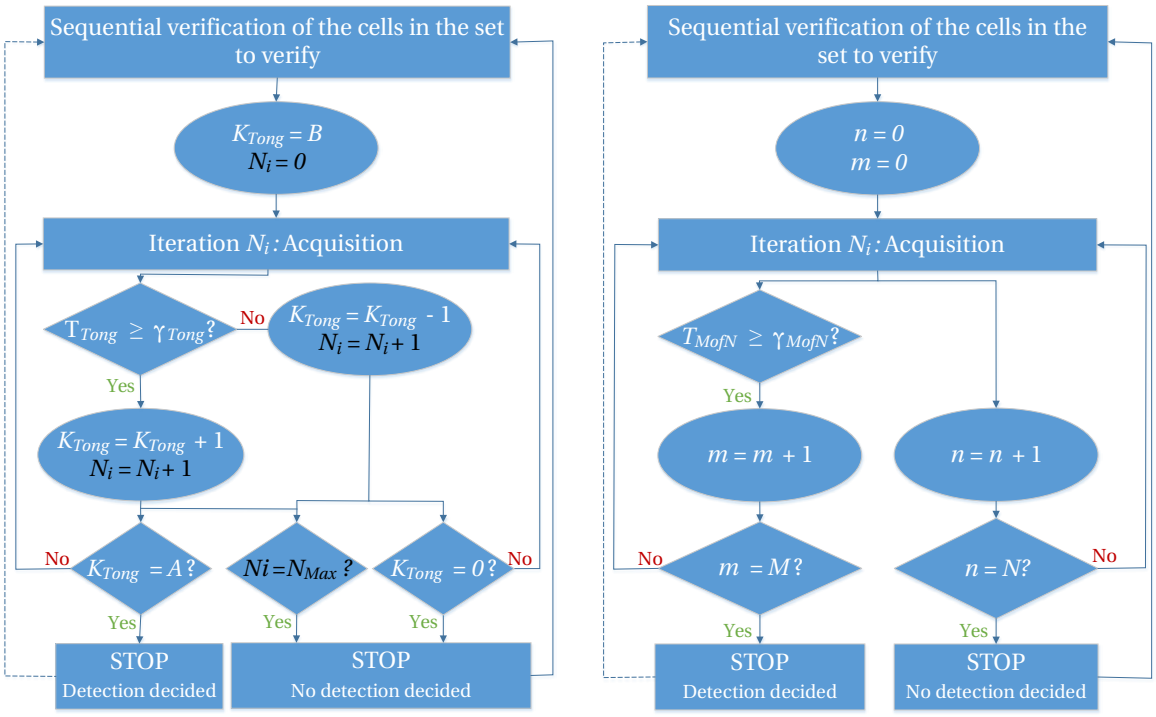

(a) Tong detector (b) M of N detector

Figure 3.18 Non-immediate rejection verification techniques

The main difference between both is the induced step of verification execution time, which is known for the M of N detector and unlimited for the Tong detector.

The principle is the same for both techniques of non-immediate rejection. Detectors are run sequentially and one or two counters are incremented or decremented as a function of the success or fail of the detection decision. When the counters reach fixed values, the step of verification confirms the presence of the signal or declares the signal absent.

Tong detector

The Tong detector, presented in [Ward, 1996] and [Hopkins, 1987] as the up-down counter, depends on two values which are the initial and final values of the counter. Indeed, the counter is initiated to a value B (taken as 1 or 2) and the Tong detector stops when the counter reaches the value A, the counter being incremented each time that a signal detection is declared and decremented each time that a no-detection is declared. To avoid infinite loop and then an infinite execution time, a threshold on the number of used detectors can be used (noted N_{Max} in Figure 3.18(a)). Clearly, the performance of this technique depends on the choice of the parameters A and B and should be a compromise, as always, between the execution time and the probabilities of detection and false alarm (given in (3.32) [Ward *et al.*, 2005b].

$$P_{D,Tong} = \frac{1-\left(\frac{1-P_D}{P_D}\right)^B}{1-\left(\frac{1-P_D}{P_D}\right)^{A+B-1}}$$
$$P_{FA,Tong} = \frac{1-\left(\frac{1-P_{FA}}{P_{FA}}\right)^B}{1-\left(\frac{1-P_{FA}}{P_{FA}}\right)^{A+B-1}} \tag{3.32}$$

Figure 3.19 presents the probabilities of detection and false alarms as a function of the parameters values of A and B (Figure (a) for $B = 1$ and Figure (b) for $B = 2$). The probability of false alarm for one detector is $P_{FA} = 10^{-1}$ and the associated probability of detection, for one detector is represented by the dashed black curve. As it can be observed, the probabilities of false alarm per cell $P_{FA,Tong}$ (presented in legend) are equivalent for $B = 1$ or $B = 2$. Furthermore, the higher the value of A is, the lower the probability of false alarm is but the lower also the probability of detection $P_{D,Tong}$ (represented by curve) is. A tradeoff on the value of A should be taken, it can be assumed that $B = 2$ is the best choice.

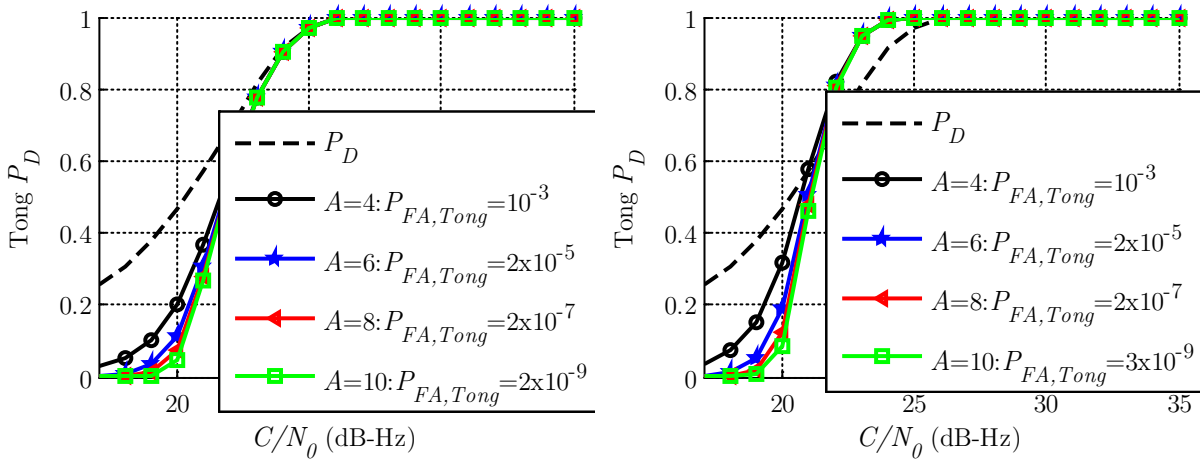

(a) $B = 1$ (b) $B = 2$

Figure 3.19 Probabilities of detection obtained for different implementations of Tong detector (Galileo E1 OS, $T_C = 4$ ms, $K = 20$, $P_{FA} = 10^{-1}$)

M of N detector

The M of N detector is one of the most famous verification technique [Ward, 1996] and is sometimes named coincidence detector [Polydoros & Weber, 1984]. The M of N detector is based on a binomial distribution $\mathcal{B}(N,p)$ where N detectors are run with a probability p (which represents the probability of false alarm or detection). It is decided that the signal is present if at least M detectors declare the signal present, in other cases the signal is declared absent. The probabilities of detection and false alarm can be easily deduced:

$$\begin{aligned} P_{D,MofN} &= \sum_{n=M}^{N} \binom{N}{n} (P_D)^n (1-P_D)^{N-n} \\ P_{FA,MofN} &= \sum_{n=M}^{N} \binom{N}{n} (P_{FA})^n (1-P_{FA})^{N-n} \end{aligned} \tag{3.33}$$

[Corazza *et al.*, 2004] proposed an improvement to reduce the M of N execution time. Instead of running all of the N detectors and compare the final counter value to M, at each run, the counter is compared to M. Then, if the first M detectors are in favor of signal presence, the step of verification stops since at least M detectors declare the signal presence. In the same way, if $N - M$ detectors declare the signal absence, it is a waste of time to run all of the N detectors since the final decision is already taken. The probabilities of detection and false alarm (3.33) stay unchanged.

Figure 3.20 presents the performance study of the M of N detector for the step of verification. Figure (a) is for $N = 8$ while Figure (b) is for $N = 10$ where N is the number of detectors. The probabilities of detection $P_{D,MofN}$ are globally higher for the highest value of N in the same conditions (C/N_0, P_{FA} for one detector of 10^{-3} and value of M) but the probabilities of false alarms $P_{FA,MofN}$ are higher. The smaller the value of M is, the higher the probability of detection is but also the higher the probability of false alarm is.

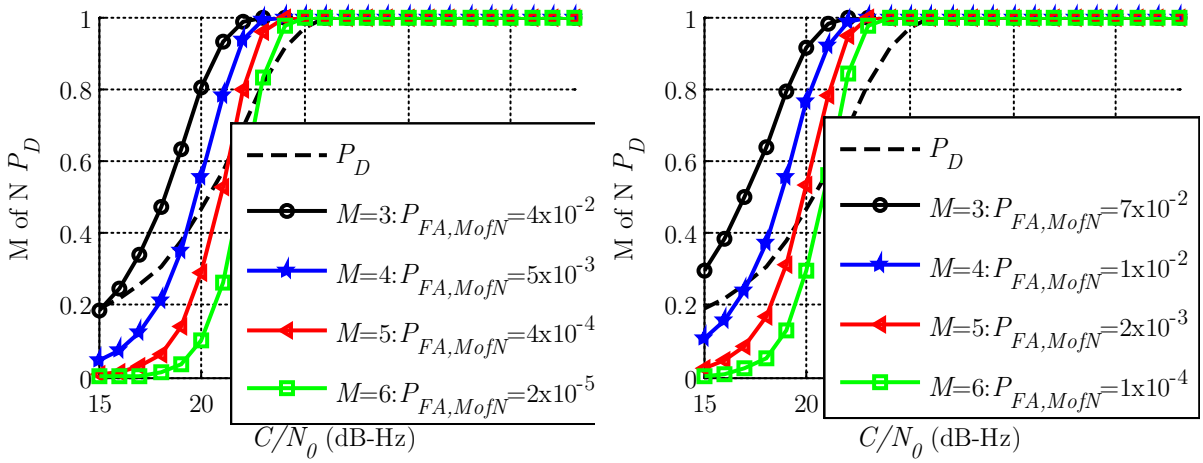

(a) $N = 8$ (b) $N = 10$

Figure 3.20 Probabilities of detection obtained for different implementations of M of N detector (Galileo E1 OS, $T_C = 4$ ms, $K = 20$, $P_{FA} = 10^{-1}$)

In comparison with the Tong detector, for the same value of C/N_0, the probability of detection can be higher with the M of N detector. However, the probability of false alarm is considerably lower for the Tong detector. A refined study should be conducted to choose in an optimal way the parameters of the step of verification, as presented in *Chapter 6*.

3.3.3 Modernized GNSS signal acquisition

Unlike the GPS L1 C/A signal, the modernized GNSS signals have two components (data and pilot) and this implies an adaptation of the acquisition methods to the signal structure. Furthermore, they are characterized by the presence of binary sequence on both components (navigation message on the data component and secondary code on the pilot component) and their bit durations correspond to the spreading code period. Two kinds of acquisition method, dedicated to the modernized GNSS signals, were developed over the last ten years: coherent integration over a single spreading code period and over multiple spreading code periods. The difference rests on the sign recovery necessity for the second case.

3.3.3.1 Coherent integration over a single spreading code period

- Acquisition of one component

The simplest acquisition method consists in ignoring the data component and only acquiring the pilot component. This method works as the traditional GPS L1 C/A signal acquisition (Table 3.7) and it has the lowest computational load. However, only a part of the available power is employed.

Correlator outputs used	$I_p(k) = \frac{A_p}{2} c_{2,p}(k) R_{c_{1,p}}\left(\varepsilon_\tau(k)\right) \cos\left(\pi \varepsilon_{f_D}(k) T_C + \varepsilon_{\phi_0}(k)\right) \operatorname{sinc}\left(\pi \varepsilon_{f_D}(k) T_C\right) + \eta_{I_p}(k)$ $Q_p(k) = \frac{A_p}{2} c_{2,p}(k) R_{c_{1,p}}\left(\varepsilon_\tau(k)\right) \sin\left(\pi \varepsilon_{f_D}(k) T_C + \varepsilon_{\phi_0}(k)\right) \operatorname{sinc}\left(\pi \varepsilon_{f_D}(k) T_C\right) + \eta_{Q_p}(k)$
Normalized acquisition detector	$T = \sum_{k=1}^{K} \left(\frac{I_p(k)}{\sigma_\eta}\right)^2 + \left(\frac{Q_p(k)}{\sigma_\eta}\right)^2$
Probability of false alarm	$P_{FA} = 1 - F_{\chi^2(2K)}(\gamma)$
Probability of detection	$P_D = 1 - F_{\chi^2(2K,\Lambda)}(\gamma)$
Non-centrality parameter	$\Lambda \approx \frac{A_p^2}{N_0} K T_C R_{c_{1,p}}^2(\varepsilon_\tau) \operatorname{sinc}^2\left(\pi \varepsilon_{f_D} T_C\right)$

Table 3.7 Performance study for the acquisition of the pilot component

For Galileo E1 OS, only 50% of the signal power is available (a loss of 3 dB) then for the acquisition of weak signals, it appears difficult to employ this acquisition method but for GPS L1C, the pilot component contains 75% of the total signal power (loss of 1.25 dB) then this acquisition method can provide satisfactory results as developed in *Chapter 4*, where the acquisition of the pilot component is compared to the acquisition of both components in terms of probability of detection.

- Non-coherent combining

When acquiring both components, to gather the total available signal power, an easy way to process is to acquire separately both components as illustrated by Figure 3.21.

As developed in [Van Dierendonck & Spilker, 1999] and [Bastide *et al.*, 2002] for GPS L5 signals, the incoming signal is separately correlated with a local data spreading code replica and with a local pilot spreading code replica. The acquisition detector which depends then on the four correlator outputs (two from the data component and two from the pilot component) follows χ^2 distributions with $4K$ degrees of freedom (Table 3.8). Let us note that the term of cross-correlation between the data and pilot spreading codes is considered as negligible. In this study, as generally done in literature (for example, [Borio, 2008]), the independence between data and pilot correlator outputs is assumed due to orthogonality properties of the spreading codes as reported in Appendix C.2.2.

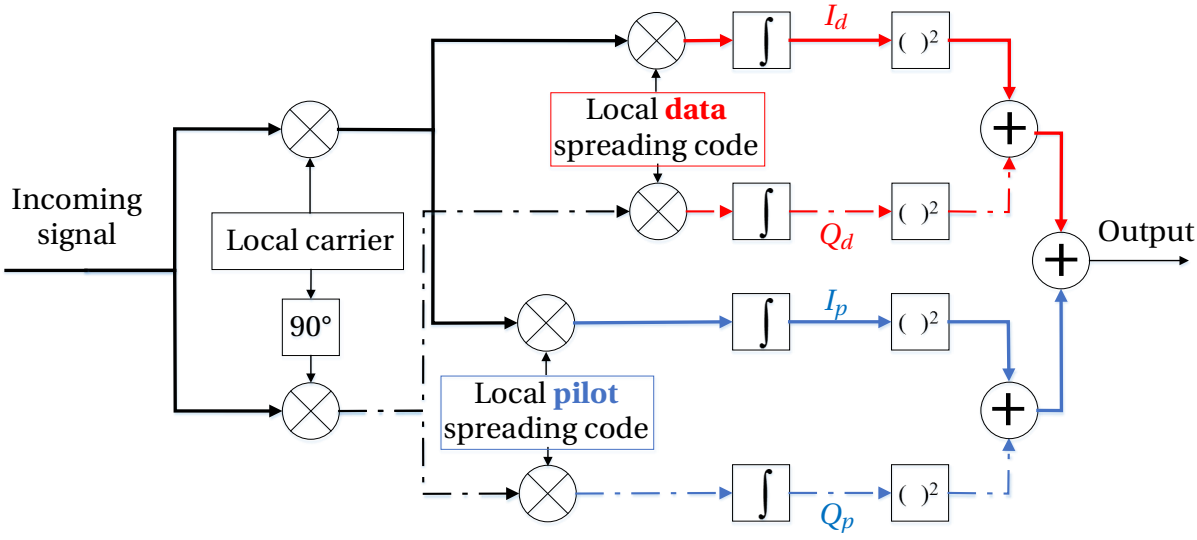

Figure 3.21 Non-coherent combining acquisition method scheme (red: data, blue: pilot, solid line: in-phase, dashed line: quadrature-phase)

Correlator outputs used	$I_d(k) \approx \frac{A_d}{2} d(k) R_{c_{1,d}}(\varepsilon_\tau(k)) \cos\left(\pi \varepsilon_{f_D}(k) T_C + \varepsilon_{\phi_0}(k)\right) \mathrm{sinc}(\pi \varepsilon_{f_D}(k) T_C) + \eta_{I_d}(k)$ $Q_d(k) \approx \frac{A_d}{2} d(k) R_{c_{1,d}}(\varepsilon_\tau(k)) \sin\left(\pi \varepsilon_{f_D}(k) T_C + \varepsilon_{\phi_0}(k)\right) \mathrm{sinc}(\pi \varepsilon_{f_D}(k) T_C) + \eta_{Q_d}(k)$ $I_p(k) \approx \frac{A_p}{2} c_{2,P}(k) R_{c_{1,p}}(\varepsilon_\tau(k)) \cos\left(\pi \varepsilon_{f_D}(k) T_C + \varepsilon_{\phi_0}(k)\right) \mathrm{sinc}(\pi \varepsilon_{f_D}(k) T_C) + \eta_{I_p}(k)$ $Q_p(k) \approx \frac{A_p}{2} c_{2,P}(k) R_{c_{1,p}}(\varepsilon_\tau(k)) \sin\left(\pi \varepsilon_{f_D}(k) T_C + \varepsilon_{\phi_0}(k)\right) \mathrm{sinc}(\pi \varepsilon_{f_D}(k) T_C) + \eta_{Q_p}(k)$
Normalized acquisition detector	$T = \sum_{k=1}^{K} \left(\frac{I_d(k)}{\sigma_\eta}\right)^2 + \left(\frac{Q_d(k)}{\sigma_\eta}\right)^2 + \left(\frac{I_p(k)}{\sigma_\eta}\right)^2 + \left(\frac{Q_p(k)}{\sigma_\eta}\right)^2$
Probability of false alarm	$P_{FA} = 1 - F_{\chi^2(4K)}(\gamma)$
Probability of detection	$P_D = 1 - F_{\chi^2(4K,\Lambda)}(\gamma)$
Non-centrality parameter	$\Lambda = \sum_{k=1}^{K} E^2\left(\frac{I_d(k)}{\sigma_\eta}\right) + E^2\left(\frac{Q_d(k)}{\sigma_\eta}\right) + E^2\left(\frac{I_p(k)}{\sigma_\eta}\right) + E^2\left(\frac{Q_p(k)}{\sigma_\eta}\right)$ $\approx \frac{1}{N_0} K T_C \left(A_d^2 R_{c_{1,d}}^2(\varepsilon_\tau) + A_p^2 R_{c_{1,p}}^2(\varepsilon_\tau)\right) \mathrm{sinc}^2(\pi \varepsilon_{f_D} T_C)$

Table 3.8 Performance study for non-coherent combining acquisition method

- Coherent combining with sign recovery

Coherent combining with sign recovery is an acquisition method dedicated to the acquisition of GNSS signals with two components. It is based on the fact that the data bit and secondary code (on the pilot component) bits are synchronized. For a given spreading code period, the data and secondary code bit can have the same sign or can have opposite sign. Then, it emerges that if they have the same sign, the incoming signal is the difference of the data and pilot component whereas if they have opposite sign, it is the sum of both components. The coherent combining with sign recovery acquisition method consists in generating two spreading code sequences $\left(c_{1,d}(nT_s)p_{1,d}(nT_s) + \alpha c_{1,p}(nT_s)p_{1,p}(nT_s)\right)$, one corresponding to the sum of data and pilot component ($\alpha = 1$) and the other one to the difference ($\alpha = -1$) and correlating both separately with the incoming signal as shown in Figure 3.22.

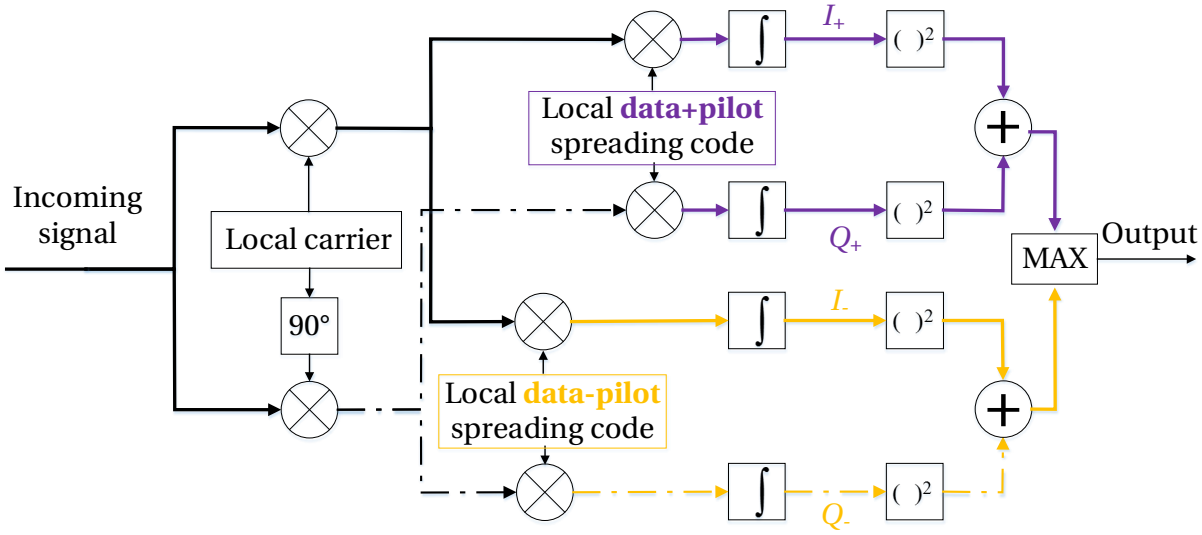

Figure 3.22 Coherent combining with sign recovery (purple: data+pilot, orange: data-pilot, solid line: in-phase, dashed line: quadrature-phase)

It seems clear that only one of both local spreading code sequence would provide a high correlation with the incoming signal (when the noise levels are low). The goal is to determine, for each spreading code period, the value of α which maximizes $R_{c_1,\alpha}(\varepsilon_\tau)$:

$$\begin{aligned} R_{c_1,\alpha}\left(\varepsilon_\tau(k)\right) &= \sum_{n=0}^{N_s-1} \left(d(nT_s)c_{1,d}(nT_s)sc_d(nT_s) - c_{2,p}(nT_s)c_{1,p}(nT_s)sc_p(nT_s)\right) \\ &\quad \times \left(c_{1,d}(nT_s)sc_d(nT_s) + \alpha c_{1,p}(nT_s)sc_p(nT_s)\right) \\ &= d(k)R_{c_{1,d}}(\varepsilon_\tau) - \alpha c_{2,p}(k)R_{c_{1,p}}(\varepsilon_\tau) + \left(\alpha d(k) - c_{2,p}\right)R_{c_{1,d/p}}\left(\varepsilon_\tau, \varepsilon_{f_D}\right) \end{aligned} \tag{3.34}$$

Theoretically (since the signs of the incoming data and secondary code bits are unknown), Table 3.9 permits to determine the optimal choice for α and then the optimal local combination spreading code sequences as a function of the sign of the data and secondary code bits.

	$c_{2,p}(k) = 1$	$c_{2,p}(k) = -1$
$d(k) = 1$	$\alpha = -1$ $d(k) + c_{2,p}(k) = 2$ $R_{c_{1,d}} + R_{c_{1,p}} - 2R_{c_1,d/p}$	$\alpha = 1$ $d(k) + c_{2,p}(k) = 0$ $R_{c_{1,d}} + R_{c_{1,p}} + 2R_{c_1,d/p}$
$d(k) = -1$	$\alpha = 1$ $d(k) + c_{2,p}(k) = 0$ $-\left(R_{c_{1,d}} + R_{c_{1,p}}\right) - 2R_{c_1,d/p}$	$\alpha = -1$ $d(k) + c_{2,p}(k) = -2$ $-\left(R_{c_{1,d}} + R_{c_{1,p}}\right) + 2R_{c_1,d/p}$

Table 3.9 Choice of α as a function of the data and secondary code bit signs

[Yang *et al.*, 2004] analyzed this method, and when no non-coherent summations is used [Borio *et al.*, 2009] provides the probability of false alarm and probability of detection reminded here in Table 3.10 (it is assumed that the signal power is equally distributed in both components and that $A_d = A_p = A$). When non-coherent summations are used, the statistical model of the acquisition detector seems difficult to directly derive since it is a sum of maximum of χ^2 distributions but can be approximated (by using Newton-Raphson algorithm and Gaussian approximation for the probability of false alarm).
Some explanations are required to clarify the performance study.

Under H_0: $I_d(k)$ and $I_p(k)$ are centered Gaussian distributions.

$$I_{\pm}(k) = I_d(k) \pm I_p(k) \approx_{H_0} \eta_{I_d}(k) \pm \eta_{Q_p}(k) \sim \mathcal{N}\left(0, 2\sigma_\eta^2\right) \tag{3.35}$$

Then $\frac{I_+(k)}{\sqrt{2}\sigma_\eta} = \frac{I_d(k)+I_p(k)}{\sqrt{2}\sigma_\eta}$ is a unit Gaussian distribution. $T_{\pm}$ can be seen as the difference of two χ^2 distributions with 2 degrees of freedom.

Under H_1: either T_+ or T_- is a non-central χ^2 random variable with 2 degrees of freedom and the other a central χ^2 random variable with 2 degrees of freedom since only one corresponds to the signal presence.

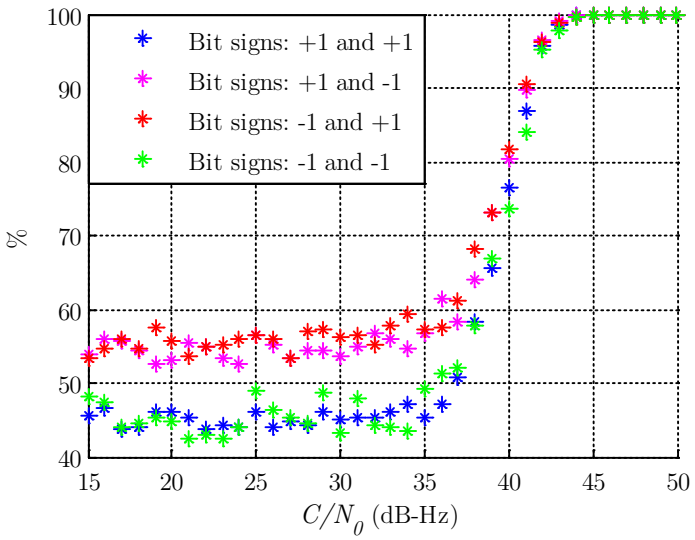

Figure 3.23 Experimental probability to correctly determines the optimal spreading code sequence between data+ pilot and data-pilot (Galileo E1 OS, $K = 1$, $T_C = 4$ ms)

The issue when using this method is to know the probability that the maximum of T_+ and T_- corresponds to the right sequence. Figure 3.23 presents this probability and as it is shown, for weak signal, the maximum result is not reliable since the probability is around 0.5. That means that below 41 dB-Hz, it can be assumed that the maximum is mainly determined on a noise criterion.

Correlator outputs used	$I_+(k) \approx \frac{A}{2} R_{c_1,+}(\varepsilon_\tau(k)) \cos\left(\pi\varepsilon_{f_D}(k)T_C + \varepsilon_{\phi_0}(k)\right) \mathrm{sinc}(\pi\varepsilon_{f_D}(k)T_c) + \eta_{I_+}(k)$ $Q_+(k) \approx \frac{A}{2} R_{c_1,+}(\varepsilon_\tau(k)) \sin\left(\pi\varepsilon_{f_D}(k)T_C + \varepsilon_{\phi_0}(k)\right) \mathrm{sinc}(\pi\varepsilon_{f_D}(k)T_c) + \eta_{Q_+}(k)$ $I_-(k) \approx \frac{A}{2} R_{c_1,-}(\varepsilon_\tau(k)) \cos\left(\pi\varepsilon_{f_D}(k)T_C + \varepsilon_{\phi_0}(k)\right) \mathrm{sinc}(\pi\varepsilon_{f_D}(k)T_c) + \eta_{I_-}(k)$ $Q_-(k) \approx \frac{A}{2} R_{c_1,-}(\varepsilon_\tau(k)) \sin\left(\pi\varepsilon_{f_D}(k)T_C + \varepsilon_{\phi_0}(k)\right) \mathrm{sinc}(\pi\varepsilon_{f_D}(k)T_c) + \eta_{Q_-}(k)$
Normalized acquisition detector	$T_+ = \left(\frac{I_+(k)}{\sqrt{2}\sigma_\eta}\right)^2 + \left(\frac{Q_+(k)}{\sqrt{2}\sigma_\eta}\right)^2$ and $T_- = \left(\frac{I_-(k)}{\sqrt{2}\sigma_\eta}\right)^2 + \left(\frac{Q_-(k)}{\sqrt{2}\sigma_\eta}\right)^2$ $T = \max(T_+, T_-)$
Probability of false alarm	$P_{FA} = P(T > \gamma) = 1 - P\big((T_+ \le \gamma) \cap (T_- \le \gamma)\big)$ $= 1 - \left(F_{\chi^2(2)}(\gamma)\right)\left(F_{\chi^2(2)}(\gamma)\right)$
Probability of detection	$P_D = 1 - \left(F_{\chi^2(2)}(\gamma)\right)\left(F_{\chi^2(2K,\Lambda)}(\gamma)\right)$
Non-centrality parameter	$\Lambda = \frac{A^2}{4 \times 2\sigma_\eta^2}\left(R_{c_{1,d}}(\varepsilon_\tau) + R_{c_{1,p}}(\varepsilon_\tau)\right)^2 \mathrm{sinc}^2(\pi\varepsilon_{f_D}T_C)$ $= \frac{A^2}{2N_0} T_C \left(R_{c_{1,d}}(\varepsilon_\tau) + R_{c_{1,p}}(\varepsilon_\tau)\right)^2 \mathrm{sinc}^2(\pi\varepsilon_{f_D}T_C)$

Table 3.10 Performance study for coherent combining with sign recovery acquisition method

- Differentially coherent combining

An acquisition approach, initially applied to the GPS L1 C/A signal evaluates the acquisition detector from two consecutive correlator output pairs. Indeed, there should be a high degree of correlation between the phases of 2 successive correlator outputs when the signal is present whereas when the signal is absent, the correlator outputs should be essentially independent under the influence of the noise [O'Driscoll, 2007].

This method can be applied to modernized GNSS signals, instead of considering two consecutive correlator output pairs, the acquisition detector considers the two correlator output pairs provided by both component, as illustrated in Figure 3.24.

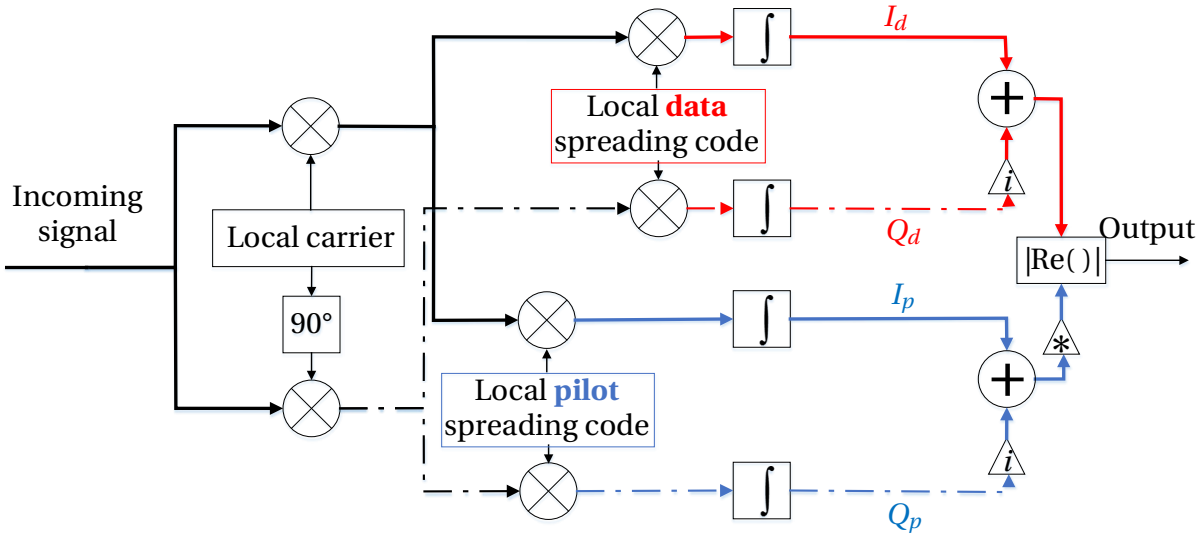

Figure 3.24 Differentially coherent combining acquisition method scheme (red: data, blue: pilot, solid line: in-phase, dashed line: quadrature-phase)

Based on [Avila-Rodriguez *et al.*, 2004], [Borio *et al.*, 2009] and [Esteves, 2014], the performance study is given in Table 3.11.

Under H_0, T is the difference of 2 random variables χ^2 distributed. A random variable with a χ^2 distribution with 2 degrees of freedom is a special case of an exponential random variable $\mathcal{E}(1/2)$ with mean 2 (or a Gamma distribution $\Gamma(1,2)$). Furthermore, the difference of 2 exponential distributions is a Laplace distribution:

$$X_1 \sim \mathcal{E}\left(\frac{1}{2}\right), X_2 \sim \mathcal{E}\left(\frac{1}{2}\right), X_1 \text{ and } X_2 \text{ independent} \Rightarrow \frac{1}{2}(X_1 - X_2) \sim \text{Laplace}(0,1) \tag{3.36}$$

Then, under H_0, the acquisition criterion T is Laplace distributed which parameters are 0 (for the location) and 1 (for the scale).

Under H_1, T is the difference of a non-central χ^2 random variable with 2 degrees of freedom and a central χ^2 random variable with 2 degrees of freedom. The distribution of acquisition detector, under H_1, is more complicated to determine. The probability of detection cannot be analytically expressed [Avila-Rodriguez *et al.*, 2004]. [O'Driscoll, 2007] can be used as a reference for the approximated expressions of the probability of detection.

It is then difficult to compare the acquisition performance of this acquisition method from a theoretical point of view.

Correlator outputs	$I_d(k), Q_d(k)$ $I_p(k), Q_p(k)$
Normalized acquisition detector	$T = \left\| \mathrm{Re}\left(\left(\frac{I_d(k)}{\sigma_\eta} + i\frac{Q_d(k)}{\sigma_\eta} \right) \left(\frac{I_p(k)}{\sigma_\eta} + i\frac{Q_p(k)}{\sigma_\eta} \right)^* \right) \right|$ $= \left(\left(\frac{I_+(k)}{\sqrt{2}\sigma_\eta} \right)^2 + \left(\frac{Q_+(k)}{\sqrt{2}\sigma_\eta} \right)^2 \right) - \left(\left(\frac{I_-(k)}{\sqrt{2}\sigma_\eta} \right)^2 + \left(\frac{Q_-(k)}{\sqrt{2}\sigma_\eta} \right)^2 \right)$ $= \frac{1}{\sigma_\eta^2} \left\| I_d(k) I_p(k) + Q_d(k) Q_p(k) \right\|$ $\approx \left\| \frac{1}{\sigma_\eta^2} \frac{A^2}{2} R_{c_{1,d}}(\varepsilon_\tau(k)) R_{c_{1,p}}(\varepsilon_\tau(k)) \mathrm{sinc}^2(\pi \varepsilon_{f_D} T_C) \cos(\phi_d - \phi_p) + \eta_{DCC} \right\|$
Probability of false alarm	$P_{FA} = 1 - F_{\mathrm{Laplace}(0,1)}(\gamma)$
Probability of detection	P_D approximated

Table 3.11 Performance study for differentially coherent combining acquisition method

where:

- ϕ_d and ϕ_p are the respective phases ($\pi \varepsilon_{f_D}(k) T_C + \varepsilon_{\phi_0}(k)$) obtained with the data and the pilot components. When the Doppler frequency is well estimated, both phases are close and the difference is null,
- η_{DCC} is the resulting noise of the product of the data and pilot correlator output pairs.

Furthermore, [Zarrabizadeh & Sousa, 1997] and [Pulikkoonattu & Antweiler, 2004] proposed a variant to accumulate more signal energy by extending the total accumulation time: a differentially coherent integration version and a differentially non-coherent integration respectively.

3.3.3.2 Coherent integration over multiple spreading code periods

When the coherent integration time is increased, several bit sign transitions can occur and it implies that the binary sequences modulating the data and pilot components should be estimated. The higher the coherent integration time is, the higher the number of bit combinations is and the higher the number of acquisition grid cells in the domain frequency is. Then, two strategies can be chosen on the bit sign combinations search.

- Exhaustive bit sign combinations

The exhaustive bit sign combination consists in testing all possible sign combinations of data and pilot components D_K. The acquisition detector is then the maximum variable for all the bit sign combinations (Table 3.12) and the correct estimation of the bit sign combinations can be thus obtained.

Bit sign combination set	$D_K = \left\{ \left(\hat{d}(k), \hat{c}_{2,p}(k) \right), \hat{d}(k) \in \{-1,+1\}, \hat{c}_{2,p}(k) \in \{-1,+1\} \right\}^K$
Normalized acquisition detector	$T = \max_{D_K} \left| \sum_{k=1}^{K} \left(\hat{d}(k) I_d(k) - \hat{c}_{2,p}(k) Q_p(k) \right)^2 + \left(\hat{d}(k) Q_d(k) + \hat{c}_{2,p}(k) I_p(k) \right)^2 \right|$

Table 3.12 Exhaustive sign search acquisition method

The main drawback of this acquisition method is the computational load since the number of bit sign combinations grows exponentially with K.

- Primary code acquisition based on multi-hypotheses secondary code

Only a partial set of bit sign can be considered, for example on the pilot component. Based on the same principle as previously, [Corazza *et al.*, 2007] proposed to build a secondary code hypotheses tree. When acquiring only the pilot component, the secondary code ambiguity is handled by considering all possible combinations of the K consecutive secondary code bits.

- Coherent integration on the pilot secondary code period

The secondary code on the pilot component being known, an acquisition method consists in coherently correlating on the secondary code period. That means that, for example, for Galileo E1 OS, 100 ms of incoming signal is correlated with a local pilot component replica containing 25 repetitions of the spreading code, each one affected by the sign of the secondary code. This permits to simultaneously acquire the spreading code and the secondary code. This method is further detailed in *Chapter 7* which is dedicated to the acquisition of the secondary code.

3.4 Discussion

This *Chapter 3* was dedicated to the acquisition process and in particular to the two first steps: the *search step* and the *verification step*.

The acquisition process is based on the correlation operation, presented at the beginning of this chapter. To do so, and as generally presented in the literature, it is assumed that during the correlation interval the data bit sign does not change. For GPS L1 C/A, a data bit sign transition occurs, in average, every 40 ms (corresponding to 40 spreading code periods) but for the modernized GNSS signals, a bit sign transition occurs, in average, at each spreading code period (since there are two components). One can thus understand that this model does not reflect the reality of the acquisition (no knowledge about the location of the bit transition) and this implies to express the correlation operation outputs considering bit sign transition during the correlation interval (it is one of the objectives of the *Chapter 4*) and adapt the acquisition strategy.

- *Search step*

The first analyzed acquisition method is the serial acquisition method which consists in serially exploring an acquisition grid, representing the 2D search domain and containing all the possible couples of incoming signal parameters estimates.

To speed up the search step, some optimized acquisition methods, based on parallelization in frequency (PFS) or time domain (PCPS), or based on a double parallelization (Double-Block Zero-Padding), were developed. This method is known for its efficiency for the acquisition of the GPS L1 C/A signal from the point of view of the execution computation. It is why, as presented in *Chapter 5,* a variant of this method, Transition-Insensitive, designed for the acquisition of the modernized GNSS signals, is proposed and studied.

Indeed, the introduction of the modernized GNSS signals induced the development of specific acquisition methods. The main differences with GPS L1 C/A is the split into two components and the presence of frequent bit sign transition and one of the challenges is to counter the presence of frequency bit sign transition, for example by exploring or taking hypothesis on the sign combination of the data and secondary code bits, as presented in the state-of-the-art of the modernized GNSS acquisition methods.

For the acquisition of modernized GNSS signals, the acquisition methods based on a coherent integration over multiple spreading code periods do not seem appropriate in real-time processing (or close to real-time). The exploration of multiple bit sign combinations can lead to long execution time. In low C/N_0 conditions, the acquisition of one component or the coherent combining with sign recovery acquisition method do not seem satisfactory. The non-coherent combining scheme appears as the acquisition method which fits for the acquisition of Galileo E1 OS signals at low C/N_0.

At the end of the acquisition process, it would be too computationally expensive that there are remaining doubts on the estimation of the incoming signal parameters. It is why a verification step permits to eliminate false alarms and validate the good estimation of the signal parameters. For computation reasons, the verification step can be only used to verify a reduced set. In addition to the known searching strategies (serial, maximum and hybrid strategies), an innovative searching strategy is also presented. It is a mix between the maximum and the hybrid strategies. The verification step should verify at the maximum a predefined number of cells for which the acquisition detector amplitude are the highest ones. The interest of this strategy is to provide a reduced set of cells to verify, set which is not reduced to a singleton (less constraining than the maximum strategy) and with a choice of cell to verify smarter than the hybrid strategy.

- *Verification step*

Once the search step provides a set of potential estimates of the incoming signal parameters, the verification step should determine the couple which is the closest to the incoming signal parameters couple. Mainly two techniques are proposed in literature, the M of N detector and the Tong detector. They are based on the repetition of experiments which test the signal presence. The number of repetition and the signal presence detection should be parameterized.

The challenge, now, is to dimension the acquisition process in order to reach the targeted acquisition performance and by optimizing the execution computation. This includes:

- Individually, choose the optimal acquisition parameters for each acquisition step,
- Globally, choose the good compromise between each acquisition step.

In the shape of this thesis, the acquisition strategy should, in priority, aim at the acquisition of Galileo E1 OS, in low C/N_0 conditions. The discussion leading to the choice of the acquisition parameters is given in *Chapter 6.*

Chapter 4
Investigation of Acquisition Degradation Sources

The objective of this chapter is to study the typical main sources of performance degradation of the GNSS acquisition process and to assess their effects on the acquisition, in particular, of new GNSS civil signals. The three sources, uncertainties brought by the choice of the acquisition grid, the non-compensation of the code Doppler and the presence of bit sign transition are studied independently. For each one, the mathematical model of the probability of detection is provided and illustrated by Matlab simulations.

The purpose of this study is to provide an overview of the impact of each source of degradation and compute a representative figure to compare the performance degradations. It is worth noting that the focus is on the probability of detection and the objective is to maximize it in presence of potential sources of degradations.

Contents

4.1 Introduction 66
4.2 Acquisition grid uncertainties 66
4.3 Effect of code Doppler 68
4.3.1 Generalities on code Doppler effect 70
4.3.2 Mathematical model of the distorted correlation function 72
4.3.3 Acquisition performance when considering uncompensated code Doppler . 74
4.4 Effect of data message 80
4.4.1 GNSS signal detection statistical model in presence of bit sign transition . 81
4.4.2 Application to the acquisition of GNSS signals 86
4.4.3 Comparison of modernized GNSS signals with GPS L1 C/A 98
4.5 Discussion 101

4.1 Introduction

The three main sources of acquisition performance degradation are:

- The uncertainty on the acquisition grid cell,
- The code Doppler, which implies a change in the received spreading code period,
- The bit sign transition, data bit transition on the data component and secondary code bit transition on the pilot component for the modernized GNSS signals.

In literature, there is a lack on a quantization of the acquisition performance degradations for each source, in particular for the modernized GNSS signals. Some studies propose to quantify the degradations losses (for example for the uncertainty on the acquisition grid cell). In this work, the approach is to study the loss on the probability of detection for each of the three sources and when two sources affect simultaneously the acquisition. To do so, the starting point is to compute the acquisition parameters to reach a targeted acquisition performance when not considering the source of degradation, and then to study the average probability of detection when the source of degradation is present.

The common acquisition parameters are:

- The probability of false alarm is fixed to $P_{FA} = 10^{-3}$ [RTCA, Inc, 2008],
- The reference case (without degradations) is a probability of detection of $P_D = 95\%$ for a signal at 27 dB-Hz (this corresponds to approximately the probability of detection of the search step),
- The code delay and the Doppler frequency are roughly well estimated, which means that the right cell in the acquisition grid is found.

4.2 Acquisition grid uncertainties

The acquisition degradation due to the acquisition grid uncertainties is inherent to the serial search acquisition method. Indeed, the acquisition grid is defined by a number of cells and this implies residual estimation errors due to the cell width. Δ_f is the uncertainty width in the frequency search space which is equal to the Doppler frequency search space length divided by the number of frequency cells N_f. In the same way, Δ_τ is the uncertainty width in the code delay search space which is equal to the code delay search space length divided by N_τ. The acquisition grid represents a discretization of the 2D search space, and the objective of the acquisition search step is to find the cell $\left(\hat{f}_D, \hat{\tau}\right)$ which parameters are the closest to the incoming signal parameters.

There are residual errors δ_{f_D} and δ_τ corresponding to the correct bin. These residual errors are defined by the difference between the cell central value and the true value of the estimated parameters. The residual error is then smaller than half the width of the cell in the time and frequency domains respectively. In many references, the probability of detection is computed assuming that there is no residual error cell but as it will be observed, the residual errors can

have a dramatic impact on the probability of detection even if the incoming signal parameters are roughly estimated. To consider the residual errors, one option is to compute the probability of detection for an equivalent C/N_0, which is the sum of the received C/N_0 and losses due to residual errors [Van Diggelen, 2009]. In this work, the approach evaluates the average probability of detection on the "right" cell, it seems to be a more relevant figure.

As done in [RTCA, Inc, 2008], the average probability of detection is obtained by taking the expectation value assuming a uniform distribution of the residual Doppler frequency and code delay errors:

$$P_{D,(\delta_{f_D},\delta_\tau)} = E_{(\delta_{f_D},\delta_\tau)}\left(P_D\left(\delta_{f_D},\delta_\tau\right)\right) \tag{4.1}$$

It should be noticed that $P_D\left(\delta_{f_D},\delta_\tau\right)$ depends on the residual Doppler frequency and code delay errors through the non-centrality parameter (section 3.2.3.1). Indeed, when the signal is present and the incoming signal parameters roughly estimated (under H_1), the non-centrality parameter is:

$$\lambda_0 = \frac{A^2}{N_0} T_C R_{c_1}^2(\delta_\tau)\,\mathrm{sinc}^2\left(\pi\delta_{f_D}T_C\right) \tag{4.2}$$

As an example with GPS L1 C/A, to reach a probability of detection of 95% in the center of the right cell, the acquisition parameters are the following: for a received C/N_0 of 27 dB-Hz, a probability of false alarm of $P_{FA} = 10^{-3}$ and a total integration duration of $T_I = 126$ ms (coherent duration of $T_C = 1$ ms). Figure 4.1 shows the probability of detection as a function of the Doppler frequency uncertainty and of the code delay uncertainty created by the cell size for the right cell. In the worst cases (edge of the cell), the probability of detection falls from 95% to 81% and 43% respectively. A more representative figure is thus the average probability of detection over the cell assuming that the actual Doppler frequency error and code delay error are random variables uniformly distributed over the entire bin.

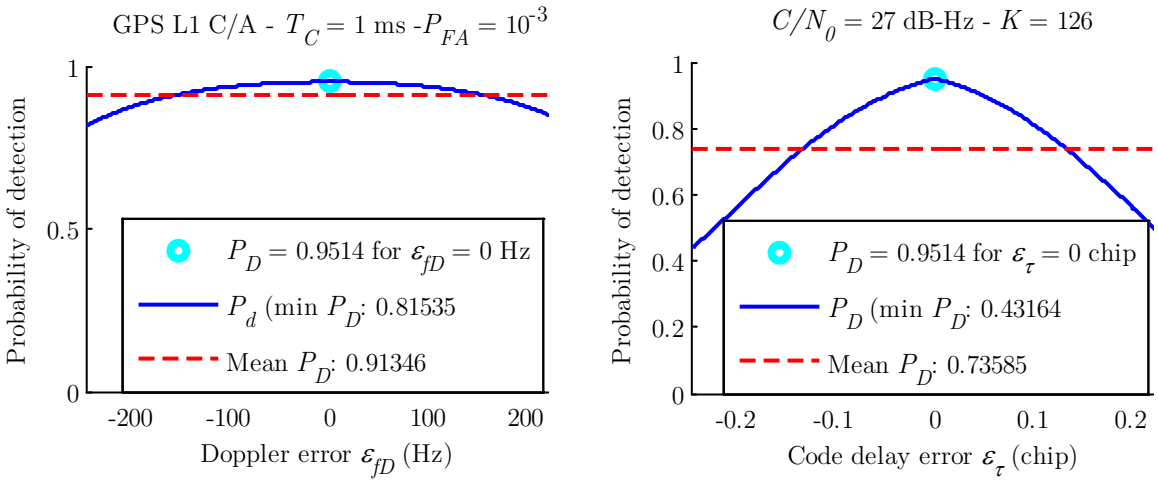

(a) In the frequency domain (b) In the time domain

Figure 4.1 Probability of detection on the right cell in frequency and time domains

The acquisition grid, as defined in section 3.2.1, implies at most a loss of the equivalent received C/N_0 of 3.4 dB (0.9 dB in the frequency domain and 2.5 dB in the time domain) assuming a very wide band front-end filter. If the worst cases in the frequency and time domains are combined, it results in a probability of detection down to 25.35% instead of 95%. The average probability of detection over the entire cell is however around 67.06% as presented in Figure 4.2.

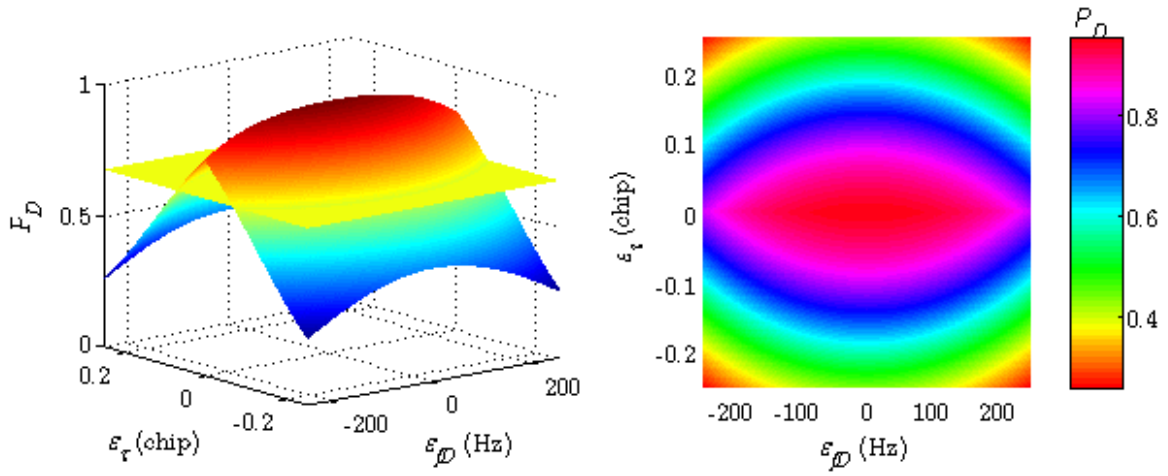

(a) In the frequency domain (b) In the time domain

Figure 4.2 Probability of detection in the right cell (GPS L1 C/A, $T_C = 1$ ms and $C/N_0 = 27$ dB-Hz)

In conclusion, even if the acquisition algorithm explores the correct cell, the detection may fail due to the uncertainties on the cell size. This loss is generally not considered in the general literature to dimension the acquisition parameters but the previous results show that to be realistic, the aforementioned source of degradation should be considered by adapting the acquisition parameters or by refining the acquisition grid.

4.3 Effect of code Doppler

A second source of degradation is presented, it is the effect of uncompensated code Doppler. The Doppler frequency, mainly caused by the satellite motion and the local oscillator [Van Diggelen, 2009], affects the received signal by modifying:

- The carrier frequency,
- The code frequency (chipping rate).

If f_{c_1} denotes the chipping rate without Doppler, f_L the carrier frequency without Doppler and f_D the Doppler frequency affecting the received carrier, the chipping rate, denoted $f_{c_1,D}$, can be expressed as:

$$f_{c_1,D} = f_{c_1}\left(1 + \frac{f_D}{f_L}\right) = f_{c_1} + \delta_{f_{c_1},D}$$
$$\delta_{f_{c_1},D} = f_{c_1,D} - f_{c_1} = f_{c_1} \times \frac{f_D}{f_L} \quad (4.3)$$

where $\delta_{f_{c_1,D}}$ corresponds to the code Doppler shift.

The modification of the code frequency leads to a change in the spreading code period as can be seen in Figure 4.3 where 3 periods of a four-chip spreading code are represented.

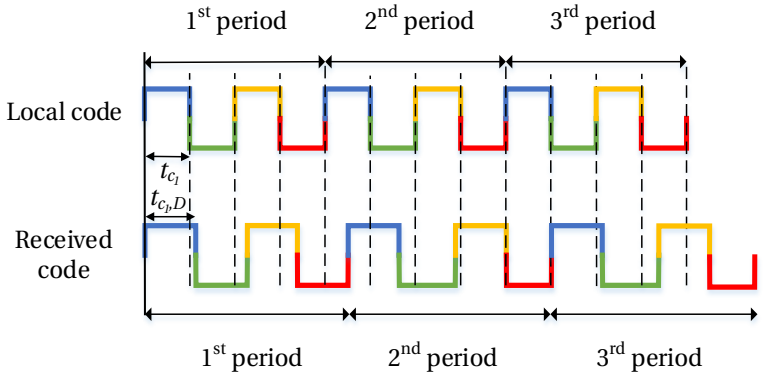

Figure 4.3 Code Doppler effect on the spreading code period

where $t_{c_1,D}$ is the spreading code chip duration defined by:

$$t_{c_1,D} = \frac{1}{f_{c_1,D}} = t_{c_1}\left(\frac{f_L}{f_D + f_L}\right) \tag{4.4}$$

A positive Doppler frequency causes the spreading code duration to shrink ($t_{c_1,D} < t_{c_1}$) and a negative Doppler frequency causes an expansion of the spreading code duration ($t_{c_1,D} > t_{c_1}$).

$$\begin{aligned} f_D > 0 \Rightarrow \delta_{f_{c_1,D}} > 0 \Rightarrow f_{c_1,D} > f_{c_1} \Rightarrow t_{c_1,D} < t_{c_1} \\ f_D < 0 \Rightarrow \delta_{f_{c_1,D}} < 0 \Rightarrow f_{c_1,D} < f_{c_1} \Rightarrow t_{c_1,D} > t_{c_1} \end{aligned} \tag{4.5}$$

If the incoming Doppler frequency in absolute value is small (depending on the signal), the code Doppler effect can be ignored. However, in high Doppler conditions, the code Doppler impact on the acquisition performance can be significant. For an incoming Doppler frequency of 10 kHz, the code Doppler impact translates into one spreading code chip slip in 154 ms for GPS L1 C/A. In this case, the Doppler impact on the code frequency is generally overlooked in the literature in classical conditions (low correlation duration) since even if the Doppler frequency is relatively high, the impact is weak. But for the acquisition of the modernized GNSS signals which can have a large chipping rate, or for the acquisition of weak signals which might require long dwell times, it becomes extremely difficult to neglect it.

If the receiver does not take the code Doppler into account during the acquisition phase (the local PRN code has a null code Doppler), this can result in degraded correlator outputs that will degrade the acquisition capability of the receiver. It is thus relevant to discuss the code Doppler effect on GNSS acquisition performance by expressing for example the degradations on the acquisition performance in terms of probability of detection if the code Doppler is not compensated by the receiver.

This effect of code Doppler on the GPS L1 C/A signal acquisition has been thoroughly studied in the literature. The motivation behind the below investigation is to apply this study to the new generation of GNSS signals to provide careful instructions concerning the acquisition

of these signals. In this study the Doppler frequency is assumed to be constant over the total accumulation duration since the maximum rate of change of the Doppler frequency is very slow (on the order of 1 hertz per second [Van Diggelen, 2009] without user motion).

The Doppler frequency of the received signal at the antenna depends upon the L-band central frequency, the relative satellite/receiver motion and the oscillator quality. The simulations results are presented for the same value of Doppler for each signal. To be rigorous, the Doppler frequency should be adapted for each signal. The study does not take into account the Doppler frequency changes over time.

4.3.1 Generalities on code Doppler effect

As previously explained, the code Doppler results in a change of the spreading code period. Table 4.1 presents the time (in ms and in spreading code periods) after which a slip of one chip occurs for GPS L1 C/A and the modernized GNSS signals, considering different incoming Doppler frequencies and assuming a synchronization at the beginning. The linear expression is reminded in *Appendix E.1.1.* Indeed, if the shift between the received spreading code and the local spreading code (without Doppler) exceeds 1 chip during the correlation duration, then the correlation process (summation) no longer makes sense. As it can be read, the time before the slip of 1 chip is really shorter for signals in the L5 band (on the order of a few tens of ms) compared to signals in L1 band (on the order of a few hundreds of ms) due to their chipping frequency f_{c_1}, which is 10 times higher for signals in the L5 band. Furthermore, for the modernized GNSS signals, this implies that a slip of 1 chip occurs after only a few tens of spreading code periods for an incoming Doppler frequency of 10 kHz (for Galileo E1 OS it is a few tens of spreading code periods). As it can be understood, the acquisition performance would suffer from the rapid slip of chips. The Galileo E5a signal is similar to the GPS L5 signal from the point of view of the code Doppler effect on acquisition and Galileo E5b is very close.

Signal	Incoming Doppler frequency Offset of 1 chip (ms) Offset of 1 chip (number of spreading code periods)				
	2 kHz	4 kHz	6 kHz	8 kHz	10 kHz
GPS L1 C/A	770 770	385 385	257 257	193 193	154 154
Galileo E1 OS	770 192.5	385 96.25	257 64.25	193 48.25	154 38.5
GPS L1C	770 77	385 38.5	257 25.7	193 19.3	154 15.4
GPS L5	58 58	29 29	20 20	15 15	12 12

Table 4.1 Time to get an offset of 1 chip depending on the incoming Doppler frequency

To be rigorous, since the Doppler frequency depends on the transmitting frequency and satellite constellation, the received Doppler frequency of a signal emitted by one satellite is not the same whether the signal of interest is GPS L5 or GPS L1 C/A for example.

Before the slip of one chip, the slip of a few samples leads to degradations on the correlation function. Due to the use of high sampling frequency and BOC modulations (CBOC, TMBOC…), the slip of one sample can occur very rapidly.

As an example, for an incoming Doppler frequency of 10 kHz and a sampling frequency of 40.96 MHz, the slip of 1 sample in the Galileo E1 OS data spreading code occurs after 3.85 ms, which means less than a spreading code period. Figure 4.4 shows the sampling of the first and the penultimate chips of the first spreading code of the local code and the received code affected by a code Doppler shift. As it can be observed, the sampled first chips of the received and local spreading codes are exactly the same. However, after 4 ms, there is a delay of around 1/40 chip between both sequences for an incoming Doppler frequency of 10 kHz. As illustrated, this implies a shift of one sample and, then, 12 samples over 40 do not describe the same portion of the subcarrier.

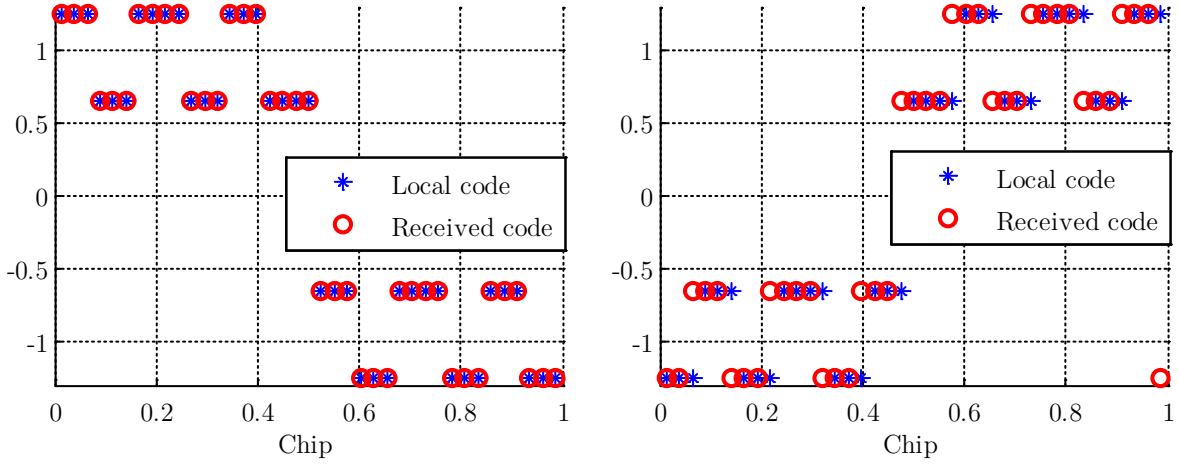

(a) Sampling of the 1^{st} chip

(b) Sampling of the 4091^{st} chip

Figure 4.4 Sampling of 2 chips of the Galileo E1 OS spreading code PRN B/1 for an incoming Doppler frequency of 10 kHz and a sampling frequency of 40.96 MHz

4.3.2 Mathematical model of the distorted correlation function

One approach to model the spreading code period change, used by [Psiaki, 2001] [O'Driscoll, 2007], is to resort to the parameter $\frac{f_D}{f_L}$ and then the received spreading code can be written as:

$$\begin{aligned} &\text{For the received signal without code Doppler effect:} && c_1(t) \\ &\text{For the received signal affected by code Doppler effect:} && c_1\left(\left(1+\frac{f_D}{f_L}\right)t\right) \end{aligned} \tag{4.6}$$

For the need of this study, another approach is proposed. The rectangular shape of the spreading code permits to express the received signal when it is affected by code Doppler.

The u-th chip of the PRN code can be modeled as:

$$\begin{aligned} &\text{For the received signal without code Doppler effect:} && \sum_{u=1}^{N_{c_1}} c_1(u)\,\mathrm{rect}\left(\frac{t}{t_{c_1}}-u\right) \\ &\text{For the received signal affected by code Doppler effect:} && \sum_{u=1}^{N_{c_1}} c_1(u)\,\mathrm{rect}\left(\frac{t}{t_{c_1,D}}-u\right) \end{aligned} \tag{4.7}$$

where the rectangular function is defined by:

$$\mathrm{rect}\left(\frac{t}{T}-u\right)=\mathrm{rect}\left(\frac{t-uT}{T}\right)=\begin{cases}1, (u-1)T \le t \le uT \\ 0, \text{otherwise}\end{cases} \tag{4.8}$$

The mathematical model of the autocorrelation function when the received signal is affected by code Doppler is developed and is denoted $R_{c_1}(f_D, \varepsilon_\tau)$, f_D referring to as the incoming signal parameter and the second parameter ($\varepsilon_\tau = 0$) to the initial delay. To do so, some assumptions need to be taken:

- The model is valid for BPSK-modulated signals. The values taken by the spreading code sequence are 1 or -1,
- There is no code delay error at the start of the correlation between the incoming and local PRN sequences, this means that $\tau = \hat{\tau} = 0$ chip and the first chips of the received and local spreading code begin simultaneously

Furthermore, if $a \le b$, then $\int \mathbf{1}_{[a,b]}(t)\,dt = \int_a^b dt = (b-a)$ and $\mathbf{1}_{[b,a]}(t) = 0$ where $\mathbf{1}_{[a,b]}(t)$ is the indicator function, not null on the interval $[a, b]$.

The autocorrelation function on the first local spreading code period when the received spreading code is affected by code Doppler is given by (4.9). The complete expression is presented in *Appendix E.1.2* and is illustrated by Figure 4.5.

$$
\begin{aligned}
R_{c_1}(f_D,0) &= \frac{1}{T_C}\int_0^{T_C}\left(\sum_{u=1}^{N_{c_1}} c(u)\,\mathrm{rect}\left(\frac{t}{t_{c_1}}-u\right)\right)\left(\sum_{v=1}^{N_{c_1}} c(v)\,\mathrm{rect}\left(\frac{t}{t_{c_1,D}}-v\right)\right)dt \\
&= \frac{1}{T_C}\sum_{u=1}^{N_{c_1}}\int_{(u-1)t_{c_1}}^{ut_{c_1}} c(u)\sum_{v=1}^{N_{c_1}} c(v)\,\mathbf{1}_{\left[\max\left((u-1)t_{c_1},(v-1)t_{c_1,D}\right),\min\left(ut_{c_1},vt_{c_1,D}\right)\right]}(t)dt \\
&= \frac{1}{T_C}\left(N_{c_1}\max\left(t_{c_1},t_{c_1,D}\right)-\left|\delta_{t_{c_1,D}}\right|\frac{N_{c_1}\left(N_{c_1}+1\right)}{2}\right. \\
&\quad \left.+\left|\delta_{t_{c_1,D}}\right|\left(\sum_{u=1}^{N_{c_1}-1} uc(u)c(u+1)+N_{c_1}c(1)c\left(N_{c_1}\right)\mathbf{1}_{\left[t_{c_1,D}\le t_{c_1}\right]}\right)\right)
\end{aligned}
\tag{4.9}
$$

The absolute difference between the duration of one chip of the local and received spreading codes is denoted by $\delta_{t_{c_1,D}} = \left|t_{c_1,D} - t_{c_1}\right|$.

The autocorrelation function is composed of two terms:

- $N_{c_1}\max\left(t_{c_1},t_{c_1,D}\right)-\left|\delta_{t_{c_1,D}}\right|\frac{N_{c_1}\left(N_{c_1}+1\right)}{2}$ corresponds to the cumulative sum (green zones) where the chip "u" of the local code is multiplied by the same chip "u" of the incoming code,
- $\left|\delta_{t_{c_1,D}}\right|\left(\sum_{u=1}^{N_{c_1}-1} uc(u)c(u+1)+N_{c_1}c(1)c\left(N_{c_1}\right)\mathbf{1}_{\left[t_{c_1,D}\le t_{c_1}\right]}\right)$ corresponds to the potential degradations (red zones) due to the product of two adjacent chips results in 1 or -1, with a probability of 50%

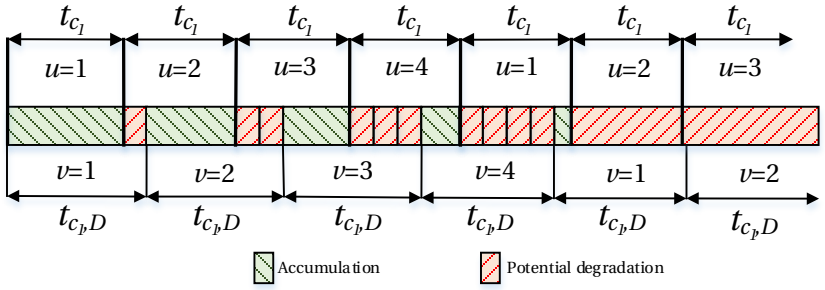

Figure 4.5 Autocorrelation process: same spreading code but with different length due to code Doppler

The expression of the autocorrelation function seems to be difficult to extend to a more general case (for instance, CBOC-modulated signals, with initial delay, non-coherent summations…).

4.3.3 Acquisition performance when considering uncompensated code Doppler

Table 4.2 indicates the dwell time to reach a probability of detection of 95% for a C/N_0 of 27 dB-Hz (total signal power). To do so, it is assumed that the code delay and Doppler frequency are well estimated and that there is no code Doppler. These parameters will be used in the simulations within this section.

	GPS L1 C/A		Galileo E1 OS	GPS L1C	GPS L5
	$T_C = 1$ ms	$T_C = 20$ ms (optimal)	$T_C = 4$ ms	$T_C = 10$ ms	$T_C = 1$ ms
T_I (ms)	126	40	80	50	217
K	126	2	20	5	217

Table 4.2 Required dwell time to acquire signal with a C/N_0 of 27 dB-Hz for a desired probability of detection (obtained from theoretical study 3.2.3.1)

4.3.3.1 Non-coherent summation

This section focuses on the effect of uncompensated code Doppler on the acquisition performance when considering non-coherent summation. The first correlator outputs are slightly degraded whereas the last suffers from a big shift between the local and the incoming signals, as depicted in Figure 4.6.

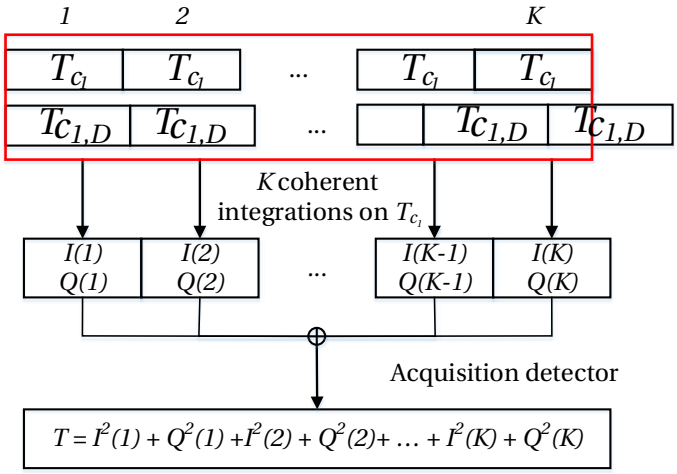

Figure 4.6 Non-coherent summation scheme when considering code Doppler on the received signal

The question is now to understand the resulting effect on the correlation function. In Figure 4.7, Figure 4.8 and Figure 4.9, the average value of the square autocorrelation function affected by a code Doppler (4.10) is represented for negative incoming Doppler frequencies (to have a positive induced code delay $\delta_\tau(f_D)$).

$$\frac{1}{K}\sum_{k=1}^{K} R_{c_1}^2\left(f_d, \varepsilon_\tau(k)\right) \tag{4.10}$$

The reference case, this means when no Doppler is present is represented in cyan; the worst case, in black, represents an incoming Doppler frequency of -10 kHz.

Figure 4.7 represents the GPS L1 C/A cases. As it can be observed, the autocorrelation function shape becomes rounded and offset compared to the reference squared triangle. The amplitude of the maximum value is also reduced and the peak is shifted to positive induced code delay. The effect is accentuated when the dwell time is longer (Figure 4.7(b)).

Indeed, over 126 ms, between the local and the received signals, there is a shift of 0.81 chip for an incoming Doppler frequency of 10 kHz. In this situation, the correlation function is maximum for an induced code delay of 0.42 chip (around half of 0.81 chip). In comparison, in Figure 4.7(a), for an integration time of 40 ms, the correlation peak for an induced code delay of 0.15 chip.

The effect of code Doppler is more marked for the modernized GNSS signals. For the BOC-modulated signals, such as Galileo E1 OS (Figure 4.8) and GPS L1C (Figure 4.9(a)), the secondary peaks which characterize the correlation function tend to disappear leading to a single rounded peak.

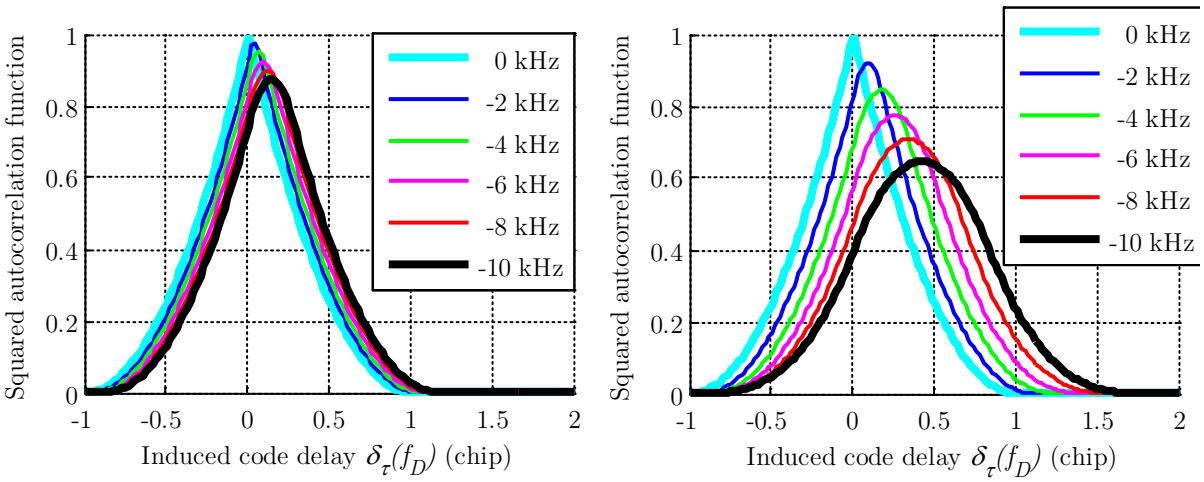

(a) $T_C = 20$ ms, $T_I = 40$ ms (b) $T_C = 1$ ms, $T_I = 126$ ms

Figure 4.7 Normalized squared autocorrelation function when considering code Doppler (GPS L1 C/A)

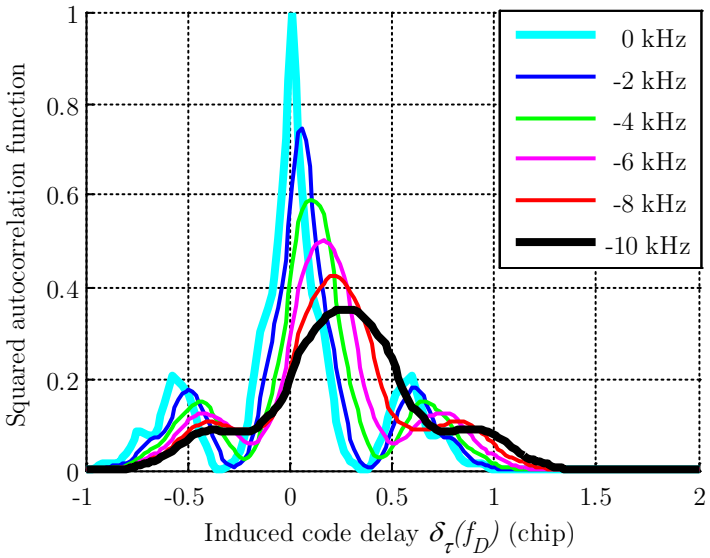

Figure 4.8 Normalized squared autocorrelation function when considering code Doppler (Galileo E1 OS, $T_I = 80$ ms, $K = 20$)

From the point of view of the acquisition, if the correlation function peak is attenuated, the acquisition detector for a right estimation of the signal parameters may not exceed the acquisition threshold and then the detection might fail. From the wide shape of the correlation function, it is even possible that the detector crosses the acquisition threshold for several "cells", as illustrated with an incoming Doppler frequency of -10 kHz (black curve in Figure 4.8).

For the new BPSK-modulated signals, such as GPS L5, with a rapid chipping rate, the correlation peak offset has moved by more than one chip over the 217 milliseconds dwell time for an incoming Doppler frequency higher than 2 kHz (Table 4.1) and the acquisition seems impossible since the shape of the autocorrelation function is flat and close to 0 (Figure 4.9(b)).

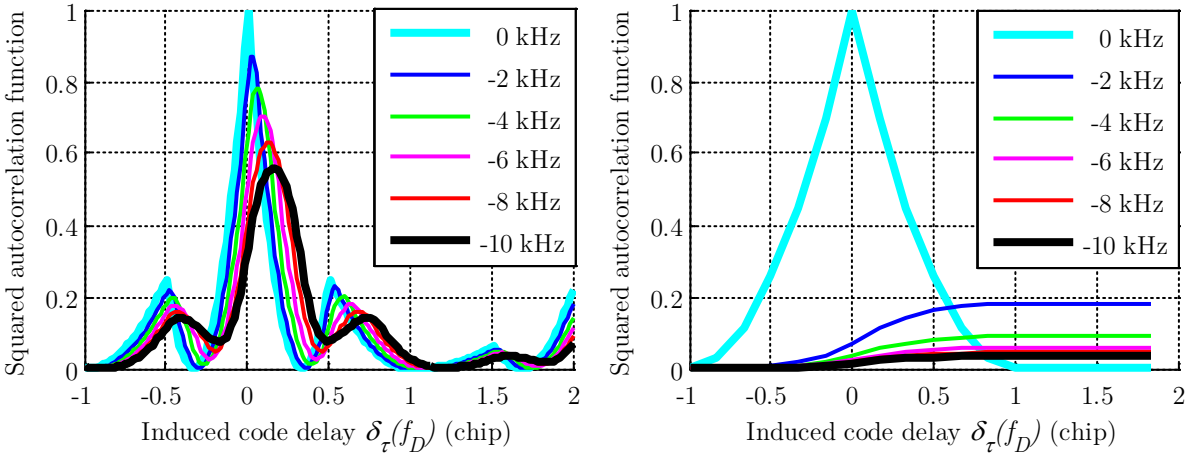

(a) GPS L1C on $T_I = 50$ ms (b) GPS L5 on $T_I = 217$ ms

Figure 4.9 Normalized squared autocorrelation function when considering code Doppler

Let us note that the slip of 1 chip occurs after 217 milliseconds if the incoming Doppler frequency is 500 Hz that means even for very small Doppler frequencies (in the order of a few hundreds of hertz), the code Doppler has a considerable and not negligible impact on the acquisition performance.

As a synthesis on the autocorrelation function considering uncompensated code Doppler, Figure 4.10 describes the main peak (amplitude and induced code delay for which it is obtained) of the squared autocorrelation function affected by code Doppler for different values of incoming Doppler frequencies. Clearly, its amplitude is attenuated, in particular in the case of BOC-modulated signals Figure 4.10(b). The considerable shift of the peak (argmax code delay) when the incoming Doppler increases can then create a detection problem as several cells could trigger a detection. The acquisition grid cell in the time domain is represented by a dashed black line.

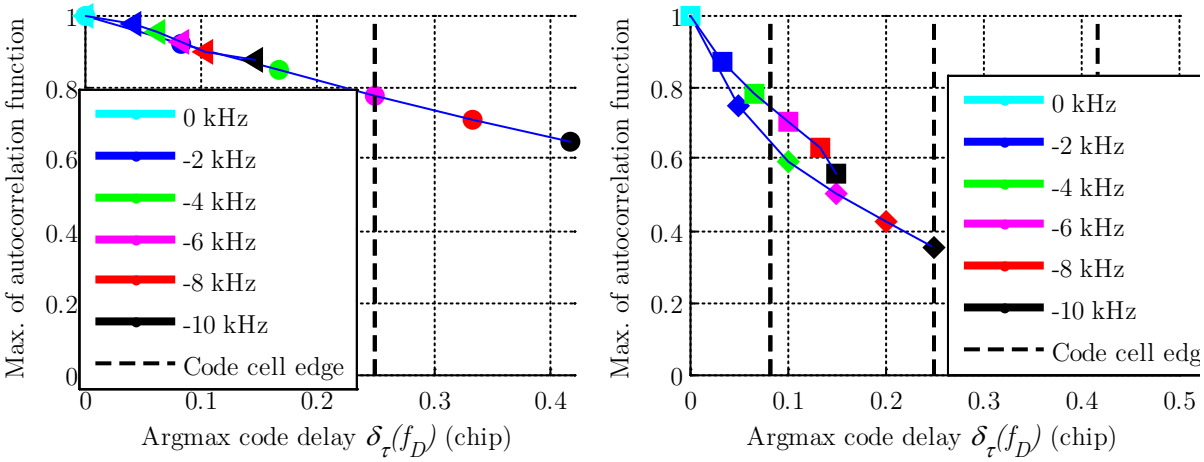

(a) GPS L1 C/A
Circle: $T_C = 1$ ms, Triangle: $T_C = 20$ ms
$\Delta_\tau \approx 0.5$ chip

(b) Diamond: Galileo E1 OS
Square: GPS L1C
$\Delta_\tau \approx \frac{1}{6}$ chip

Figure 4.10 Description of the peak (amplitude and argmax) of the autocorrelation function

The losses on the amplitude of the main peak of the autocorrelation function affected by code Doppler and for all signals are presented in Figure 4.11. Clearly, the higher the incoming Doppler frequency is, the higher the loss on the autocorrelation function is. The worst case is for the modernized GNSS signals (2.5 dB for GPS L1C, 4.5 dB for Galileo E1 OS and close to 15 dB for GPS L5). The consequence of this loss on the autocorrelation function amplitude is detection failures as presented in Figure 4.12.

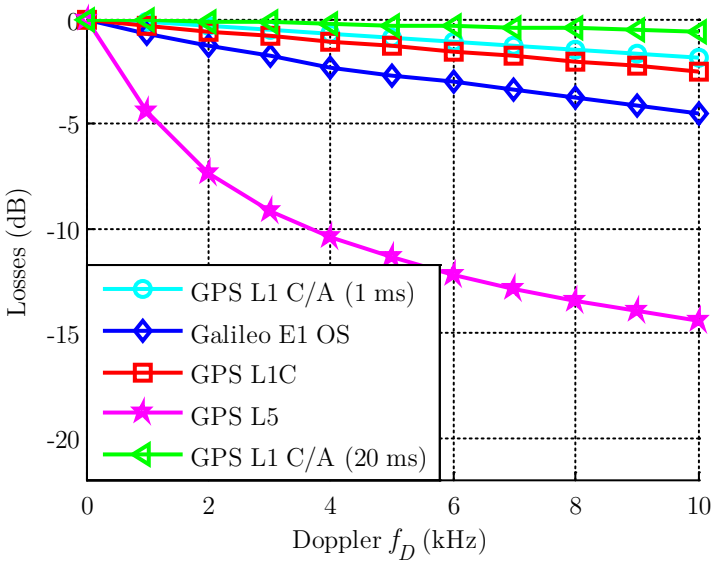

Figure 4.11 Losses on the autocorrelation function due to code Doppler

The considered dwell time was fixed to achieve a detection probability of 95% at 27 dB-Hz assuming that the code Doppler was perfectly aligned. However, when the uncompensated Doppler frequency increases, the probability of detection falls as shown in Figure 4.12.

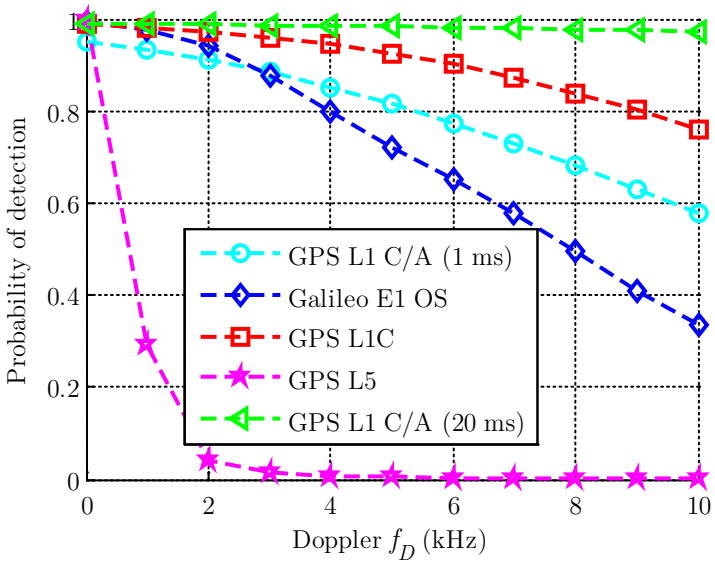

Figure 4.12 Probability of detection when considering code Doppler (no Doppler frequency error)

4.3.3.2 Coherent summation

It is debatable whether the effect of code Doppler on the acquisition performance is accentuated by coherent summation instead of non-coherent summation for the same dwell time T_I, as depicted in Figure 4.13.

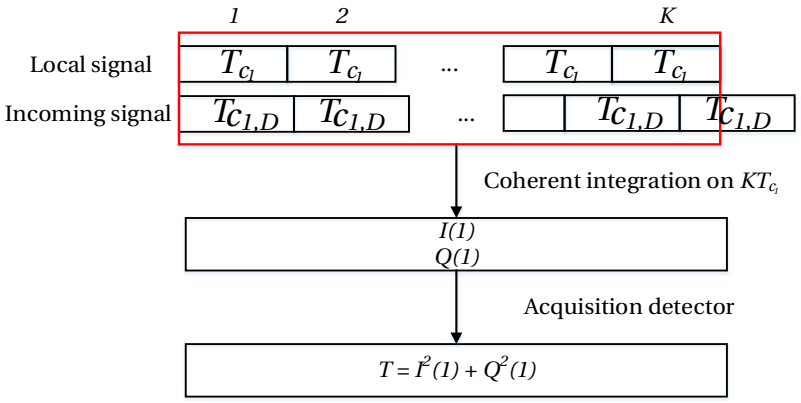

Figure 4.13 Coherent summation scheme when considering code Doppler on the received signal

Obviously, for the considered dwell time presented in Table 4.2, one or several bit sign transitions occur. But ignoring these potential bit sign transitions and their impact on the acquisition performance, Figure 4.14 and Figure 4.15 present the squared autocorrelation function considering the impact of the code Doppler on the received spreading code. Comparing with Figure 4.7, Figure 4.8 and Figure 4.9, it can be concluded that the phenomenon of rounding and shifting is more visible for coherent summations for BPSK and BOC-modulated signals. However, even if the autocorrelation function amplitude is more attenuated for coherent accumulation, the probability of detection is less degraded.

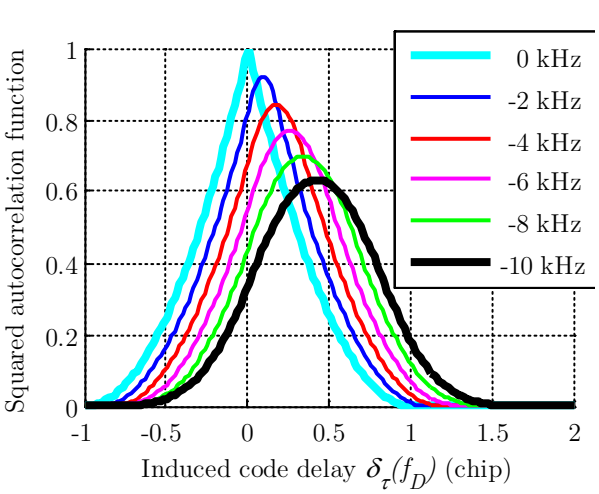

(a) GPS L1 C/A on $T_I = 126$ ms

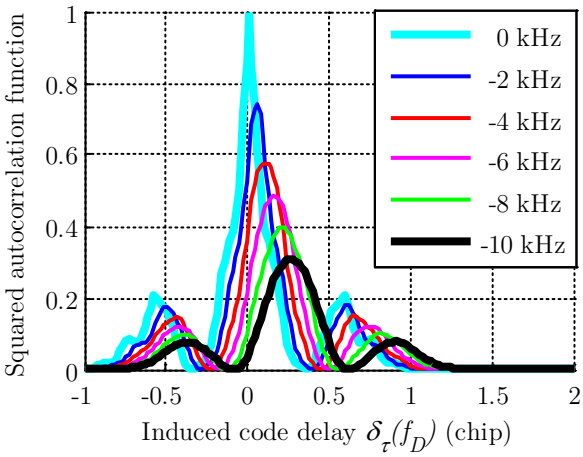

(b) Galileo E1 OS on $T_I = 80$ ms

Figure 4.14 Normalized squared autocorrelation function when considering code Doppler (coherent summation – GPS L1 C/A and Galileo E1 OS)

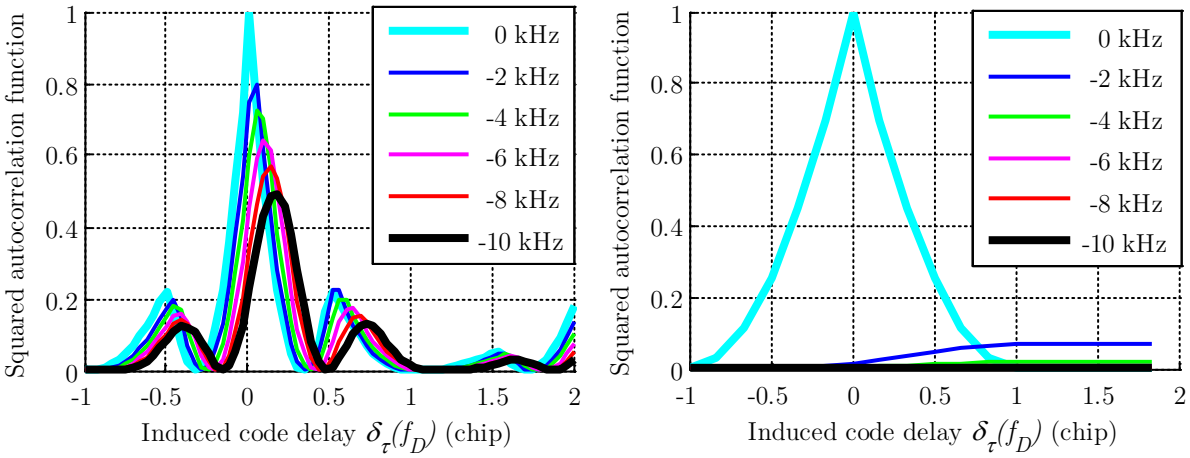

(a) GPS L1C on $T_I = 50$ ms

(b) GPS L5 on $T_I = 217$ ms

Figure 4.15 Normalized squared autocorrelation function when considering code Doppler (coherent summation – GPS L1C and L5)

As a conclusion of this study on the impact of code Doppler on the acquisition performance, it was demonstrated that the code Doppler clearly needs to be dealt with for modernized GNSS signals since the autocorrelation function peak is attenuated and shifted. As shown, when the chipping rate is high such as the GPS L5 signal, an incoming Doppler frequency higher than a few hundreds of hertz

A few code Doppler compensation methods were developed such as [Jiao *et al.*, 2012], [Psiaki, 2001], [Ziedan, 2006] and [Akopian, 2001].

4.4 Effect of data message

The last presented source of degradation is also inherent to the signal and is the effect of the presence of a data message. During the acquisition process, there is no reason that the integration interval is aligned with the data bit since the receiver has not yet achieved bit synchronization. When the same slice of the received signal is correlated with different replicas of the local code affected by different code delays, the bit sign transition occurring within the coherent integration interval may cause degradations on the correlation operation. Indeed, if a data bit sign transition occurs within the coherent integration interval, the autocorrelation function amplitude is attenuated since a part of the terms in the integration has a different sign.

In order to overcome the data bit sign transitions (and avoid the losses implied by these sign transitions), some acquisition methods have been proposed, mainly for the GPS L1 C/A signal, based:

- On the correlation of $2T_{c_1}$ ms of signal with a zero-padded T_{c_1} ms of local code, performed by DFT [Yang *et al.*, 2004]. Initially, used for GPS L1 C/A, this method is called "1+1 ms" in this work.
- On the application of the correlation operation on two separate slices of incoming signal, resulting in two correlator outputs pairs. Applied to GPS L1 C/A, the incoming signal is split into blocks of 10 ms since the data bit duration is equal to 20 ms. Then, if a data bit sign transition occurs, only one of the correlator output pair is affected by the sign transition whereas the other one is guaranteed to be without bit sign transition (called "alternate half-bits method" in [Psiaki, 2001]).
- On the application of the correlation operation on several slices of incoming signal and with a coherent integration time equal to the data bit duration. Presented as "full-bit method" in [Psiaki, 2001] and applied to GPS L1 C/A, 20 correlators on 20 ms are implemented with an offset from one another of one spreading code period (1 ms). The maximum correlator output is chosen with the hope that the correlation integration corresponds to the data bit.
- On a two-step acquisition scheme (estimation of the code delay and then estimation of the Doppler frequency) such as [Sun & Lo Presti, 2010].

In the next chapter, an innovative acquisition method will be proposed but before, a complete study of the impact of the bit sign transition on the acquisition performance is proposed. This study was initiated in [O'Driscoll, 2007] but it is extended by providing the expression of the correlator output and the optimal GNSS acquisition parameters when considering bit sign transitions.

4.4.1 GNSS signal detection statistical model in presence of bit sign transition

4.4.1.1 Correlator output in presence of bit sign transition

Let us first define the terminology used in the following:

- A bit transition is defined as the transition between 2 consecutive bits of the useful data sequence or secondary code,
- During a bit transition, a sign transition can occur or not. Assuming that the data sequence is random and each bit value is independent from the previous one, a data bit sign transition occurs with a probability of ½.

In *Chapter 3*, the correlator outputs were expressed assuming that the useful data sequence is constant during the correlation process. If this assumption is no longer valid, the presented results become radically different.

To consider this case, let us assume without loss of generality that:

- For signals containing two components, only one component is acquired. The acquisition of both components can be easily derived.
- The correlation duration is assumed to be shorter than or equal to the data bit duration $T_C \leq T_d$. As a consequence, one bit sign transition can occur at most within the correlation interval,
- The correlation interval is chosen to be $[0, T_C]$ (if $T_C < T_d$, as it is the case for GPS L1 C/A, if there is a bit transition, it is assumed that it occurs in the interval $[0, T_C]$),
- A bit sign transition occurs at t_0 with $0 \leq t_0 \leq T_C$. Without loss of generality, the bit sign before the bit sign transition is "+1":

$$d(t) = \begin{cases} +1, t \in [0, t_0] \\ -1, t \in]t_0, T_C] \end{cases} \tag{4.11}$$

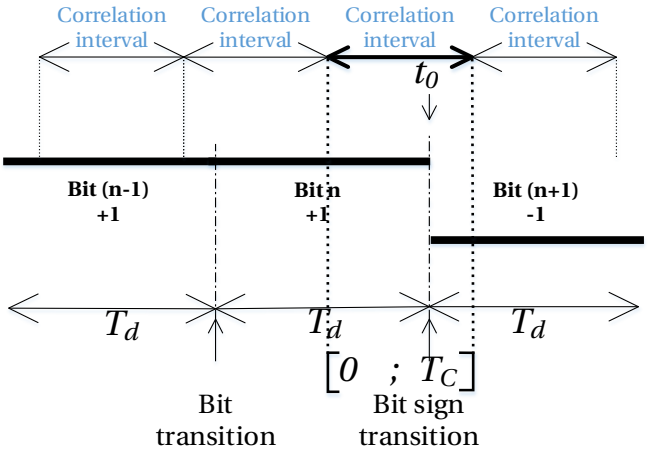

Figure 4.16 Bit sign transition scheme

Figure 4.16 illustrates the previously presented assumptions, in which 2 bit transitions are represented but there is only one bit sign transition between the bit n and the bit $n+1$.

The development of the correlator outputs in presence of bit sign transition is presented in *Appendix E.2*, it results that the in-phase and quadrature-phase correlator outputs $I(t_0, k)$ and $Q(t_0, k)$, considering a bit sign transition at t_0 can be expressed as follows:

$$I(t_0, k) = \frac{A}{2} R_{c_1}(\varepsilon_\tau) \left(-\sin\left(\pi \varepsilon_{f_D} T_C + \phi_0(k)\right) \frac{\cos\left(\pi \varepsilon_{f_D} T_C\right)}{\pi \varepsilon_{f_D} T_C} + \frac{\sin\left(2\pi \varepsilon_{f_D} t_0 + \phi_0(k)\right)}{\pi \varepsilon_{f_D} T_C} \right) + \eta_{I(t_0)}(k)$$

$$Q(t_0, k) = \frac{A}{2} R_{c_1}(\varepsilon_\tau) \left(\cos\left(\pi \varepsilon_{f_D} T_C + \phi_0(k)\right) \frac{\cos\left(\pi \varepsilon_{f_D} T_C\right)}{\pi \varepsilon_{f_D} T_C} - \frac{\cos\left(2\pi \varepsilon_{f_D} t_0 + \phi_0(k)\right)}{\pi \varepsilon_{f_D} T_C} \right) + \eta_{Q(t_0)}(k) \tag{4.12}$$

4.4.1.2 Discussion on the non-centrality parameter when no non-coherent summation is used

Considering that the acquisition is only based on one correlator output (that means $K = 1$ and only one component of the modernized GNSS signals is used), then in presence of a data bit transition, the normalized acquisition detector becomes:

$$T(t_0) = \frac{I^2(t_0,k)}{\sigma_\eta^2} + \frac{Q^2(t_0,k)}{\sigma_\eta^2} \tag{4.13}$$

Similarly to the ideal case (no bit transition):

Under H_0, $T(t_0)$ follows a χ^2 distribution with 2 degrees of freedom,

Under H_1, $T(t_0)$ follows a non-central χ^2 distribution with 2 degrees of freedom with a non-centrality parameter $\lambda(t_0)$ (which expression is developed in *Appendix E.2.2):*

$$\lambda(t_0) = \frac{1}{\sigma_\eta^2}\left(\frac{A}{2}R_{c_1}(\varepsilon_\tau)\right)^2 \frac{\left(1+\cos^2(\pi\varepsilon_{f_D}T_C) - 2\cos(\pi\varepsilon_{f_D}T_C)\cos\left(\pi\varepsilon_{f_D}(T_C-2t_0)\right)\right)}{\left(\pi\varepsilon_{f_D}T_C\right)^2} \tag{4.14}$$

The probability of detection knowing that a bit sign transition occurs at t_0 in the correlation interval is then expressed as a function of $\lambda(t_0)$, which depends on the code delay, Doppler frequency error and on the bit sign transition location t_0:

$$P_{D_1}(t_0) = 1 - F_{\chi^2(2,\lambda(t_0))}(\gamma) \tag{4.15}$$

The expression of the non-centrality parameter when not considering bit sign transition λ_0 (3.15) which can be found with $\lambda(t_0 = T_C)$ ($t_0 = T_C$ is equivalent to no transition during the correlation interval). Figure 4.17 represents the non-centrality parameter $\lambda(t_0)$ as a function of the Doppler frequency error and the ratio t_0/T_C in the case of a coherent integration of 4 ms (Galileo E1 OS) and for a received signal C/N_0 of 30 dB-Hz assuming no Doppler frequency and code delay errors.

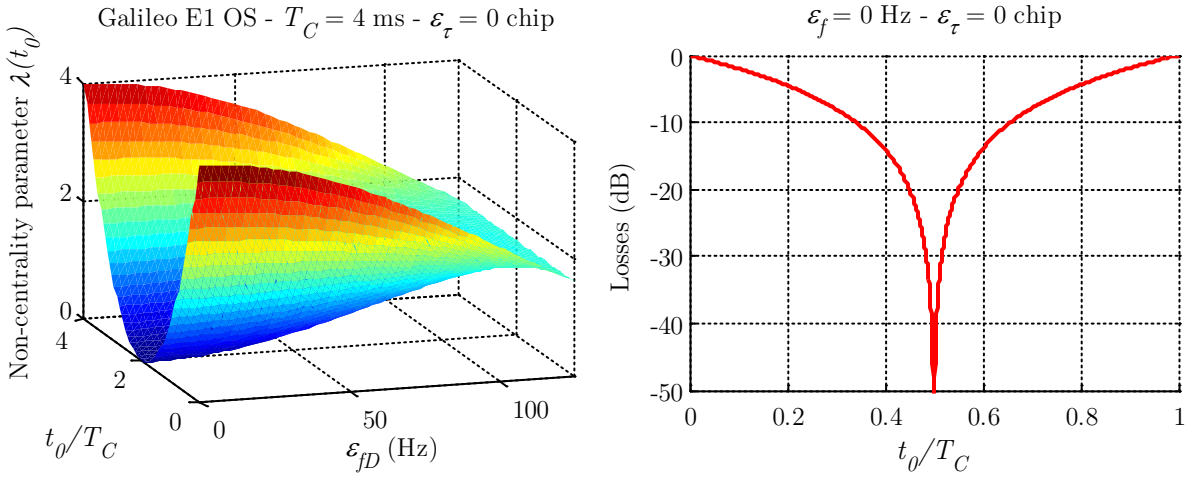

(a) Non-centrality parameter (b) Zoom on the transition location domain

Figure 4.17 Non-centrality parameter in presence of a bit sign transition

Thanks to Figure 4.17(a) and (4.14) it can be noted that the non-centrality parameter $\lambda(t_0)$ depends on:

- The code delay error ε_τ in the same way as for λ_0. So, the non-centrality parameter and the instant of bit sign transition can be considered independent because a bit sign transition occurs at the beginning of the spreading code period. In the following, ε_τ will be assumed to be equal to 0.
- The Doppler frequency error ε_{f_D},
- The location of the bit sign transition t_0, through $\cos\left(\pi\varepsilon_{f_D}(T_C - 2t_0)\right)$ in (4.14). Note that the worst location for the bit sign transition is in the middle of the correlation interval ($t_0 = T_C/2$). In this case, for $\varepsilon_{f_D} \neq 0$, the non-centrality parameter, denoted $\lambda\left(t_0 = \frac{T_C}{2}\right)$ to notify the Doppler frequency error for which it is true, is:

$$\begin{aligned}\lambda\left(t_0 = \frac{T_C}{2}\right) &= \frac{A^2}{N_0} T_C {R_{c_1}}^2(\varepsilon_\tau) \frac{\left(1 + \cos^2\left(\pi\varepsilon_{f_D} T_C\right) - 2\cos\left(\pi\varepsilon_{f_D} T_C\right)\right)}{\left(\pi\varepsilon_{f_D} T_C\right)^2} \\ &= \frac{A^2}{N_0} T_C {R_{c_1}}^2(\varepsilon_\tau) \frac{\left(1 - \cos\left(\pi\varepsilon_{f_D} T_C\right)\right)^2}{\left(\pi\varepsilon_{f_D} T_C\right)^2}\end{aligned} \tag{4.16}$$

If $\varepsilon_{f_D} = 0$, then $\lambda(t_0)$ needs to be evaluated carefully since ε_{f_D} is in the denominator in (4.14). As presented in *Appendix E.2.2*, in this case, the non-centrality parameter can be approximated by:

$$\lambda\left(t_0, \varepsilon_{f_D} \approx 0\right) \approx \frac{A^2}{N_0} T_C {R_{c_1}}^2(\varepsilon_\tau) \left(1 + 4\left(\frac{t_0}{T_C}\right)^2 - 4\frac{t_0}{T_C}\right) \tag{4.17}$$

Another fact, firstly presented in [O'Driscoll, 2007] is that the non-centrality parameter is constant for a Doppler frequency error equal to $\varepsilon_{f_D} = \frac{1}{2T_C}$:

$$\lambda\left(t_0, \varepsilon_{f_D} = \frac{1}{2T_C}\right) = \frac{A^2}{N_0} T_C {R_{c_1}}^2(\varepsilon_\tau) \frac{4}{\pi^2} \tag{4.18}$$

4.4.1.3 Probability of detection for any number of non-coherent summations

The previous analysis can be extended over several non-coherent summations in order to give the general expression of the probability of detection. Over the dwell time $T_I = KT_C$, K correlator pairs are computed, some can be affected by a bit sign transition. Let us denote by N_d the number of bit transitions (with sign transition of not), it can be expressed as:

$$N_d = \left\lceil \frac{T_I}{T_d} \right\rceil \tag{4.19}$$

Knowing that, over T_I, at maximum N_d bit transitions occur, let us denote by N_{t_0} the maximum number of bit sign transitions which can be equal to N_d or $N_d - 1$, depending on the overlap of the integration interval and the data bits, as represented in Figure 4.18.

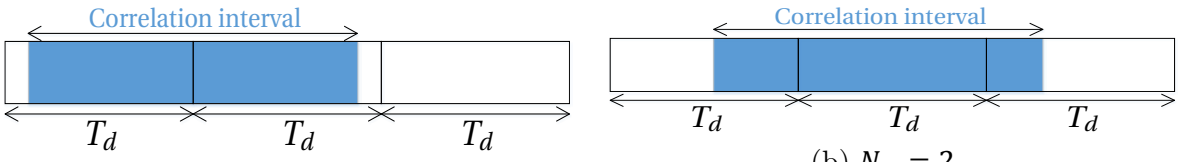

(a) $N_{t_0} = 1$ (b) $N_{t_0} = 2$

Figure 4.18 Illustration of different parameters related to bit sign transition

If the coherent integration time is strictly shorter than the data bit duration, for example the GPS L1 C/A signal with $T_C = 5$ ms and if we fix the dwell time T_I to 35 ms, then N_d equals 2. As illustrated in Figure 4.18(a), $N_{t_0} = 1$ in 25% of the cases that means that only one bit sign transition can occur within the dwell time (when the second bit transition is in the interval [35,40] ms) and in 75% of the cases, 2 bit sign transition can occur (Figure 4.18(b)). When the spreading code period is equal to the data bit duration, $N_{t_0} = N_d$ since $N_d = T_I/T_d$ (integer number).

In practice, depending on the considered slice of received signal, j bit sign transition occur (with $j = 0, 1, \ldots, N_{t_0}$) with a probability of occurrence $P_{j/N_{t_0}}$. Then, among the K computed correlator outputs, j correlator outputs are affected by a bit sign transition. And so, the corresponding probability of detection, knowing that j bit sign transitions, is $P_{D_j}(t_0)$:

$$P_{D_j}(t_0) = 1 - F_{\chi^2(2,\Lambda)}(\gamma) \tag{4.20}$$

where the non-centrality parameter Λ depends on j, the number of correlator pairs K, the coherent integration time T_C and the errors ε_{f_D} and ε_τ:

$$\Lambda = j\lambda(t_0) + (K - j)\lambda_0 \tag{4.21}$$

In order to consider all the cases, it seems more appropriate to provide the average probability of detection considering the distribution of the occurrences of a bit sign transition.

The probability of detection $P_D(t_0)$ represents the average probability of detection on the number of bit sign transition occurring in T_I ms and knowing that at maximum N_{t_0} bit sign transitions occur:

$$P_D(t_0) = \sum_{j=0}^{N_{t_0}} P_{j/N_{t_0}} \times P_{D_j}(t_0) \tag{4.22}$$

which depends on j, λ_0, $\lambda(t_0)$, the number of correlator pairs K, the coherent integration time T_C and the errors ε_{f_D} and ε_τ.

In the specific case of GPS L1 C/A for which several spreading sequences are within one data bit, the probability of detection $P_D(t_0)$ should take into account both values of the maximum number of bit sign transitions ($N_{t_0} = N_d$ and $N_{t_0} = N_d - 1$) depending on the start of the first correlation.

The generic probability of detection is then:

$$\begin{aligned} P_D(t_0) &= \sum_{j=0}^{N_d-1} P_{j/N_d-1} \times P_{D_j}(t_0) + \sum_{j=0}^{N_d} P_{j/N_d} \times P_{D_j}(t_0) \\ &= \sum_{j=0}^{N_d-1} \left(P_{j/N_d-1} + P_{j/N_d}\right) P_{D_j}(t_0) + P_{N_d/N_d} \times P_{D_{N_d}}(t_0) \end{aligned} \tag{4.23}$$

For GPS L1 C/A, considering a coherent integration time as an integer divider of the data bit duration (that means $T_C \in \{1, 2, 4, 5, 10, 20\}$ ms), the average probability of detection $P_D(t_0)$ can then be expressed as:

$$P_D(t_0) = \sum_{j=0}^{N_d-1} \left(\alpha_{N_d-1}\binom{N_d-1}{j} + \alpha_{N_d}\binom{N_d}{j}\right) P_{D_j}(t_0) + \alpha_{N_d} P_{D_{N_d}}(t_0) \tag{4.24}$$

with (as developed in Appendix E.2.3)

$$\alpha_{N_{t_0}} = \frac{1}{2^{N_{t_0}}}\left(1 - \left|N_{t_0} - \frac{T_I}{T_d}\right|\right) \tag{4.25}$$

α_{N_d} and α_{N_d-1} depend on the realization of the events $\{N_{t_0} = N_d\}$ and $\{N_{t_0} = N_d - 1\}$ respectively.

When the data bit duration is equal to the spreading code period and assuming that the probability of a bit sign transition is equal to 50% (such as for Galileo E1 OS signal data component), the maximum number of bit sign transitions is $N_{t_0} = N_d = K$ and the probability of occurrence of j bit sign transitions can be modeled by a binomial distribution $\mathcal{B}\left(K, \frac{1}{2}\right)$. Knowing the probability of occurrence $P_{j/K} = \frac{1}{2^K}\binom{K}{j}$, the average probability of detection $P_D(t_0)$ is then:

$$P_D(t_0) = \frac{1}{2^K} \sum_{j=0}^{K} \binom{K}{j} P_{D_j}(t_0) \tag{4.26}$$

A last step consists in evaluating the average probability of detection over the bit sign transition location:

$$P_{D,t_0} = E_{t_0}\left(P_D(t_0)\right) \tag{4.27}$$

4.4.2 Application to the acquisition of GNSS signals

Previously, it was assumed that the probability of a bit sign transition is 50% when a bit transition occurs. However, this is not the case for all components of the new generation of GNSS signals. That is why the average probability of detection is extended to the new GNSS signals when acquiring both components. GPS L1 C/A and three new GNSS signals are presented since they cover all the possible cases:

- The spreading code period is equal to or shorter than the data bit duration,
- Due to the presence of secondary codes on the data and pilot component, the probability that a bit transition can be different from 50%,
- There is an inequality in the signal power repartition between both components.

So new notations should be introduced:

- p_d is the probability of a bit sign transition on the data component (assumed to be ½ if there is no secondary code on the data component),
- p_p is the probability of a bit sign transition on the pilot component, it depends on the secondary code on the pilot component ($\overline{p_p} = 1 - p_p$),
- A_x is the amplitude of the received signal on the x component (A_d for data and A_p for pilot),
- $\lambda_{0,x}$ and $\lambda_x(t_0)$ correspond to the non-centrality parameters when only one correlator output pair is computed on the x component, when the data is considered absent (based on (3.15)) or when it is present and one bit sign transition occur (based on (4.14)).

For each signal, some results on the probability of detection are then presented, they result from a simulation on the developed model of the probability of detection.

4.4.2.1 GPS L1 C/A

The case of GPS L1 C/A is particular because the spreading code period is shorter than the data bit duration.

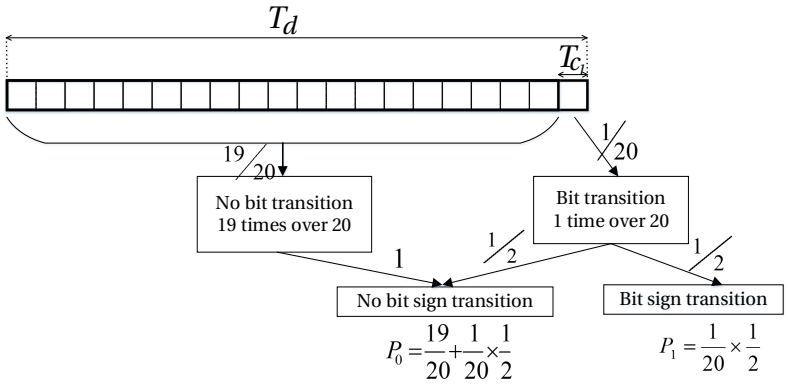

Figure 4.19 Scheme to determine the probability of detection (GPS L1 C/A) with $T_I = 20$ ms

Over 20 successive 1-ms correlations, only one can be affected by a data bit transition which involves a sign transition with a probability of 50%. The 19 other 1-ms correlations will necessarily be free of bit transition. Figure 4.19 presents the scheme to compute the probability of occurrence of one bit sign transition for one integration and for a coherent integration time of $T_C = 1$ ms. It can be extended to any coherent integration time which is an integer divider of $T_d = 20$ ms, as presented in Table 4.3.

$T_I = KT_C = 20$ ms		$P_D(t_0) = P_{0/1} \times P_{D_0} + P_{1/1} \times P_{D_1}(t_0)$ $P_{D_0} = 1 - F_{\chi^2(2K,\Lambda)}(\gamma)$ with $\Lambda = K\lambda_0$ $P_{D_1}(t_0) = 1 - F_{\chi^2(2K,\Lambda)}(\gamma)$ with $\Lambda \approx (K-1)\lambda_0 + \lambda(t_0)$
T_C	K	
1 ms	20	$\left(\frac{19}{20} + \frac{1}{20} \times \frac{1}{2}\right) P_{D_0} + \left(\frac{1}{20} \times \frac{1}{2}\right) P_{D_1}(t_0)$
2 ms	10	$\left(\frac{9}{10} + \frac{1}{10} \times \frac{1}{2}\right) P_{D_0} + \left(\frac{1}{10} \times \frac{1}{2}\right) P_{D_1}(t_0)$
4 ms	5	$\left(\frac{4}{5} + \frac{1}{5} \times \frac{1}{2}\right) P_{D_0} + \left(\frac{1}{5} \times \frac{1}{2}\right) P_{D_1}(t_0)$
5 ms	4	$\left(\frac{3}{4} + \frac{1}{4} \times \frac{1}{2}\right) P_{D_0} + \left(\frac{1}{4} \times \frac{1}{2}\right) P_{D_1}(t_0)$
10 ms	2	$\left(\frac{1}{2} + \frac{1}{2} \times \frac{1}{2}\right) P_{D_0} + \left(\frac{1}{2} \times \frac{1}{2}\right) P_{D_1}(t_0)$
20 ms	1	$\frac{1}{2} P_{D_0} + \frac{1}{2} P_{D_1}(t_0)$

Table 4.3 Probability of detection for an integration time of 20 ms (GPS L1 C/A)

It is well known that the performance of the GPS L1 C/A signal acquisition when not considering bit sign transitions depends on the correlation duration and that it is preferable to have a long coherent integration time to improve the acquisition detection performance [Bastide *et al.*, 2002].

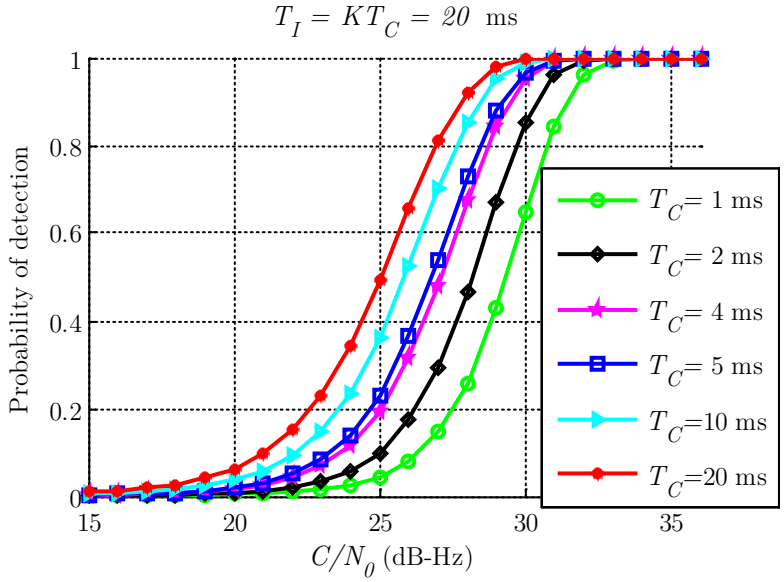

Figure 4.20 Probabilities of detection for different coherent integration times when not considering bit sign transition (GPS L1 C/A)

In Figure 4.20, the curve with green circles, representing the probability of detection for a coherent integration time of 1 ms, is clearly below the curve with red points (which refers to a coherent integration time of 20 ms). For example, at 30 dB-Hz, the detection seems obvious (probability higher than $P_D = 0.99$) with the longest coherent integration time whereas with the shortest, the detection appears more challenging (only $P_D = 0.65$).

In contrast, when considering bit sign transitions, a long coherent integration time provides one of the worst performance since the effect of the bit sign transition is significant. When the integration time is too short, the effect of the bit sign transition is slight, but it does not allow for optimal detection.

Two examples of bit sign transition location are presented in Figure 4.21: $t_0 = T_C/4$ and $t_0 = T_C/2$. The integration time is $T_I = 20$ ms, which means that only one data bit sign transition can occur. As an example, if $T_C = 5$ ms with $K = 4$ and $t_0 = T_C/2$, it is similar to say that 3 integrations are not affected by bit sign transition and one integration is affected by a bit sign transition occurring with a probability of 50%, at $t_0 = 2.5$ ms after the beginning of the coherent integration interval. Figure 4.21 gives a representation of the probability of detection considering bit sign transitions as presented in Table 4.3. As it was expected, for high C/N_0, the curve with red points ($T_C = 20$ ms) goes below the other curves (with shorter coherent integration times). When the bit sign transition occurs in the middle of the coherent integration time, the more observable degradations are for a coherent integration time of 20 ms and in this case, the probability of detection stays at $P_D = 0.5$ even for high C/N_0.

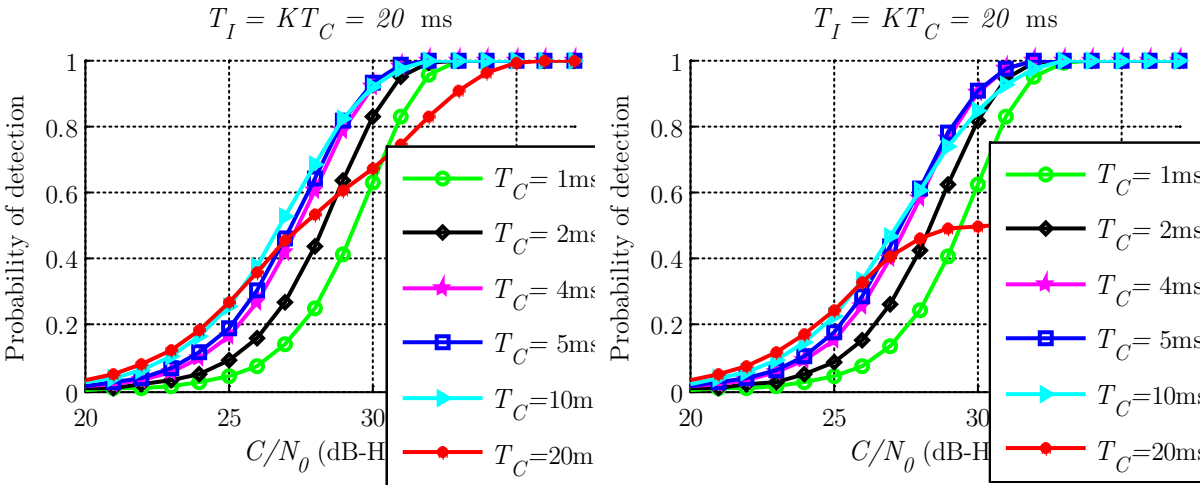

(a) $t_0 = T_C/4$ (b) $t_0 = T_C/2$

Figure 4.21 Probabilities of detection for different coherent integration times and different location of the transition when considering bit sign transition (GPS L1 C/A)

Figure 4.23(a) presents the resulting average probability of detection on all the possible bit sign transition location for an integration time of 20 ms. It seems clear that $T_C = 1$ or $T_C = 2$ ms are not optimal coherent integration times except maybe for very high C/N_0. To complete the results presented in the figures, Table 4.4 provides the optimal coherent integration time as a function of the bit sign transition location and the sensitivity. The higher the C/N_0 is, the shorter the optimal coherent integration time is (at 39 dB-Hz, a coherent integration time of 1 ms is sufficient). For weak C/N_0, a long coherent integration time is required to accumulate enough energy to be able to detect even if the bit sign transition degradations are significant.

To complete the previous result, in the case of weak signals, an example on an integration duration of $T_I = 40$ ms is proposed, for a C/N_0 of 27 dB-Hz and a probability of false alarm of $P_{FA} = 10^{-3}$. It is assumed that there are 2 bit transitions and only one leads to a bit sign transition, occurring at 10.5 ms, as illustrated in Figure 4.22.

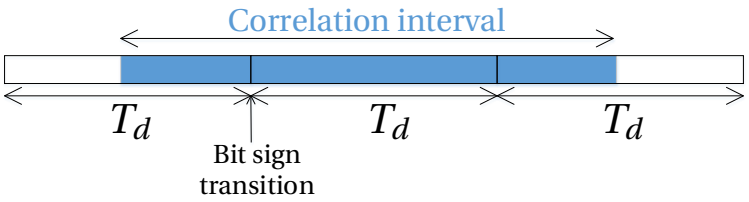

Figure 4.22 Illustration of a bit sign transition for a total integration time of 40 ms

If the coherent integration duration is the shortest ($T_C = T_{c_1} = 1$ ms), there is 1 accumulation which is affected by a bit sign transition at $t_0 = 0.5$ ms and 39 accumulations are free of bit sign transition. When the coherent integration time is 1 ms, the probability of detection when one bit sign transition occurs is 35.76%.

$$P_{D_1}(t_0) = 1 - F_{\chi^2(2\times 40,\Lambda)}(\gamma) \approx 35.76\% \text{ with } \Lambda \approx 39\lambda_0 + \lambda(t_0) \tag{4.28}$$

If the coherent integration time is the longest ($T_C = T_d = 20$ ms), there is 1 accumulation affected by a bit sign transition at $t_0 = 10.5$ ms (and the associated non-centrality parameter is very close to 0) and 1 accumulation is free of bit sign transition. When the coherent integration time is 20 ms, the probability of detection when one bit sign transition occurs is 70.02%.

$$P_{D_1}(t_0) = 1 - F_{\chi^2(2\times 2,\Lambda)}(\gamma) \approx 70.02\% \text{ with } \Lambda \approx \lambda_0 + \lambda(t_0) \tag{4.29}$$

On this example on 40 ms, it can be observed that the probability of detection is higher when the coherent integration time is 20 ms even if one accumulation is strongly degraded. This explains that in presence of weak signals, the priority is to accumulate energy with long coherent integrations.

It is important to note that the coherent integration time T_I has an impact on the size of the cell in the Doppler frequency (which is inversely proportional to the coherent integration time). A long coherent integration time implies a thin cell and then more cells to explore in the frequency domain.

It is interesting to observe that for medium C/N_0, the optimal coherent integration times seem to be the intermediate ones $T_C = 10$ ms, $T_C = 4$ or $T_C = 5$ ms. Table 4.5 provides the associated probabilities of detection for the optimal coherent integration time.

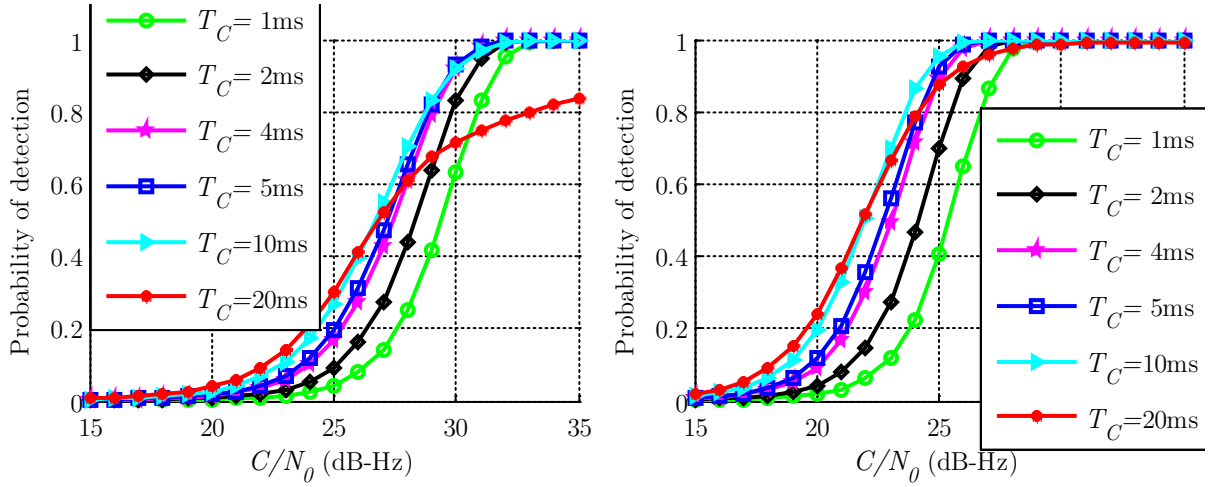

(a) $T_I = 20$ ms (b) $T_I = 100$ ms

Figure 4.23 Average probabilities of detection on t_0 for different coherent integration times when considering bit sign transition (GPS L1 C/A)

Bit sign transition location $t_0 = \frac{a}{b} T_C$	C/N_0 (dB-Hz) 25	27	29	31	33	35	37	39
$\frac{a}{b} = 0$	20	20	20	20	20	20	2	1
$\frac{1}{16}$	20	20	20	20	10	10	2	1
$\frac{2}{16} = \frac{1}{8}$	20	20	10	10	10	5	4	1
$\frac{3}{16}$	20	10	10	5	5	5	4	1
$\frac{4}{16} = \frac{1}{4}$	20	10	10	5	5	4	4	1
$\frac{5}{16}$	20	10	5	5	4	4	4	1
$\frac{6}{16} = \frac{3}{8}$	20	10	5	5	4	4	4	1
$\frac{7}{16}$	20	10	5	5	4	4	4	1
$\frac{8}{16} = \frac{1}{2}$	20	10	5	5	4	4	4	1
Average	20	10	10	5	4	4	4	1

Table 4.4 Optimal coherent integration time T_C (in ms) for $T_I = 20$ ms (GPS L1 C/A)

$P_D(t_0)$		C/N_0 (dB-Hz)							
		25	27	29	31	33	35	37	39
Bit sign transition location $t_0 = \frac{a}{b}T_C$	$\frac{a}{b} = 0$	0.49	0.81	0.98	1	1	1	1	1
	$\frac{1}{16}$	0.41	0.72	0.94	1	1	1	1	1
	$\frac{2}{16} = \frac{1}{8}$	0.34	0.61	0.90	0.99	1	1	1	1
	$\frac{3}{16}$	0.29	0.56	0.86	0.98	1	1	1	1
	$\frac{4}{16} = \frac{1}{4}$	0.26	0.53	0.82	0.98	1	1	1	1
	$\frac{5}{16}$	0.25	0.60	0.80	0.98	1	1	1	1
	$\frac{6}{16} = \frac{3}{8}$	0.25	0.48	0.79	0.98	1	1	1	1
	$\frac{7}{16}$	0.25	0.47	0.78	0.97	1	1	1	1
	$\frac{8}{16} = \frac{1}{2}$	0.25	0.47	0.78	0.97	1	1	1	1
Average P_{D,t_0}		0.30	0.55	0.83	0.98	1	1	1	1

Table 4.5 Probability of detection for the optimal coherent integration time (Table 4.4) for $T_I = 20$ ms (GPS L1 C/A)

To conclude this section on the GPS L1 C/A signal detection when considering bit sign transitions, it has been observed that the optimal coherent integration time depends on the C/N_0 (in general unknown), the integration time (as an example, $T_I = 20$ and $T_I = 100$ ms as presented in Figure 4.23) and on the bit sign transition location t_0. The average probability of detection on the bit sign transition location seems the highest for $T_C = 10$ ms among the 6 considered coherent integration times and for a C/N_0 higher than 23 dB-Hz. When the C/N_0 is lower, it is better to choose the longest possible coherent integration time.

It can be interesting to extend these results to any coherent integration time and not to restrict as done to $T_C \in \{1, 2, 4, 5, 10, 20\}$, such as $T_C = 6$ ms for example. Some key elements to compute the average probability of detection are proposed using as an example a dwell time of 60 ms. Let us assume that there is a shift of 1 ms between the local and the incoming signal, it can be deduced that there is a bit sign transition:

- At $t_0 = 1$ ms during the 1st integration $[0,6]$ ms (data bit transition at 1 ms)
- At $t_0 = 3$ ms during the 4th integration $[18, 24]$ ms (data bit transition at 21 ms)
- At $t_0 = 5$ ms during the 7th integration $[36, 42]$ ms (data bit transition at 41 ms)

But for instance, if there are two bit sign transitions, the average probability of detection is not the same if they occur at the first and the second bit transitions or at the first and the third. The average probability of detection should then take into account all the potential combinations on the locations of bit sign transitions (which depend on the correlation intervals).

4.4.2.2 Galileo E1 OS

The Galileo E1 OS signal is characterized by a spreading code period T_{c_1} of 4 ms which corresponds to the data bit duration on the data component. On the pilot component, there is a unique 25-bit secondary code, each bit has also a duration of 4 ms. The representation of the Galileo E1 OS secondary code is given by Figure 4.24. Due to its number of bits (odd number), the probability of a secondary code bit sign transition is $p_p = \frac{12}{25} = 0.48$ close to 0.5 and then $p_d = p_p \approx 0.5$.

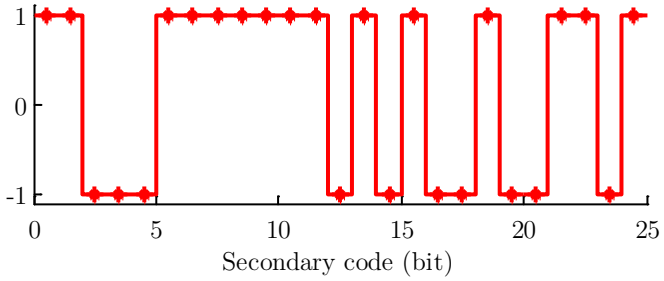

Figure 4.24 Secondary code on the Galileo E1 OS pilot component

When K non-coherent summations are computed, the probability of occurrence of j bit sign transitions (with $j = 0, 1, \ldots, 2K$) follows a binomial distribution $\mathcal{B}(2K, 1/2)$. Because the total signal power is split in 50% on each component, $\lambda_{0,d} = \lambda_{0,p}$ and $\lambda_{t_0,d} = \lambda_{t_0,p}$.

The probability of detection $P_D(t_0)$ is then:

$$P_D(t_0) = \frac{1}{2^{2K}} \sum_{j=0}^{2K} \binom{2K}{j} P_{D_j}(t_0)$$
$$P_{D_j}(t_0) = 1 - F_{\chi^2(4K,\Lambda)} \qquad (4.30)$$
$$\Lambda = j\lambda_x(t_0) + (2K - j)\lambda_{0,x}$$

Figure 4.25(a) presents the probabilities of detection when 0, 1 bit sign transition on each component occur during one integration interval which integration time is equal to the spreading code period. For a good interpretation, it is important to insist on the fact that the plotted C/N_0 on the x-axis of the figures represents the total received signal power and then does not take into account potential differences in the transmitted power.

If one bit sign transition occurs on each component, that means there is a data bit sign transition on the data component and a secondary code bit sign transition on the pilot component. This configuration occurs as many times as when no bit sign transition occurs on both component $P_{0/2} = P_{2/2} = 1/4$. One bit sign transition means that there is a data bit sign transition and no secondary code bit sign transition or vice versa, it explains why the probability of occurrence is two times higher $P_{1/2} = 1/2$. The average probability of detection for $K = 1$ is presented in Figure 4.25(b). As it can be observed, it converges to 0.75 for high C/N_0 since $P_{D_2} = 0$ ($\lambda_d\left(t_0 = \frac{T_C}{2}\right) = \lambda_p\left(t_0 = \frac{T_C}{2}\right) = 0$).

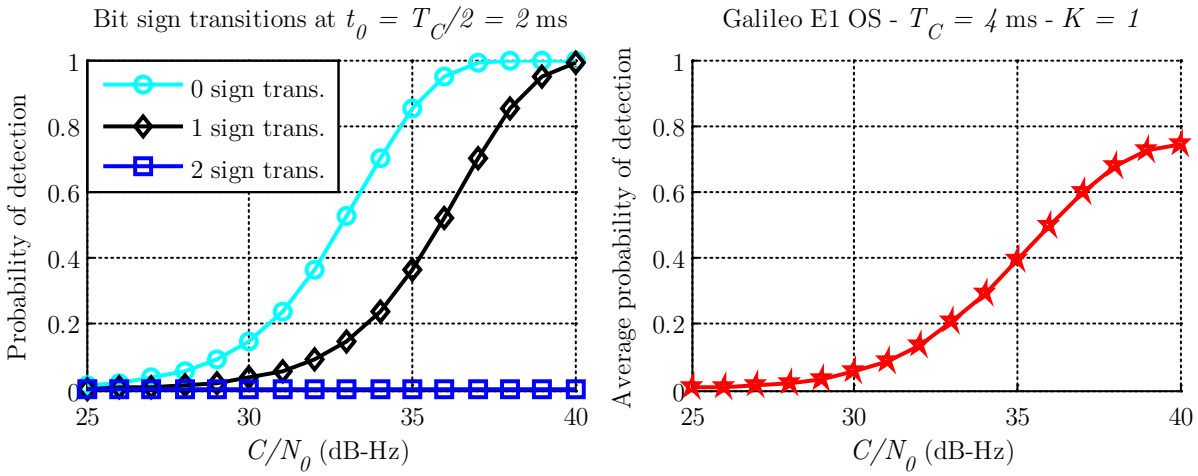

(a) P_{D_j} for $j = 0, 1, 2$ (b) $P_D(t_0) = \frac{1}{4}P_{D_0} + \frac{1}{2}P_{D_1}(t_0) + \frac{1}{4}P_{D_2}(t_0)$

Figure 4.25 Probabilities of detection P_{Dj} and $P_D(t_0)$ for one integration ($K = 1$) on 4 ms on both components and considering a bit sign transition in the middle of the integration interval (Galileo E1 OS)

Figure 4.26 presents the probability of detection when not considering bit sign transitions and the average probability of detection when considering bit sign transitions in the case $K = 5$. To optimize the probabilities of detection, it is preferable to acquire both components. The degradations on the probability of detection due to bit sign transitions is comparable for both techniques (acquisition of one or both components), around 2 dB for a C/N_0 around 30 dB-Hz.

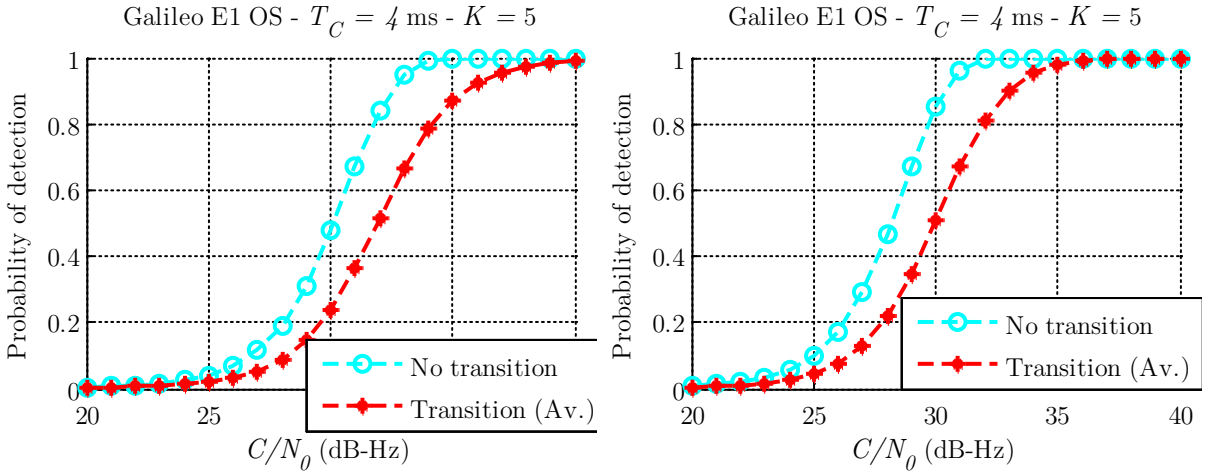

(a) Acquisition of one component (b) Acquisition of both components

Figure 4.26 Probabilities of detection on $T_I = 20$ ms when considering or not bit sign transitions (Galileo E1 OS)

4.4.2.3 GPS L5

On the data component of the GPS L5 signal, a secondary code, a 10-bit Neuman-Hofman code and denoted by $c_{2,d} = NH_{10}$ (given in [Navstar, 2012c] and represented in Figure 4.27(a)) multiplies the data sequence, which is assumed to be random. It results in a binary sequence with a rate of 1 kbit/s.

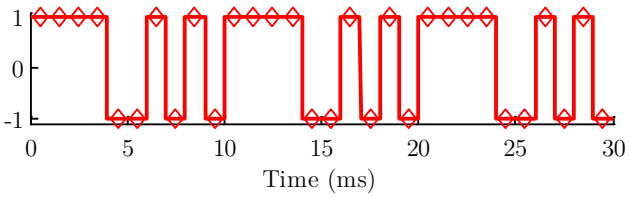

(a) NH_{10}

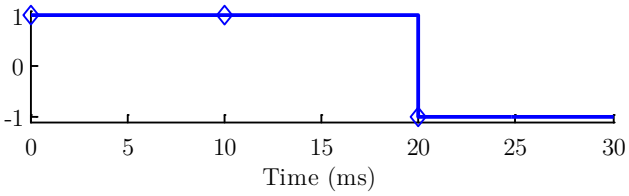

(b) $Data$

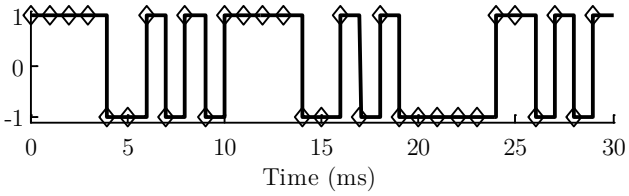

(c) $Data \times NH_{10}$

Figure 4.27 Product of data sequence and secondary code on the GPS L5 data component

This implies that a bit sign transition on the data component does not occur with the same probability as a bit transition without bit sign transition. Knowing that:

- There is a sign transition between the last and the first data secondary code bits (since the first bit is 1 and the last one -1),
- The data bit cannot change sign during the NH period (10 ms),

it can be established that a bit sign transition occurs:

- When the data bit changes without sign change because the secondary code changes sign,
- When the secondary code bit changes (with a probability of $5/9$ without considering the sign transition between the last and the first NH_{10} bits)

In the end, the probability that there is a bit sign transition (product of the data and secondary code) on the data component is:

$$p_d = \frac{1}{10}\left(1 \times \frac{1}{2} + 9 \times \frac{5}{9}\right) = 0.55 \tag{4.31}$$

On the GPS L5 pilot component, the secondary code is unique for all signals and is a 20-bit Neuman-Hofman code (presented in Figure 4.28). As it can be observed, a secondary code bit transition can result in a sign transition with a probability of ½.

$$p_p = \overline{p_p} = 0.5 \tag{4.32}$$

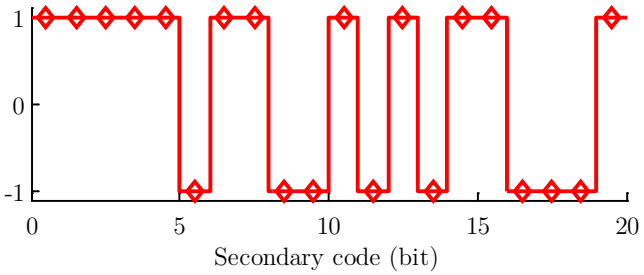

Figure 4.28 Secondary code on the GPS L5 pilot component

Since, on the data component, a bit sign transition occurs more often than a bit transition without sign transition, to compute the probability of detection, the number of bit sign transitions on the data component should be distinguished to differentiate the behavior on the data component from this on the pilot component. Over K spreading code periods, if j bit sign transitions occur, the number of bit sign transition on the data component can be denoted by j_d (and, consequently, on the pilot component $j - j_d$ bit sign transitions occur). It implies that j_d is bounded by:

- $j_d \leq \min(K, j)$ because the number of bit transitions on the data component is at maximum equal to the number of spreading code periods and obviously to the number of bit sign transitions,
- $j_d \geq \max(j - K, 0)$. For example, if $j = 2K$ (maximum number of bit sign transitions), this implies that on each component, K bit sign transition occurs and then $j_d = K$.

Then, the probability of occurrence of j bit sign transitions knowing that j_d bit sign transitions occur on the data component is:

$$P_{j,j_d} = \binom{K}{j_d}\binom{K}{j - j_d} p_d^{j_d}(1 - p_d)^{K - j_d} p_p^{j - j_d}\left(1 - p_p\right)^{K - (j - n_d)} \tag{4.33}$$

It results that the probability of detection becomes:

$$\begin{aligned} P_D(t_0) &= \sum_{j=0}^{N_{t_0}} \sum_{j_d=\max(j-K,0)}^{\min(K,j)} P_{j,j_d} \times P_{D_j}(t_0) \\ P_{D_j}(t_0) &= 1 - F_{\chi^2(4K,\Lambda)} \\ \Lambda &= j\lambda_x(t_0) + (2K - j)\lambda_{0,x} \end{aligned} \tag{4.34}$$

The same approach can be applied to Galileo E5a and Galileo E5b signals since on both components the probability that a Galileo E5 secondary codes transition does not lead to a bit sign transition close to 50% (between 46% and 54%).

Even if the probability that a bit sign transition occurs when a bit transition occurs on the data component is higher than 0.5, the average probability of detection of the pilot or of the data components are very close. It seems preferable to acquire both GPS L5 components to optimize the probability of detection and the average probability of detection when considering bit sign transitions (Figure 4.29). The effect of bit sign transition on the acquisition performance is very strong, in the case of the acquisition of both components of a received signal at 32 dB-Hz, the average probability of detection is around 40% when considering bit sign transition whereas the probability of detection considering the absence of bit sign transitions is higher than 80%, the losses being higher than 2 dB.

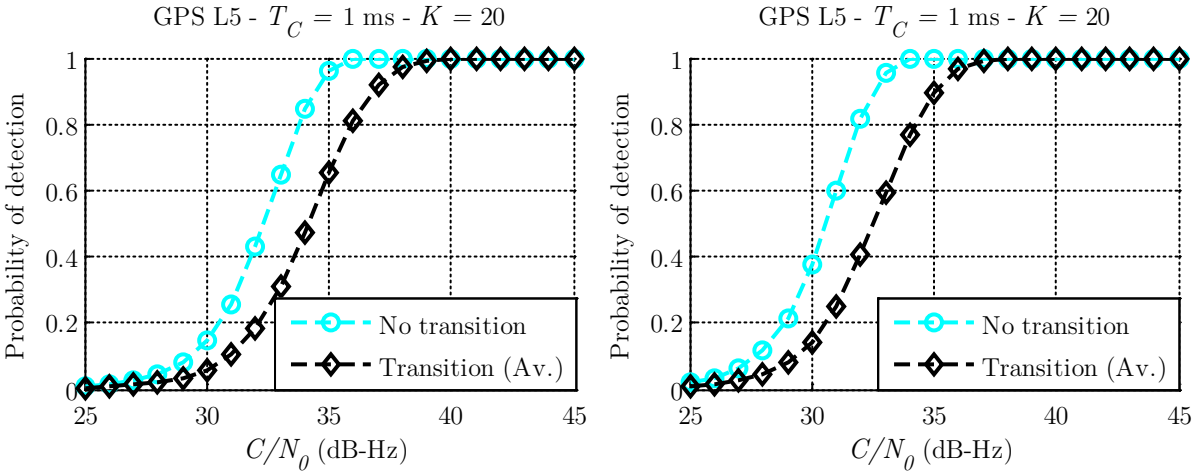

(a) Acquisition of the pilot component (b) Acquisition of both components

Figure 4.29 Probabilities of detection when considering or not bit sign transitions (GPS L5)

4.4.2.4 GPS L1C

Unlike Galileo E1 OS, GPS L5 and Galileo E5, there are as many secondary codes as satellites on the GPS L1C pilot component and they are extremely long (1800 bits). Let us admit that the bit sign transition location distribution is uniform ($p_p = \overline{p_p} = 0.5$). Furthermore, the GPS L1C signal is characterized by a difference in power on both components. This implies a difference on the non-centrality parameters expressions since $\lambda_{0,d} \neq \lambda_{0,p}$ and $\lambda_d(t_0) \neq \lambda_p(t_0)$. Once again, but for different reasons than GPS L5, the number of bit sign transition on the data component j should be considered. Over K spreading code periods, the non-centrality parameter contains:

- K terms from the data component: j considering bit sign transitions and $K - j$ without bit sign transition,

- K terms from the pilot component: $j - j_d$ considering bit sign transitions and $K - (j - j_d)$ without bit sign transition

Because the probability of bit sign transitions on each component is assumed to be one half, the probability of detection can be expressed as follows:

$$P_D(t_0) = \sum_{j=0}^{N_{t_0}} \sum_{j_d=\max(j-K,0)}^{\min(K,j)} \frac{1}{2^{2K}} \binom{K}{j_d} \binom{K}{j-j_d} \times P_{D_{j,j_d}}(t_0)$$
$$P_{D_{j,j_d}}(t_0) = 1 - F_{\chi^2(4K,\Lambda)} \quad (4.35)$$
$$\Lambda = \left(j_d \lambda_d(t_0) + (K - j_d)\lambda_{0,d}\right) + \left((j - j_d)\lambda_p(t_0) + \left(K - (j - j_d)\right)\lambda_{0,p}\right)$$

As shown in Figure 4.30, the acquisition of the GPS L1C pilot component provides an average probability of detection similar to the one for the acquisition on both components since the pilot component contains 75% of the signal power.

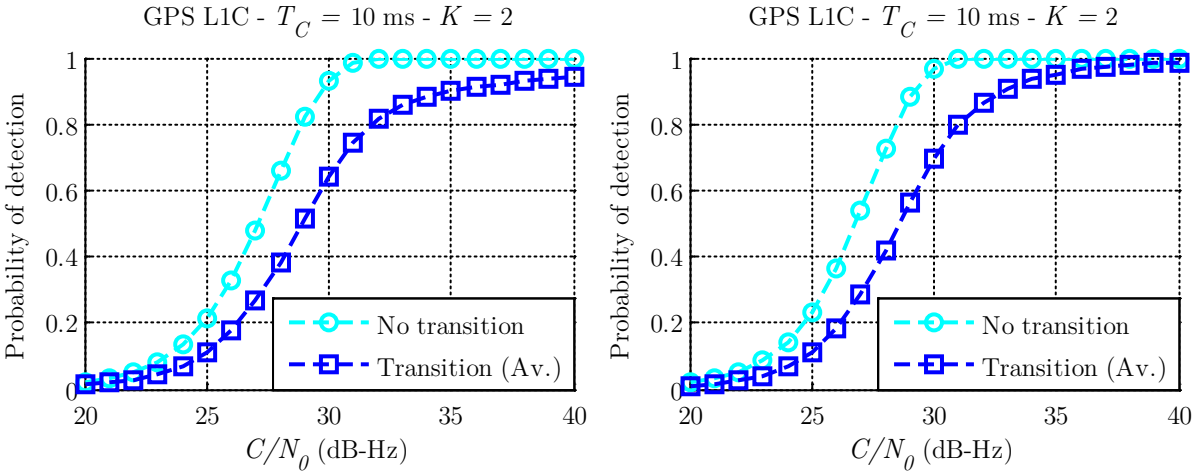

(a) Acquisition of the pilot component (b) Acquisition of both components

Figure 4.30 Probabilities of detection on $T_I = 20$ ms when considering or not bit sign transitions (GPS L1C)

4.4.3 Comparison of modernized GNSS signals with GPS L1 C/A

In this section, the acquisition performance of the modernized GNSS signals is studied. Firstly, the three considered modernized signals are compared on a common dwell time of $T_I = 20$ ms and for the same total received signal power (data and pilot) and without considering potential difference in transmitted power. Since the correlation duration is different ($T_C = 1$ ms for GPS L5, $T_C = 4$ ms for Galileo E1 OS, $T_C = 10$ ms for GPS L1C), the acquisition detectors have different distributions.

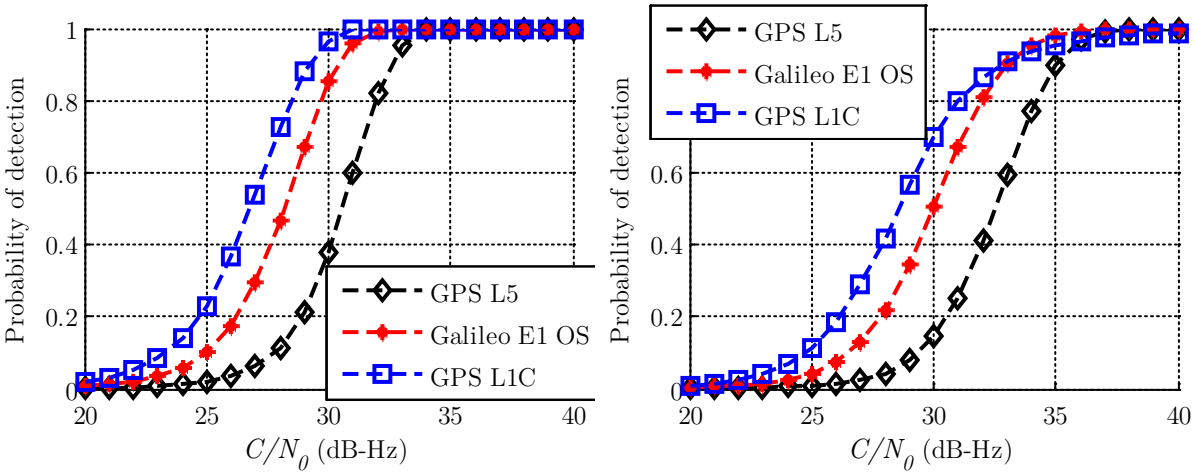

(a) No bit sign transition (b) Acquisition using both components

Figure 4.31 Probabilities of detection for $T_I = 20$ ms when considering or not bit sign transitions (modernized GNSS signals)

. When considering the absence of bit sign transition on both components, the best probability of detection is for the signal for which the coherent integration time is the longest (GPS L1C in Figure 4.31(a)). When considering bit sign transition on both components, the average probabilities of detection are obviously degraded. For GPS L1C, over 20 ms, at best there can be 4 bit sign transitions (few compared to 40 for GPS L5) but the effect of a bit sign transition is stronger for longer coherent integration time and this explains why for high C/N_0, the GPS L1C average probability of detection is lower than the Galileo E1 OS and GPS L5 average probabilities of detection Figure 4.31(b)).

This result on the new GNSS signals can be compared to the results provided for GPS L1 C/A. The conclusions stay unchanged, even if the number of bit sign transitions is higher for the modernized GNSS signals. Indeed, the average probabilities of detection are higher when the coherent integration time is 10 ms (GPS L5), the worst case being 1 ms (GPS L5).

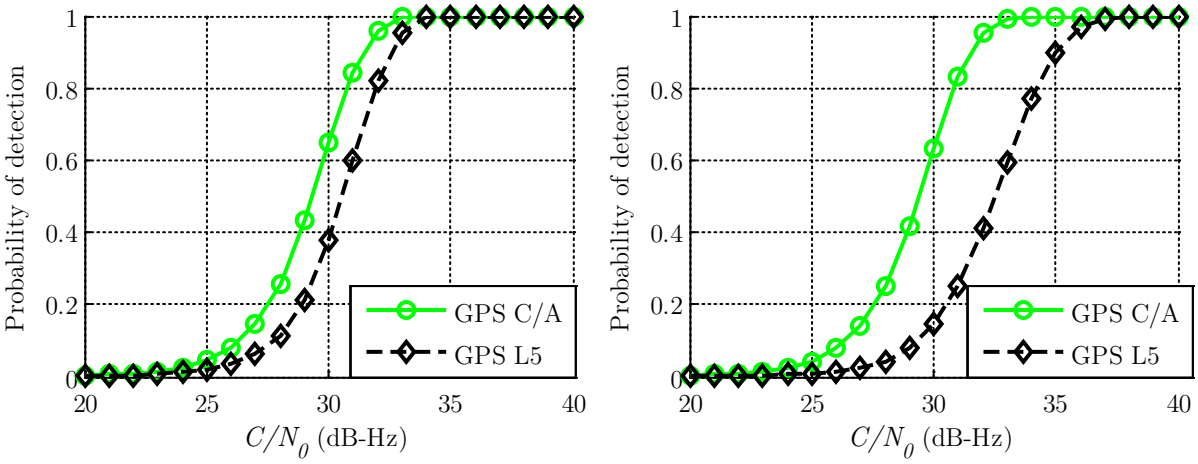

(a) No bit sign transition (b) Bit sign transition

Figure 4.32 Probabilities of detection when considering or not bit sign transitions on T_I =20 ms and $T_C = 1$ ms for GPS L1 C/A and GPS L5

This study can go further by comparing the acquisition performance of new GNSS signals with GPS L1 C/A on the same coherent integration time and for a dwell time of $T_I = 20$ ms. Figure 4.32, Figure 4.33 and Figure 4.34 present the probability of detection when not considering bit sign transitions and the average probability of detection for GPS L1 C/A and for a modernized GNSS signal on the same coherent integration time. GPS L1 C/A is represented by a continuous curve whereas the modernized GNSS signal is represented by a dashed curve.

When considering absence of bit sign transition (Figures(a)), the GPS L1 C/A probability of detection is always higher than the associated modernized GNSS signal probability of detection. A difference of around 1 dB can be observed between GPS L1 C/A and modernized GNSS signals (the shorter the coherent integration time, the higher the difference is). From the statistical point of view, this is due to the distribution of the acquisition detector which has only $2K$ degrees of freedom for GPS L1 C/A instead of $4K$ for the other signals that have data/pilot components) for the same integration time KT_C and the same signal power. Obviously, if only one component is acquired (which implies a loss of 3 dB), the probability of detection is highly attenuated, as presented in example, in Figure 4.33).

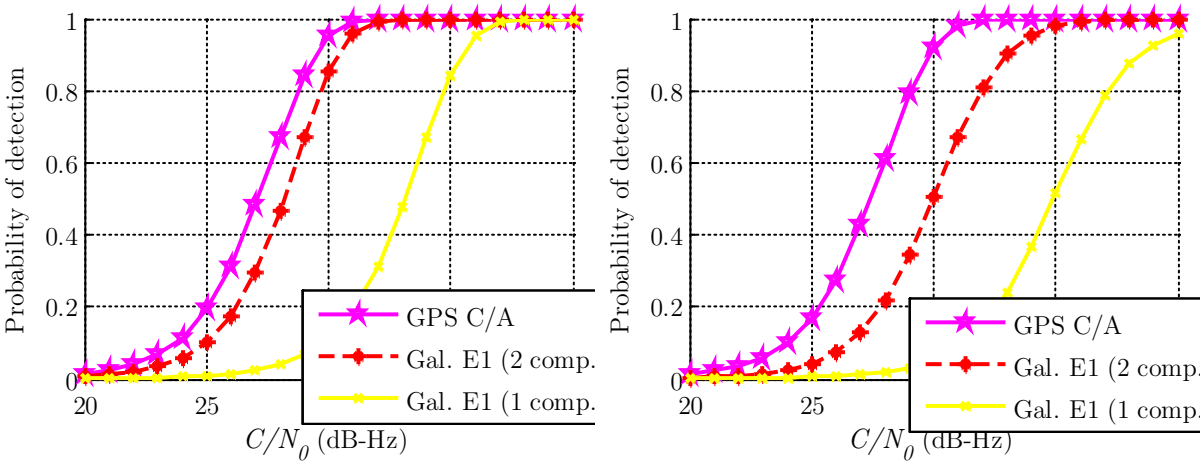

(a) No bit sign transition

(b) Bit sign transition

Figure 4.33 Probabilities of detection when considering or not bit sign transitions on $T_I = 20$ ms and $T_C = 4$ ms for GPS L1 C/A and Galileo E1 OS

When considering bit sign transitions, the average probabilities of detection for modernized GNSS signals are more affected than the average probability of detection for GPS L1 C/A, in particular for the shortest coherent integration time where a difference of more than 3 dB is observed.

From the point of view of the acquisition performance, it appears then clear that it is essential to consider the presence of data when deciding upon the acquisition parameters, in particular for modernized GNSS signals for which a Transition-Insensitive acquisition method seems necessary. However, this can imply acquisition execution times longer than for classical acquisition methods which are not Transition-Insensitive.

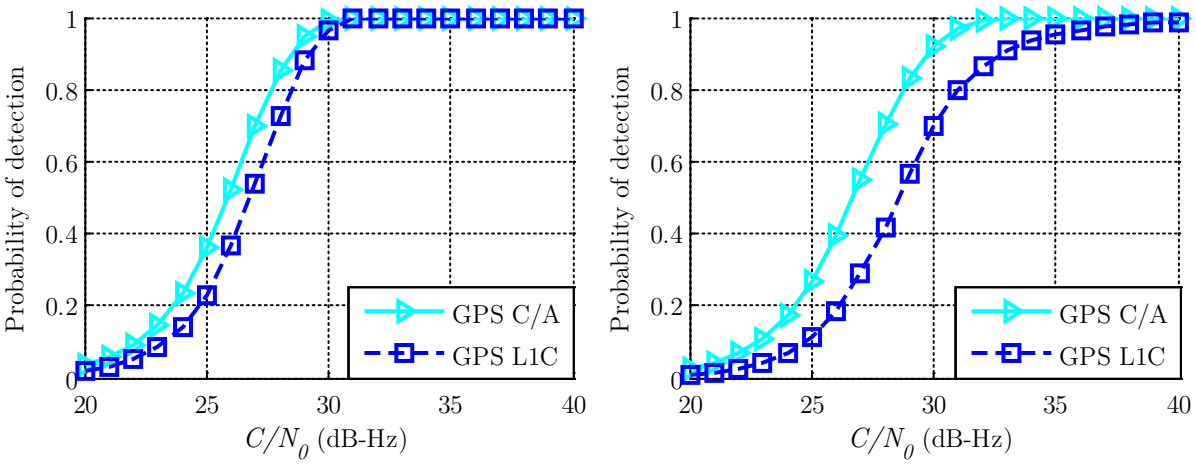

(a) No bit sign transition

(b) Bit sign transition

Figure 4.34 Probabilities of detection when considering or not bit sign transitions on $T_I = 20$ ms and $T_C = 10$ ms for GPS L1 C/A and GPS L1C

4.5 Discussion

To conclude this chapter on the main point of acquisition performance degradation, some results on the joint effect of 2 sources of degradations are presented. In Table 4.6 and Table 4.7, the required integration time to reach a probability of detection of 95% for a C/N_0 of 27 dB-Hz in several cases for GPS L1 C/A and Galileo E1 OS is provided. The first line provides the integration time and the optimal coherent integration time for GPS L1 C/A. For each probability of detection case, in the line, there is a value in italics (higher than 95%) and the corresponding column gives the required integration time.

The second step consists in evaluating the joint effect of several sources of acquisition degradations. To evaluate the effect of the code Doppler on the probability of detection, the average probability of detection taken on 6 values of Doppler frequency (0, 2, 4, 6, 8 and 10 kHz) $P_{D,f_D}(t_0 = 0, \varepsilon_{f_D} = 0)$ is provided. In this case, it is assumed that there is no code delay and Doppler frequency initial errors and is computed for a sampling frequency of 40.96 MHz. The probability of detection is computed by means of non-coherent summations and is taken for the maximum amplitude and this implies a resulting non-null code delay error.

For GPS L1 C/A, where no errors on the code delay and Doppler frequency are considered and no data modulation, $T_I = 40$ ms is needed (with a coherent integration time of 10 ms or 20 ms) for $P_D(t_0 = 0, \varepsilon_{f_D} = 0, \varepsilon_\tau = 0)$ higher than 95%. $T_I = 60$ ms is the optimal integration time when taking the average probability of detection on the code delay and Doppler frequency errors and no data modulation $P_{D,(\varepsilon_{f_D},\varepsilon_\tau)}(t_0 = 0)$, the associated coherent integration time is (5 or 10 ms). It is also the optimal required time when taking the average probabilities of detection on the bit sign transition location (and no Doppler frequency and code delay errors) $P_{D,t_0}(\varepsilon_{f_D} = 0, \varepsilon_\tau = 0)$ but the optimal coherent integration time is 20 ms. When considering

the average probability of detection on the code delay, Doppler frequency errors and on the bit sign transition location when data modulates the signal, the required integration time becomes $T_I = 100$ ms.

If the Galileo E1 OS required integration time is compared to GPS L1 C/A ones, they are significantly higher (more than twice). Indeed, in the basic case (no residual code delay and Doppler frequency errors) 80 ms are required. If the average probability of detection is considered over the residual errors and over bit sign transition location, the required integration times are 160 and 200 ms respectively. For GPS L1 C/A, in both cases, it is the same required integration time. Galileo E1 OS suffers more from the bit sign transition location.

T_I	40 ms		60 ms			100 ms
T_c	10 ms	20 ms	5 ms	10 ms	20 ms	10 ms
$P_D(t_0 = 0, \varepsilon_{f_D} = 0, \varepsilon_\tau = 0)$	*96.7%*	*98.99%*	98.41%	99.78%	99.27%	100%
$P_{D,f_D}(t_0 = 0, \varepsilon_{f_D} = 0)$	94.83%	98.25%	96.18%	99.25%	99.86%	97.74%
$P_{D,(\varepsilon_{f_D},\varepsilon_\tau)}(t_0 = 0)$	87.03%	76.29%	*96.11%*	*96.94%*	87%	99.87%
$P_{D,t_0}(\varepsilon_{f_D} = 0, \varepsilon_\tau = 0)$	79.75%	89.26%	83.14%	93.44%	*97.62%*	99.37%
$P_{D,(t_0,\varepsilon_{f_D},\varepsilon_\tau)}$	66.56%	62.55%	77.42%	84.53%	77.58%	*96.93%*

Table 4.6 Average probabilities of detection for different integration times and considering potential sources of acquisition degradations at 27 dB-Hz (GPS L1 C/A)

In terms of probability of detection performance degradations, it can be noted that the impact of the code Doppler is not negligible for Galileo E1 OS as it can be for GPS L1 C/A. Indeed, for GPS L1 C/A, for all of the considered integration times, the losses on the probability of detection when not considering any residual errors and data modulation are no more than 2.5% (maximum losses for the longest integration time). On the contrary, for Galileo E1 OS, since the integration times are longer and as studied, the BOC-modulated signals really suffer from the code Doppler, the detection is compromised (less than 60%). As it can be observed, for both signals, it seems appropriate to consider residual errors and bit sign transition impacts on the acquisition performance.

	80 ms	160 ms	200 ms	372 ms
$P_D(t_0 = 0, \varepsilon_{f_D} = 0, \varepsilon_\tau = 0)$	*95.45%*	99.98%	100%	100%
$P_{D,f_D}(t_0 = 0, \varepsilon_{f_D} = 0)$	44.52%	59.66%	44.45%	40.59%
$P_{D,(\varepsilon_{f_D},\varepsilon_\tau)}(t_0 = 0)$	70.56%	*95.06%*	98.03%	99.96%
$P_{D,t_0}(\varepsilon_{f_D} = 0, \varepsilon_\tau = 0)$	63.26%	90.19%	*95.21%*	99.84%
$P_{D,(t_0,\varepsilon_{f_D},\varepsilon_\tau)}$	37.69%	68.81%	78.15%	95.16%

Table 4.7 Average probabilities of detection for different integration times and considering potential sources of acquisition degradations at 27 dB-Hz (Galileo E1 OS)

Chapter 5
Acquisition Method based on DBZP

In this chapter, the well-known Double-Block Zero-Padding (DBZP) acquisition method, known for his efficiency, is deeply analyzed to highlight its strengths and weaknesses. As it will be proved, the DBZP suffers from the occurrence of data bit transitions. As previously explained, the acquisition of the modernized GNSS signals can be seriously degraded by the presence of bit sign transitions at each spreading code period. It appears clear that there is a need to use an acquisition method which is bit sign transition insensitive. To tackle this problem an improved and innovative acquisition method, the Double-Block Zero-Padding Transition Insensitive (DBZPTI) is proposed. Besides this major improvement, other developments are proposed to limit losses on the acquisition performance, in particular due to the incoming signal Doppler frequency. The chapter will focus on the study of the acquisition of weak Galileo E1 OS signals with a wide Doppler frequency uncertainty. The performance study and the results point out the efficiency of this method for the acquisition of weak Galileo E1 OS signals, in comparison with a classical acquisition method which is also data insensitive.

Contents

5.1 Double-Block Zero-Padding (DBZP) method 106
5.1.1 DBZP method algorithm 106
5.1.2 DBZP performance study 113
5.2 Proposed DBZP improvements 118
5.2.1 Data transition insensitivity 119
5.2.2 Dependence on the incoming Doppler frequency 120
5.2.3 Sub-sampling 124
5.3 Software implementation and results 125
5.3.1 Matlab implementation 125
5.3.2 Computation efficiency 126
5.4 Discussion 130

5.1 Double-Block Zero-Padding (DBZP) method

As previously seen, several acquisition methods have been developed that aim at accelerating the correlation process. In many of these, the search is parallelized based on the discrete Fourier transform, implemented using Fast Fourier Transform (FFT) algorithms. In this case, the complexity of such a method depends on the size of the vector over which the FFT is executed, and the number of FFTs computed. One approach to optimize the correlation process execution time is to deal with vectors which size is a fraction of the spreading code period. The most well-known acquisition method based on this approach is the Double-Block Zero-Padding as presented initially in literature in [Lin *et al.*, 1999]. It has been demonstrated by [Lin & Tsui, 2000] and [Chibout, 2008] that the DBZP consumes less time and power compared to other classical acquisition methods, also based on FFTs.

5.1.1 DBZP method algorithm

The general mathematical model of the Double-Block Zero-Padding acquisition method can be described in 5 steps. The block diagram of the DBZP method is shown in Figure 5.6. The concept of the DBZP is the use of many partial correlations over a duration equivalent to a few tens of chips. To do so, the incoming signal and the local code are split into blocks.

5.1.1.1 Initialization

The input parameters of the DBZP are:

- The coherent integration time T_C,
- The Doppler uncertainty range $[f_{D,Min}, f_{D,Max}]$ where $f_{D,Max}$ is the maximum expected value of the incoming Doppler frequency and $f_{D,Min}$ the minimum. The central frequency of the Doppler frequency range is denoted $f_{D,Med}$.

In a typical acquisition scheme, the coherent integration time is in general chosen to be equal to the spreading code period T_{c_1}. For an application on GPS L1 C/A signal, it can be several spreading code periods.

The Doppler frequency range is in general symmetric with respect to 0 when there is no a priori knowledge on the Doppler. Even if the Doppler frequency range is not symmetric, it is easy to go to the case $f_{D,Med} = 0$, by multiplying the local carrier by $\exp(-2i\pi f_{D,Med} n T_s)$ with $(n = 0, 1, \dots, N_s - 1)$. Then $f_{D,Min} = -f_{D,Max}$.

Unlike the serial search acquisition method, the number of DBZP Doppler frequency bins and their resolutions are fixed by the algorithm and cannot be chosen by the user. The number of Doppler frequency bins, denoted N_b is determined by:

$$N_b = \frac{f_{D,Max} - f_{D,Min}}{\frac{1}{T_C}} = 2 f_{D,Max} \times T_C \tag{5.1}$$

The number of code delay blocks is chosen to be equal to the number of Doppler frequency bins [Ziedan, 2006]. It can be deduced that:

- The duration of one block t_b is:

$$t_b = \frac{T_C}{N_b} = \frac{1}{2f_{D,Max}} \tag{5.2}$$

- The number of samples per block N_{spb} is equal to:

$$N_{spb} = \frac{N_s}{N_b} = t_b \times f_s \tag{5.3}$$

- The Doppler frequency resolution Δ_f is:

$$\Delta_f = \frac{2f_{D,Max}}{N_b} = \frac{1}{T_C} \tag{5.4}$$

For example, for an incoming Doppler frequency between -10 and 10 kHz, the duration of one block t_b is equal to 50 µs (a twentieth of one millisecond, equivalent to $N_{cpb} = 51.15$ chips). For a coherent integration time of $T_C = 4$ ms, the Doppler frequency resolution, Δ_f, is 250 Hz, which is twice wider than for the serial search acquisition method for which $\Delta_f = 1 / 2T_C$. In the time domain, the resolution Δ_τ corresponds to the sampling period T_s. Indeed, the code delay uncertainty space is discretized at the sampling frequency. There are thus as many possible code delay (N_τ) as the number of sample per spreading code period (N_s).

5.1.1.2 Step 1: Pre-processing of the incoming signal

Firstly, the received signal is pre-processed. Indeed, the received complex signal is converted into baseband by multiplying it by a complex carrier $\exp(-2i\pi f_{IF} n T_s)$ depending only on the intermediate frequency f_{IF}, which means that the local complex carrier does not try to compensate the incoming Doppler frequency. It is important to understand that only one carrier replica, which does not depend on a Doppler frequency estimate, is generated.

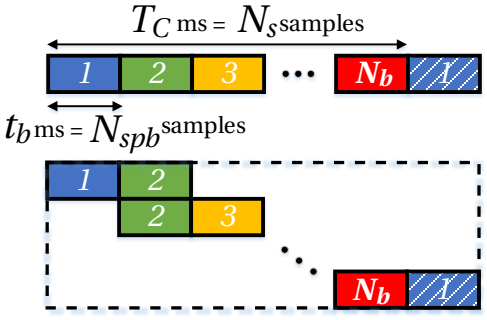

Figure 5.1 Pre-processing of the incoming signal

The resulting T_C-long baseband samples are arranged into N_b blocks of equal length. Each couple of two consecutive blocks is grouped to form N_b blocks of size $2N_{spb}$ (thus the name "Double-Block") and denoted B^s_{l+1}, with $l = 0, 1, \ldots, N_b - 1$ referring to as the block index. The last block is combined with additional samples as illustrated in Figure 5.1.

5.1.1.3 Step 2: Generation of the local spreading code

The second step consists in conditioning the local spreading code. As for the incoming signal, T_C ms of the local code are generated and splitted up into N_b blocks of N_{spb} samples. Then, each block is zero-padded and denoted B^c_{l+1}, this means that N_{spb} samples of value 0 are appended to each block as illustrated in Figure 5.2, where the N_{spb}-block composed of 0s is represented by a black box.

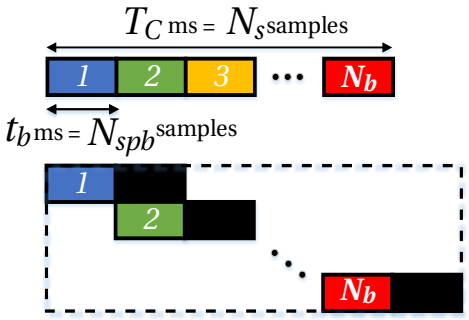

Figure 5.2 Pre-processing of the local code

5.1.1.4 Step 3: Partial correlations on the split signals

The third step aims at evaluating the correlation output, computing it by means of FFT. The first $2N_{spb}$-samples block of the incoming signal is circularly correlated with the first zero-padded code block. This results in a partial circular correlation, and only the first half is preserved.

Some points in this step should be developed. The N_{spb} output samples represent a partial correlation on t_b ms (much shorter than a spreading code period) over N_{spb} possible code delays. The partial correlation is illustrated in Figure 5.3 and can be compared with the full correlation.

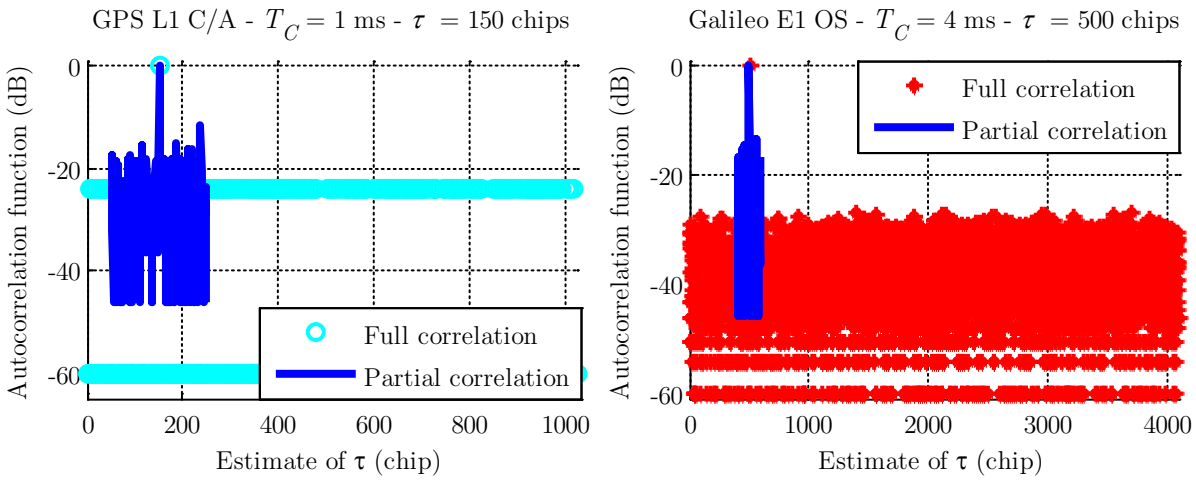

(a) GPS L1 C/A (b) Galileo E1 OS

Figure 5.3 Full and partial GPS L1 C/A and Galileo E1 OS autocorrelations

When the local and incoming spreading codes are perfectly aligned (or the estimated code delay is in the neighborhood of the right code delay), the normalized partial correlation is equivalent to the normalized full autocorrelation. The drawback of the partial correlation is that the correlation is done on only a part of the whole spreading code and thus the periodicity and the properties of the spreading code are not kept (the isolation is degraded as it can be observed in Figure 5.3).

In the DBZP acquisition method, the Zero-Padding is used to go over the non-periodicity of the partial code blocks. Indeed, as illustrated in Figure 5.4(a), when the zero-padding is not used, the normalized autocorrelation function peak is highly attenuated. On the contrary, when the partial correlation is computed using $2t_b$ of signal and zero-padding the local partial code, the normalized autocorrelation function peak is highly isolated and not attenuated (Figure 5.4(b), even when there is a bit sign transition). Let us note that only the first part of the correlation is kept, corresponding to the one with the potential peak. On the figures, the partial correlation is done over t_b for a code delay of 27 chips

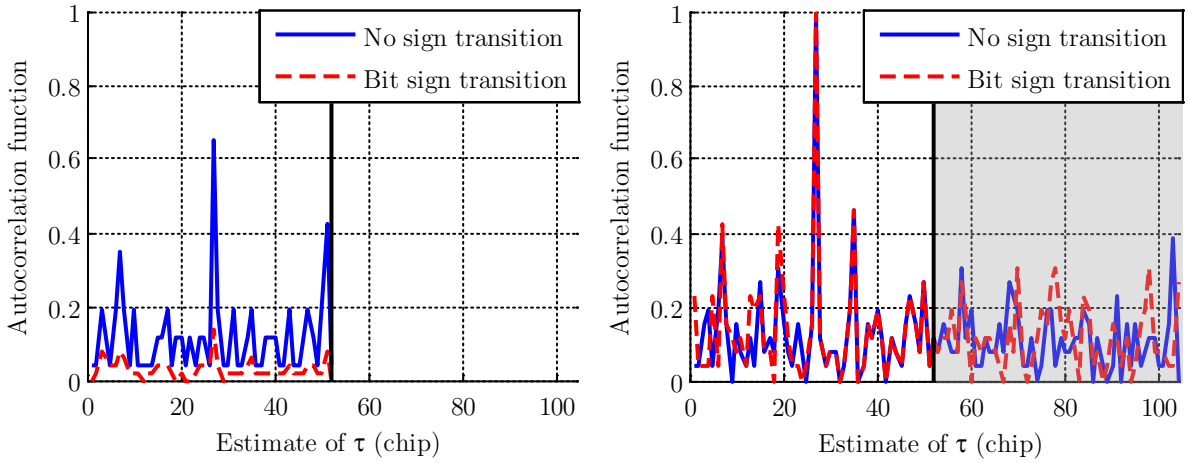

(a) Without zero-padding (b) With zero-padding

Figure 5.4 Illustration of the use of the zero-padding for the partial correlation

Knowing that $l = 0, 1, .., N_b - 1$ defines the code block pair, the coherent integration interval is assumed to be:

$$[T_0 + (k-1)T_C + lt_b, T_0 + (k-1)T_C + (l+1)t_b] \tag{5.5}$$

Furthermore, the phase at $t = T_0 + (k-1)T_C + lt_b$ is assumed to be:

$$\phi_0(k,l) = 2\pi f_D(T_0 + (k-1)T_C + lt_b) \tag{5.6}$$

Based on the classical correlator outputs (presented in the previous chapter), the partial in-phase correlator output is:

$$\widetilde{I}_l(k) = \frac{1}{t_b}\int_{T_0+(k-1)T_C+lt_b}^{T_0+(k-1)T_C+(l+1)t_b} B_{l+1}^c(t) \times B_{l+1}^s(t)dt \tag{5.7}$$

In the end, for small Doppler frequency and code delay errors (refer to section 3.1.2.3), their expressions are:

$$\begin{aligned}\tilde{I}_l(k) &= \frac{A}{2} d(k) \tilde{R}_{c_1}\left(\varepsilon_\tau(k,l)\right) \cos\left(\pi f_D t_b + \varepsilon_{\phi_0}(k,l)\right) \operatorname{sinc}(\pi f_D t_b) + \eta_{\tilde{I}_l}(k) \\ \tilde{Q}_l(k) &= \frac{A}{2} d(k) \tilde{R}_{c_1}\left(\varepsilon_\tau(k,l)\right) \sin\left(\pi f_D t_b + \varepsilon_{\phi_0}(k,l)\right) \operatorname{sinc}(\pi f_D t_b) + \eta_{\widetilde{Q_l}}(k)\end{aligned} \tag{5.8}$$

where:

- $l = 0, 1, \ldots, N_b - 1$ stands for the l-th partial correlation,
- $\tilde{I}_l$ and $\widetilde{Q_l}$ are the in-phase and quadrature phase l-th partial correlator output,
- $\tilde{R}_{c_1}$ is the partial autocorrelation function,
- $\varepsilon_\tau(k,l)$ is the code delay in $[T_0 + (k-1)T_C + lt_b\ ,\ T_0 + (k-1)T_C + (l+1)t_b]$. Strictly speaking, $\varepsilon_\tau(k,l)$ depends on the slice of time, but it is assumed that the parameters of the incoming signal and local replica are constant during the correlation process and then, it is assumed that $\varepsilon_\tau(k,l) = \varepsilon_\tau$,
- $\varepsilon_{\phi_0}(k,l) = \phi_0(k,l) - \hat{\phi}_0$ is the carrier phase error at the beginning of the interval $[T_0 + (k-1)T_C + lt_b\ ,\ T_0 + (k-1)T_C + (l+1)t_b]$,
- $\eta_{\tilde{I}_l}$ and $\eta_{\widetilde{Q_l}}$ are the noises at the partial correlator outputs with a variance of

$$\sigma^2_{\tilde{\eta}} = \frac{N_0}{4t_b} = \frac{N_0 N_b}{4T_C} \tag{5.9}$$

It is worth noting that the phase $\pi f_D t_b + \varepsilon_{\phi_0}(k,l)$ depends on:

- The incoming Doppler frequency f_D (if $\hat{f}_D$ is null, otherwise on $\varepsilon_{f_D} = f_D - \hat{f}_D$),
- The $(l+1)^{th}$ signal block B^s_{l+1}

The partial correlator outputs can be stored in a matrix of size $N_b \times N_{spb}$ where:

- There are as many columns as possible code delays: each column contains all the partial correlator outputs for a given code delay error,
- There are as many rows as partial correlations: each row contains the partial correlator outputs for a given slice of time

5.1.1.5 Step 4: Application of the FFT

An N_b-point FFT is applied to the set of the partial correlation outputs corresponding to a given code delay. This permits to determine the Doppler frequency of the incoming signal.

It can be assumed that $\frac{A}{2}\tilde{R}_{c_1}(\varepsilon_\tau)\operatorname{sinc}(\pi f_D t_b)$ is constant for all l in $[\![0, N_{b-1}]\!]$ and can be approximated by $\frac{A}{2}R_{c_1}(\varepsilon_\tau)\operatorname{sinc}(\pi f_D t_b)$ in the neighborhood of $\varepsilon_\tau = 0$. Thus, the FFT of the partial correlator outputs provides the DBZP outputs, denoted $\iota(k,m)$ and $\rho(k,m)$, which are (development in *Appendix F.1*):

$$\begin{aligned}\iota(k,m) &= \mathcal{F}\left(\widetilde{I_l}(k)\right) \\ &= \frac{A}{2} d(k) R_{c_1}(\varepsilon_\tau)\,\mathrm{sinc}(\pi f_D t_b)\,\mathcal{F}\left(\cos\left(\pi f_D t_b + 2\pi f_D l t_b + \varepsilon_{\phi_0}(k,0)\right)\right) \\ &\quad + \eta_\iota(m) \\ &= \frac{A}{2} d(k) R_{c_1}(\varepsilon_\tau)\,\mathrm{sinc}(\pi f_D t_b)\, N_b \frac{\mathrm{sinc}\left(\pi(m - f_D T_C)\right)}{\mathrm{sinc}\left(\pi \frac{m - f_D T_C}{N_b}\right)} \cos\left(\phi(k)\right) + \eta_\iota(m) \\ \rho(k,m) &= \mathcal{F}\left(\widetilde{Q_l}(k)\right) \\ &= \frac{A}{2} d(k) R_{c_1}(\varepsilon_\tau)\,\mathrm{sinc}(\pi f_D t_b)\, N_b \frac{\mathrm{sinc}\left(\pi(m - f_D T_C)\right)}{\mathrm{sinc}\left(\pi \frac{m - f_D T_C}{N_b}\right)} \sin\left(\phi(k)\right) + \eta_\rho(m)\end{aligned} \tag{5.10}$$

where:

- $\phi(k) = \pi f_D t_b + \pi \frac{(N_b-1)}{N_b}(f_D T_C - m) + \varepsilon_{\phi_0}(k,0)$,
- $m = 0, \ldots, N_b - 1$ is the point where the FFT is taken and corresponds to a Doppler frequency bin,
- η_ι and η_ρ are the complex noises at the DBZP outputs, which expression and variance $\sigma^2_{\eta_{DBZP}}$ is developed in *Appendix F.1*:

$$\sigma^2_{\eta_{DBZP}} = \frac{N_b^2 N_0}{4T_C} \tag{5.11}$$

It is interesting to note that the width of the main peak of the sinc term $\mathrm{sinc}(\pi f_D t_b)$ is $2\frac{N_b}{T_C}$ which is larger than the main peak of the sinc term $\mathrm{sinc}(\pi \varepsilon_{f_D} T_C)$ (classical serial search) which is $2\frac{1}{T_C}$.

However, due to the additional presence of the second sinc term, in the frequency domain, the DBZP output should provide a peak for the frequency bin that corresponds to the right estimation of the incoming Doppler frequency as presented in Figure 5.5, for a right estimation of the code delay. The peak width corresponds to the frequency resolution $1/T_C$.

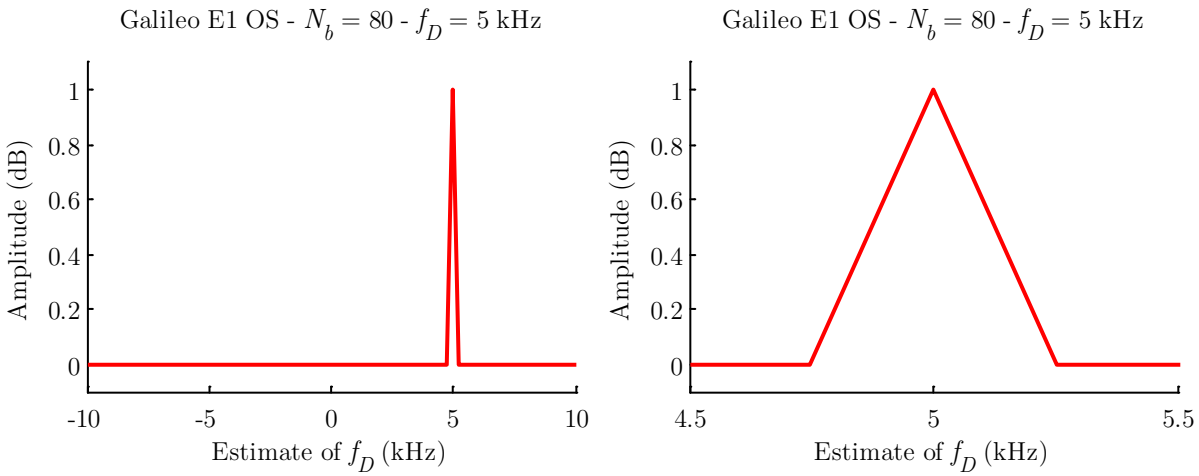

(a) Entire frequency domain (b) Zoom

Figure 5.5 DBZP output in frequency domain

5.1.1.6 Step 5: Permutation of code blocks

In the process previously described, only code delays in the first code delay time slice $[0, t_b[$ are tested. To try all code delays, the local code blocks are circularly permutated: the N_b-th block becomes the first block, the first block becomes the second block, etc (the permutation is illustrated in Figure 5.6). N_r permutations like this can be done to explore the whole code delays. The incoming signal blocks are kept unchanged.

Let us note that if the coherent integration time T_C is equal to the spreading code period, the number of circular permutations corresponds to the number of blocks $N_r = N_b$. However, if T_C is longer than one spreading code period (e.g. for GPS L1 C/A with $T_C = 10$ ms [Ziedan, 2006]), the number of circular permutations reduces to $N_r = \frac{N_b}{T_C/T_{c_1}}$ due to the spreading code periodicity. Indeed, the code block $B^c_{N_r+1}$ is equal to the code block B^c_1 because the first N_r blocks describe spreading code period and the next N_r blocks are a repetition of the first N_r blocks.

At the end, the DBZP matrix output is of size $(N_b \times N_r N_{spb})$, each row corresponding to a Doppler frequency bin and each column to a code delay.

As a synthesis, the block diagram of the DBZP is presented in Figure 5.6.

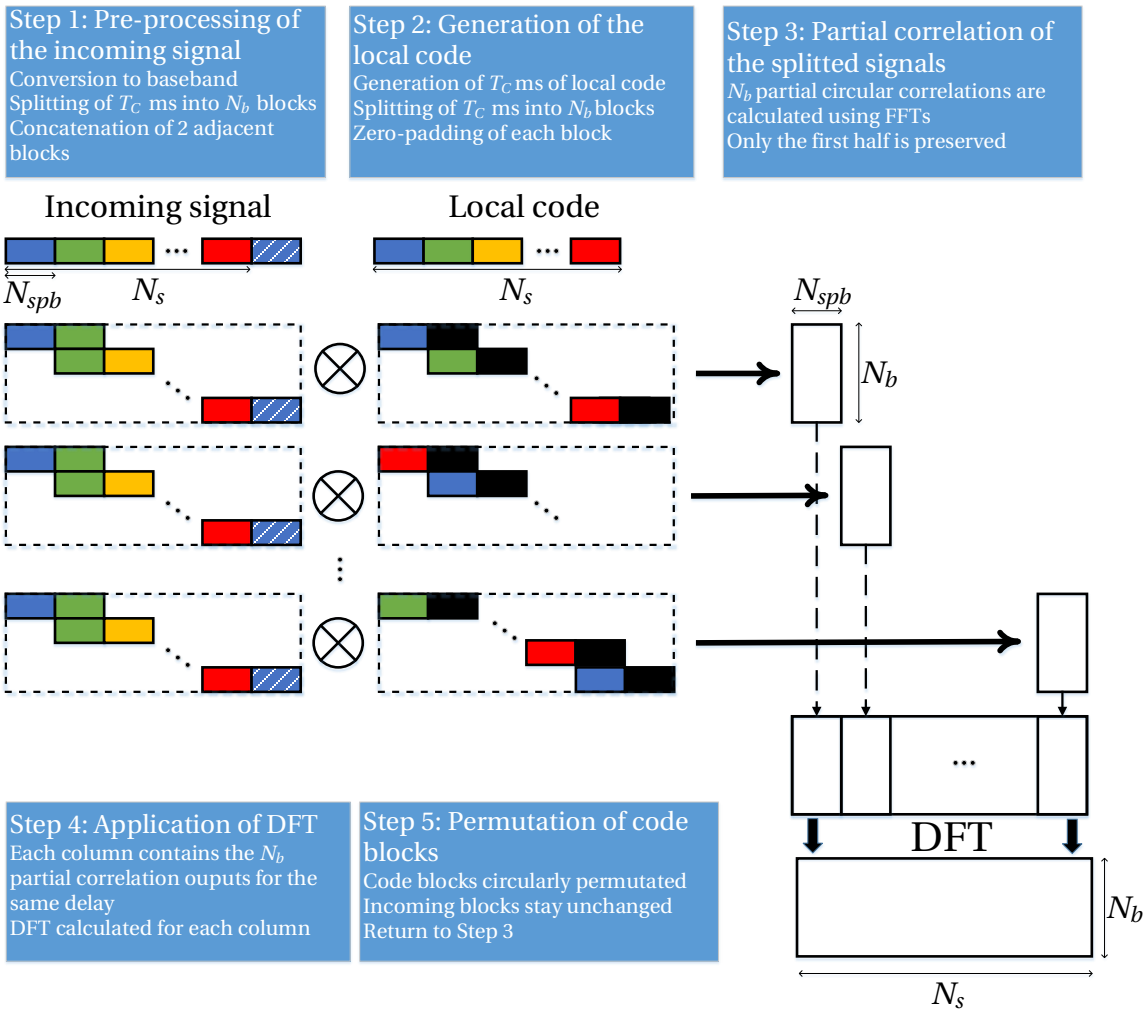

Figure 5.6 Double-Block Zero-Padding (DBZP) method block diagram

5.1.2 DBZP performance study

The performance study of the DBZP is presented for the acquisition of the GPS L1 C/A signal. It is also valid for the case of the acquisition of one component of the modernized GNSS signals. It can be easily extended for the acquisition of both components of modernized GNSS signals.

5.1.2.1 DBZP criterion

The normalized DBZP acquisition detector is:

$$T = \sum_{k=1}^{K} \left(\left(\frac{\iota(k,m)}{\sigma_{\eta_{DBZP}}} \right)^2 + \left(\frac{\rho(k,m)}{\sigma_{\eta_{DBZP}}} \right)^2 \right) \tag{5.12}$$

Under H_0:

Under the null hypothesis, the DBZP outputs (5.10) can be seen as noise only η_ι and η_ρ. Then the normalized acquisition detector under the null hypothesis follows a χ^2 distribution with $2K$ degrees of freedom:

$$T \quad \sim_{H_0} \quad \chi^2(2K) \tag{5.13}$$

where η_ι and η_ρ are assumed to be complex Gaussian noise with null mean and variance σ_ι^2 and then $\frac{\eta_\iota}{\sigma_{\eta_{DBZP}}}$ and $\frac{\eta_\rho}{\sigma_{\eta_{DBZP}}}$ are unit Gaussian distribution. $\left(\frac{\eta_\iota}{\sigma_{\eta_{DBZP}}}\right)^2$ follows a centered χ^2 distribution.

The knowledge of the desired probability of false alarm permits to determine the acquisition threshold:

$$\begin{aligned} P_{FA} &= P_{H_0}(T > \gamma) = 1 - F_Z(\gamma) \\ \gamma &= F_Z^{-1}(1 - P_{FA}) \end{aligned} \tag{5.14}$$

where $Z \sim \chi^2(2K)$ and F_Z is its cumulative distribution function

Under H_1:

The useful signal is assumed to be present and the code delay error ε_τ is assumed small (less than 1 chip). In this case, the distributions of the DBZP outputs are:

$$\begin{aligned} \iota(k,m) &\sim \mathcal{N}\left(E\left(\iota(k,m)\right), \sigma^2_{\eta_{DBZP}}\right) \\ \rho(k,m) &\sim \mathcal{N}\left(E\left(\rho(k,m)\right), \sigma^2_{\eta_{DBZP}}\right) \end{aligned} \tag{5.15}$$

With

$$\begin{aligned} E\left(\iota(k,m)\right) &= \frac{A}{2} R_{c_1}(\varepsilon_\tau)\, \mathrm{sinc}(\pi f_D t_b)\, N_b \frac{\mathrm{sinc}\left(\pi(m - f_D T_C)\right)}{\mathrm{sinc}\left(\pi \frac{m - f_D T_C}{N_b}\right)} \cos\left(\phi(k)\right) \\ E\left(\rho(k,m)\right) &= \frac{A}{2} R_{c_1}(\varepsilon_\tau)\, \mathrm{sinc}(\pi f_D t_b)\, N_b \frac{\mathrm{sinc}\left(\pi(m - f_D T_C)\right)}{\mathrm{sinc}\left(\pi \frac{m - f_D T_C}{N_b}\right)} \sin\left(\phi(k)\right) \end{aligned} \tag{5.16}$$

Under the alternative hypothesis, the normalized acquisition detector follows a non-central χ^2 distribution with $2K$ degrees of freedom:

$$T \sim_{H_1} \chi^2(2K, K\lambda) \tag{5.17}$$

The detector is then characterized by a non-central χ^2 distribution. Assuming that ε_τ is the same for all of the K DBZP outputs and does not depend on the slice of time, the non-centrality parameter is equal to $K \times \lambda$ with:

$$\begin{aligned}\lambda &= E^2\left(\frac{\iota(k,m)}{\sigma_{\eta_{DBZP}}}\right) + E^2\left(\frac{\rho(k,m)}{\sigma_{\eta_{DBZP}}}\right) \\ &\approx \frac{A^2}{N_0} T_C R_{c_1}^2(\varepsilon_\tau)\,\mathrm{sinc}^2(\pi f_D t_b)\frac{\mathrm{sinc}^2\big(\pi(m - f_D T_C)\big)}{\mathrm{sinc}^2\left(\pi\frac{m - f_D T_C}{N_b}\right)}\end{aligned} \tag{5.18}$$

The probability of detection P_D is then:

$$P_D = P_{H_1}(T > \gamma) = 1 - F_{\chi^2(2K,K\lambda)}(\gamma) \tag{5.19}$$

5.1.2.2 Strengths of the DBZP algorithm

- Signal-to-Noise Ratio

The Signal-to-Noise Ratio (SNR) at the DBZP output is first analyzed. The power of the noise P_{η_ι} at the DBZP output is:

$$P_{\eta_\iota} = \sigma^2_{\eta_{DBZP}} = \frac{N_b^2 N_0}{4T_C} \tag{5.20}$$

The power of the useful signal at the DBZP output, denoted P_s, is:

$$\begin{aligned}P_s &= \left(\frac{A}{2} R_{c_1}(\varepsilon_\tau) N_b\right)^2 \mathrm{sinc}^2(\pi f_D t_b)\frac{\mathrm{sinc}^2\big(\pi(m - f_D T_C)\big)}{\mathrm{sinc}^2\left(\pi\frac{m - f_D T_C}{N_b}\right)} \\ &\approx \frac{A^2}{4} R_{c_1}^2(\varepsilon_\tau) N_b^2\end{aligned} \tag{5.21}$$

Then the SNR is:

$$\frac{P_s}{P_{\eta_\iota}} \approx \frac{\frac{A^2}{4} R_{c_1}^2(\varepsilon_\tau) N_b^2}{\frac{N_b^2 N_0}{4T_C}} \approx \frac{A^2}{N_0} T_C \tag{5.22}$$

As presented in [Julien, 2008] for the classical acquisition method, it can be concluded that there is no additional noise when acquiring with the DBZP acquisition method compared to the classical acquisition method because the SNR at the correlator output and at the DBZP output are the same. Both acquisition methods are equivalent in terms of SNR at the output.

- Width of the peak

In the frequency domain, the width of the main peak (for the right code delay and for the right incoming Doppler frequency) is the same for the DBZP acquisition method $1/T_C$ (Figure 5.5). The width of the main peak corresponds to the interval between two FFT outputs m.

5.1.2.3 Weaknesses of the DBZP algorithm

- Code Doppler impact on partial correlations

As explained in the previous chapter, the code Doppler can have a significant impact on the acquisition performance. For the DBZP, in (5.8), the assumption of the constancy of the

partial autocorrelation function was taken (for all $l = 0, 1, \dots, N_b - 1$, $\tilde{R}_{c_1}\left(\varepsilon_\tau(k,l)\right) \approx R_{c_1}(\varepsilon_\tau)$). When considering code Doppler, this assumption is not valid anymore, and the autocorrelation function depends on l: $\tilde{R}_{c_1}\left(\varepsilon_\tau(l)\right)$. The application of the FFT (5.10) (development given in *Appendix F.1*) becomes:

$$\begin{aligned}&\mathcal{F}\left(\tilde{R}_{c_1}\left(\varepsilon_\tau(l)\right)\cos\left(2\pi f_D l t_b + \tilde{\phi}_0(k)\right)\right)\left(m_{m=0,\dots,N_b-1}\right)\\&\approx \mathrm{Re}\left(e^{i\tilde{\phi}_0(k)}\sum_{l=0}^{N_b-1} R_{c_1}\left(\varepsilon_\tau(k,l)\right)e^{2i\pi l\left(\frac{f_D T_C - m}{N_b}\right)}\right)\end{aligned} \tag{5.23}$$

Between the incoming signal blocks B_1^s and $B_{N_b}^s$, the time delay is $(N_b - 1)t_b$, which can be approximated by T_C. For $l = 0$, $R_{c_1}\left(\varepsilon_\tau(l)\right)$ is estimated to be 1 and should be compared to $R_{c_1}\left(\varepsilon_\tau(l)\right)$ for $l = N_b - 1$ (worst case). This is done in Table 5.1, for different incoming Doppler frequencies and signals.

$\varepsilon_\tau(N_b - 1) \approx T_C f_{c_1} \frac{f_D}{f_L}$		$f_D = 1$ kHz	$f_D = 5$ kHz	$f_D = 10$ kHz
GPS L1 C/A $T_C = 1$ ms $R_{c_1}(\varepsilon_\tau) \approx 1 - \lvert\varepsilon_\tau\rvert$	$\varepsilon_\tau(N_b - 1)$ (in chip)	0.00065	0.0032	0.0065
	$R_{c_1}\left(\varepsilon_\tau(N_b - 1)\right)$	0.999	0.997	0.993
Galileo E1 OS $T_C = 4$ ms $R_{c_1}(\varepsilon_\tau) \approx 1 - 3\lvert\varepsilon_\tau\rvert$	$\varepsilon_\tau(N_b - 1)$ (in chip)	0.0026	0.013	0.026
	$R_{c_1}\left(\varepsilon_\tau(N_b - 1)\right)$	0.992	0.961	0.922

Table 5.1 Impact of the code Doppler on the partial autocorrelation terms

In the worst case (maximum incoming Doppler frequency $f_D = 10$ kHz and the acquisition of the Galileo E1 OS signal), the last partial autocorrelation term seems to be attenuated (0.922). However, it should be noted that the phenomenon is taken in average (on the spreading code period) and the attenuation is less important.

The second impact of the code Doppler is on the code delay resolution. In an ideal case, the code delay resolution Δ_τ corresponds to the sampling period. But the code Doppler implies that the distance between two code delay errors is reduced or expanded because the code Doppler changes the spreading code period.

In the original DBZP version, only one code replica, not code Doppler compensated, is used but [Ziedan, 2006] proposes a variant of the DBZP handling code Doppler in the Modified DBZP (MDBZP). The code Doppler problem is handled in the MDBZP by dividing the whole Doppler frequency range into several ranges. A local code replica is generated taking into account a code Doppler associated with the middle frequency of the smaller frequency range. The DBZP is then computed for all of the frequency ranges. Clearly, this can improve the DBZP performance but a trade-off should be chosen between the number of local code replicas and the performance gain. Indeed, the higher the number of local code replicas is, the better the sensitivity performance is but also the higher the execution time is.

- Dependence on the incoming Doppler frequency

The useful part of the DBZP output (5.10) has 2 terms that depend on the incoming Doppler frequency f_D, which is very unusual compared to the classical acquisition scheme.

First, the amplitude of $\text{sinc}(\pi f_D t_b)$ entails a degradation of the amplitude of the useful part of the criterion for high values of the incoming Doppler frequency (in absolute value), which leads to a maximum loss of 4 dB as it can be observed in Figure 5.7 (a).

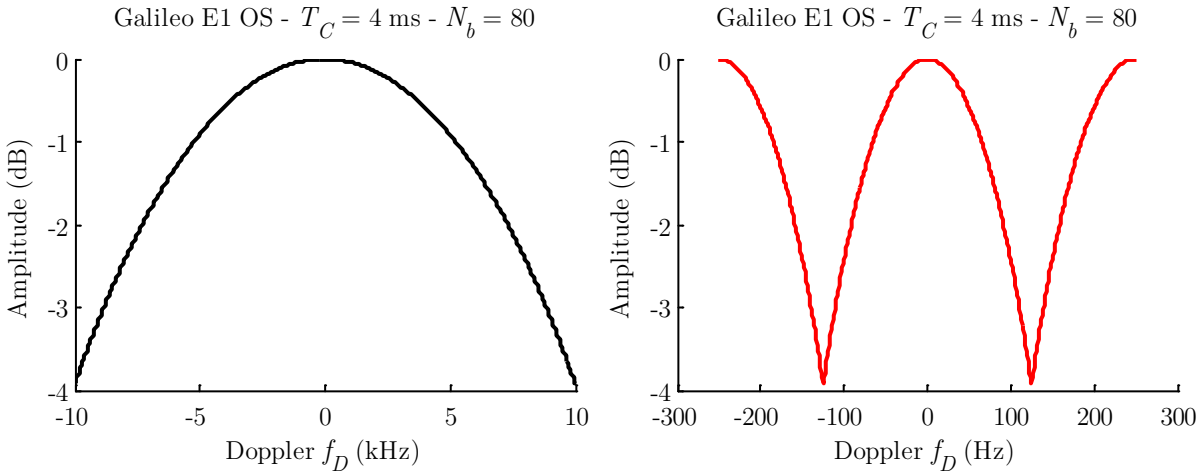

(a) $\text{sinc}(\pi f_D t_b)$ (b) $\frac{\text{sinc}(\pi(m-f_D T_C))}{\text{sinc}\left(\pi\frac{m-f_D T_C}{N_b}\right)}$

Figure 5.7 Degradations of the criterion due to incoming Doppler frequency

Let's remark that:

$$f_D t_b = \frac{T_C}{N_b} f_D = \frac{1}{2}\frac{f_D}{f_{D,Max}} \tag{5.24}$$

As a consequence, this degradation depends on the Doppler uncertainty interval through $f_{D,Max}$ (Figure 5.8).

Secondly, the ratio of sinc in (5.10) depends on the value of $m - f_D T_C$ where m is the FFT index within $[\![0, N_b - 1]\!]$. If $m - f_D T_C$ is an integer, which is equivalent to f_D being a multiple of $1/T_C$, then it is exactly a Dirac function:

$$\frac{\text{sinc}\big(\pi(m - f_D T_C)\big)}{\text{sinc}\left(\pi\dfrac{m - f_D T_C}{N_b}\right)} = \delta_0(m - f_D T_C) \tag{5.25}$$

In the worst case, if f_D is exactly between two multiples of $1/T_C$ ($f_D = \left(m + \frac{1}{2}\right) T_C$) the DBZP output degradation reaches 4 dB (Figure 5.7 (b)).

Let us note that when the value of m is the closest on $f_D T_C$, the term (5.25) can be approximated by $\text{sinc}(\pi \varepsilon_{f_D} T_C)$ with $\varepsilon_{f_D} = -\frac{1}{2T_C} + \left(f_D + \frac{1}{2T_C}\right) \bmod \frac{1}{T_C}$ where $a \bmod b$ is the remainder of the Euclidean division of a by b.

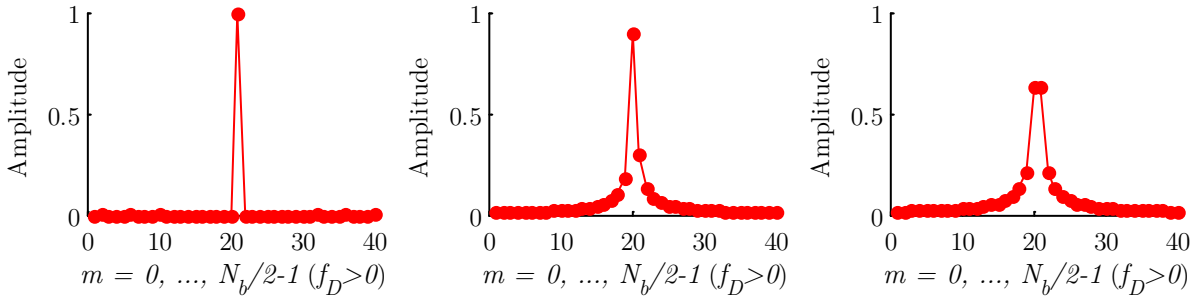

(a) $f_D = 5000$ Hz (b) $f_D = 5062.5$ Hz (c) $f_D = 5125$ Hz

Figure 5.8 Representation of (5.25) for different incoming Doppler frequencies

Based on the aforementioned investigation, Figure 5.9 represents the overall DBZP output power loss due to the incoming signal Doppler frequency.

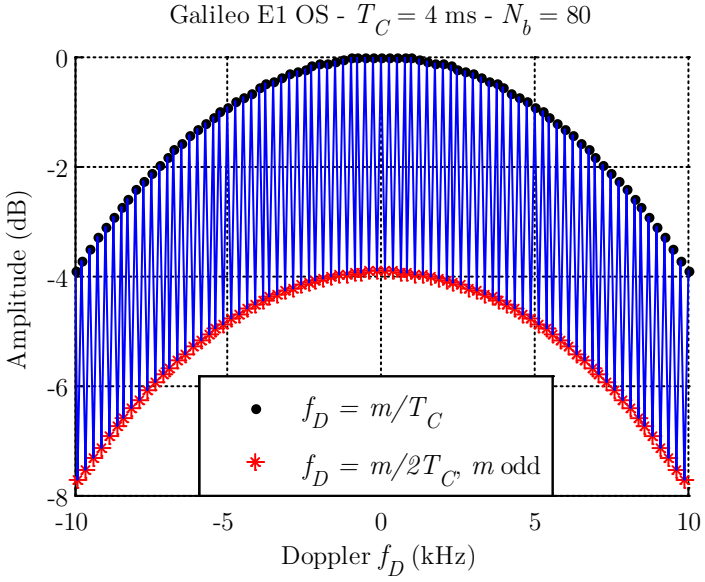

Figure 5.9 Losses due to the incoming Doppler frequency

The conclusion on the DBZP acquisition criterion is that its amplitude has a strong dependence on the incoming Doppler frequency, which is the counter part of using only a single local replica with a pre-defined Doppler for the whole acquisition grid. In particular, its amplitude can be greatly degraded for Doppler frequencies between two multiples of $\frac{1}{T_C}$ and for high Doppler frequencies. It is very important to highlight that this inherent drawback of the DBZP has never been reported in the literature.

Obviously, the resulting probability of detection will suffer from the amplitude losses of the non-central parameters due to the incoming Doppler frequency. Figure 5.10(a) provides the DBZP probability of detection as a function of the incoming Doppler frequency. The acquisition parameters ($T_C = 4$ ms, $K = 20$, $P_{FA} = 10^{-3}$) are chosen so that the acquisition of both Galileo E1 OS signal components provides a probability of detection at 95% when there

is no incoming Doppler frequency. Knowing that the Doppler frequency resolution is $\Delta_f = 1/T_C$, it is possible to take the average probability of detection per Doppler frequency "cell", it is presented in Figure 5.10(b). Even for the small incoming Doppler frequencies, the average probability of detection is 74% since for example when $f_D = 125$ Hz, the probability of detection is only 23%. When the incoming Doppler frequencies are the highest (higher than 9875 kHz), the average probability of detection is 13%.

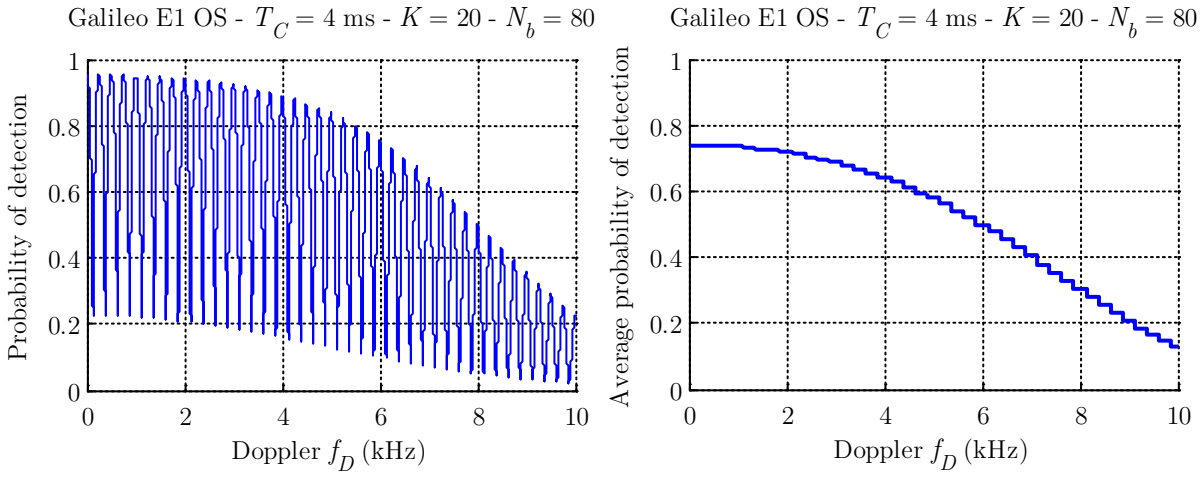

(a) Probability of detection (b) Average probability of detection

Figure 5.10 Probability of detection as a function of the incoming Doppler frequency for the DBZP acquisition method (no code delay error)

- Bit transition sensitivity

As the serial-search acquisition method, the DBZP suffers from the bit sign transition. As explained previously, the sign of the data bit can differ from the first to the last partial correlations. The DBZP output –after application of the FFT– is thus highly affected because the presence of a data bit sign transition completely destroys the code periodicity so leading to serious impairments. The short data bit duration makes the acquisition of Galileo E1 OS more sensitive to transition compared to GPS L1 C/A, and it appears important to solve for this problem when designing a Galileo E1 OS signal acquisition method for high sensitivity.

5.2 Proposed DBZP improvements

Some evolutions have been presented in literature such as the Modified Double-Block Zero-Padding (MDBZP) [Ziedan, 2006] and the Fast Modified Double-Block Zero-Padding (FMDBZP) [Zhang & Ghogho, 2010]. These improved versions of the original DBZP circumvent some problems to handle the unknown data bit transition and the Doppler effect on the spreading code, to extend the integration time and further reduce the computation processing. However, they are mainly addressed to the acquisition of GPS L1 C/A signal and do not focus on the acquisition of Galileo E1 OS.

5.2.1 Data transition insensitivity

To be resistant to the effect of data bit transition on the Galileo E1 OS signal, a variant of the DBZP, the Double-Block Zero-Padding Transition-Insensitive (DBZPTI) is proposed. The parameters of the DBZP described earlier are kept the same.

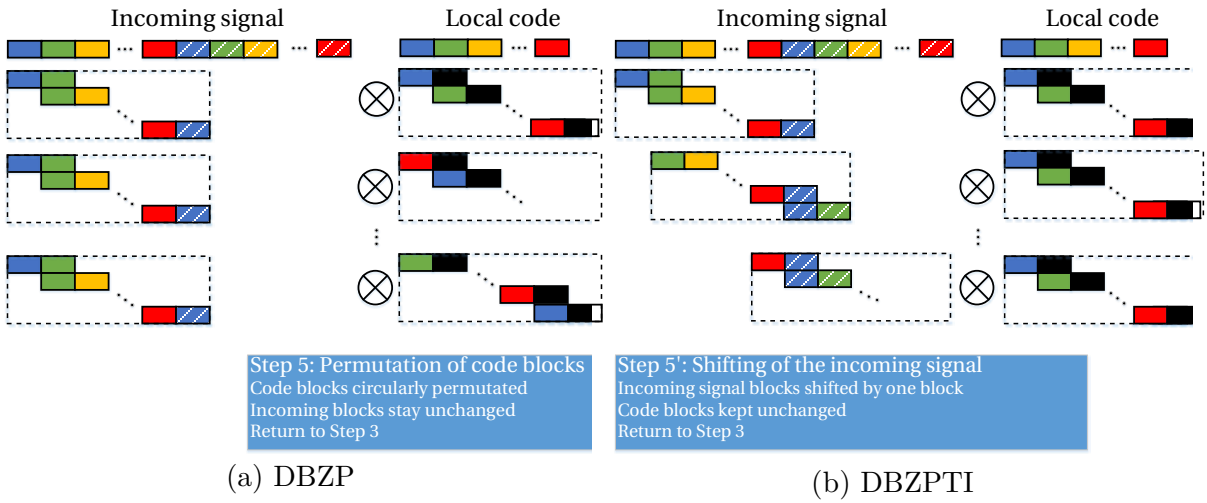

(a) DBZP (b) DBZPTI

Figure 5.11 Difference DBZP/DBZPTI

The difference between the DBZP and the DBZPTI is presented in Figure 5.11. The DBZP principle is kept, the difference rests on the management of the incoming signal and local code blocks.

5.2.1.1 Step 1': Pre-processing of the incoming signal

In the case of the DBZPTI, $2T_c$ ms of incoming signal are needed instead of $T_c + t_b$. The coherent integration time stays T_c and the number of blocks N_b.

5.2.1.2 Step 5': Shifting of the incoming signal

Instead of circularly permuting the code blocks to simulate all possible code delays, it is the incoming signal that is time-shifted by one block in a linear way (this means $2T_c$ ms of incoming signal are used). Thereby, when the coherent integration time is one code period, the correlation interval is free of data (and secondary code) bit sign transition since the correlation interval corresponds to the data bit.

Indeed, the acquisition process consists in finding the beginning of a spreading code period (in the case of Galileo E1 OS acquisition, it means also when a data bit or secondary code bit occurs). As can be seen in Figure 5.12 if a data transition occurs during the integration time, the incoming code and the local code are properly aligned for the DBZP but there is a transition. However, for the DBZPTI, it is the principle of a sliding windows of length T_c ms (the length of a data bit). This method has the advantage to compute the correlation output on the duration of one code period and not over two code periods.

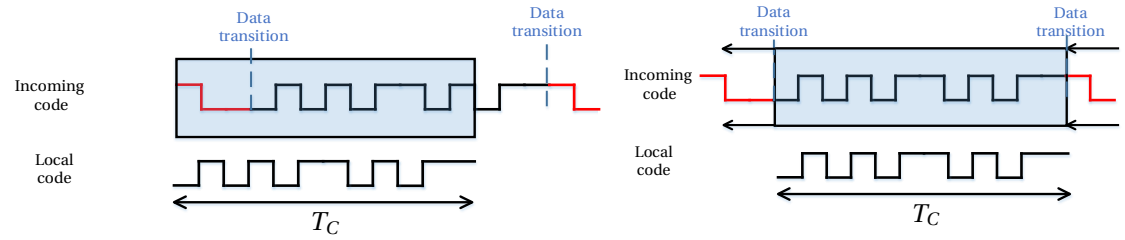

(a) DBZP (b) DBZPTI

Figure 5.12 Transition insensitivity of the DBZPTI

It is very important to understand that, for the DBZPTI, the correlation is computed on only one spreading code period, and not on two spreading code periods as it is usually the case for example with the "1+1 ms" technique.

5.2.2 Dependence on the incoming Doppler frequency

Two dependences on the incoming Doppler frequency were previously discussed. To overcome this problem, two solutions have been proposed in [Foucras *et al.*, 2013].

The first concerns the losses due to high incoming Doppler frequencies. Indeed, the term $\mathrm{sinc}(\pi f_D t_b)$ implies a maximum degradation of 4 dB for the maximal expected value of the incoming Doppler frequency (in Figure 5.7 (a)). It is possible to double the number of blocks N_b (and then decrease t_b) by artificially doubling the theoretical uncertainty Doppler frequency interval. The update of the step 1 and its effect are presented in Figure 5.13. For $f_D = 10$ kHz (real maximal expected value), the degradation is less than 1 dB (green line) instead of 4 dB (in dash-dot black line).

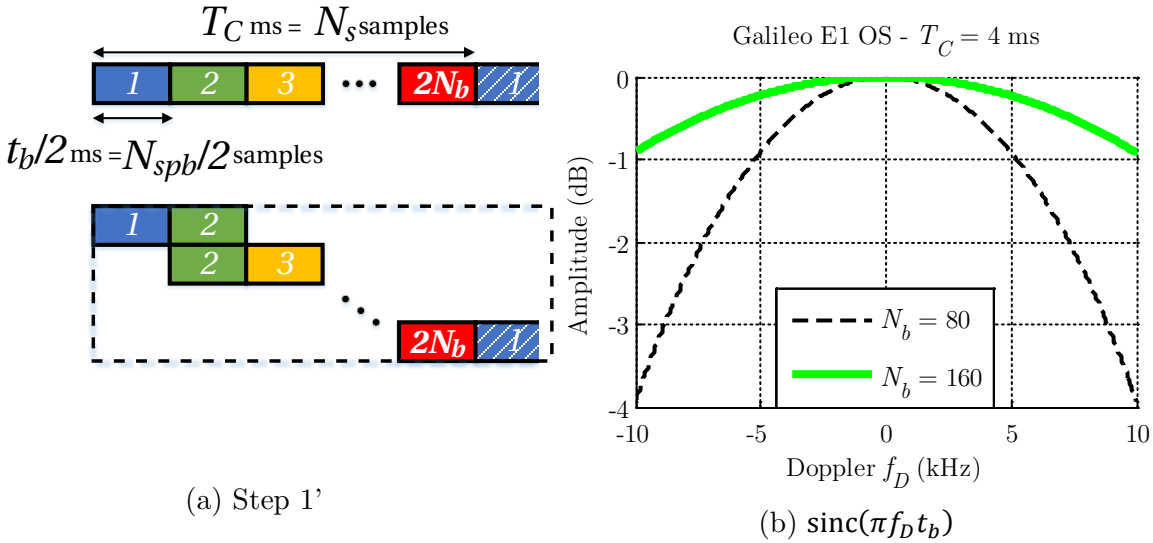

(a) Step 1' (b) $\mathrm{sinc}(\pi f_D t_b)$

Figure 5.13 Losses reduction due to high Doppler frequencies

From an implementation point, the doubling of the number of blocks implies the processing of blocks of size N_{spb} divided by 2.

Reducing the number of samples per blocks is a-priori an advantage; the disadvantages are that:

- The size of the vector for the Step 4 (on which the last FFT is applied) is doubled,
- The number of partial correlations and the number of repetitions of the process (N_r) are doubled.

Now, let us have a look on the second point of degradation. The step 4 of the DBZPTI uses a DFT on a vector that is the set of partial correlation outputs for a given code delay (with a size equal to the number of blocks N_b). The DFT result allows determining the incoming Doppler frequency thanks to the term (5.10). But it implies a maximum degradation of 4 dB (in Figure 5.7 (b)) for f_D multiple of $1/2T_C$.

From (5.10), it can be understood that the DBZPTI output will present a peak for the value of m that is the nearest to the incoming Doppler frequency f_D. To overcome this problem it is suggested to zero-pad (using β blocks of size $\left(N_b \times N_r N_{spb}\right)$) because the zero-padding is equivalent to oversample the FFT result. Indeed, the more points there are to describe the FFT, the smaller is the gap between $f_D T_C$ and m and the smaller is the degradation.

$$\begin{aligned}&\mathcal{F}\left(\cos\left(2\pi f_D l t_b + \tilde{\phi}_0(k)\right)\right)\left(m_{m=0,\dots,N_b+\beta N_b-1}\right)\\&= N_b \frac{\operatorname{sinc}\left(\pi \dfrac{m-(1+\beta)f_D T_C}{(1+\beta)}\right)}{\operatorname{sinc}\left(\pi \dfrac{m-(1+\beta)f_D T_C}{(1+\beta)N_b}\right)} \cos\left(\tilde{\phi}_0(k) + \pi \frac{(N_b-1)}{(1+\beta)N_b}(m-(1+\beta)f_D T_C)\right)\end{aligned} \tag{5.26}$$

The expression of the FFT output is given in (5.26) (the development is in *Appendix F.2*) to support the result in Figure 5.14. The DFT is applied on this matrix of size $\left((1+\beta)N_b \times N_r N_{spb}\right)$.

Two candidates for β are proposed as an example. When $\beta = 1$ (the size of the original matrix is doubled), the maximum degradation is divided by 4 (0.9 dB) because the number of lobes (local maxima) is doubled and every second one matches with the original lobes ($\beta = 0$) (red curve in Figure 5.14). For $\beta = 3$ (in blue curve in Figure 5.14), the result is more interesting because the worst degradation is only 0.19 dB.

Another option is to take β such that $(1+\beta)N_b$ is a power of 2 (in this case, β might not be an integer number) to speed up the FFT execution. Obviously, the associated performance gain is very interesting. The frequency resolution is then not anymore an integer dividing $1/T_C$.

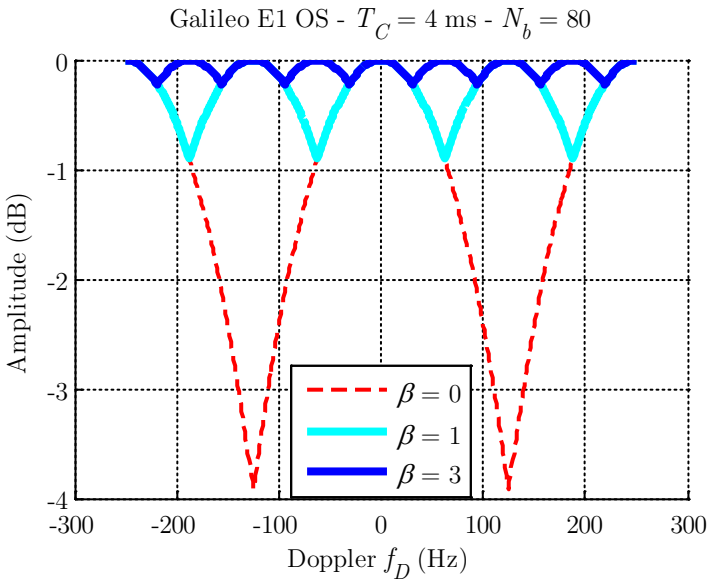

Figure 5.14 Losses reduction at intermediate incoming Doppler frequencies

As a conclusion of these improvements on the Doppler frequency dependency, Figure 5.15(a) presents the amplitude losses as a function of the Doppler frequency. In the worst case, when no modification is used in the DBZP technique, the degradations of the non-centrality parameter can be as high as 8 dB (Figure 5.9) but with the proposed modification, the worst degradation is 1.1 dB (for $\beta = 3$). It is worth noting that doubling the number of blocks has no effect on (5.26) because the sinc terms are very close to 1. The average probability of detection is presented in Figure 5.15(b) and should be compared with Figure 5.10(b). Even for the highest incoming Doppler frequencies, the average probability of detection is higher than 0.8. This shows the important gain of the proposed DBZP improvements on the probability of detection.

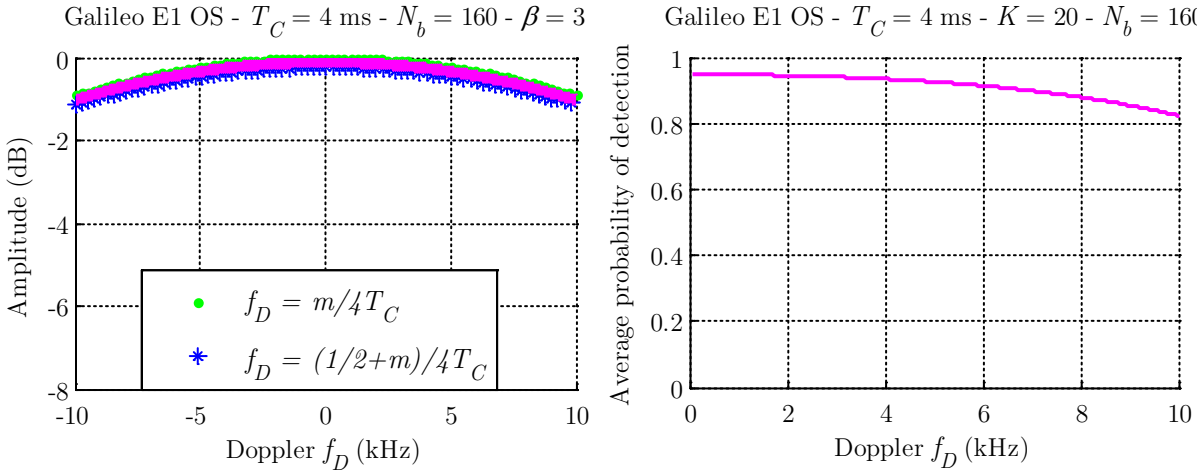

(a) Amplitude losses (b) Average probabilities of detection

Figure 5.15 Losses due to the incoming Doppler frequency after improvements

As a synthesis of all the proposed improvements, Figure 5.16 presents the block diagram of the Double-Block Zero-Padding Transition-Insensitive acquisition method. It should be noted that in the case of the DBZPTI, the number of blocks is:

$$N_b = 2 \times \frac{f_{D,Max} - f_{D,Min}}{\frac{1}{T_C}} = 4 f_{D,Max} \times T_C \tag{5.27}$$

And then the number of samples per block is:

$$N_{spb} = \frac{N_s}{N_b} = \frac{f_s}{4 f_{D,Max}} \tag{5.28}$$

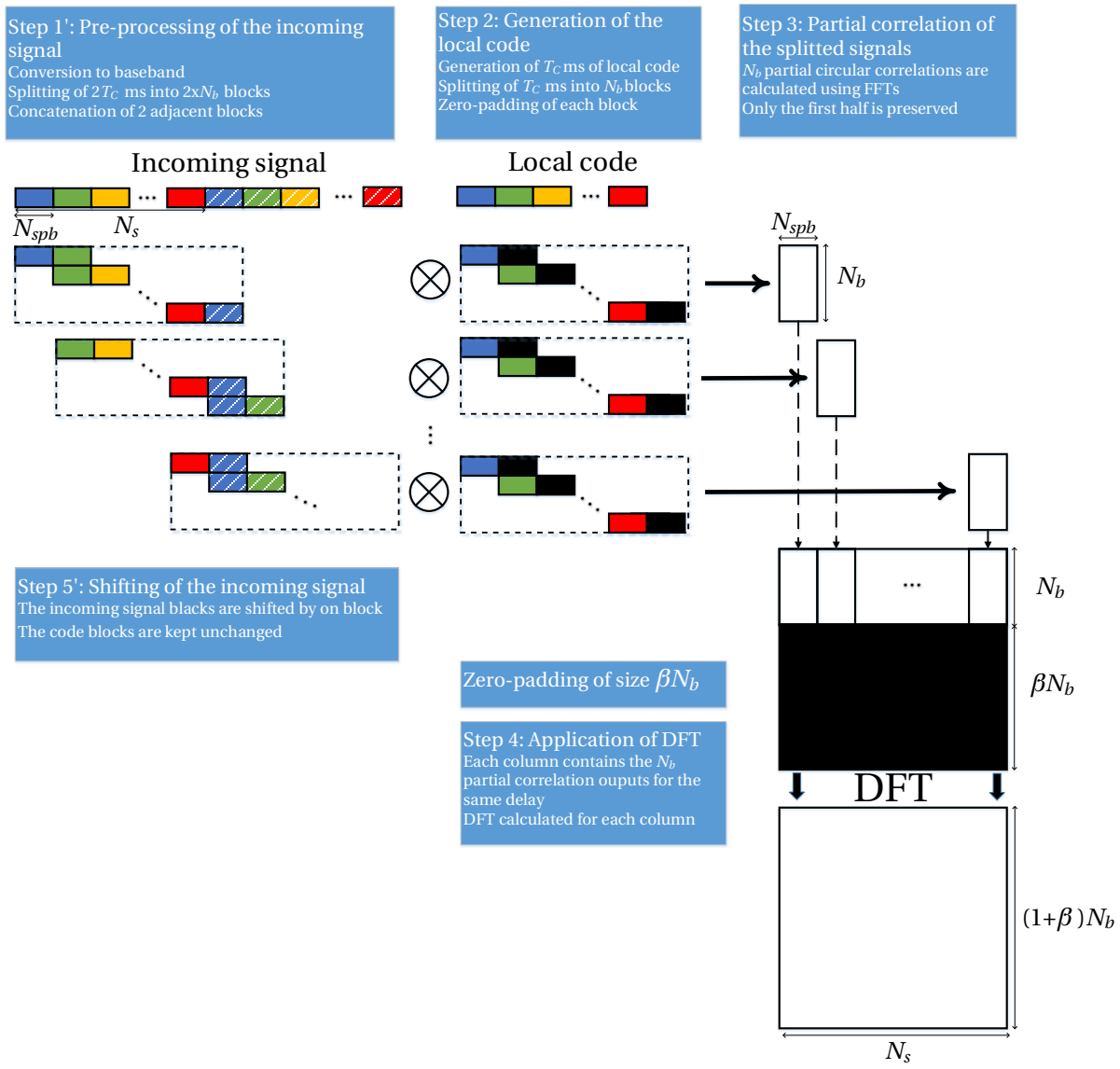

Figure 5.16 DBZPTI method block diagram

Three improvements are brought to the DBZP acquisition method, leading to the Double-Block Zero-Padding Transition-Insensitive acquisition method.

Let us recap the improvements and present their impacts:

- The transition insensitivity: $2T_C$ ms of signal are processed instead of T_C ms for the DBZP,
- Losses less important for high incoming Doppler frequency: the number of blocks is doubled. From the point of view of the implementation, this implies twice more blocks to process which size is divided by 2,
- Losses less important for incoming Doppler frequencies at the edge of the initial Doppler frequency "cell": DBZP matrix containing the partial correlator outputs is zero-padded and the last DFT is applied to this extended matrix. Obviously, the size of the vectors on which the last DFT is applied is higher and can have an impact on the execution of the DBZPTI when comparing with the execution of the DBZP.

The comparison of the computation efficiency of the DBZPTI acquisition method with the DBZP and the reference acquisition methods is detailed in section 5.3.2.

Nevertheless, as the DBZP acquisition method, the DBZPTI acquisition method is:

- Sensitive to the incoming Doppler frequency but to a lesser extent, leading to a worst case degradation of 1.13 dB for the maximum incoming Doppler frequency, instead of 8 dB,
- Sensitive to code Doppler. It would be possible, as for the MDBZP [Ziedan, 2006] to generate as many local replicas as Doppler frequency "cells" and run the DBZPTI with each replica. This however compromises the efficiency of the DBZPTI since there are as DBZPTI runs as number of Doppler frequency "cells" for one computation of the DBZPTI.

5.2.3 Sub-sampling

To reduce the size of the manipulated vectors, blocks, matrices, it is possible to subsample the signal. The sub-sampling can be applied whichever the acquisition method (DBZP/DBZPTI or reference acquisition). This section focuses only on the DBZP/DBZPTI acquisition methods. In this case, the sub-sampling can occur:

- Before step 1 when the incoming signal is processed: the number of samples per spreading code period N_s is updated and then, the number of samples per blocks is computed in function of the updated N_s,
- Before step 4 when all the partial correlations are computed: the number of columns on which the last DFT is applied, is reduced by taking only one column over 2 or over 3…

Clearly, from the point of view of the implementation, when the subsampling is applied at the beginning of the process, the number of samples to process is reduced and there is a high gain in the computation. Reducing the number of the "last DFT" permits to considerably improve the computation efficiency. It seems a good compromise between computation gain

and acquisition performance. For GPS L1 C/A, the number of samples describing the signal can be reduced to 1 sample per chip. For the Galileo E1 OS signal, to have satisfactory performance, the number of samples per chip cannot be below 6 due to the CBOC modulation. Another option for the Galileo E1 OS signal is to locally generate a BOC carrier since 10/11 of the signal is contained in the main the BOC lobes. In this case, 2 samples can be sufficient to describe each chip.

It can be interesting to study the impact of the sub-sampling on an in-depth study on the acquisition performance and on the computation gain. This is not done in this work but it can be assimilated to studies lead on the sampling frequency [Qaisar & Dempster, 2007].

5.3 Software implementation and results

5.3.1 Matlab implementation

For the implementation of the DBZP/DBZPTI, a vectorized implementation, for example with Matlab, seems well-adapted. Each step of the Matlab implementation is presented. The implementation of the DBZPTI is presented (to have a point of comparison between both acquisition methods, N_b refers to the number of blocks for the DBZP acquisition method):

- Step 1 or 1' and 5 or 5': generation of the local carrier for the baseband conversion (vector of length $(1 \times 2N_s)$) and multiplication of T_C ms of the incoming signal with the complex vector (Hadamard product). The incoming signal, splitted up into N_b blocks, can re-arranged in only one matrix (for all code blocks permutations (step 1) or incoming signal blocks shift (step 1')) of size $\left(N_r N_b \times 2N_{spb}\right)$ as illustrated in Figure 5.17. Then, for the DBZPTI, there are 2 more signal blocks than for the DBZP,
- Step 2-5/5': generation of the local code. To minimize the execution time, the local code is often generated only once and stored in memory for later use (non-coherent summations) [Ledvina *et al.*, 2003], [Petovello *et al.*, 2009]. To optimize the processing gain, the conjugate of the DFT of each code zero-padded block can be generated and stored. The local code (or DFT) is then stored in a matrix of size $\left(N_r N_b \times 2N_{spb}\right)$,
- Step 3: the partial correlations are computed in a circular way through the DFT operation. Once again, all of the partial correlator outputs (for all code delays) can be computed in one shot due to the matrix form. Care should be taken when manipulating the Matlab DFT operator because the DFT of a matrix consists in evaluating the DFT of each column. The size of the matrix output is $\left(N_r N_b \times N_{spb}\right)$,
- Step 4: the matrix containing all of the partial correlator outputs is zero-padded and then the DFT on each column is applied,
- End: the DBZP output matrix of size $\left(N_r N_b \times N_{spb}\right)$ is then squared and potentially summed with the matrix of the previous non-coherent summations. This final matrix is then compared to the threshold. Let us note that for the DBZPTI, only the rows describing the real Doppler frequency uncertainty space are kept (which corresponds to an half).

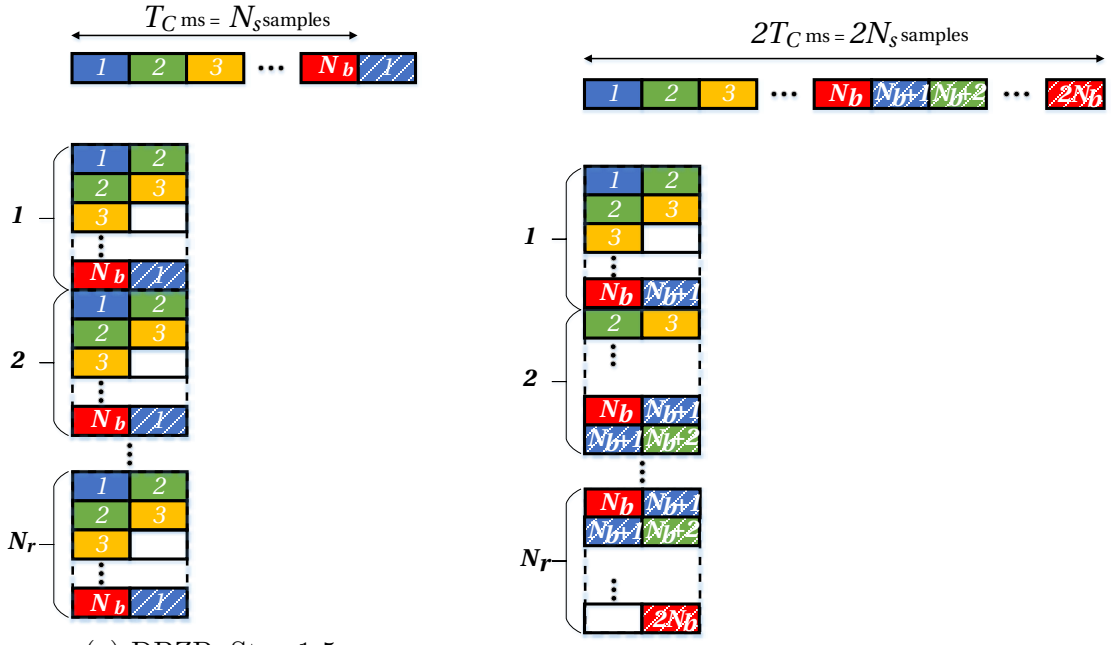

(a) DBZP: Step 1-5

(b) DBZPTI: Step 1'-5'

Figure 5.17 Implementation of Step1/1'-5/5'

For the acquisition of Galileo E1 OS signals, both data and pilot components are acquired independently and the DBZP/DBZPTI output matrices are summed together.

5.3.2 Computation efficiency

5.3.2.1 Count of the number of operations for each acquisition method

It is extremely complex to exactly quantify the number of operations required for the execution of an acquisition method and compare the performance between several acquisition methods on this criterion. In this section, the number of complex basic operations (multiplications and additions) is globally analyzed.

There exist efficient implementations of DFT such as the Fast Fourier Transform (FFT). When the size of the vector n on which the FFT is applied is a power of 2, it can be admitted that the required number of complex operations is: $\frac{3}{2}n\log_2(n)$ [Cooley & Tukey, 1965]. Nowadays, lots of optimized DFT algorithms are developed (Bruun's FFT algorithm, Winograd FFT algorithm…), based on the Cooley-Tukey FFT algorithm but which do not require a power of 2 [Leclère, 2014]. To have an order of magnitude, and because the complexity of the FFT is $\mathcal{O}(n\log(n))$ (instead of $\mathcal{O}(n^2)$ for a DFT), it is admitted that all the executions of DFTs are based on a FFT which required $\frac{3}{2}n\log_2(n)$ complex operations for a vector of size n. However, even if the size of the processed vector is not a power of 2, due to the used of optimized algorithms, the execution of the FFT can be relatively rapid and comparable to the Cooley and Tukey algorithm execution applied to vectors in power of 2.

The number of complex operations for the execution of the DBZP (Table 5.2), the DBZPTI (Table 5.4) and the reference acquisition method (Table 5.3) are detailed step by step. It is worth noting that it is not a rigorous analysis and does not take into account:

- The computation of the local carrier,
- The complex conjugate since it corresponds to only changing the bit sign and can hardly be compared to a multiplication or addition,
- The normalization by a real value,
- The access to memory,
- The split in blocks and concatenation for the DBZP/DBZPTI acquisition methods.

		Size of the vector	Operations	Number of times
Multiplication by local carrier		N_s	N_s	1
Step 3	DFT of the signal	$2\frac{N_s}{N_b}$	$3\frac{N_s}{N_b}\log_2\left(2\frac{N_s}{N_b}\right)$	N_b
	DFT of the local code	$2\frac{N_s}{N_b}$	$3\frac{N_s}{N_b}\log_2\left(2\frac{N_s}{N_b}\right)$	N_b
	DFT .× DFT	$2\frac{N_s}{N_b}$	$2\frac{N_s}{N_b}$	$N_b N_r$
	IDFT	$2\frac{N_s}{N_b}$	$3\frac{N_s}{N_b}\log_2\left(2\frac{N_s}{N_b}\right)$	$N_b N_r$
Step 4: DFT		N_b	$\frac{3}{2}N_b\log_2(N_b)$	N_s
Squaring		N_b	N_b	N_s

Table 5.2 Number of required operations for the execution of the DBZP acquisition method

	Size of the vector	Operations	Number of times
Multiplication by the local carrier	$2N_s$	$2N_s$	N_f
FFT of the signal	$2N_s$	$3N_s\log_2(2N_s)$	N_f
FFT of the local code	$2N_s$	$3N_s\log_2(2N_s)$	1
FFT .× FFT	$2N_s$	$2N_s$	N_f
IFFT	$2N_s$	$3N_s\log_2(2N_s)$	N_f
Squaring	$2N_s$	$2N_s$	N_f

Table 5.3 Number of required operations for the execution of the PCPS with 1+1 ms acquisition method (reference acquisition method)

		Size of the vector	Operations	Number of times
Multiplication by local carrier		$2N_s$	$2N_s$	1
Step 3	FFT of the signal	$2\frac{N_s}{N_b}$	$3\frac{N_s}{N_b}\log_2\left(2\frac{N_s}{N_b}\right)$	$2N_b$
	FFT of the local code	$2\frac{N_s}{N_b}$	$3\frac{N_s}{N_b}\log_2\left(2\frac{N_s}{N_b}\right)$	N_b
	FFT .× FFT	$2\frac{N_s}{N_b}$	$2\frac{N_s}{N_b}$	N_bN_r
	IFFT	$2\frac{N_s}{N_b}$	$3\frac{N_s}{N_b}\log_2\left(2\frac{N_s}{N_b}\right)$	N_bN_r
Step 4: FFT		$(1+\beta)N_b$	$\frac{3}{2}(1+\beta)N_b\log_2\left((1+\beta)N_b\right)$	N_s
Squaring		$\frac{(1+\beta)N_b}{2}$	$\frac{(1+\beta)N_b}{2}$	N_s

Table 5.4 Number of required operations for the execution of the DBZPTI acquisition method

5.3.2.2 Comparison of the number of operations of each acquisition method applied to the acquisition of GPS L1 C/A and Galileo E1 OS

As a synthesis, the number of operations for each acquisition method is computed and presented in Table 5.5. Two numerical applications are performed for the acquisition of GPS L1 C/A and for the acquisition of one component of the Galileo E1 OS signal.

Obviously, the DBZP acquisition method is the most efficient acquisition method (around 17 and 5 times less operations in comparison with the reference acquisition method for the GPS L1 C/A and Galileo E1 OS respectively). The execution of the DBZPTI requires around 1.2 less operations than the reference acquisition method.

When comparing the DBZPTI with the DBZP acquisition method, the number of samples per block is divided by 2 for the DBZPTI but the number of blocks is multiplied by 2. This implies 2 times more partial correlations and the last DFT is applied on vectors which are $2(1+\beta)$ longer (for example, for Galileo E1 OS, it is 640 instead of 80) but N_s DFTs are repeated and this relatively small difference can have a significant impact on the computation efficiency.

For all the acquisition methods, it can be seen that the acquisition of one component of Galileo E1 OS requires around 16 times more operations than the acquisition of the GPS L1 C/A signal. Indeed, N_s is 4 times higher for Galileo E1 OS because the coherent integration time 4 ms. In the same way, N_b or N_r and N_f are multiplied by 4 for Galileo E1 OS.

		GPS L1 C/A	Galileo E1 OS (1 component)
Acquisition parameters	T_C / N_s	1 ms/ 40960	4 ms/163840
	N_b (DBZP) / N_b(DBZPTI)	20 / 40	80 / 160
	N_r (DBZP) / N_r (DBZPTI)	20 / 40	80 / 160
	N_f	40	160
	β (DBZPTI)	3	3
DBZP acquisition method	$N_s\left(\begin{matrix}3(N_r+2)\log_2\left(2\frac{N_s}{N_b}\right)\\+\frac{3}{2}N_b\log_2(N_b)\\+(2N_r+N_b+1)\end{matrix}\right)$	4.02×10^7	6.47×10^8 (× 16.1 GPS/DBZP)
DBZPTI acquisition method	$N_s\left(\begin{matrix}3(N_r+3)\log_2\left(2\frac{N_s}{N_b}\right)\\+\frac{3}{2}N_b(1+\beta)\log_2((1+\beta)N_b)\\+\left(2N_r+\frac{N_b(1+\beta)}{2}+2\right)\end{matrix}\right)$	1.37×10^8 (× 3.4 GPS/DBZP)	2.45×10^9 (× 3.8 Galileo/DBZP)
Reference acquisition method	$N_s\left(6N_f+3\left(2N_f+1\right)\log_2(2N_s)\right)$	1.72×10^8 (× 4.3 GPS/DBZP)	3.05×10^9 (× 4.7 Galileo/DBZP)

Table 5.5 Comparison of the number of operations for the different acquisition methods and for GPS L1 C/A and Galileo E1 OS signals

For Galileo E1 OS, for example, the execution of the DBZPTI requires 3.8 times more operations than for the DBZP but this represents only 80% of the number of the operations required for the reference acquisition method. In conclusion, for both signals, the DBZPTI is less efficient than the DBZP, in terms of computation but still more efficient than the reference acquisition method and there is a gain of 20% of operations.

5.3.2.3 Comparison of the number of operations when using sub-sampling

Table 5.6 provides an order of magnitude of the gain in terms of operations when sub-sampling. The numerical application is for Galileo E1 OS and assuming that the sampling frequency is divided by $\zeta = 4$. For the reference acquisition method, the number of operations is divided by approximately ζ (4.46 for $\zeta = 4$) when comparing the last rows of Table 5.5 with no sub-sampling and Table 5.6 with a sub-sampling of parameter ζ. The gain in number of operations is provided in the second column of Table 5.6, and it is 6.47×10^8 operations.

		$\zeta = 4$	Galileo E1 OS (1 comp.)
DBZPTI acquisition method	Step 1	$\frac{\zeta-1}{\zeta}N_s\left(\begin{array}{c}3(N_r+3)\log_2\left(2\frac{N_s}{N_b}\right)\\+\frac{3}{2}N_b\,(1+\beta)\log_2((1+\beta)N_b)\\+\left(2N_r+\frac{N_b(1+\beta)}{2}+2\right)\end{array}\right)+\frac{3N_s}{\zeta}(N_r+3)\log_2(\zeta)$	-1.88×10^8 ($/4.28\ \zeta=1$)
	Step 4	$\frac{\zeta-1}{\zeta}N_sN_b(1+\beta)\left(\frac{3}{2}\log_2((1+\beta)N_b)\right)$	-1.14×10^8 ($/1.87\ \zeta=1$)
Reference acquisition method		$\frac{\zeta-1}{\zeta}N_s\left(6N_f+3\left(2N_f+1\right)\log_2(2N_s)\right)+3N_s\frac{\log_2(\zeta)}{\zeta}\left(2N_f+1\right)$	-6.47×10^8 ($/4.46\ \zeta=1$)

Table 5.6 Comparison of the gain on the number of operations for the different acquisitions methods and for Galileo E1 OS

For the DBZPTI acquisition method, two sub-sampling can be done. The first one (noted Step 1 in Table 5.6), consists in sub-sampling the local and incoming codes. In this case, the gain is also approximately ζ (around 4.28). The other option is to sub-sample before step 4 to limit the number of DFT computed on the columns of the DBZP matrix containing all the partial correlation outputs. In this case, the gain is 1.87. This result should be compared to the acquisition performance in terms of probability of detection.

5.4 Discussion

The intention of this chapter has been to propose a new computationally efficient Galileo E1 OS acquisition method for GNSS software receivers. From the literature, it results that methods based on parallelization (in time or frequency domain) perform the acquisition operation efficiently due to the use of FFT.

In general, it is more efficient to perform many FFTs on small vectors than one FFT on a large vector. Based on this, the Double-Block Zero-Padding (DBZP) is pointed out as one of the most computationally efficient acquisition method for GPS L1 C/A due the use of partial correlations and a high level of parallelization (in code and frequency).

In Section 5.1, all steps of the DBZP acquisition method were delved into details. This analysis permitted to mathematically express the DBZP outputs and investigate its performance. It has been shown that the signal-to-noise ratio at the DBBZP output and at the classical correlator output are the same.

However, it has been highlighted that significant performance losses can appear due to:

- High incoming Doppler frequencies (in absolute values),
- Incoming Doppler frequencies between two frequency bins,
- Bit sign transition (but this is also the case for the classical acquisition technique).

As presented in Section 5.2, due to the presence of potential bit sign transitions on each component at every spreading code period for Galileo E1 OS, it has been decided to propose a modified DBZP acquisition method which is Transition-Insensitive (DBZPTI). Some improvements were added to the DBZPTI to reduce the inherent performance losses of the DBZP due to the incoming Doppler frequency value. Then, the maximum losses are reduced from 8 dB to 1.1 dB. When these losses on the maximum incoming Doppler frequencies are interpreted in terms of probability of detection (for a $C/N_0 = 27$ dB-Hz, $P_{FA} = 10^{-3}$ and a total integration time $T_I = KT_C$ which permits a detection with a probability of $P_D = 95\%$ for a null Doppler frequency), there is a gain of around 70%.

In Section 5.3, some points of clarification with respect to the Matlab implementation were presented permitting to evaluate the computational efficiency of the proposed acquisition method in a general case and applied to the acquisition of Galileo E1 OS. The number of required operations for the DBZPTI is higher than for the DBZP (factor of 3.8) but it is lower than for the reference acquisition method (factor of 80%).

The analysis of the DBZP permitted to propose a Transition-Insensitive acquisition method with comparable computational efficiency. In the next chapter, the attention is turned to define a global acquisition strategy to reach the acquisition objective.

Chapter 6
Global Acquisition Strategy

The objective of this chapter is to design the global acquisition strategy to permit the acquisition of the Galileo E1 OS signal with a targeted C/N_0 of 27 dB-Hz and a probability of success of 90%. To do so, the acquisition parameters of the search step and of the step of verification are discussed. The theoretical performance of the global acquisition strategy based on the DBZPTI is compared with the performance of the global acquisition strategy based on the reference acquisition method and also on the DBZP acquisition method.

Several configurations will be studied such as the Doppler frequency uncertainty space: wide (uncertainty of 20 kHz) or restricted (4 kHz), the consideration or not of the Doppler frequency and code delay errors. The design of the acquisition strategy is also proposed for the acquisition of the GPS L1 C/A signal at 27 dB-Hz.

A comparison of the performance and the integration times for different values of C/N_0 is then proposed to evaluate the importance of the C/N_0 in the design of the acquisition strategy.

Contents

6.1 Discussion on the acquisition steps 134
6.1.1 Preliminary discussion 134
6.1.2 Search step 134
6.1.3 Step of verification 138
6.2 Discussion on the acquisition parameters at 27 dB-Hz 141
6.2.1 Wide Doppler frequency uncertainty space 141
6.2.2 Restricted Doppler frequency uncertainty space 144
6.2.3 Acquisition of the GPS L1 C/A signal 145
6.3 Acquisition of signals not at 27 dB-Hz 146
6.4 Discussion 148

6.1 Discussion on the acquisition steps

6.1.1 Preliminary discussion

The previous chapters provided some points of design of the acquisition of Galileo E1 OS signals of interest at 27 dB-Hz. It was shown in *Chapter 3* that for the weak Galileo E1 OS signals, it is preferable to acquire both components to collect the total signal power. In addition, even if long coherent integration is preferable, due to the presence of bit transitions on both components at each spreading code period, the coherent integration time must be equal to the spreading code period, $T_C = T_{c_1} = 4$ ms. Indeed, as explained in *Chapter 4* and *Chapter 5*, the search acquisition method DBZPTI is designed to be insensitive to one sign transition and if more bit sign transitions occur (coherent integration time longer than the spreading code period), it jeopardizes the acquisition success.

The acquisition strategy is divided into two steps: the search step consists in providing a set of estimated parameters couples which can be close to the incoming one. As discussed in *Chapter 3*, the objective is to reach a probability of detection $P_{D,acq}$ of 90% knowing that:

$$P_{D,acq} = P_{D,search} \times P_{D,verif} \tag{6.1}$$

This implies that $P_{D,search}$ and $P_{D,verif}$ should be between 0.9 and 1. Since the execution of the step of verification is shorter than the execution of the search step, the probability of detection of the step of verification is chosen very high (98 or 99%). The probability of the search step can then be around 91%.

6.1.2 Search step

6.1.2.1 DBZPTI acquisition method

An innovative acquisition method, the DBZPTI, insensitive to bit sign transition was developed and presented in *Chapter 5*, it is the chosen acquisition method for the search step.

The main drawback of this method is that the acquisition performance depends on the incoming Doppler frequency, as presented in *Chapter 5* in equation (5.19). Figure 6.1 presents the degradations on the probability of detection when the incoming Doppler frequency increases. When the Doppler frequency is null, the probability of detection is 95% and it falls down to less than 23% for the maximum real incoming Doppler frequency (dashed black curve with the initial number of blocks). When the number of blocks is doubled, the degradations are greatly reduced since the probability of detection is around 84% for an incoming Doppler frequency of 10 kHz. It is why it is decided that the computation of the probability of success in the signal detection should take into account these potential degradations due to the incoming Doppler frequency and then the objective of the design of the acquisition is to reach an average probability of detection on the incoming Doppler frequency, higher than at least 90%.

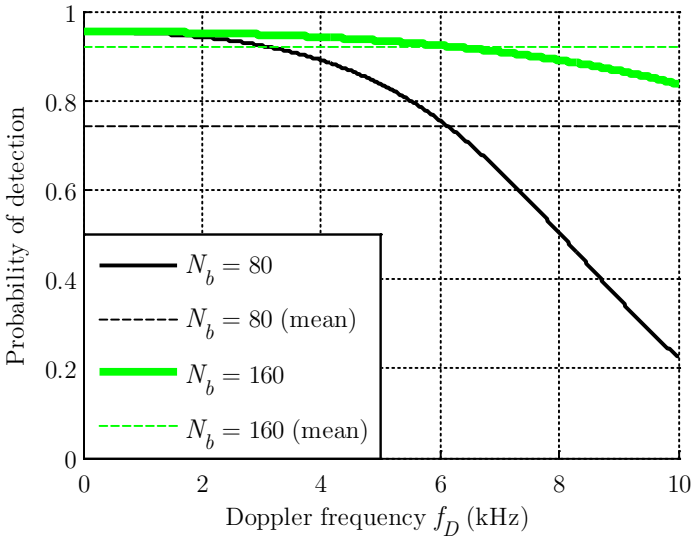

Figure 6.1 Probability of detection as a function of the incoming Doppler frequency (Galileo E1 OS, $T_C = 4$ ms, $K = 40$, $C/N_0 = 27$ dB-Hz, $P_{FA} = 10^{-3}$, $\varepsilon_\tau = 0$)

As a reminder, the number of blocks in the considered case (Galileo E1 OS acquisition) is:

$$N_b = \left(f_{D,Max} - f_{D,Min}\right) \times T_C = 20 \times 10^3 \times 4 \times 10^{-3} = 80 \tag{6.2}$$

The maximum number of tested code delays depends on the sampling frequency, assumed here to be 40.96 MHz:

$$N_s = f_S \times T_C = 40.96 \times 10^6 \times 4 \times 10^{-3} = 163\,840 \tag{6.3}$$

The matrix at the output of the DBZPTI depends on the number of blocks N_b, on the number of cell describing the spreading code period N_s and on β. For example, for $\beta = 0$, the number of cells is $N_c = 1.31 \times 10^7$.

6.1.2.2 Reference acquisition method

To evaluate the performance of the developed acquisition method, it is compared to a reference acquisition method, which is the Parallel Code Search with the "1+1 ms" technique, presented in *Chapter 3*. The acquisition grid of the reference acquisition method is defined as follows for the acquisition of Galileo E1 OS:

- In the frequency domain1+1: the width of a frequency cell is $1/2T_C$, that means 125 Hz. The Doppler frequency uncertainty space, assumed to be $[-10,10]$ kHz in cold start, is then divided in 160 cells,
- In the time domain: the width of a code delay cell is set to $1/6$ chip (to account for the CBOC modulation). The spreading code, which length is 4092 chips, is then discretized into 24 552 cells.

In the end, the number of cells in the acquisition grid is $N_c \approx 3.93 \times 10^6$.

6.1.2.3 Number of verified cells

If the probability of false alarm is chosen at 10^{-3}, a classic value, then an average of 13 107 false alarms could be declared over the DBZPTI acquisition matrix. It appears clear that this is too much for a workable acquisition strategy. The objective is thus to reduce the size of the set of false alarms. In this work, N_v was chosen to 10, that means that at the output of the search step, in average, there are 10 false alarms.

Three approaches will be studied in details to obtain in average N_v parameter estimation couples and applied to the DBZPTI acquisition method with a null incoming Doppler frequency and $\beta = 0$.

- Approach 1

The approach 1 uses a very small probability of false alarm and implies the verification all the cells exceeding the threshold. The average number of false alarms is equal to the number of cells in the search space multiplied by the probability of false alarm:

$$P_{FA,Approach1} = \frac{N_v}{N_c} = \frac{10}{1.31 \times 10^7} = \frac{1}{1.31} \times 10^{-6} \approx 7.63 \times 10^{-7} \tag{6.4}$$

Based on this probability of false alarm, let us determine the required number of non-coherent summations K such as $P_{D,search} \approx 0.95$. It can be observed with Figure 6.2 that K equal to 36 provides a probability of detection of 95.28%.

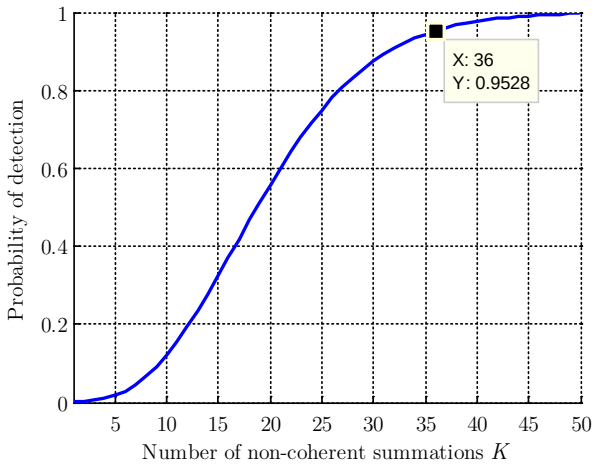

Figure 6.2 Required number of non-coherent summations for the Approach 1 (C/N_0= 27 dB-Hz)

- Approach 2

As presented in *Chapter 3,* a searching strategy consists in retaining only a few acquisition cells corresponding to an acquisition detector crossing the threshold. The approach 2 uses a relatively high probability of false alarm and implies the verification of only a reduced set of the cells exceeding the threshold. These cells are chosen to be the highest ones being over the threshold. For different integration times (associated to a number of non-coherent summations K), Figure 6.3 provides the probability of detection of the strategy $P_{D,Maxq}$ which depends on

$P_{D,cell}$, (in the legend) the probability of detection of the correct cell for a probability of false alarm fixed to $P_{FA,cell}$ of 10^{-3}. For each value of K, $P_{D,cell}$ is very close to 1 but the probability of detection of the strategy varies between 92% and 98% for a number of verified cells of 10.

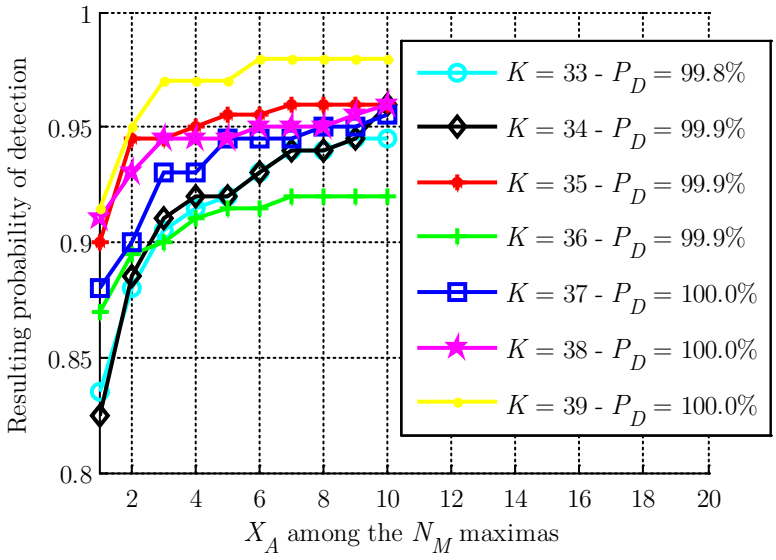

Figure 6.3 Required number of non-coherent summations for the Approach 2 ($C/N_0 = 27$ dB-Hz)

- Approach 3

The Approach 3 aims at obtaining the same probability of false alarm as the Approach 1 by running twice the acquisition search method and selecting only the cells that have crossed twice the threshold. The main drawback of this approach is that the resulting probability of detection is the product of both probability of detection.

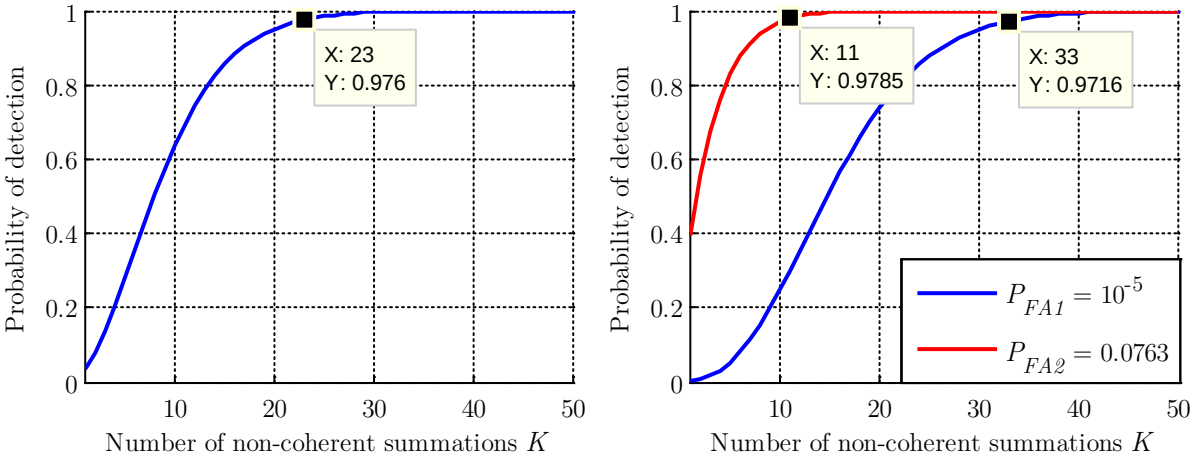

(a) $P_{FA_1} = P_{FA_2} = \sqrt{\frac{N_v}{N_c}}$

$T_I = 2 \times 23 \times T_C = 46 \times T_C$

(b) $P_{FA_1} = 10^{-5}, P_{FA_2} = \frac{\frac{N_v}{N_c}}{P_{FA_1}}$

$T_I = (11 + 33) \times T_C = 44 \times T_C$

Figure 6.4 Examples of acquisition performance for 2 choices of probabilities of false alarm for Approach 3 ($C/N_0 = 27$ dB-Hz)

Figure 6.5 permits to determine the optimal choice between both probabilities of false alarm for a C/N_0 of 27 dB-Hz. In green, the probability of detection is shown and in blue the total number of non-coherent summations is shown. For small probability of false alarm, results presented in Figure 6.4(a) can be found, 46 non-coherent summations are required to reach a probability of detection of 95%. The best choice (to have the lowest total number of non-coherent summations (blue curve) is the extreme case where P_{FA_1} is equal to 1 and P_{FA_2} is equal to N_v/N_c. It corresponds to the case presented in Figure 6.2, where there is only one probability of false alarm. Let us remark that the number of non-coherent summations is 37 instead of 36 because for the $P_{FA_1} = 1$, one summation is anyway required and is added to the 36 non-coherent summations required for $P_{FA_2} = N_v/N_c$.

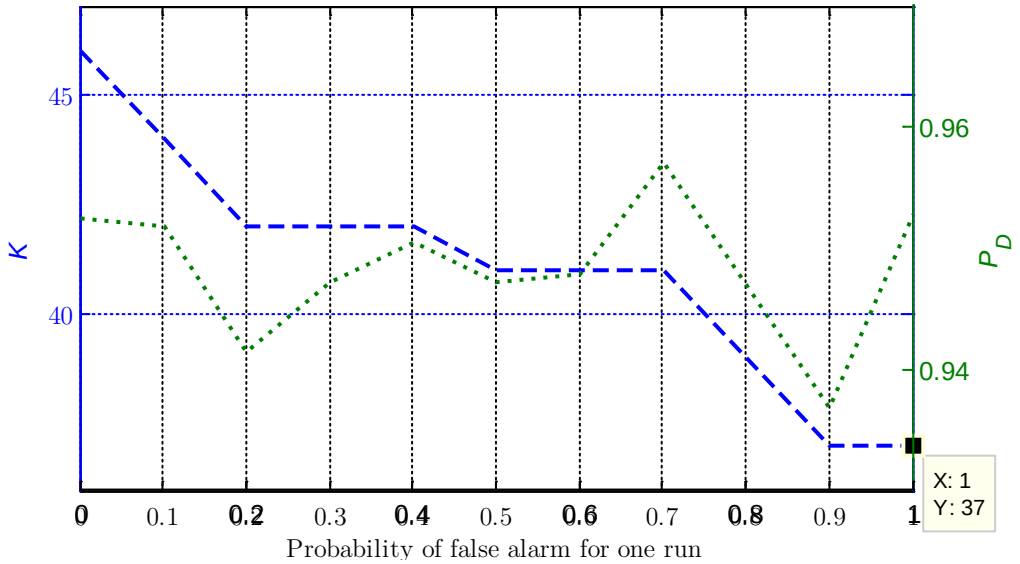

Figure 6.5 Required number of non-coherent summations for Approach 3

Some approaches to select only a set of a few cells to verify in the step of verification were compared. As it can be observed, in the case of a desired size of 10 cells at maximum and a resulting probability of detection of 95%, the integration time is close for the three approaches. The best option seems to be Approach 1, based on a very small probability of false alarm, with an integration time of $T_I = 144$ ms ($K = 36$). This approach will be selected for the development of the global acquisition strategy of acquisition. Furthermore, the Approach 1 is the simplest one because the other approaches require two steps and seems a priori the less resources consuming.

6.1.3 Step of verification

The input to the step of verification is a set of cells (Doppler, code delay) among which might be the correct cell. The step of verification aims at eliminating all the false alarms and selecting the correct cell (hopefully). The cells which will be verified have a priori no link (because the false alarms are assumed randomly distributed on the acquisition grid) and an acquisition method based on a parallelization in the time or frequency domains does not seem

appropriate. Each parameters couple is thus verified sequentially. For a parameter couple $(\hat{\tau}, \hat{f}_D)$, the acquisition method of the step of verification is the classic one which consists in generating a local code replica with the estimate of the code delay $\hat{\tau}$ and a local carrier depending on the estimate of the Doppler frequency $\hat{f}_D$. This acquisition method is not data bit sign Transition-Insensitive but it is not a big problem for the step of verification. Indeed, if it is the correct bin that is checked, the local code replica can be generated to coincide with the beginning of the spreading code sequence within a fraction of a chip.

For the design of the GNSS receiver, it is preferable to ensure that the tracking is running with a correct estimation of the signal parameters. If the receiver tracks the signal with a bad estimation of the parameters, the loops would not be locked and the acquisition should be re-run to provide the correct estimation of the signal parameters. This leads to a considerable loss of time in GNSS signal processing. In the design of the developed receiver, it was arbitrarily chosen that a false alarm can occur in average only 1 time over 1000 runs of the acquisition process, this is equivalent to say that the number of false alarm is $N_{FA} = 0.001$. The probability of false alarm of the acquisition step is then in the order of 10^{-10}.

Knowing that the probability of false alarm of the search step was fixed to $P_{FA,search} = N_v / N_c$, the probability of false alarm of the step of verification can be easily determined:

$$P_{FA,acq} = P_{FA,search} \times P_{FA,cell} = \frac{N_v}{N_c} \times P_{FA,verif}$$
$$P_{FA,acq} = \frac{N_{FA}}{N_c} \tag{6.5}$$

$$\frac{N_{FA}}{N_c} = \frac{N_v}{N_c} \times P_{FA,verif} \Leftrightarrow P_{FA,verif} = \frac{N_{FA}}{N_v} \approx \frac{0.001}{10} = 10^{-4} \tag{6.6}$$

The objective is then to determine the acquisition parameters of the step of verification, knowing that $P_{D,verif} = 99\%$ and $P_{FA,verif} = 10^{-4}$. For the step of verification, the Tong detector or the M of N detector techniques can be used. For the Tong detector technique, 4 acquisition parameters should be determined.

- Tong detector

Simulations were run to determine the best choice of the parameters which permits to reach the probabilities of detection and false alarm. The criterion is the smaller value of $(A - B) \times K$ which can reflect an execution time. Indeed, the minimum number of detectors to detect the presence of the signal of the step of verification is $(A - B)$ and for each one, K non-coherent summations were run.

The 4 acquisition parameters and the tested values are given:

- B, the initial value of the counter, which can take the values 1 or 2,
- A, the value of the counter for which the detection is decided, which can take minimum value is $B + 1$, the maximum value was set to 20,
- P_{FA}, the probability of false alarm for one detector, ($P_{FA} \in \{0.5, 0.1, 0.05, 0.001\}$)
- K, the number of non-coherent summations for one detector ($K = 1, 2, \ldots, 20$).

Table 6.1 provides the optimal (in the sense described earlier) choice of the acquisition parameters for the Tong detector technique. The probability of detection P_D for one detector is deduced from P_{FA} and K.

	B	A	P_{FA}	K	P_D
No errors	2	4	0.1	6	90.25%

Table 6.1 Acquisition parameters for the Tong detector technique

For this choice of parameters, the probability of detection of the step of verification is $P_{D,verif} = 98.83\%$ and $P_{FA,verif} = 2 \times 10^{-5}$.

- M of N detector

For the M of N detector technique, also, 4 acquisition parameters should be determined:

- N, the maximum number of detectors, which is chosen to be 8 or 10 (values taken from literature, for example, [Ward *et al.*, 2005b] chose $N = 8$),
- M, the minimum number detectors which success the detection for which the detection in the step of verification is decided (M varies between 3 and N),
- P_{FA} and K.

The criterion to choose the acquisition parameters for the step of verification is $\left(\frac{M+N}{2} \times K\right)$, which can be assimilated to a mean time of acquisition. Based on the acquisition parameters presented in Table 6.2, the probability of detection of the step of verification is $P_{D,verif} = 98.87\%$ and $P_{FA,verif} = 6 \times 10^{-5}$.

	M	N	P_{FA}	K	P_D
No errors	5	10	0.05	5	77.64%

Table 6.2 Acquisition parameters for the M of N detector technique

It is clear that the "best" choice of the acquisition parameters for the step of verification is strongly dependent on the desired performance. As it can be observed, the performance in terms of probabilities of false alarm and detection are equivalent for both techniques. Because a choice between both should be done, the Tong detector technique is preferred for two reasons. The first one is that the probability of detection for one detector P_D is higher (given as an indication in the last column of Table 6.1 and Table 6.2). The step of verification was designed assuming no code delay or Doppler frequency errors, so with potential residual errors due to the discretization of the acquisition grid, the probability of detection $P_{D,verif}$ is higher for the Tong detector (41% instead of 28% for the M of N technique, assuming a code delay error of 1/12 chip and a Doppler frequency error of 62.5 Hz). The second argument is that the rough estimation of the minimum execution time is shorter for the Tong detector technique because after the computation of only 2 detectors, the presence of the signal can be decided (instead of 5 detectors for the M of N detector technique).

6.2 Discussion on the acquisition parameters at 27 dB-Hz

6.2.1 Wide Doppler frequency uncertainty space

It is assumed that there is no a-priori knowledge on the incoming Doppler frequency. The Doppler frequency uncertainty space if then wide since it is $[-10, 10]$ kHz.

6.2.1.1 No Doppler frequency and code delay errors

		DBZPTI acquisition method $\beta = 3$	Reference acquisition method
Acquisition method parameters	Number of rows	$N_b = 160$ $\Rightarrow (1+\beta)\frac{N_b}{2} = 320$	$N_f = 160$
	Number of columns	$N_s = 163840$	$N_\tau = 163\,840$
	Number of cells	$N_c \approx 5.24 \times 10^7$	$N_c \approx 2.62 \times 10^7$
	Number of verified cells	$N_v = 10$	
Doppler frequency and code delay error(s)		$f_D \in [-10{,}10]$ kHz $\varepsilon_{f_D} = 0$ Hz	
		$\varepsilon_\tau = 0$ chip	
Search Approach 1	Probability of false alarm	$P_{FA} = \frac{N_v}{N_c} \approx 1.9 \times 10^{-7}$	$P_{FA} = \frac{N_v}{N_c} \approx 3.8 \times 10^{-7}$
	Non-coherent summations	$K = 40$	$K = 34$
	Probability of detection	$P_{D,search} = 91.15\%$	$P_{D,search} = 91.63\%$
Final probability of detection		$P_D = P_{D,search} \times P_{D,verif} = 90.08\%$	$P_D = P_{D,search} \times P_{D,verif} = 90.56\%$

Table 6.3 Acquisition parameters with a correct estimation of the incoming signal parameters (DBZPTI/Reference)

In Table 6.3, for each method, the number of rows (frequency domain) and columns (time domain) is enumerated to determine the number of cells in the acquisition matrix and then the probability of false alarm which is set by the Approach 1.

When there is no error on the Doppler frequency and code delay, to reach a final probability of detection higher than 91%, the required integration time is:

- For the DBZPTI acquisition method: 160 ms,
- For the reference acquisition method: 136 ms.

6.2.1.2 Uncertainties on the Doppler frequency and code delay errors

When considering residual Doppler frequency and code delay errors (more realistic), the required integration time (presented in Table 6.4) is:

- For the DBZPTI acquisition method: 176 ms,
- For the reference acquisition method: 168 ms.

The number of non-coherent summations for the search step for both acquisitions methods is relatively close, when considering potential errors, the DBZPTI acquisition method has a small disadvantage of 8 ms for the total dwell time (which represented less than 5%).

It is possible to compare the number of operations to reach the same probability of detection using the DBZPTI or the reference acquisition method. For the DBZPTI, 44 non-coherent summations are required and one summation needs 2.45×10^9 operations, then 1.08×10^{11} are required for the DBZPTI. It corresponds to a gain of 15% on the number of operations when comparing with the reference acquisition (42 summations of 3.05×10^9 operations).

<table>
<tr><th colspan="2"></th><th>DBZPTI acquisition method
$\beta = 3$</th><th>Reference acquisition method</th></tr>
<tr><td colspan="2" rowspan="2">Doppler frequency and code delay error(s)</td><td colspan="2">$f_D \in [-10,10]$ kHz</td></tr>
<tr><td>$\varepsilon_{f_D} \in \left[-\frac{1}{8T_C}, \frac{1}{8T_C}\right] \in [-31.25, 31.25]$ Hz</td><td>$\varepsilon_{f_D} \in \left[-\frac{1}{4T_C}, \frac{1}{4T_C}\right] \in [-62.5, 62.5]$ Hz</td></tr>
<tr><td colspan="2"></td><td colspan="2">$\varepsilon_\tau \in \left[-\frac{f_{c_1}}{2f_s}, \frac{f_{c_1}}{2f_s}\right] = \left[-\frac{1}{80}, \frac{1}{80}\right]$ chip</td></tr>
<tr><td rowspan="3">Search</td><td>Non-coherent summations</td><td>$K = 44$</td><td>$K = 42$</td></tr>
<tr><td>Dwell time</td><td>$T_I = 176$ ms</td><td>$T_I = 168$ ms</td></tr>
<tr><td>Probability of detection</td><td>$P_{D,search} = 91.20\%$</td><td>$P_{D,search} = 91.75\%$</td></tr>
</table>

Table 6.4 Acquisition parameters with a rough estimation of the incoming signal parameters (DBZPTI/Reference)

It is interesting to compare the required dwell time for the DBZP and DBZPTI acquisition methods. As presented in Table 5.5, the DBZP acquisition method has been shown to be more efficient computationally that the DBZPTI since the number of operations is less important (by a factor of 4 approximately) for the DBZP acquisition method but the question is to know if the DBZPTI acquisition method compensates by a reduced dwell time and in which proportions. Table 6.5 compares the dwell time (for the search step) of both acquisition methods, based on the same average probability of detection obtained for the uncertainty search spaces.

As a reminder, one of the improvements of the DBZP (and then in the DBZPTI) is that the Doppler frequency error is reduced by 4, if $\beta = 3$. This implies that the size of the DBZPTI output matrix is also 4 times greater and then the probability of false alarm is reduced in the same way. As a synthesis, in comparison with the DBZPTI acquisition method, for the DBZP acquisition method:

- The Doppler frequency uncertainty is higher (disadvantage),
- The probability of false alarm is higher.

and the number of non-coherent summations is nearly the double. That means that the dwell time is 340 ms for the DBZP acquisition method whereas it is only 176 ms for the DBZPTI acquisition method.

<table>
<tr><th colspan="2"></th><th>DBZPTI acquisition method
$\beta = 3$</th><th>DBZP acquisition method</th></tr>
<tr><td rowspan="4">Acquisition method parameters</td><td>Number of rows</td><td>$N_b = 160$
$\Rightarrow (1+\beta)\frac{N_b}{2} = 320$</td><td>$N_b = 80$</td></tr>
<tr><td>Number of columns</td><td colspan="2">$N_s = 163\,840$</td></tr>
<tr><td>Number of cells</td><td>$N_c \approx 5.24 \times 10^7$</td><td>$N_c \approx 1.31 \times 10^7$</td></tr>
<tr><td>Number of verified cells</td><td colspan="2">$N_v = 10$</td></tr>
<tr><td colspan="2" rowspan="2">Doppler frequency and code delay error(s)</td><td colspan="2">$f_D \in [-10{,}10]$ kHz</td></tr>
<tr><td>$\varepsilon_{f_D} \in \left[-\frac{1}{8T_C}, \frac{1}{8T_C}\right] \in [-31.25, 31.25]$ Hz</td><td>$\varepsilon_{f_D} \in \left[-\frac{1}{2T_C}, \frac{1}{2T_C}\right] \in [-125, 125]$ Hz</td></tr>
<tr><td colspan="2"></td><td colspan="2">$\varepsilon_\tau \in \left[-\frac{f_{c_1}}{2f_s}, \frac{f_{c_1}}{2f_s}\right] = \left[-\frac{1}{80}, \frac{1}{80}\right]$ chip</td></tr>
<tr><td rowspan="3">Search</td><td>Probability of false alarm</td><td>$P_{FA} = \frac{N_v}{N_c} \approx 1.9 \times 10^{-7}$</td><td>$P_{FA} = \frac{N_v}{N_c} \approx 3.8 \times 10^{-7}$</td></tr>
<tr><td>Non-coherent summations</td><td>$K = 44$</td><td>$K = 85$</td></tr>
<tr><td>Probability of detection</td><td>$P_{D,search} = 91.20\%$</td><td>$P_{D,search} = 91.28\%$</td></tr>
</table>

Table 6.5 Acquisition parameters with a rough estimation of the incoming signal parameters (comparison DBZPTI/DBZP)

In the end, the execution of the DBZPTI acquisition method is, in average, 2 times less than the execution of the DBZP acquisition method for the same theoretical acquisition performance. It is worth noting that the DBZPTI acquisition method is Transition-Insensitive and this important feature does not appear in the comparison. To reach the same acquisition performance in presence of bit sign transitions, the dwell time for the DBZP acquisition method should be extended (difficult to compute it, since as previously presented, it highly depends on the bit sign transition location and an average value does not ensure detection, especially in worst cases).

When comparing the DBZP with the DBZPTI, the number of operations is reduced by 2 in favor of the DBZP (85 summations of 6.47×10^8) but this does not take into account the data insensitivity of the DBZPTI. For two data bit transition insensitive acquisition methods, the DBZPTI presents a gain of 15% on the number of operations and in addition presented a high level of parallelization. This proves the efficiency of the DBZPTI.

6.2.2 Restricted Doppler frequency uncertainty space

If the Doppler frequency uncertainty space is restricted, due to an a-priori knowledge, it would be interesting to compare the acquisition performance of both acquisition methods.

<table>
<tr><th colspan="2"></th><th>DBZPTI acquisition method
$\beta = 3$</th><th>Reference
acquisition method</th></tr>
<tr><td rowspan="4">Acquisition method parameters</td><td>Number of rows</td><td>$N_b = 32 \Rightarrow (1+\beta)\frac{N_b}{2} = 64$</td><td>$N_f = 32$</td></tr>
<tr><td>Number of columns</td><td>$N_s = 163\,840$</td><td>$N_\tau = 163\,840$</td></tr>
<tr><td>Number of cells</td><td>$N_c \approx 1.05 \times 10^7$</td><td>$N_c \approx 5.24 \times 10^6$</td></tr>
<tr><td>Number of verified cells</td><td colspan="2">$N_v = 10$</td></tr>
<tr><td colspan="2" rowspan="2">Doppler frequency and code delay error(s)</td><td colspan="2">$f_D \in [-2, 2]$ kHz</td></tr>
<tr><td>$\varepsilon_{f_D} \in \left[-\frac{1}{8T_C}, \frac{1}{8T_C}\right] \in [-31.25, 31.25]$ Hz</td><td>$\varepsilon_{f_D} \in \left[-\frac{1}{4T_C}, \frac{1}{4T_C}\right] \in [-62.5, 62.5]$ Hz</td></tr>
<tr><td colspan="2"></td><td colspan="2">$\varepsilon_\tau \in \left[-\frac{f_{c_1}}{2f_s}, \frac{f_{c_1}}{2f_s}\right] = \left[-\frac{1}{80}, \frac{1}{80}\right]$ chip</td></tr>
<tr><td rowspan="3">Search</td><td>Probability of false alarm</td><td>$P_{FA} = \frac{N_v}{N_c} \approx 9.5 \times 10^{-7}$</td><td>$P_{FA} = \frac{N_v}{N_c} \approx 1.7 \times 10^{-6}$</td></tr>
<tr><td>Non-coherent summations</td><td>$K = 35$</td><td>$K = 40$</td></tr>
<tr><td>Probability of detection</td><td>$P_{D,search} = 91.11\%$</td><td>$P_{D,search} = 91.37\%$</td></tr>
</table>

Table 6.6 Acquisition parameters with a rough estimation of the incoming signal parameters (restricted Doppler frequency uncertainty space)

Because the Doppler frequency uncertainty space $[-2, 2]$ kHz is centered in 0, the number of blocks is, as given by (5.27), $N_b = 4 \times (2 \times 10^3) \times (4 \times 10^{-3}) = 32$. Since the number of blocks is divided by 5, the number of samples per blocks N_{spb} is then multiplied by 5.

Based on Table 5.5, the number of operations is globally divided also by 5 for both acquisition methods. From the point of view of the acquisition parameters, reducing the Doppler frequency uncertainty space permits to decrease the number of cells N_c.

As presented in Table 6.6, for the reference acquisition method, this permits to lower by 4 the number of non-coherent summations, which means 16 ms processed signal. For the DBZPTI

acquisition method, the gain is higher (9 non-coherent summations, which means 36 ms on the total dwell time). Unlike a wide Doppler frequency uncertainty space, when the Doppler frequency uncertainty space is reduced, there is a small advantage for the DBZPTI acquisition method.

6.2.3 Acquisition of the GPS L1 C/A signal

The same theoretical study on the DBZPTI acquisition parameters is lead for the acquisition of the GPS L1 C/A. Two cases are presented in Table 6.7: when there are no residual errors and when there are residuals errors and the probability of detection is the average of the average probabilities of detection for each potential couple of residual code delay and Doppler frequency errors.

If Table 6.7 (GPS L1 C/A) is compared with Table 6.3 (Galileo E1 OS), it can be observed that the number of cells N_c is smaller for GPS L1 C/A. Indeed, in the time domain, the number of cells is divided by 4 because the coherent integration time is divided by 4. This implies also a number of blocks divided by 4.

		DBZPTI acquisition method ($\beta = 3$)	
Acquisition method parameters	Number of rows	$N_b = 40 \Rightarrow (1+\beta)\frac{N_b}{2} = 80$	
	Number of columns	$N_s = 40\,960$	
	Number of cells	$N_c \approx 3.28 \times 10^6$	
	Number of verified cells	$N_v = 10$	
Doppler frequency and code delay error(s)		$f_D \in [-10, 10]$ kHz	
		$\varepsilon_{f_D} = 0$ Hz	$\varepsilon_{f_D} \in \left[-\frac{1}{8T_C}, \frac{1}{8T_C}\right] \in [-125, 125]$ Hz
		$\varepsilon_\tau = 0$ chip	$\varepsilon_\tau \in \left[-\frac{f_{c_1}}{2f_s}, \frac{f_{c_1}}{2f_s}\right] = \left[-\frac{1}{80}, \frac{1}{80}\right]$ chip
Search	Probability of false alarm	$P_{FA} = \frac{N_v}{N_c} \approx 3.6 \times 10^{-6}$	
	Non-coherent summations	$K = 189$	$K = 228$
	Probability of detection	$P_{D,search} = 91.19\%$	$P_{D,search} = 91.21\%$

Table 6.7 Acquisition parameters for the acquisition of the GPS L1 C/A signal ($T_C = 1$ ms)

When there are no residual errors, the integration time (on the search step) is $T_I = 189$ ms (with $T_C = 1$ ms) whereas it is $T_I = 160$ ms for Galileo E1 OS. This can be explained by the coherent time. Indeed, with $T_C = 20$ ms, the integration time becomes $T_I = 80$ ms ($K = 4$) for an equivalent probability of detection $P_{D,search}$. On this example, it can be noted that for the acquisition of the GPS L1 C/A signal, the choice of the coherent integration must be studied to take advantage of the strengths of the DBZPTI.

6.3 Acquisition of signals not at 27 dB-Hz

The design of the acquisition parameters, previously discussed, targeted a C/N_0 of 27 dB-Hz. Figure 6.6 provides the average probability of detection as a function of the C/N_0 with the acquisition parameters presented in Table 6.4. At 27 dB-Hz, the probability of detection is 95%, for higher C/N_0, the probability of detection is equal to 1. For weaker signals, the probability of detection falls down. For example, at 24 dB-Hz, the probability of detection is around 10%. At 26 dB-Hz (only 1 dB-Hz below the targeted C/N_0), the probability of detection is 64%. This means that the acquisition of weak signals requires to make a considerable effort.

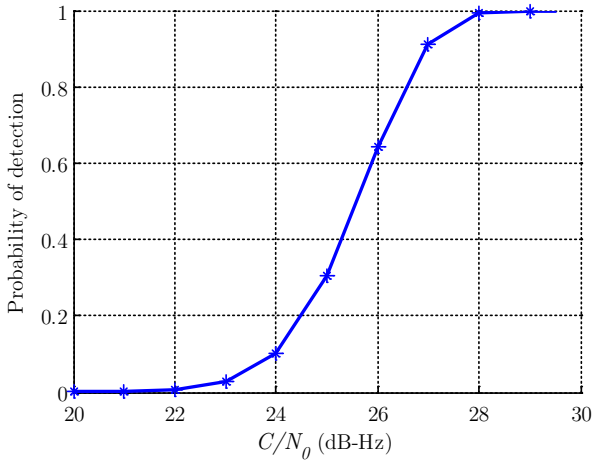

Figure 6.6 Probability of detection for different values of C/N_0 with the DBZPTI acquisition parameters given in Table 6.4

To give an order of idea, to reach an average probability of at least 90%, at 27 dB-Hz, the number of non-coherent summations K is 44 but in the same conditions, at 26 dB-Hz, the number of non-coherent summations should be 64 (Table 6.8). The integration time is then 256 ms, which represents an increase higher than 45% (80 ms).

C/N_0	24 dB-Hz	25 dB-Hz	26 dB-Hz	27 dB-Hz	28 dB-Hz	29 dB-Hz	30 dB-Hz
K	140	96	64	44	30	22	15
T_I	560 ms	384 ms	256 ms	176 ms	120 ms	88 ms	60 ms

Table 6.8 Search step integration time for different value of C/N_0

The design of the presented acquisition strategy is based on a dimensioning that considers the weakest desired signals. However, this strategy is not adapted for stronger signals (as introduced previously) and thus results in a waste of time and resources. It is then possible to set up a strategy in two steps, depend on the power received signals. As an example, let us assume that the probability of detection should be at least $P_D = 95\%$ whatever the C/N_0 and the probability of false alarm $P_{FA} = 10^{-3}$. As presented in Figure 6.7, the required number of

non-coherent summations K can be easily determined for each C/N_0 to reach the desired probability of detection. It can be seen that the number of non-coherent summations decreases strongly with the C/N_0.

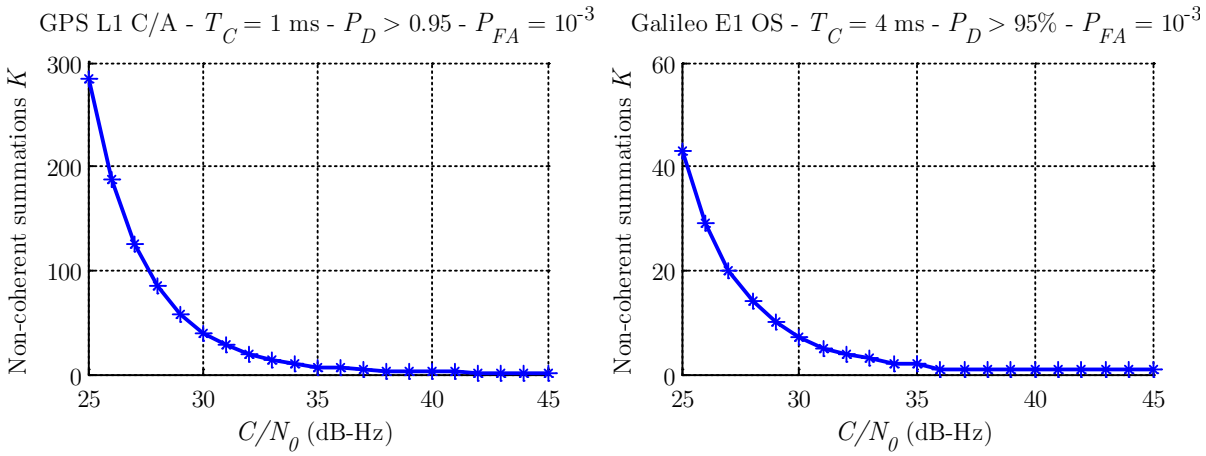

(a) GPS L1 C/A (b) Galileo E1 OS

Figure 6.7 Required number of non-coherent summations as a function of the C/N_0 (DBZPTI method, no errors, null incoming Doppler frequency)

For example, for GPS L1 C/A (Figure 6.7 (a)) (the same discussion can be lead to Galileo E1 OS, based on Figure 6.7 (b)), the "strong C/N_0 threshold" can be set to 33 dB-Hz. For this C/N_0, the number of non-coherent summations is $K = 14$, it is more than 8 times less than the required number of non-coherent summations for a C/N_0 of 27 dB-Hz ($K = 126$). The resulting smaller dwell time implies a high gain on the global acquisition execution time.

With $K = 14$, the probability to detect weak signals is very low ($P_D \approx 9\%$ for a $C/N_0 = 27$ dB-Hz). To resume, the acquisition strategy in presence of several signals with different received C/N_0 consists in the following:

- Only a few non-coherent correlator outputs are used to compute the acquisition detector. The acquisition detector is then compared to the corresponding threshold: if the threshold is passed, the signal is acquired probably because it is strong; otherwise the signal is first supposed weak.
- More correlator outputs are used to compute a second acquisition detector based on more non-coherent summations: if the second threshold is passed, the signal is acquired; otherwise the signal is supposed absent.

In function of the satellites visibility, the distribution of the received C/N_0 and designer's choices, the first threshold should be determined to optimize the performance. Indeed, this strategy permits to have a better management of the resources and acquisition execution time and to avoid to waste time for the acquisition of strongest signals.

6.4 Discussion

In this chapter, the design of a global acquisition strategy for the acquisition of the Galileo E1 OS signal at 27 dB-Hz was discussed.

From the theoretical point of view, the integration times for the search step based on the DBZPTI or on the reference acquisition method are equivalent (176 ms). For this integration time, the probability of detection is in average higher than 91% whatever the incoming Doppler frequency and code delay (and then considering potential residual errors). The step of verification using the Tong detector with $B = 2$ and $A = 4$ and 6 non-coherent summations (with a probability of false alarm per detector at 0.1) permits to reach the predefined objective of success of the acquisition 90% of the time. The probability of false alarm of the acquisition process is 2×10^{-10}, ensuring that less than 1 times 100 runs of the global acquisition strategy, a false alarm can occur in average.

From the point of view of the execution time, the DBZPTI has a high power of parallelization, then an adapted development of the DBZPTI in function of the targeted platform should permit a quicker execution of the DBZPTI. When comparing the DBZP with the proposed variant of the DBZP, the integration time is divided by approximately 2, in favor of the DBZPTI. In addition, the transition sensitivity is not taken into account. When comparing the DBZPTI with the reference acquisition method, there is a gain of 15% on the number of operations for the same acquisition performance.

The optimized implementation of the DBZPTI on the targeted platform and simulations on real or simulated signals should permit to check:

- The insensitivity of the DBZPTI and the reference acquisition methods,
- The theoretical performance (average probability of detection, dependence on the incoming Doppler frequency…)
- The efficiency of the DBZPTI in terms of execution time.

In addition, it permits to evaluate:

- The impact of bit sign transitions on the average probability of detection using the DBZP acquisition method,
- The impact of the code Doppler on the average probability of detection using the DBZPTI acquisition or the reference acquisition method,
- The impact of the RF front-end filter on the average probability of detection for all the acquisition methods.

Chapter 7
Acquisition-to-Tracking Transition

The last step of the acquisition process, as presented in this thesis, aims at ensuring the success of the tracking process once the right cell has been detected and validated at the targeted C/N_0. For GPS L1 C/A, that means that the frequency estimate is sufficiently refined by means of Frequency Lock Loops (FLL) in order to lock the Phase Lock Loop (PLL). This does not pose a significant problem, as already presented in the literature and reminded here.

For the acquisition of modernized GNSS signals, some works should be done. Indeed, to permit long coherent integrations on the pilot component during the tracking process, the secondary code should be acquired. The acquisition of the secondary code consists in determining the location of its first bit since the secondary code is synchronized with the spreading code. This is possible only if the Doppler frequency error is small enough. The bit transitions at each spreading code period make the frequency refinement by FLL a non-trivial step. A study is then lead to determine the best FLL scheme to be able to lock the FLL at 27 dB-Hz.

Contents

7.1 FLL frequency refinement 150
7.1.1 FLL and frequency discriminators 150
7.1.2 Discriminator combination techniques 157
7.1.3 Simulation scheme 161
7.1.4 Simulation results 162
7.2 Pilot secondary code acquisition 174
7.2.1 Pilot secondary code features 175
7.2.2 Pilot secondary code acquisition methods 177
7.2.3 Simulation results 180
7.3 Discussion 185

7.1 FLL frequency refinement

This section aims at determining whether it is possible to reduce the frequency uncertainty using a FLL and choose the best FLL scheme. Since the frequency refinement occurs after the acquisition process, it can be assumed that the Doppler frequency error is within $\left[-\frac{1}{4T_C}, \frac{1}{4T_C}\right]$ where the coherent integration time T_C is limited to a spreading code period because the secondary code on the pilot component is not acquired.

7.1.1 FLL and frequency discriminators

The FLL are used in a wide range of communication systems as a means of achieving carrier synchronization [Curran *et al.*, 2012]. In the area of GNSS signal processing, they are used to track the Doppler frequency of the incoming signal which is dominated by the satellite-to-receiver motion and the user clock drift. It is well known that the FLL is more robust than the PLL that aims at tracking the phase of the incoming signal. The FLL plays thus a key role in facilitating reliable signal tracking. The performance of the FLL will be driven by the number of correlator outputs, the nature of the discriminator and the discriminator combination technique.

7.1.1.1 Frequency Lock Loop

The FLL tracks the carrier frequency by using a frequency tracking error estimate between the received and the local signals. As any other classical feedback control loop, this estimate is filtered by a low-pass filter and then used to control a Numerically Controlled Oscillator (NCO). A simplified block diagram of this operation is depicted in Figure 7.1.

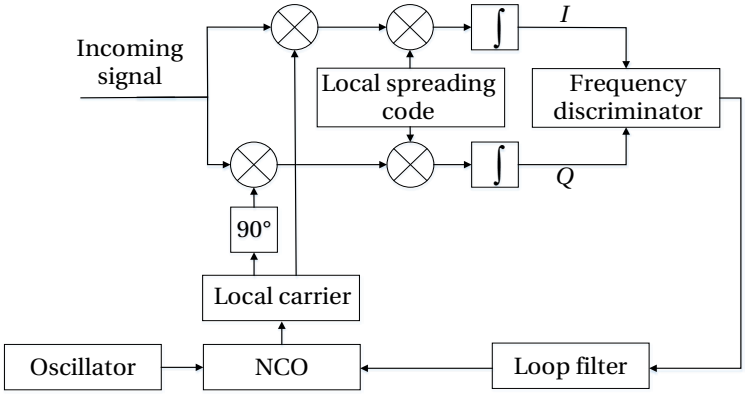

Figure 7.1 Block diagram of a typical frequency lock loop

The carrier frequency error can be computed by means of frequency discriminators. A frequency discriminator is generally a function that produces an estimate of the frequency error from two consecutive correlator output (I/Q) pairs (3.3).

The notation $\varepsilon_\phi(k) = \pi\varepsilon_{f_D}(k)T_C + \varepsilon_{\phi_0}(k)$ can be used to simplify the mathematical expressions. Let us note that in the context of this work, it is assumed that the incoming frequency f_D is constant.

7.1.1.2 Frequency discriminators

In this section, four popular frequency discriminators are analyzed by summarizing their main characteristics such as the data sensitivity/insensitivity, linear region (which contains the frequency error range for which the noise-free discriminator response has a linear shape). For more details, the reader is invited to read [Curran, 2010] for an overview of all of the discriminators. The below analysis on the FLL discriminators is presented assuming the tracking of only one component, the data component, without loss of generalities. Clearly, the results are applicable to the pilot component by substituting the data bit $d(k)$ by the secondary code bit $c_{2,p}(k)$ because the two sequences (data and secondary code) have the same rate. For simplification, for the GPS L5 signal, the term "data" corresponds to the product of the data and secondary code on the data component.

This transition between acquisition and tracking is after the acquisition step, then it is assumed that the code delay is well estimated and then the normalized autocorrelation function value is thus close to 1.

- Cross Product (CP) Discriminator

The first presented discriminator, is the Cross Product discriminator (noted as CP). It is known as one of the most computationally efficient discriminator [Ward *et al.*, 2005b]. It is defined as:

$$\begin{aligned} e_{CP}(k) &= \frac{Cross}{T_C} = \frac{Q_d\,(k)I_d(k-1) - I_d(k)Q_d(k-1)}{T_C} \\ &= A_{CP}d(k-1)d(k)\frac{\sin\left(\varepsilon_\phi(k) - \varepsilon_\phi(k-1)\right)}{T_C} + \eta_{CP}(k) \\ &\approx_{\varepsilon_{f_D}\approx 0} \frac{A_d^2}{2}\pi\,\mathrm{sinc}^2\left(\pi\varepsilon_{f_D}(k)T_C\right)d(k-1)d(k)\times\varepsilon_{f_D}(k) + \eta_{CP}(k) \end{aligned} \tag{7.1}$$

where

- $A_{CP} = \frac{A_d^2}{4}\mathrm{sinc}\left(\pi\varepsilon_{f_D}(k-1)T_C\right)\mathrm{sinc}\left(\pi\varepsilon_{f_D}(k)T_C\right)$ is the amplitude term where the product of the sinc can be approximated by $\mathrm{sinc}^2\left(\pi\varepsilon_{f_D}(k)T_C\right)$ because $\varepsilon_{f_D}(k)$ is close to $\varepsilon_{f_D}(k-1)$,
- $\eta_{CP}(k)$ is the discriminator output noise

The discriminator output $e_{CP}(k)$ is expressed as a sine function of the difference of two consecutive phase errors, which can be approximated by a ε_{f_D} for small Doppler frequency error. Furthermore, the frequency error estimate produced by the Cross Product discriminator must be normalized by $\frac{A_d^2}{2}\pi$ but this normalization is not a significant problem. Secondly, it is evident from (7.1) that the sign of frequency estimate depends on the data bit signs associated to the consecutive correlator outputs. That means that the frequency estimate would be inverted each time $d(k)$ differs from $d(k-1)$. This would lead to significant performance degradation. Then, care must be taken when applying it to data modulated signals.

Figure 7.2 represents the mean discriminator response to frequency error for GPS L1 C/A and Galileo E1 OS for different values of C/N_0. It can be observed that its shape does not depend upon the C/N_0 which is one of its advantages, in particular at low C/N_0. The linear region, where the frequency discriminators can produce an accurate estimate (in the figures, where the black curve representing the noise-free case can be approximated by a line) is approximately within $[-30; 30]$ Hz for Galileo E1 OS.

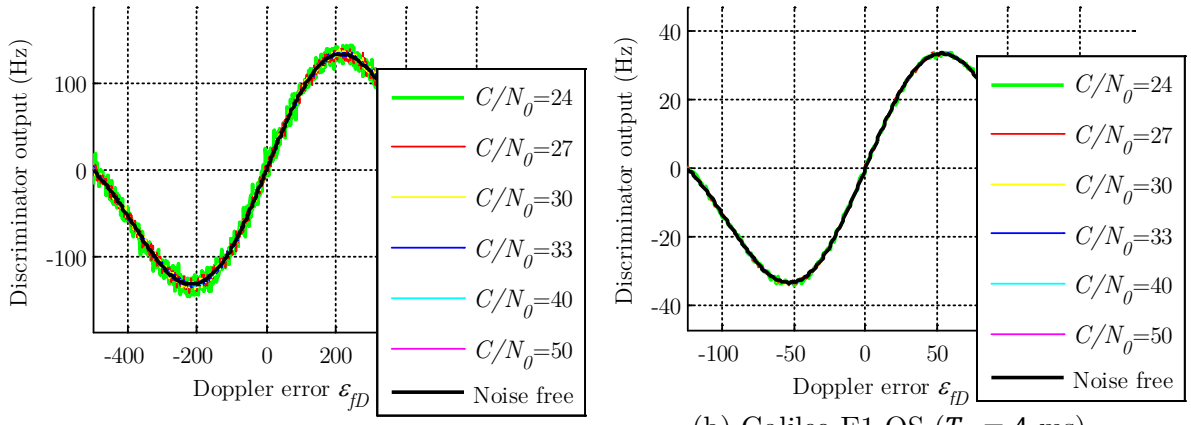

(a) GPS L1 C/A ($T_C = 1$ ms) (b) Galileo E1 OS ($T_C = 4$ ms)

Figure 7.2 Average CP discriminator response to frequency error for a noise-free signal and different C/N_0 cases

- Decision Directed Cross Product (DDCP) Discriminator

As previously seen, the Cross Product discriminator is affected by the presence of data bit transitions. If there is a data bit sign transition, the Cross Product discriminator estimates the opposite of the frequency error. The Decision Directed Cross Product, denoted as DDCP, solves the problem by modulating the Cross Product discriminator with the sign of the dot product:

$$\begin{aligned} Dot &= I(k)I(k-1) + Q(k)Q(k-1) \\ &\approx A_{CP}d(k-1)d(k)\cos\left(\varepsilon_\phi(k-1)\right)\cos\left(\varepsilon_\phi(k)\right) \\ &\quad + A_{CP}d(k-1)d(k)\sin\left(\varepsilon_\phi(k-1)\right)\sin\left(\varepsilon_\phi(k)\right) \\ &\approx A_{CP}d(k-1)d(k)\cos\left(\varepsilon_\phi(k) - \varepsilon_\phi(k-1)\right) \end{aligned} \tag{7.2}$$

Knowing that $\text{sign}(x) = x/|x|$, the DDCP frequency response is then:

$$\begin{aligned} e_{DDCP}(k) &= e_{CP}(k) \times \text{sign}\big(I(k)I(k-1) + Q(k)Q(k-1)\big) \\ &= \frac{A_{CP}}{T_C} \times \frac{\sin\left(\varepsilon_\phi(k) - \varepsilon_\phi(k-1)\right)\cos\left(\varepsilon_\phi(k) - \varepsilon_\phi(k-1)\right)}{\left|\cos\left(\varepsilon_\phi(k) - \varepsilon_\phi(k-1)\right)\right|} \\ &= \frac{A_{CP}}{2} \times \frac{\sin\left(2\left(\varepsilon_\phi(k) - \varepsilon_\phi(k-1)\right)\right)}{T_C \times \left|\cos\left(\varepsilon_\phi(k) - \varepsilon_\phi(k-1)\right)\right|} \\ &= \frac{A_d^2}{2}\pi\text{sinc}^2\big(\pi\varepsilon_{f_D}(k)T_C\big)d(k-1)d(k) \times \frac{\varepsilon_{f_D}(k)}{\left|\cos\big(2\pi\varepsilon_{f_D}(k)T_C\big)\right|} \end{aligned} \tag{7.3}$$

Without noise, the estimated frequency error in (7.3) is a sine function of twice the difference of phase errors.

The linear region for the DDCP discriminator for the noise-free case (in Figure 7.3) is similar to that of the CP discriminator. As it is shown, unlike the Cross Product discriminator, the mean response is dependent upon the C/N_0. Indeed, the term $\mathrm{sign}(Dot)$ might provide the wrong sign when the noise level is too high.

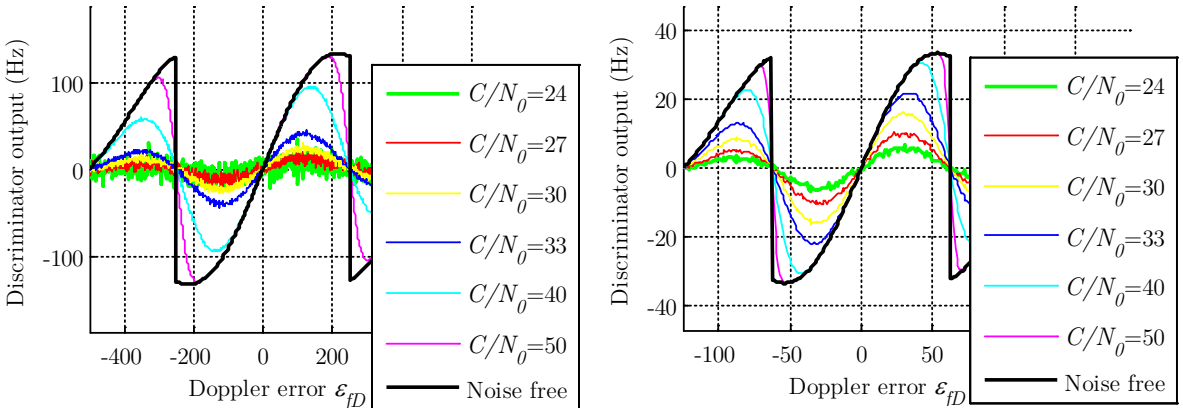

(a) GPS L1 C/A ($T_C = 1$ ms) (b) Galileo E1 OS ($T_C = 4$ ms)

Figure 7.3 DDCP discriminator response to frequency error for a noise-free signal and different C/N_0 cases

- Differential Arctangent (Atan) Discriminator

One of the optimal phase estimators, from a Maximum Likelihood sense, is $\widehat{\varepsilon_\phi}(k) = \tan^{-1}\big(Q(k)/I(k)\big)$. Then, based on this, a frequency discriminator can be computed using the difference of the phase estimator at two consecutive instants.

$$e_{Atan}(k) = \frac{1}{2\pi T_C}\mathrm{UW}\left(\tan^{-1}\left(\frac{Q(k)}{I(k)}\right) - \tan^{-1}\left(\frac{Q(k-1)}{I(k-1)}\right)\right) \tag{7.4}$$

where UW is a phase-unwrapping function that maps the phase estimate from $[-\pi, \pi]$ to the interval $\left[-\frac{\pi}{2}, \frac{\pi}{2}\right]$ defined by:

$$\mathrm{y} = \mathrm{UW}(x) \Leftrightarrow \begin{cases} y = x + \pi \in \left[0, \frac{\pi}{2}\right], x \in \left[-\pi, -\frac{\pi}{2}\right] \\ y = x \in \left[-\frac{\pi}{2}, \frac{\pi}{2}\right], x \in \left[-\frac{\pi}{2}, \frac{\pi}{2}\right] \\ y = x - \pi \in \left[-\frac{\pi}{2}, 0\right], x \in \left[\frac{\pi}{2}, \pi\right] \end{cases} \tag{7.5}$$

This discriminator mitigates the effect of the data modulation on the frequency estimate by reducing the estimate of the phase increment to the interval $\left[-\frac{\pi}{2}, \frac{\pi}{2}\right]$ [Curran *et al.*, 2012].

As depicted in Figure 7.4, the linear region of the Differential Arctangent discriminator is $\left[-\frac{1}{4T_C}, \frac{1}{4T_C}\right]$ in the noise-free case. However, the mean response is dependent upon the $\mathrm{C/N_0}$ as it is based on the arctangent of the ratio of 2 correlator outputs.

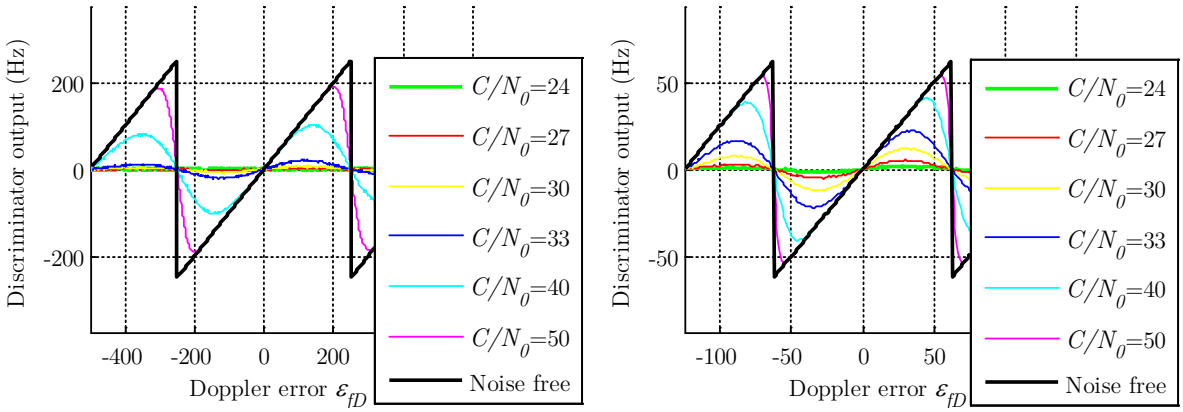

(a) GPS L1 C/A ($T_C = 1$ ms) (b) Galileo E1 OS ($T_C = 4$ ms)

Figure 7.4 Atan discriminator response to frequency error for a noise-free signal and different C/N_0 cases

- Four-Quadrant Arctangent (Atan2) Discriminator

The last presented discriminator is the Atan2 discriminator, which is self-normalized as the Differential Arctangent discriminator. The sign of $e_{Atan2}(k)$ depends on the sign of $d(k-1)d(k)$ and then care must be taken when applying it to data modulated signals [Curran *et al.*, 2012].

$$\begin{aligned} e_{Atan2}(k) &= \frac{1}{2\pi T_C}\operatorname{atan2}(Cross, Dot) \\ &= \frac{1}{2\pi T_C}\tan^{-1}\left(\frac{d(k-1)d(k)\sin\left(\varepsilon_\phi(k)-\varepsilon_\phi(k-1)\right)}{1+d(k-1)d(k)\cos\left(\varepsilon_\phi(k)-\varepsilon_\phi(k-1)\right)}\right) \end{aligned} \tag{7.6}$$

where the acrtangent function with 2 arguments atan2 is defined by:

$$\begin{aligned} \mathrm{z} = \operatorname{atan2}(y,x) &= 2\tan^{-1}\left(\frac{y}{x+\sqrt{x^2+y^2}}\right) \\ &\Leftrightarrow \begin{cases} z = \tan^{-1}\left(\frac{y}{x}\right) \in \left]-\frac{\pi}{2},\frac{\pi}{2}\right[, x>0 \\ z = \tan^{-1}\left(\frac{y}{x}\right)-\pi \in \left]-\pi,-\frac{\pi}{2}\right[, x<0, y<0 \\ z = \tan^{-1}\left(\frac{y}{x}\right)+\pi \in \left]\frac{\pi}{2},\pi\right[, x<0, y>0 \\ z = \frac{\pi}{2}\times\operatorname{sign}(y), x=0, y\neq 0 \\ \text{undefined}, x=0, y=0 \end{cases} \end{aligned} \tag{7.7}$$

If $\cos\left(\varepsilon_\phi(k)-\varepsilon_\phi(k-1)\right)$ and $\sin\left(\varepsilon_\phi(k)-\varepsilon_\phi(k-1)\right)$ are strictly positive and the data bits have the same sign, without noise, $\operatorname{atan2}(Cross, Dot) = \varepsilon_\phi(k)-\varepsilon_\phi(k-1)$. But if the data bits do not have the same sign, it results that $Cross$ and Dot are negative and then $\operatorname{atan2}(Cross, Dot) = \left(\varepsilon_\phi(k)-\varepsilon_\phi(k-1)\right)-\pi$ and the resulting frequency estimate is $\varepsilon_{f_D}-\frac{1}{2T_C}$.

From Figure 7.5, the linear region is the widest compared to the previous discriminators and it is evident that the response is also sensitive to the received C/N_0.

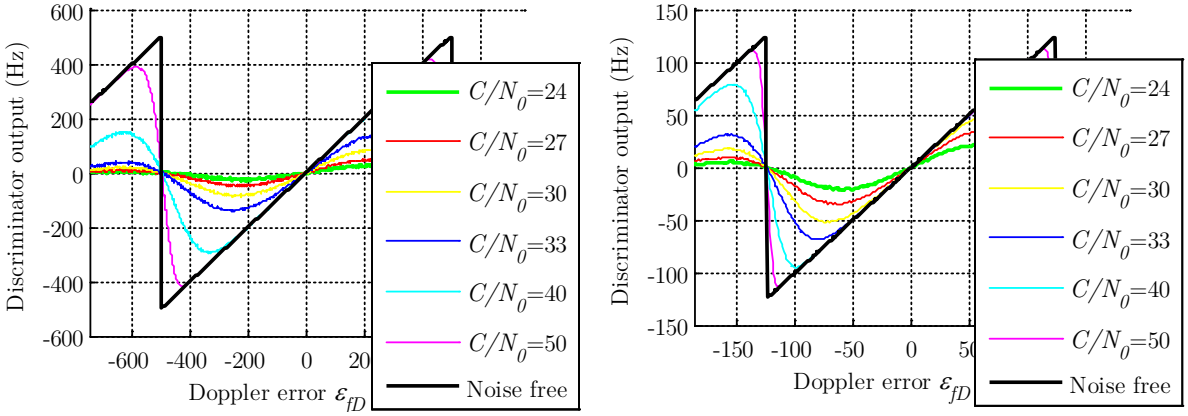

(a) GPS L1 C/A ($T_C = 1$ ms) (b) Galileo E1 OS ($T_C = 4$ ms)

Figure 7.5 Atan2 discriminator response to frequency error for a noise-free signal and different C/N_0 cases

7.1.1.3 Discussion

- Linear region and discriminator gain

As previously said, for most of the discriminators, the linear region changes with the C/N_0. It is worth noting that the linear region should be as large as possible to ensure a better stability of the loop for large errors. For the Cross-Product and Decision Directed Cross Product discriminators, the linear region is the narrowest $\left[-\frac{1}{8T_C}, \frac{1}{8T_C}\right]$ whereas it is the widest $\left[-\frac{1}{2T_C}, \frac{1}{2T_C}\right]$ for the Atan2 discriminator (the Atan discriminator linear region is $\left[-\frac{1}{4T_C}, \frac{1}{4T_C}\right]$).

The discriminator gain K_D is defined as the slope of the discriminator function when the frequency error is zero. A carrier frequency estimate can under certain conditions (discussed in [Curran, 2010]) be approximated by the gain plus an independent corrupting noise noted η^w:

$$e(k) \approx \frac{1}{T_C} K_D \left(\varepsilon_\phi(k) - \varepsilon_\phi(k-1)\right) + \eta^w(k) \tag{7.8}$$

Under strong signal power condition, the slope is approximately unity. As the C/N_0 is reduced, the slope of the discriminator function usually becomes flatter, as seen in Figure 7.4 and Figure 7.5 for instance. As the relationship is nonlinear, discriminator gains in function of C/N_0 are estimated using Monte-Carlo simulations and approximations models are given in [Curran, 2010].

$$\begin{aligned} \text{CP: } K_D &= 1 \\ \text{DDCP: } K_D &\approx 1 - e^{-0.388 \times 2 \frac{C}{N_0} T_C} \\ \text{Atan: } K_D &\approx \left(1 - e^{-0.368 \times 2 \frac{C}{N_0} T_C}\right)^2 \\ \text{Atan2: } K_D &\approx 1 - e^{-0.7683 \times 2 \frac{C}{N_0} T_C} \end{aligned} \tag{7.9}$$

In Figure 7.6, the line curves correspond to the theoretical gains given by (7.9). Markers represent the experimental gains which result in the slope computation from the discriminator response curves. It can be observed that they agree well for both signals.

Note that it is important for the proper function in the loop that the slope is well taken into account. Indeed, if this is not the case, then the discriminator will under- or over- evaluate the actual frequency tracking error which will put the loop into danger of losing lock, and will certainly make it work in a sub-optimal way.

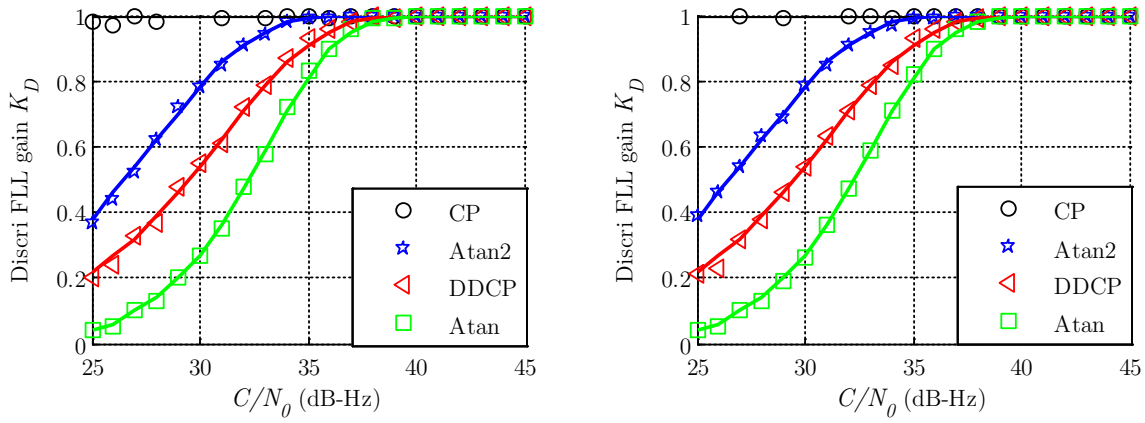

(a) GPS L1 C/A ($T_C = 1$ ms) (b) Galileo E1 OS ($T_C = 4$ ms)

Figure 7.6 Theoretical and estimated discriminator gains

- FLL tracking error

Due to thermal noise and dynamic stress error, the frequency estimate at the output of the FLL is not perfect, there is an error, denoted η_f. The Doppler frequency error can be modeled as:

$$\varepsilon_{f_D} = f_D - \hat{f}_D + \eta_f \tag{7.10}$$

The general expression of the FLL tracking loop jitter due to thermal noise is given by [Ward *et al.*, 2005b] ([Natali, 1984] gives the tracking error variance for each discriminator):

$$\sigma_{FLL} = \sqrt{var(\eta_f)} = \frac{1}{2\pi T_C}\sqrt{\frac{4FB_L}{C/N_0}\left(1 + \frac{1}{T_C C/N_0}\right)} \tag{7.11}$$

where F is a parameter which value is 1 or 2.

Simulations were run for two discriminators to verify the correct implementation of the FLL. The variance of the FLL frequency error is computed over 10 seconds assuming a null initial error. The Galileo E1 OS is tracked, assuming potential bit sign transitions and for coherent integration on $T_C = 4$ ms, the FLL bandwidth was chosen equal to $B_L = 10$ Hz. Results are plotted in Figure 7.7(a). As it can be observed, experimental results (with marker) match perfectly the theoretical results (black solid line $F = 2$). The validation of the FLL model permits also to highlight that the tracking error variance is not a linear function of the C/N_0.

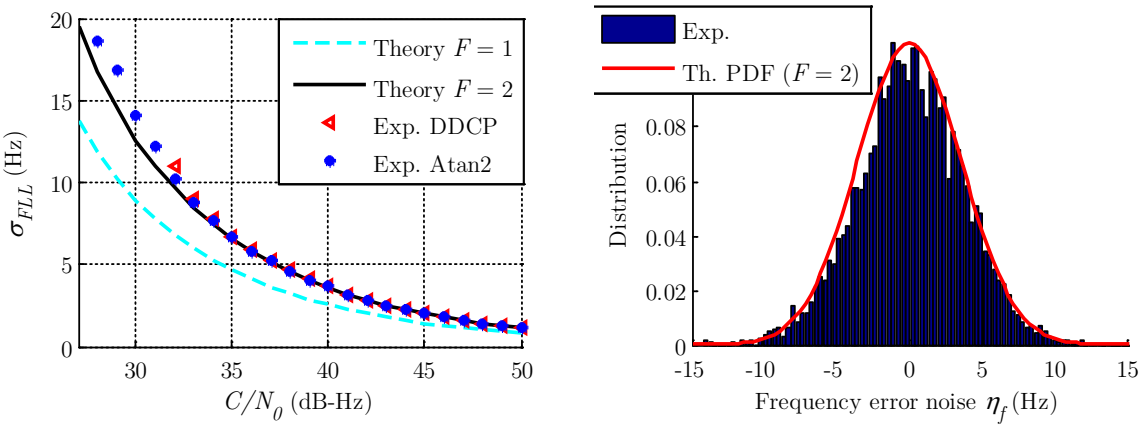

(a) Adequacy of the frequency error noise

(b) Distribution of the frequency error noise (DDCP discriminator)

Figure 7.7 Frequency error standard deviation due to thermal noise (theoretical and simulated results) (Galileo E1 OS, $T_C = 4$ ms, $B_L = 10$ Hz)

In addition, Figure 7.7(b) shows that the approximation of the frequency error noise η_f by a Gaussian distribution is justified. Then, in this chapter, it is assumed that the frequency error noise is a centered Gaussian disbribution:

$$\eta_f \sim \mathcal{N}(0, \sigma_{FLL}^2) \tag{7.12}$$

7.1.2 Discriminator combination techniques

The main contribution of this section is to investigate correlator combination techniques to strengthen frequency tracking and compare their properties and performance.

7.1.2.1 GPS L1 C/A

For GPS L1 C/A, two techniques are looked at: the classical FLL scheme, and a technique based on a frequency update every 20 ms, which corresponds to the data bit duration.

- FLL update every $2\times T_{c_1}$ (2 ms)

This technique is the classical use of a FLL. Two consecutive pairs of correlator outputs are computed and are used for the FLL discriminator computation. The frequency update is based on the FLL discriminator output. The update of the local frequency is thus taking place every two spreading code period. An illustration of this technique is presented in Figure 7.8.

Because right after the acquisition, the receiver is not synchronized with the data sequence, the data bit boundaries are not known. This implies that it is possible that, one pair of correlator outputs can straddle two data bits. This bad configuration occurs only for 1 every 10 correlator output pairs, but the data bit change does not necessary imply a sign change.

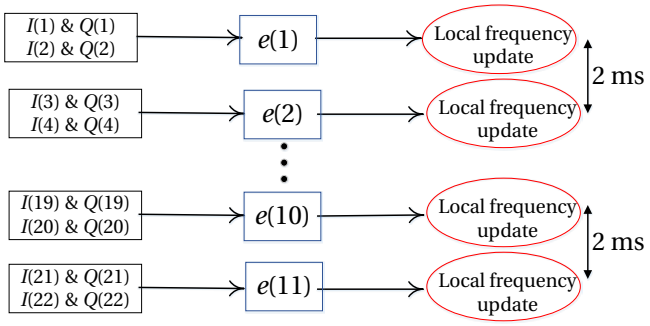

Figure 7.8 Classical FLL technique

- FLL update every 20 ms

The second GPS L1 C/A technique is briefly presented in [Van Dierendonck, 1996]. It is based on correlator outputs computed every $T_C = 1$ ms. The discriminator output is in fact an average value on the 19 discriminator outputs, computed over 20 ms (the first discriminator output is computed with the first T_C ms and the second T_C ms, the second discriminator output with the second T_C ms and the third T_C ms…). The scheme is presented in Figure 7.9.

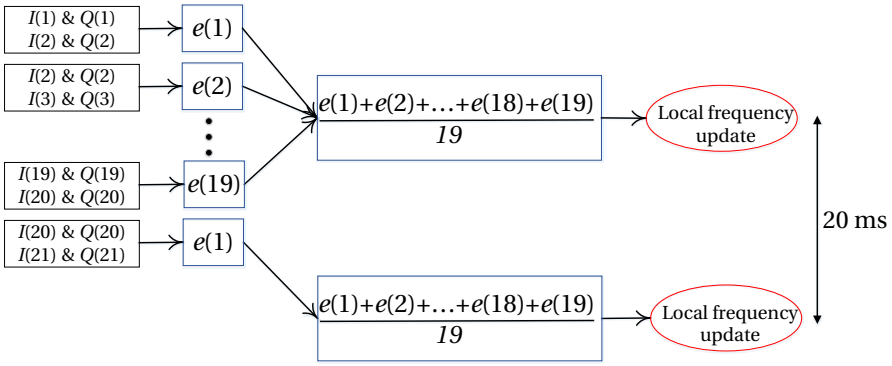

Figure 7.9 GPS L1 C/A FLL technique based on a frequency update every 20 ms

The advantages of this discriminator is that it allows refining the estimation of the frequency error and has an intrinsic mitigation of bit sign transition consisting in mixing the corresponding faulty discriminator output with 18 other ones that will not be affected by bit sign transition.

Figure 7.10 presents the considered GPS L1 C/A discriminator combination techniques. The signs + (associated to a blue cell) and – (associated to a red cell) refer to the sign of the data bit in the correlator output. The brace refers to the correlator combination: a green brace means that the sign of the data bit is the same for both correlator output pairs, a violet refers to a different sign and then potential FLL performance degradations.

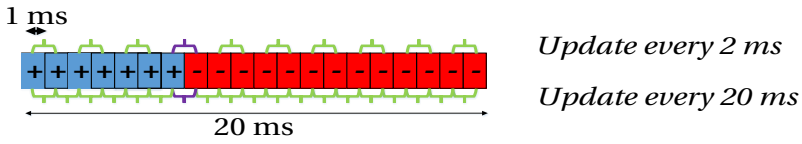

Figure 7.10 Illustration of the impact of bit sign transition for different discriminator combination technique (GPS L1 C/A)

7.1.2.2 Galileo E1 OS and modernized GNSS signals

For all of the presented techniques, a choice on the number of considered components should be done. Except for GPS L1C, which has a dissymmetry in signal power distribution between both components, when only one component is used, it does not matter whether the data or the pilot component is used since data and secondary code bits have the same duration (for GPS L5, the presence of the secondary code on the data component implies that the resulting binary sequence bit has the same duration as the pilot secondary code bit). When considering both data and pilot components to acquire the total received signal power, the data and pilot components are processed separately and each one provides a FLL discriminator output. The frequency update is based on the average value of the discriminator outputs obtained from the data and pilot components. Discriminator combinations techniques for modernized GNSS signals are illustrated on the basis of the use of both components.

- FLL update every $2\times T_{c_1}$ (8 ms for Galileo E1 OS)

The first technique for modernized GNSS signals is similar to the first one for GPS L1 C/A and it is illustrated by the Figure 7.11.

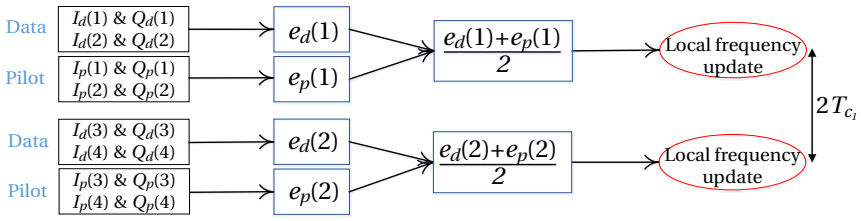

Figure 7.11 Classical FLL technique applied to data/pilot GNSS signals

- FLL update at 20 ms

To mimic what is done for the GPS L1 C/A second technique, the update of the local frequency is every 20 ms, based on an average discriminator output. Then on both components, the discriminator output is computed for each consecutive pair (for example, for Galileo E1 OS, 4 discriminators outputs on 4 ms per component over 20 ms as presented in Figure 7.12).

For GPS L1C, the spreading code period is $T_{c_1} = 10$ ms, the first and second techniques are thus similar.

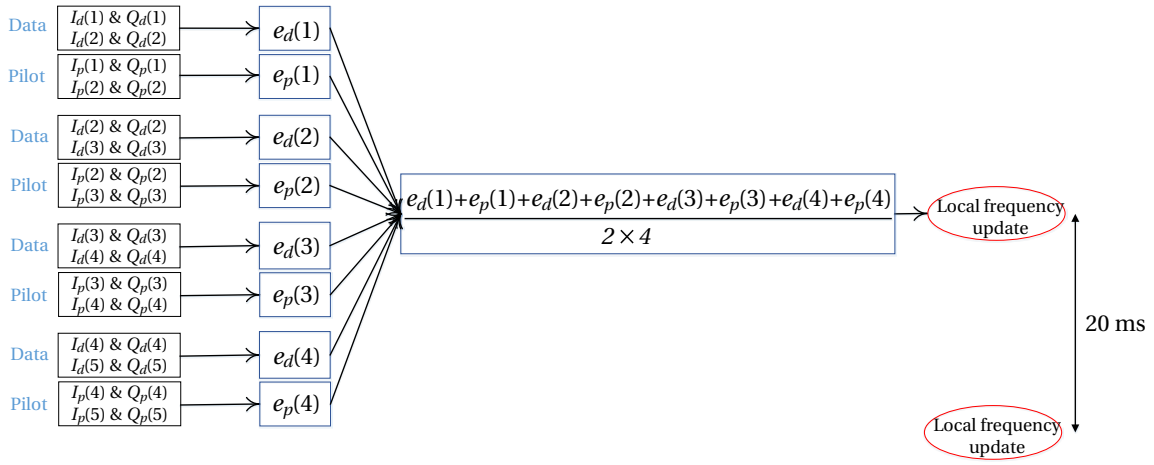

Figure 7.12 Galileo E1 OS FLL technique based on a frequency update every 20 ms

- Partial correlation outputs

Modernized GNSS signals present the particularity to have a spreading code period equal to the data (or secondary code) bit duration. This implies potential data bit sign change between any two consecutive correlator output pairs. For the frequency discriminators that are bit sign transition sensitive, producing correlator output pairs that are on the data bit will improve the FLL performance. The proposed technique thus consists in computing partial correlations that are based on at most half the duration of the PRN code. By doing so, and since the receiver is synchronized with the PRN sequences, the frequency discriminator based on consecutive partial correlation that belong to the same PRN will not be affected by data bit transition by definition. Another advantage of this technique is that by reducing the correlation duration, the pull-in region of the discriminator becomes wider. The drawback is that by reducing the coherent integration time to $T_C = \frac{T_{c_1}}{2}$ ms (for example, for Galileo E1 OS, 2 ms instead of 4 ms), the correlator outputs and discriminators will be more noisy.

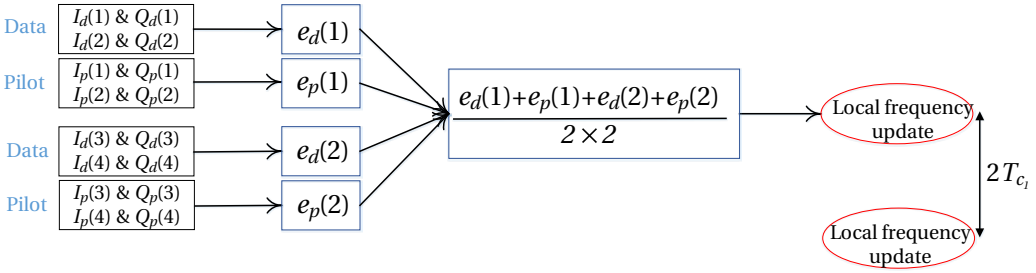

Figure 7.13 FLL technique applied to data/pilot GNSS signals using partial correlations

As previously, a variant of this technique consists in updating every 20 ms instead of $2T_{c_1}$.

Figure 7.14 provides an illustration of the discriminator combination techniques applied to Galileo E1 OS. As it can be observed, even if the beginning of the spreading code is supposed to be known, two consecutive correlator output pairs computed on the full spreading code period can have a different data bit sign (or secondary code bit sign for the pilot component) with a probability of 50% whereas two consecutive correlator output pairs computed on 2 ms in a spreading code period have the same data bit sign. Two consecutive partial correlator outputs taken in the same spreading code have the same sign and are not affected by a bit sign change.

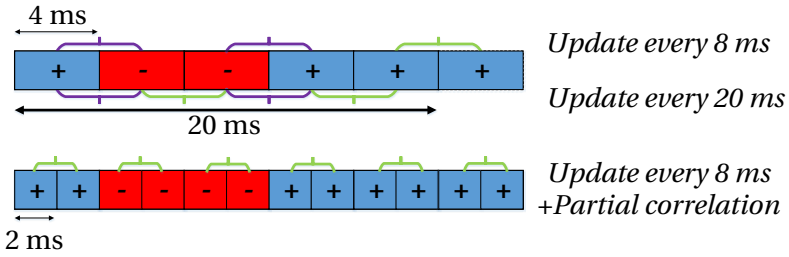

Figure 7.14 Illustration of the impact of bit sign transition for different discriminator combination technique (Galileo E1 OS)

7.1.3 Simulation scheme

The simulations results are based on Monte-Carlo simulations and present the probability to get the FLL locked after 20 seconds as a function of the considered GNSS signal, the discriminator combination technique, the loop bandwidth, the discriminator function, the input Doppler frequency error and the received C/N_0.

7.1.3.1 Simulations inputs

- Loop order and equivalent loop bandwidth

For the simulations, the loop order is chosen equal to 2 in order to be able to track jerk dynamics (this is a typical choice for FLLs).

The one-sided noise bandwidth B_L is defined in [Curran, 2010]. In this study, it can take values between 1 and 10 Hz. A system with a higher bandwidth has a faster response because the convergence time is in the order of $\frac{1}{B_L}$ (in seconds). However, a wide bandwidth also means a tracking more affected by thermal noise.

- Doppler frequency error

The uncertainty on the frequency at the initiation of the tracking is equal to half of the width of the Doppler acquisition bin i.e. $\frac{1}{4T_C}$. It is reasonable to assume that the distribution of the Doppler error at the initiation of the tracking phase is uniform and that the FLL performance does not depends on the sign of the Doppler frequency error.

To test the dependency of the FLL tracking performance as a function of the initial Doppler error, the initial uncertainty region $\left[0, \frac{1}{4T_C}\right]$ has been split into 50 sub-bins. For each sub-bin, 200 uniformly distributed initial frequencies are tested. The simulation output result is thus obtained for each sub-bin and a more general simulation result can be obtained by averaging the results from each sub-bin and provides a result per C/N_0 (average over 10 000 simulations).

7.1.3.2 Simulation output

During the simulations, it was decided that the FLL was locked when the frequency error output is in the corresponding discriminator linear region after 20 seconds, which is representative of a convergence and a stable tracking (or at least, no divergence). The probability that the FLL remains locked after 20 seconds can be seen as the convergence success rate.

The experimental probability to get locked, denoted P_l, is then the number of times that the frequency error is in the linear region after 20 seconds over the number of simulations (20 seconds is an arbitrarily value, if 20 seconds the FLL does not converge, it means that in a less time, for example 100 ms, there is no FLL lock).. For example, in Figure 7.15, the upper case does not imply an increment of the "success" counter even if the frequency estimate (represented with a red curve) crosses the linear region during the 20 seconds. For the lower case, after 20 seconds, the frequency estimate is in the linear region (materialized by black lines) and this leads to an increment of the "success" counter. Indeed, that means that the Doppler frequency error should be refined.

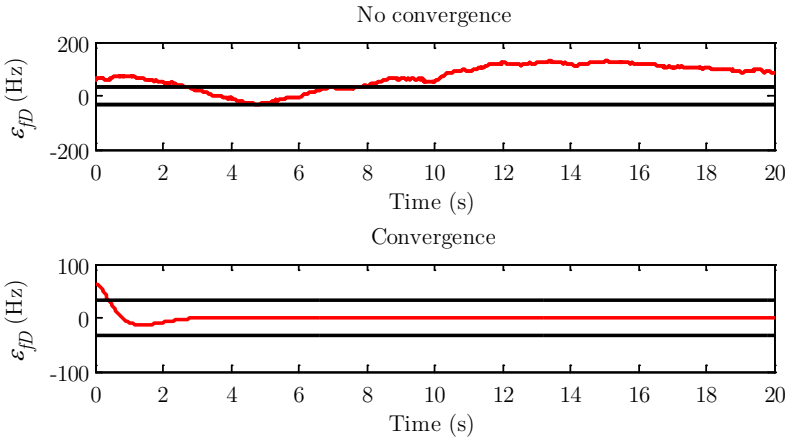

Figure 7.15 Convergence scheme

7.1.3.3 Simulation scheme

The algorithm consists in simulating the correlator output pairs, computing a frequency estimate and then running the FLL. The data and secondary code on the pilot component are implemented. For GPS L1 C/A, the data bit sign is randomly chosen among the 20 spreading code periods. For the modernized GNSS signals, on the pilot component, the first secondary code bit is randomly chosen.

7.1.4 Simulation results

Monte-Carlo simulations results are presented in this section. This permits to determine the best FLL schemes depending on several parameters such as the loop bandwidth, the discriminator, the discriminator combination technique, the coherent integration time. The criterion is the probability to get locked, experimentally obtained.

7.1.4.1 Loop bandwidth

The tested input parameter is the first loop bandwidth. Four values are tested, $B_L = 1, 2, 5, 10$ Hz. Figure 7.16 and Figure 7.17 presents the results for the different values of loop bandwidth. Whatever the discriminator and the input Doppler frequency error, it is better to choose an FLL loop bandwidth B_L that is relatively reduced even though this reduces the response time of the loop. Clearly, the curves with black circle ($B_L = 1$ Hz) and blue stars ($B_L = 2$ Hz) are higher than the other curves with higher loop bandwidth. Only one correlator output technique is presented for each signal but the trend stays unchanged whatever the used correlator output technique. In the following, $B_L = 1$ Hz is thus chosen for the simulations, this implies a convergence time of the FLL loop of 1 second, which is much smaller than 20 seconds (simulated convergence time).

Figure 7.16 and Figure 7.17 also show, as expected, that the successful convergence rate depends upon the initial Doppler frequency error: it is better to start close to the correct value.

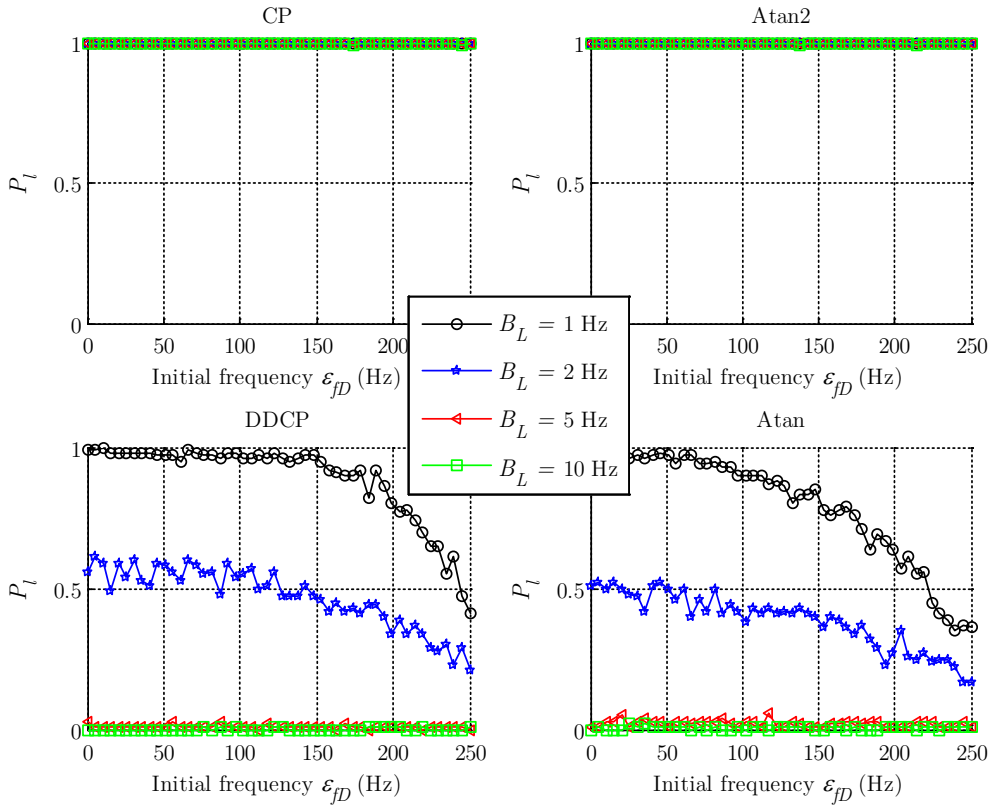

Figure 7.16 Probability to get locked in function of the FLL loop bandwidth (GPS L1 C/A, $C/N_0 = 27$ dB-Hz, frequency update every 20 ms)

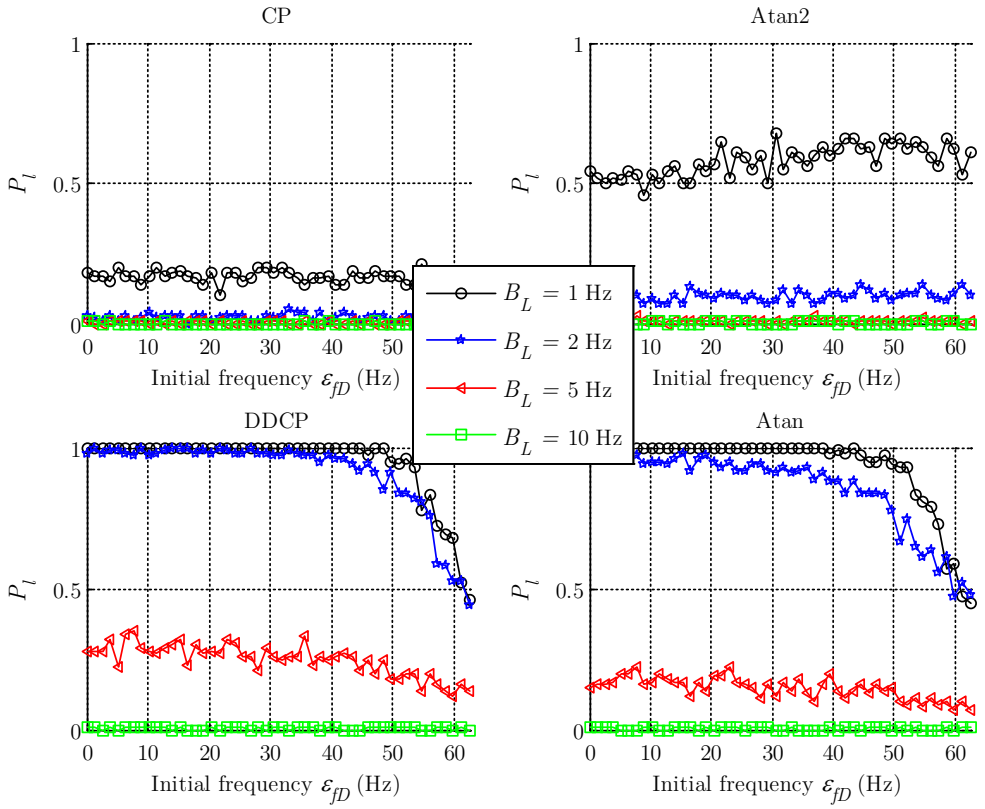

Figure 7.17 Probability to get locked in function of the FLL loop bandwidth (Galileo E1 OS (both components), $C/N_0 = 27$ dB-Hz, frequency update every 20 ms and full correlations on 4 ms)

7.1.4.2 GPS L1 C/A

From Figure 7.18, it can be observed that the discriminator combination technique does not change the trend of the probability to get locked but the technique with a frequency update every data bit duration (20 ms) provides better performance.

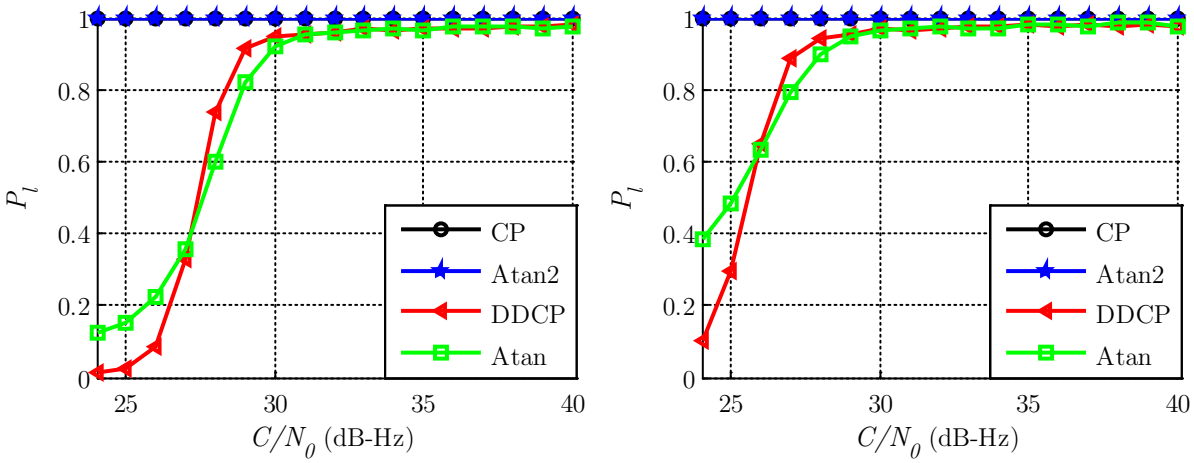

(a) Frequency update every 2 ms (b) Frequency update every 20 ms

Figure 7.18 Results for FLL schemes for GPS L1 C/A

Only one over the 19 frequency estimates is affected by a data bit transition, which can be a sign transition with a probability of 50%. This explains why the impact of a data bit sign transition is negligible when updating the frequency every 20 ms, as confirmed by Table 7.1 where the simulated correlator outputs do not take into account the presence of data in the column "No data".

The evolution of the probability to get locked at 27 dB-Hz as a function of the input Doppler frequency error is provided in Figure 7.17 ($B_L = 1$ Hz), the average value corresponding to the value presented in Figure 7.18(b).

	Data sensitive discriminators				Data insensitive discriminators			
	CP		Atan2		DDCP		Atan	
	Data	No data	Data	No data	Data	No data	Data	No data
2 ms	1	1	1	1	0.33	0.34	0.38	0.36
20 ms	1	1	1	1	0.89	0.88	0.79	0.79

Table 7.1 Average probability to get locked at 27 dB-Hz in presence/absence of data (GPS L1 C/A)

Since data bit transition does not occur at every spreading code period (as it is the case for modernized GNSS signals), the data sensitive discriminators (CP and Atan2) always allow FLL convergence at the presented C/N_0 (relatively low). More simulations were run to determine the C/N_0 threshold for which the FLL failed to lock, results are presented in Figure 7.19 for both discriminator combination techniques. When the frequency is updated every 2 ms (Figure 7.19(a)), the C/N_0 threshold is between 20 and 25 dB-Hz for both discriminators. When the frequency update is based on the average over 19 frequency estimates, the C/N_0 threshold is obviously lower (between 15 and 20 dB-Hz). It can also be seen that Atan2 discriminator provides more robustness.

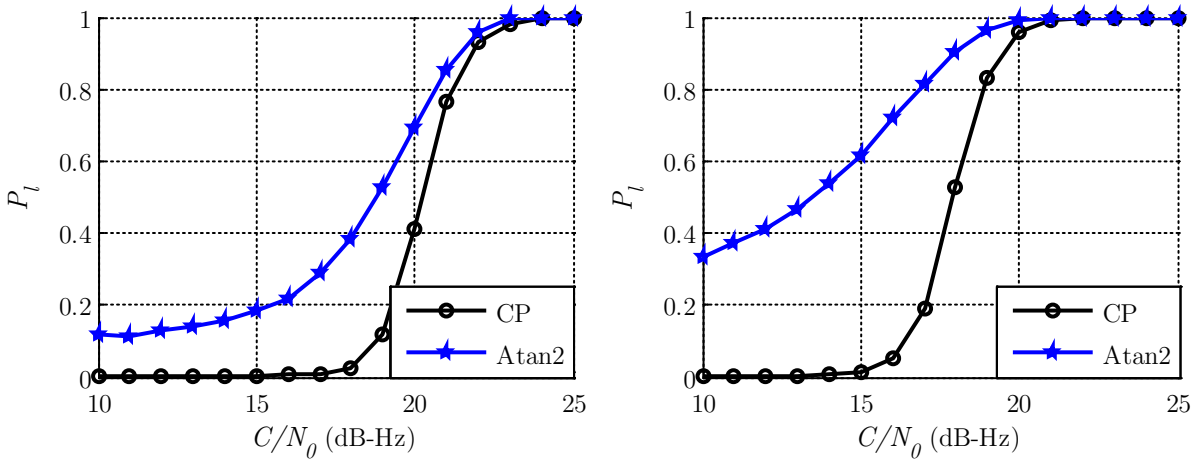

(a) Frequency update every 2 ms

(b) Frequency update every 20 ms

Figure 7.19 Results for FLL schemes for GPS L1 C/A (low C/N_0)

As a conclusion, for a GPS L1 C/A signal, at 27 dB-Hz the best discriminator choice for the FLL scheme seems to be based on a data sensitive discriminator (Atan2 from the simulations) with a frequency update over 20 ms.

7.1.4.3 Galileo E1 OS

Unlike GPS L1 C/A, Galileo E1 OS has two components and the FLL designer could choose to use one or both components. Figure 7.20 and Figure 7.21 compare the FLL performance when only pilot correlator output pairs are considered (Figure(a)) or when both correlator output pairs are used (Figure(b)). For the results presented in Figure 7.20, the frequency is updated every two spreading code periods, which means 8 ms whereas for the Figure 7.21, the frequency is updated every 20 ms. For both techniques (frequency update every 8 ms or 20 ms), the probability that the FLL is locked is higher when both components are used, and whatever the FLL discriminator, except for the CP discriminator at higher C/N_0 values. The difference is particularly pronounced for low C/N_0 and data modulation insensitive discriminators (DDCP with red triangle and Atan with green square). This demonstrates that using both components permits to average the correlator noise output and provides better performance. When considering partial correlations, only results based on the correlation on both components are presented.

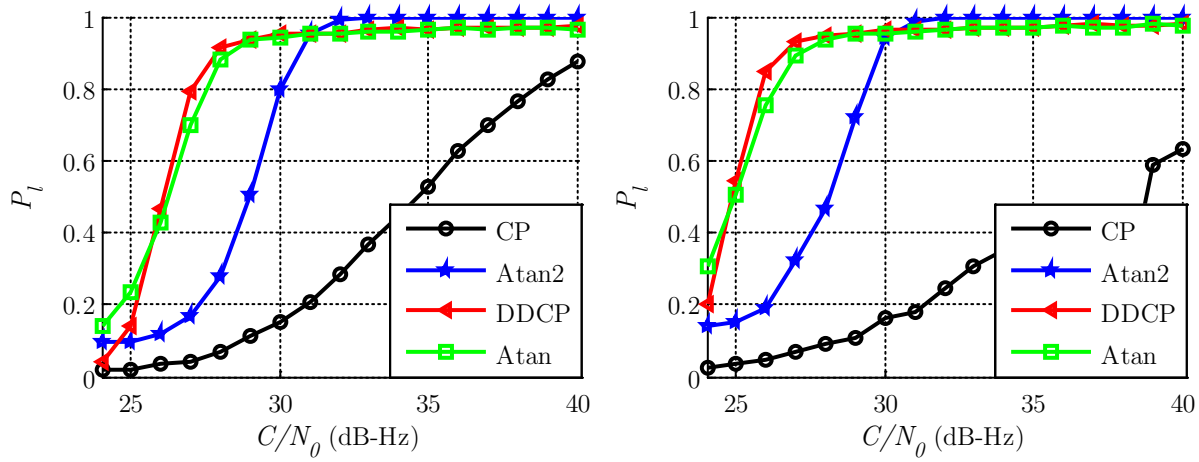

(a) Pilot component (b) Both components

Figure 7.20 Results for FLL schemes for Galileo E1 OS with a frequency update every 8 ms ($C/N_0 = 27$ dB-Hz, $T_C = 4$ ms)

For Figure 7.20(b), the frequency update is based on the average on 2 discriminator outputs. For Figure 7.21, it is based on the average of 4 and 8 respectively discriminator outputs. At low C/N_0, the FLL lock occurs more often with Atan and DDCP discriminators.

For Galileo E1 OS, when the coherent integration time is equal to the spreading code period, the data insensitive FLL discriminators (DDCP and Atan) provide higher probability to get locked whatever the discriminator combination technique (on 8 ms or 20 ms) and whatever the number of used components. This can be explained by the frequent bit sign transition on each component.

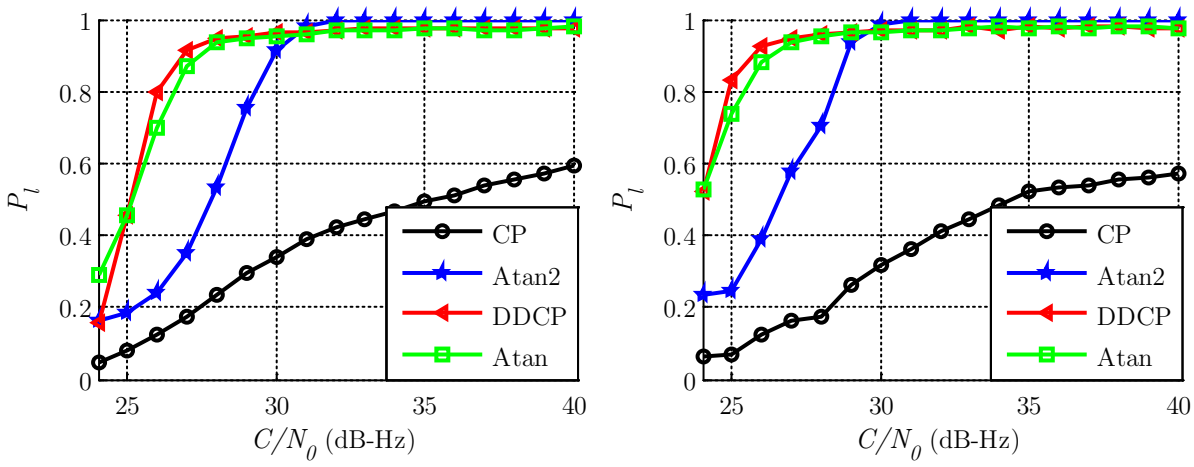

(a) Pilot component (b) Both components

Figure 7.21 Results for FLL schemes for Galileo E1 OS with a frequency update every 20 ms ($C/N_0 = 27$ dB-Hz, $T_C = 4$ ms)

To demonstrate that the performance degradation for CP and Atan2 discriminators are only due to the data modulation, the probability to get locked when there is no data and no secondary code is also computed and compared to the probability in presence of data modulation (Table 7.2). In italics appears the highest probability to get locked per discriminator which highlights the best choice among the discriminator combination technique and coherent integration time. At 27 dB-Hz, for the data insensitive discriminators (last columns), the presence of data does not change the probability to get locked. On the contrary, the probability to get locked for the data sensitive discriminators is equal to 1 when there is no data and no secondary code whereas it can very small when the simulated correlator output pairs take into account the presence of data and secondary code. In general, the probability to get locked is lower for Galileo E1 OS than for GPS L1 C/A.

Components used	T_C	Frequency update	Data sensitive discriminators				Data insensitive discriminators			
			CP		Atan2		DDCP		Atan	
			Data	No data	Data	No data	Data	No data	Data	No data
Pilot	4 ms	8 ms	0.04	1	0.17	1	0.8	0.79	0.7	0.7
		20 ms	0.18	1	0.35	1	0.91	0.92	0.87	0.87
Both		8 ms	0.07	1	0.32	1	0.93	0.93	0.89	0.9
		20 ms	0.17	1	0.58	1	*0.95*	0.95	*0.94*	0.94
	2 ms	8 ms	*1*	1	*1*	1	0.69	0.7	0.69	0.69
		20 ms	*1*	1	*1*	1	0.75	0.76	0.75	0.75
	1 ms	8 ms	*1*	1	*1*	1	0.23	0.22	0.61	0.61
		20 ms	*1*	1	*1*	1	0.27	0.27	0.66	0.67

Table 7.2 Average probability to get locked at 27 dB-Hz in presence/absence of data and secondary code (Galileo E1 OS)

Even if the performance of the FLL for Galileo E1 OS is affected by the bit sign transitions, the "best" FLL discriminator is not necessary a data insensitive discriminator. Indeed, a strategy consists in correlating on a duration shorter than the spreading code period has been presented and is investigated here. Results are presented for a coherent integration duration of 1 and 2 ms. For simulations, only consecutive correlator output pairs in the same data bit are used to compute the frequency estimate.

As it can be read in Table 7.2 and observed in Figure 7.22 and Figure 7.23, the data insensitive discriminators (DDCP and Atan) when using partial correlations are not as good as when using full correlation because they suffer from extra noise (which variance is inversely proportional to the coherent integration time). For example, for the DDCP discriminator, the probability to get locked is 95% when the coherent integration time is 4 ms and becomes 75% and 27% when the coherent integration time is respectively 2 ms and 1 ms. When the coherent integration time is smaller than the data bit duration, the probability to get locked is equal to 1 for CP and Atan2 discriminators, even for low C/N_0.

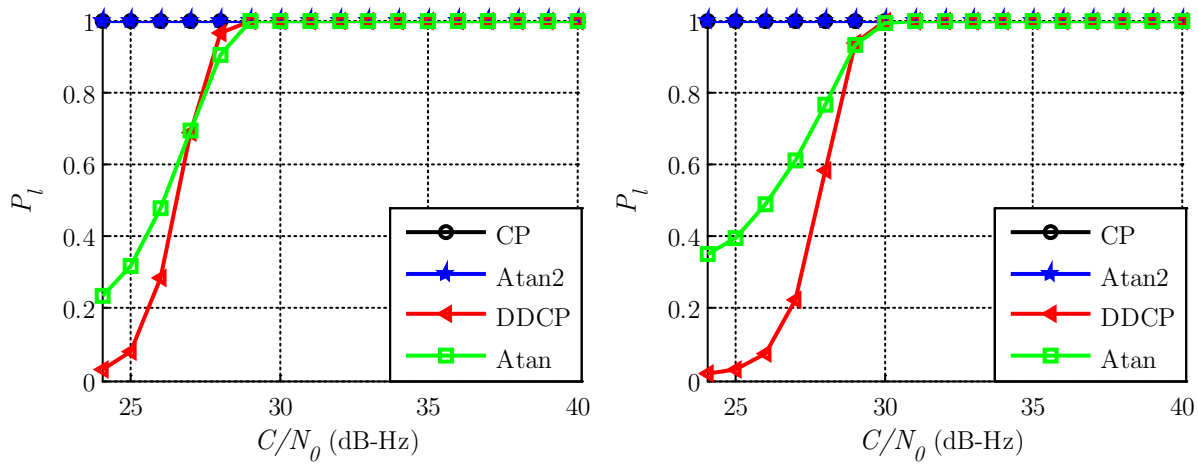

(a) $T_C = 2$ ms (b) $T_C = 1$ ms

Figure 7.22 Results for FLL schemes for Galileo E1 OS with a frequency update every 8 ms (both components)

Let us note that a coherent integration time of 1 ms improves also the probability to get FLL lock when the Atan discriminators are used. This can be explained by the fact that the frequency update is based on the average on 30 discriminator outputs e_{Atan}, (already observed in Figure 7.20(b) and Figure 7.21(b) for a frequency update of 8 or 20 ms respectively) whereas the DDCP discriminator may be more sensitive to the correlator output noise.

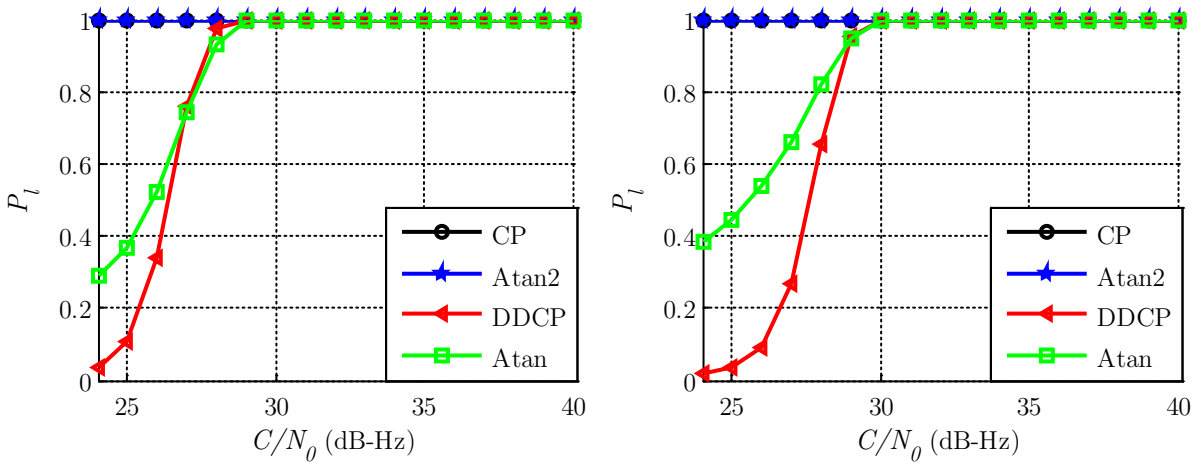

(a) $T_C = 2$ ms (b) $T_C = 1$ ms

Figure 7.23 Results for FLL schemes for Galileo E1 OS with a frequency update every 20 ms (both components)

It can be interesting to study the C/N_0 threshold for which the FLL failed to lock when using partial correlations and data sensitive discriminators.

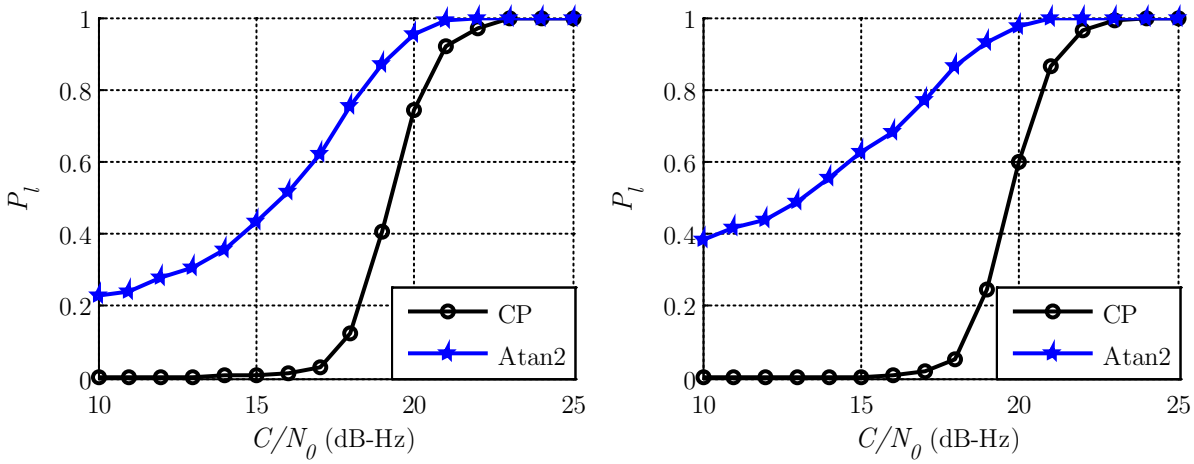

(a) $T_C = 2$ ms (b) $T_C = 1$ ms

Figure 7.24 Results for FLL schemes for Galileo E1 OS with a frequency update every 20 ms (both components) (low C/N_0)

To conclude this section on FLL performance for Galileo E1 OS, the evolution of the probability to get FLL lock as a function of the Doppler frequency error is presented for the three studied coherent integration times and for each discriminator (Figure 7.25). The FLL performance as a function of the coherent integration time is clearly observable:

- For the data sensitive discriminator (first line), the shorter T_C is, the better the probability to get locked is (and is equal to 1 in the present case),
- For data insensitive discriminator (second line), the highest probabilities to get locked are for the longest coherent integration time, except maybe for the highest Doppler frequency errors. Indeed, the probability to get locked falls down for a coherent integration time of 4 ms when the Doppler frequency error is between 50 and 62.5 Hz.

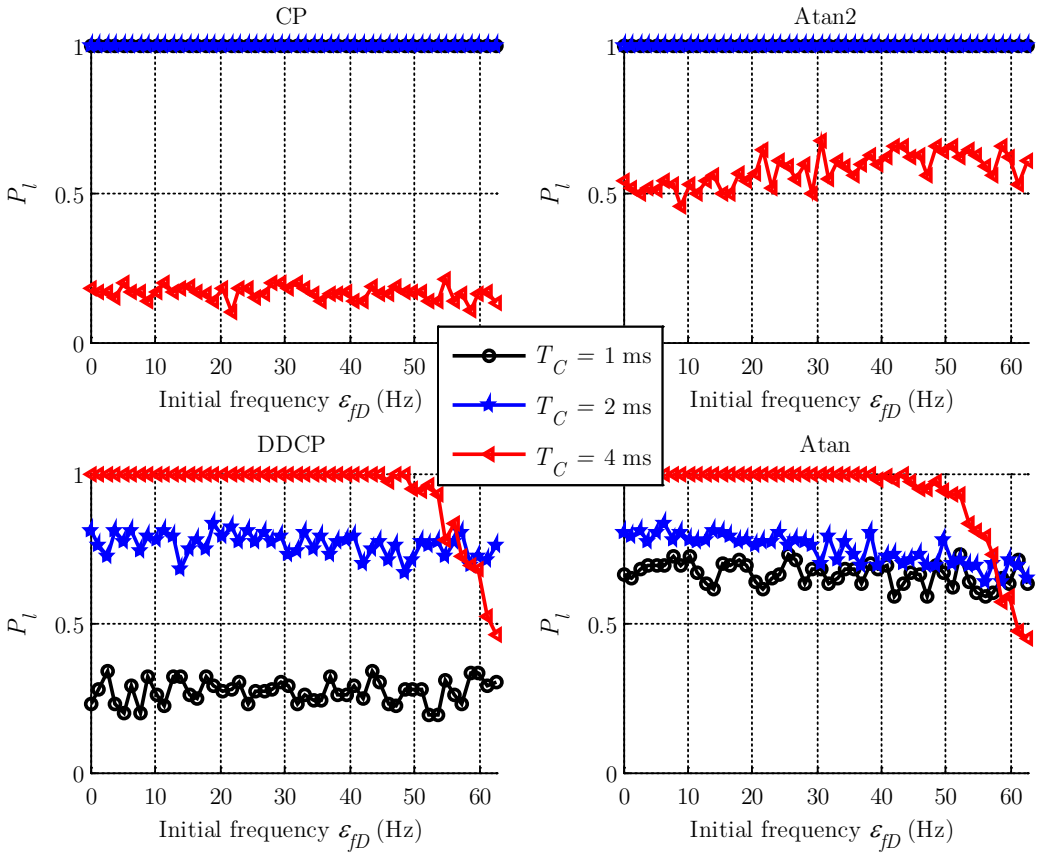

Figure 7.25 Results for FLL schemes for Galileo E1 OS with a frequency update every 20 ms at 27 dB-Hz (both components)

To refine the frequency when acquiring the Galileo E1 OS signal at 27 dB-Hz, several FLL schemes can be used providing the same probability to get locked. A further study can be lead to determine the optimal. As it was presented, it is preferable to use both components and a frequency update every 20 ms. To tackle the problem of bit sign transition, two choices appears relevant:

- Use a data sensitive discriminator (Atan2 seems preferable rather than CP) with partial correlator output computed over 1 ms for example. This implies a probability to get locked equal to 1 whatever the initial frequency error at a C/N_0 of 27 dB-Hz,
- Use a data insensitive discriminator (DDCP better than Atan) with correlator output computed over the full spreading code period. This implies a probability to get locked of 0.95 at a C/N_0 of 27 dB-Hz.

7.1.4.4 Other GNSS signals

It can be interesting to explore the feasibility of the frequency refinement for other modernized GNSS signals, for example GPS L5 and Galileo E5 (indifferently Galileo E5a or Galileo E5b and also true for GPS L5). As for Galileo E1 OS, the main constraint is the presence of potential bit sign transition at each spreading code period

.

- GPS L1C

Because the GPS L1C spreading code period is 10 ms, the FLL schemes applied to this signal only depend on the choice of using the pilot or both components and on the coherent integration time; the frequency being updated every 20 ms.

Unlike Galileo signals, the GPS L1C signal has a dissymmetry in the signal power between both components. For this signal, the computation of the correlator output pair on both components does not seem necessary. From Figure 7.26 and Figure 7.27, where Figure (a) represents the probability to get locked when using only the pilot component (which contains 75% of the total signal power) and Figure (b) the probability to get locked when using both components. The use of both components does not significantly improve the FLL performance compared to the use of the pilot component only. In both cases, the best discriminators are the data insensitive ones (Atan and DDCP).

When the coherent duration is 5 ms (use of partial correlation), the performance of the data sensitive discriminators (CP and Atan2) is greatly improved at low C/N_0 and once again, the probability to get locked in this case is equal to 1 down to 25 dB-Hz.

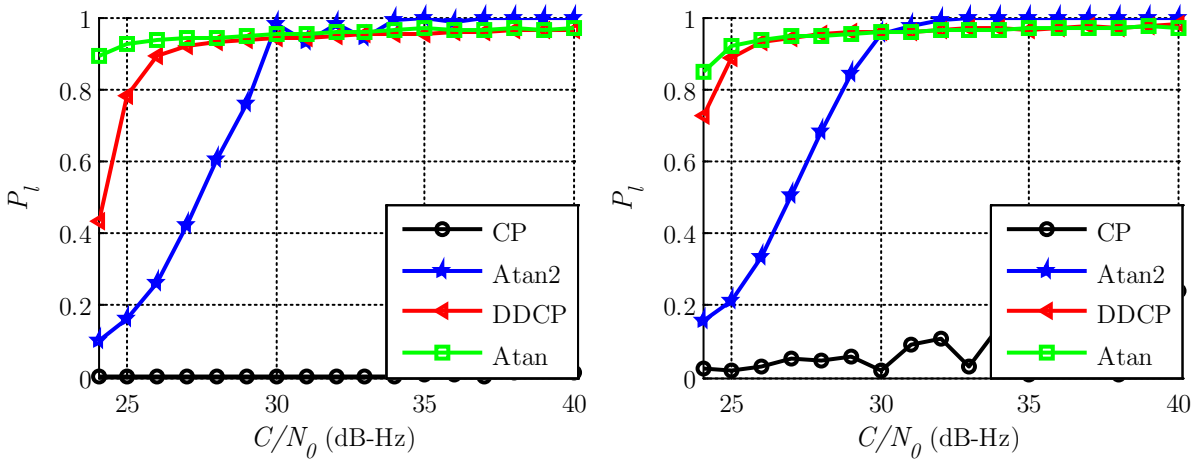

(a) Pilot component (b) Both components

Figure 7.26 Results for FLL schemes for GPS L1C with a frequency update every 20 ms ($T_C = 10$ ms)

Figure 7.28 presents the probability to get FLL lock at 27 dB-Hz as a function of the input Doppler frequency error for three values of partial integration time ($T_C = 1, 5, 10$ ms). For the data transition sensitive discriminators, the shorter the coherent integration duration is, the better the performance is, whereas it is the contrary for the other discriminators.

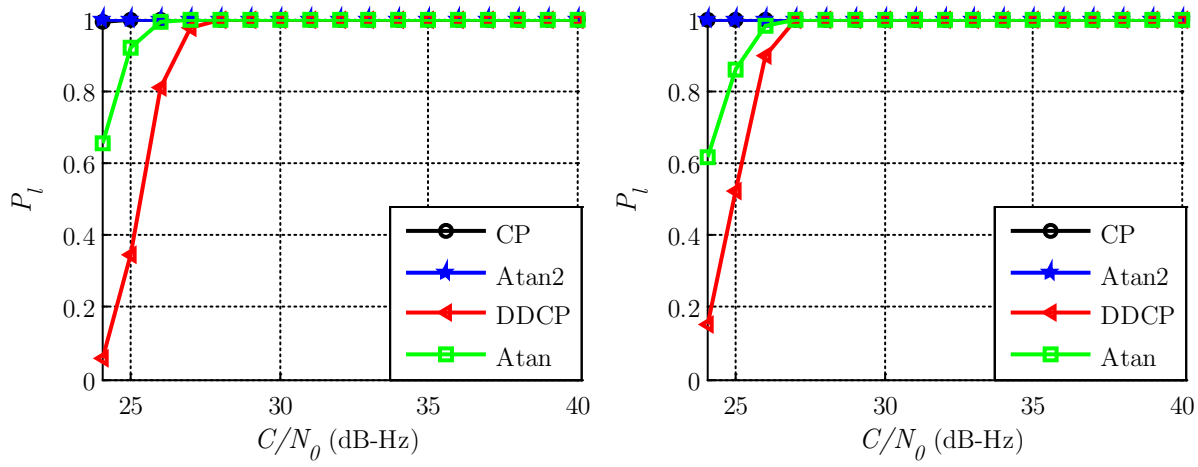

(a) Pilot component (b) Both components

Figure 7.27 Results for FLL schemes for GPS L1C with a frequency update every 20 ms ($T_C = 5$ ms)

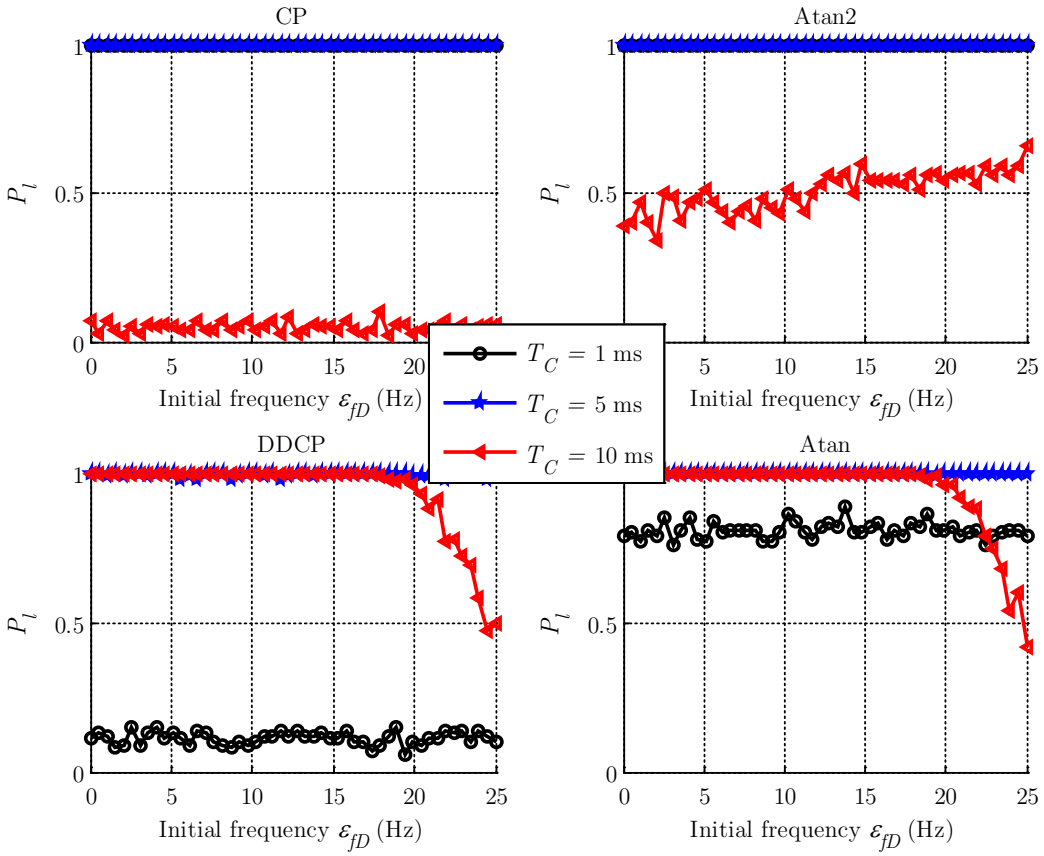

Figure 7.28 Results for FLL schemes for GPS L1C with a frequency update every 20 ms at 27 dB-Hz (both components)

- Galileo E5

The Galileo E5 signal is one of the modernized GNSS signal with the shortest spreading code period (1 ms, like GPS L1 C/A). However, the behavior of the FLL is totally different between these two signals. Indeed, it is reminded that for GPS L1 C/A, the probability to get locked is equal to 1 for the CP and Atan2 discriminators down to 25 dB-Hz. Here, for the Galileo E5 signal, as presented in Figure 7.29 and Figure 7.30, one of the best discriminators is Atan with Atan2 for low C/N_0 or with DDCP for high C/N_0. The improvement of FLL performance when updating every 20 ms (Figure 7.30) instead of 2 ms (Figure 7.29) is clearly observable for the Atan2 and Atan discriminators. As for Galileo E1 OS, the better performance is for the use of both components.

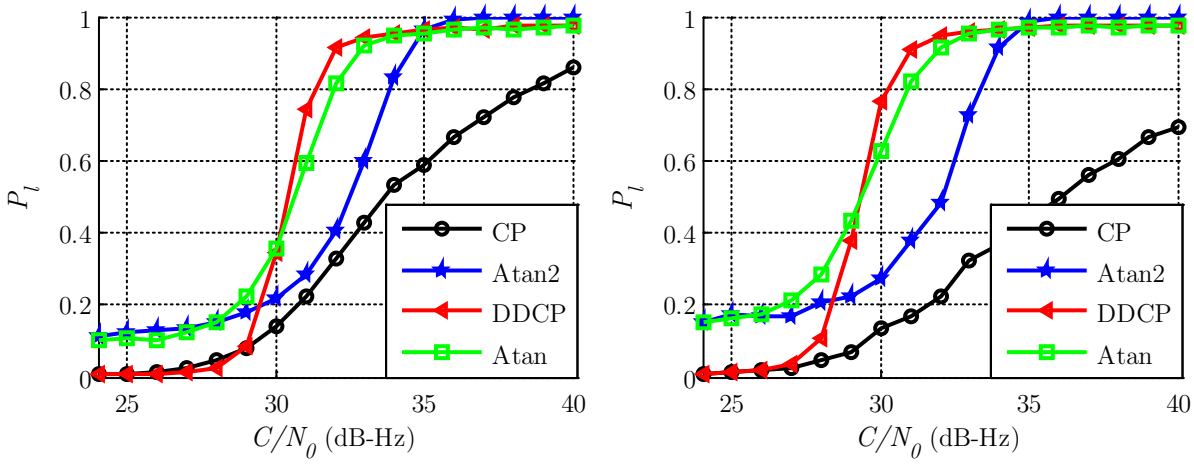

(a) Pilot component (b) Both components

Figure 7.29 Results for FLL schemes for Galileo E5 with a frequency update every 2 ms ($T_C = 1$ ms)

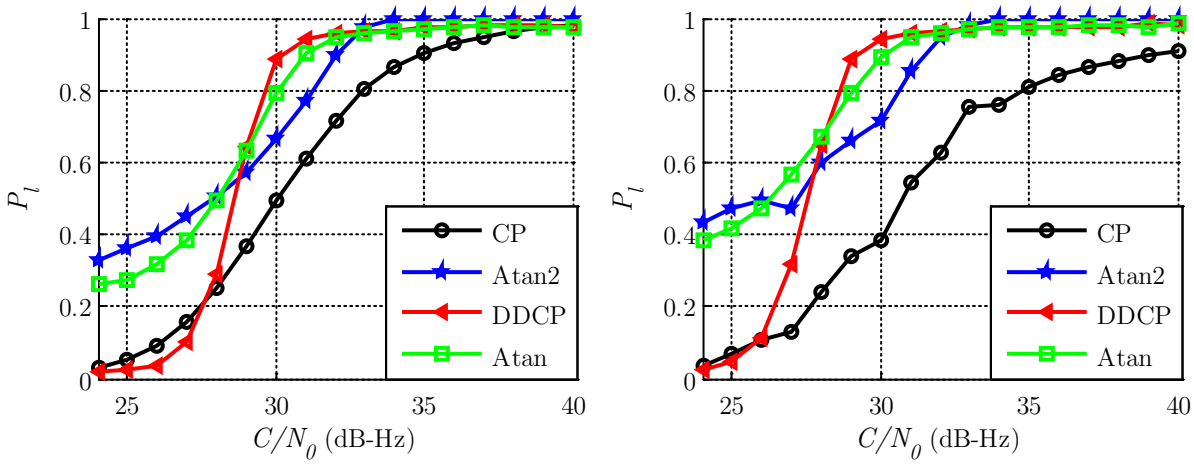

(a) Pilot component (b) Both components

Figure 7.30 Results for FLL schemes for Galileo E5 with a frequency update every 20 ms ($T_C = 1$ ms)

Figure 7.31 compares the FLL performance, at 27 dB-Hz, when correlating on the spreading code period or on half. As for the other modernized GNSS signals, it is preferable to associate

data sensitive discriminators with partial correlation and data insensitive discriminators with full correlation.

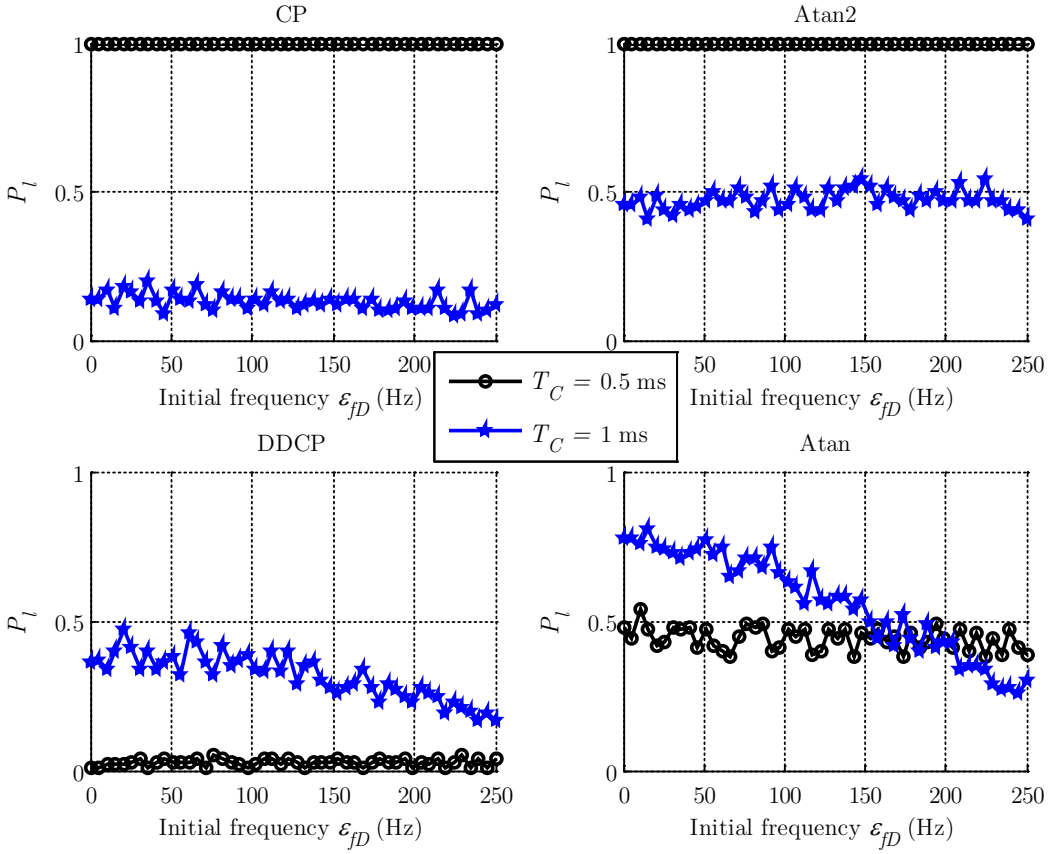

Figure 7.31 Results for FLL schemes for Galileo E5 with a frequency update every 20 ms at 27 dB-Hz (both components)

7.2 Pilot secondary code acquisition

Once the FLL has converged, the last step before tracking the modernized GNSS signal, as expected, is the acquisition of the secondary code. As explained in the previous section, the new generation of GPS and Galileo signals is composed of two components, one being the pilot component which is dataless but contains a known secondary code. The presence of secondary code breaks the periodicity of the transmitted sequence and this increases the correlation properties and speed up the bit synchronization process on the data component [Borio, 2011]. But in order to extend the coherent integration duration for a robust tracking, the secondary code should be acquired.

The objective is to ensure that, even at a weak C/N_0, the acquisition of the secondary code is a success. This study is mainly lead for Galileo E1 OS but results for the other GPS and Galileo modernized signals are also presented.

7.2.1 Pilot secondary code features

First of all, a rapid comparison on the secondary code features is presented in Table 7.3. The secondary codes are relatively short (between 20 and 100 bits) except for GPS L1C which is 1800-bit long. For all the GNSS signals, each bit of the secondary code modulates one period of the spreading code. For Galileo E1 OS and GPS L5, the secondary code on the pilot component is unique and common to all the satellites; it means it cannot be used for satellite identification. The unicity of the secondary code can be explained by its length. Indeed, there are not enough short codes with good correlation properties [Leclère, 2014] for one secondary code per satellite.

	Length	Bit duration	Number of secondary codes	Pilot power allocation	A_p
GPS L1C-P	1800 bits 18 s	10 ms (100 bit/s)	63	75% (-1.25 dB)	$\frac{\sqrt{3C}}{\sqrt{2}}$
GPS L5-Q	20 bits 20 ms	1 ms (1 kbit/s)	1	50% (-3 dB)	$\sqrt{C}$
Galileo E1-C	25 bits 100 ms	4 ms (250 bit/s)	1	50% (-3 dB)	$\sqrt{C}$
Galileo E5a-Q	100 bits 100 ms	1 ms (1 kbit/s)	50	50% (-3 dB)	$\sqrt{C}$
Galileo E5b-Q	100 bits 100 ms	1 ms (1 kbit/s)	50	50% (-3 dB)	$\sqrt{C}$

Table 7.3 Pilot secondary code features

For each considered modernized GNSS signal, the secondary code correlation function for the pilot component, defined by (7.13), is plotted (Figure 7.32 for Galileo E1 OS, Figure 7.33 for GPS L1C, Figure 7.34 for GPS L5, Figure 7.35 for Galileo E5 a/b).

$$R_{c_2}(\Delta) = \frac{1}{N_{c_2}} \sum_{y=1}^{N_{c_2}} c_{2,p}(y) c_{2,p}(y - \Delta) \tag{7.13}$$

where Δ is the secondary code bit delay.

The associated distribution of the values that can take the secondary code autocorrelation function is presented. For signals with several pilot secondary codes (GPS L1C and Galileo E5 a/b), the autocorrelation function for only the first code is represented. The maximum autocorrelation value (minimum isolation) is:

- 13.98 dB for GPS L5,
- 18.42 dB for Galileo E1 OS,
- 21.94 dB for Galileo E5 a/b (same maximum value for all of the 100 Galileo E5 secondary codes),
- 24.76 dB for GPS L1C (maximum reached for one of the 63 GPS L1C secondary codes).

Galileo E1 OS seems to be a good compromise between secondary code length and autocorrelation isolation.

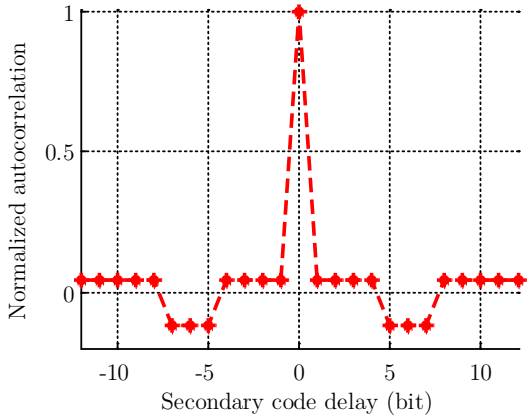

(a) Autocorrelation function shape

Autocorrelation function		Distribution	
		Over 25	In %
0.04	-27.96 dB	18	72%
-0.12	-18.42 dB	6	24%
1	0 dB	1	4%

(b) Autocorrelation function distribution

Figure 7.32 Galileo E1 OS secondary code autocorrelation function description

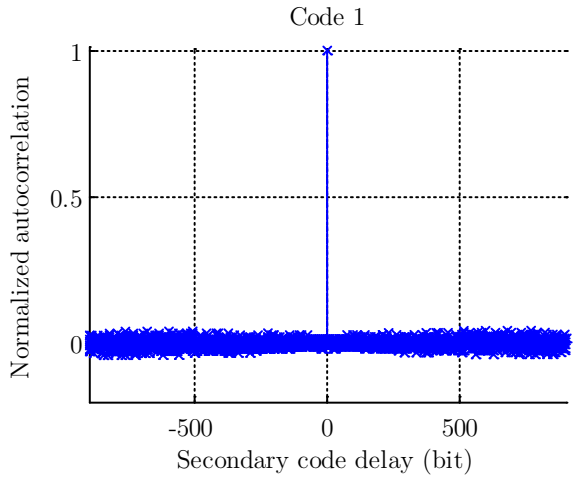

(a) Autocorrelation function shape

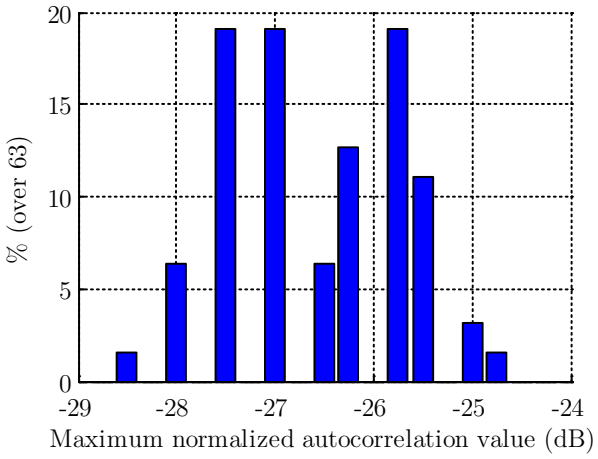

(b) Distribution of the side-peaks

Figure 7.33 GPS L1C secondary codes autocorrelation function description

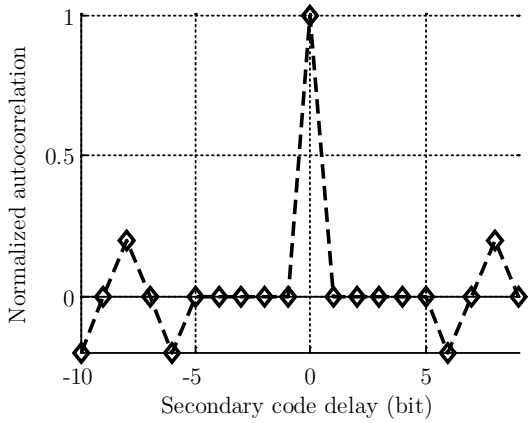

(a) Autocorrelation function shape

Autocorrelation function		Distribution	
		Over 20	In %
-0.2	-13.98 dB	3	15%
0	$-\infty$	14	70%
0.2	-13.98 dB	2	10%
1	0 dB	1	5%

(b) Autocorrelation function distribution

Figure 7.34 GPS L5 secondary code autocorrelation function description

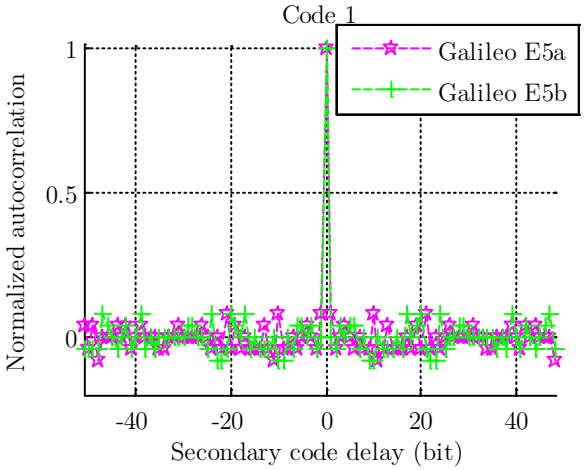

(a) Autocorrelation function shape

Autocorrelation function		Distribution Over 100	In %
0	$-\infty$	40	40%
0.04	-27.96 dB	49	49%
0.08	-21.94 dB	10	10%
1	0 dB	1	1%

(b) Distribution of the maximums

Figure 7.35 Galileo E5 a/b secondary codes autocorrelation function description

Since GPS L1C secondary codes are very long, it seems not appropriate to compare their acquisition performance with the acquisition performance of shorter secondary codes such as the ones on the pilot component of the signals GPS L5, Galileo E1 OS and Galileo E5 a/b in terms of secondary code acquisition execution time (because the acquisition of GPS L1C exceeds 18 s).

7.2.2 Pilot secondary code acquisition methods

The acquisition of the secondary code aims at determining the beginning of the secondary code knowing that each secondary code bit coincides with the spreading code period. Two acquisition techniques can be suggested, the first one considers both pilot correlator outputs (in-phase and quadrature-phase) whereas the second considers only the in-phase correlator output. Firstly, the spreading code is acquired. N_{c_2} correlator outputs, based on the pilot spreading code are then collected (N_{c_2} is the number of secondary code bits on the pilot component). As a consequence, each of these correlator outputs carries the value of a secondary code bit. As presented earlier, these successive pilot correlator outputs are:

$$\begin{aligned} I_p(k,y) &= \frac{A_p}{2} c_{2,p}(y-\Delta)\, R_{c_1,p}\left(\varepsilon_\tau(k,y)\right) \\ &\quad \cos\left(2\pi(y-1)\varepsilon_{f_D}(k,y)T_C + \varepsilon_{\phi_0}(k,y)\right) \operatorname{sinc}\left(\pi\varepsilon_{f_D}(k,y)T_C\right) + \eta_{I_p}(k,y) \\ Q_p(k,y) &= \frac{A_p}{2} c_{2,p}(y-\Delta)\, R_{c_1,p}\left(\varepsilon_\tau(k,y)\right) \\ &\quad \sin\left(2\pi(y-1)\varepsilon_{f_D}(k,y)T_C + \varepsilon_{\phi_0}(k,y)\right) \operatorname{sinc}\left(\pi\varepsilon_{f_D}(y,k)T_C\right) + \eta_{Q_p}(k,y) \end{aligned} \quad (7.14)$$

where:

- $y \in [\![1;N_{c_2}]\!]$ is the index of the considered secondary code bit,
- $I_p(k,y)$ stands for the k-th summation on the y-th secondary code bit, there are $N_{c_2}T_C = T_{c_2}$ ms between two successive integrations on the y-th bit $I_p(1,y)$ and $I_p(2,y)$,
- $\eta_{I_p}(k,y)$ and $\eta_{Q_p}(k,y)$ are the noises and can be modeled as centered Gaussian noises,

- $\varepsilon_{\phi_0}(k,y) = 2\pi\varepsilon_{f_D}(y,k)\left(T_0 + (k-1)T_{c_2} - \frac{T_C}{2}\right) - \hat{\phi}_0$,
- $\varepsilon_\tau(k,y)$ and $\varepsilon_{f_D}(k,y)$ are the code delay and Doppler frequency errors, which are assumed to be constant.

The code delay is assumed to be negligible and then $R_{c_1,p}\left(\varepsilon_\tau(y,k)\right)$ can be assumed close to 1. Furthermore, it is assumed that Doppler frequency is roughly estimated but there can be some residual Doppler frequency error.

7.2.2.1 Technique 1: Acquisition method based on the correlator output pair

As done for the spreading code acquisition and explained in [Yang *et al.*, 2004] applied to GPS L5 and [Tawk *et al.*, 2011] applied to Galileo signals, the DFT of the N_{c_2} correlator output pairs is multiplied with the complex conjugate of the DFT of the generated secondary code. Afterwards, the result is transformed back to the time domain by an inverse DFT. An illustration is proposed with Figure 7.36. The output using this technique is equivalent to the one proposed in [Macabiau *et al.*, 2003] where accumulations are done in the time domain.

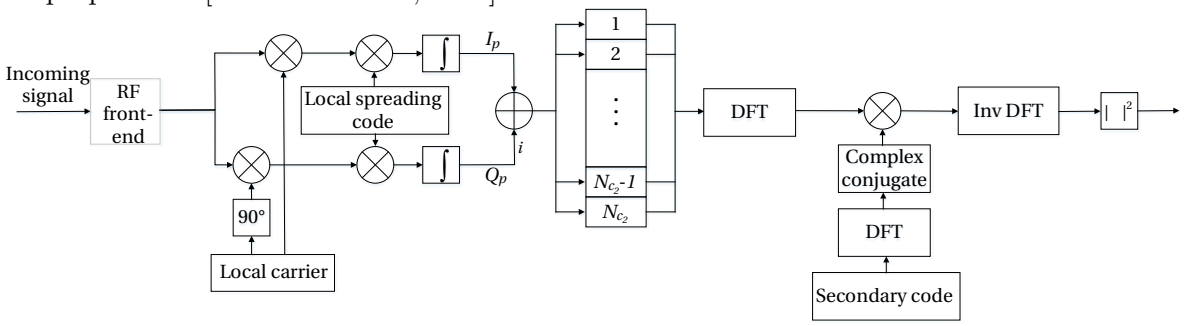

Figure 7.36 Acquisition of secondary code using both correlator outputs

The outputs of the secondary code acquisition are:

$$\begin{aligned} I_{c_2}(k) &= \frac{1}{N_{c_2}}\sum_{y=1}^{N_{c_2}} I_p(k,y)c_{2,p}\left(y-\hat{\Delta}\right) \\ &= \frac{A_p \mathrm{sinc}\left(\pi\varepsilon_{f_D}T_C\right)}{2N_{c_2}}\sum_{y=1}^{N_{c_2}} c_{2,p}(y-\Delta)c_{2,p}\left(y-\hat{\Delta}\right)\cos\left(2\pi(y-1)\varepsilon_{f_D}T_C + \varepsilon_{\phi_0}(k,y)\right) \\ &\quad + \eta_{I_{c_2}}\left(k,\hat{\Delta}\right) \\ Q_{c_2}(k) &= \frac{A_p \mathrm{sinc}\left(\pi\varepsilon_{f_D}T_C\right)}{2N_{c_2}}\sum_{y=1}^{N_{c_2}} c_{2,p}(y-\Delta)c_{2,p}\left(y-\hat{\Delta}\right)\sin\left(2\pi(y-1)\varepsilon_{f_D}T_C + \varepsilon_{\phi_0}(k,y)\right) \\ &\quad + \eta_{Q_{c_2}}\left(k,\hat{\Delta}\right) \end{aligned} \quad (7.15)$$

where the noises $\eta_{I_{c_2}}\left(k,\hat{\Delta}\right)$ and $\eta_{Q_{c_2}}\left(k,\hat{\Delta}\right)$ follow centered Gaussian distribution and their variance is σ_η^2 / N_{c_2}. $\eta_{I_{c_2}}$ and $\eta_{Q_{c_2}}$ are independent but $\eta_{I_{c_2}}\left(k,\hat{\Delta}_1\right)$ and $\eta_{I_{c_2}}\left(k,\hat{\Delta}_2\right)$ are correlated since they result from the correlation with the same PRN sequence η_{I_p}.

The correlation coefficient correspond to the autocorrelation function of the secondary code [Julien, 2005]: for $\widehat{\Delta}_1$ different from $\widehat{\Delta}_2$:

$$\mathrm{cov}\left(\widehat{\Delta}_1, \widehat{\Delta}_2\right) = R_{c_2}\left(\left|\widehat{\Delta}_1 - \widehat{\Delta}_2\right|\right) \tag{7.16}$$

In the end, the acquisition detector is:

$$T = \frac{I_{c_2}^2(k)}{\sigma_\eta^2/N_{c_2}} + \frac{Q_{c_2}^2(k)}{\sigma_\eta^2/N_{c_2}} \tag{7.17}$$

As for the spreading code acquisition, a decision test can be settled on the right estimation of the secondary code delay. Under H_0, it is assumed that $\widehat{\Delta} \neq \Delta$ and then I_{c_2} is a centered Gaussian distribution. Then, T follows a central χ^2 distribution with 2 degrees of freedom.

Under H_1, it is assumed that $\widehat{\Delta} = \Delta$ and then I_{c_2} is a non-central Gaussian distribution. The acquisition criterion follows then a non-central χ^2 distribution with 2 degrees of freedom.

For the acquisition of weak signals one secondary code period can be insufficient to accumulate enough useful energy. Then, K secondary code periods have to be considered by averaging the noise at the correlator output level. As developed in Table 7.4, the noise variance is equivalent to the noise variance for a coherent integration duration over KT_C.

Normalized acquisition detector	$\left(\frac{1}{K}\sum_{k=1}^{K}\frac{I_{c_2}(k)}{\sqrt{\sigma_\eta^2/N_{c_2}}}\right)^2 + \left(\frac{1}{K}\sum_{k=1}^{K}\frac{Q_{c_2}(k)}{\sqrt{\sigma_\eta^2/N_{c_2}}}\right)^2$
Output noise distribution	$\mathcal{N}\left(0, \frac{N_0}{4KT_C}\right)$
Probability of false alarm	$P_{FA} = 1 - F_{\chi^2(2)}(\gamma)$
Probability of detection	$P_D = 1 - F_{\chi^2(2,\Lambda)}(\gamma)$
Non-centrality parameter	$\Lambda = \frac{A_p^2}{N_0} KT_C N_{c_2} \mathrm{sinc}^2\left(\pi\varepsilon_{f_D} T_C\right)\widetilde{R_{c_2}^2}(0)$

Table 7.4 Performance study for the acquisition of the secondary based on the pilot correlator output pair

where $\widetilde{R_{c_2}}(\varepsilon_\Delta)$ given by:

$$\widetilde{R_{c_2}}(\varepsilon_\Delta) = \frac{1}{N_{c_2}}\sum_{y=1}^{N_{c_2}} c_{2,p}(y-\Delta)c_{2,p}\left(y-\widehat{\Delta}\right)\cos\left(2\pi(y-1)\varepsilon_{f_D}T_C + \varepsilon_{\phi_0}(k,y)\right) \tag{7.18}$$

can be approximated by the autocorrelation function of the secondary code $R_{c_2}(\varepsilon_\Delta)$ when the Doppler frequency error is small enough with ε_Δ the secondary code delay error ($\varepsilon_\Delta = \widehat{\Delta} - \Delta$).

7.2.2.2 Technique 2: Acquisition method based on the in-phase correlator output

When the Doppler frequency error is very small and considering no phase error, the quadrature-phase correlator output can be assimilated to noise only because the sin term in (7.14) is close to null. It is why, the second secondary code acquisition technique only considers

the in-phase correlator output. In this case, the cos term is close to 1 and then the sign of $I_p(k,y)$ is an estimator of the sign of the bit y of the secondary code $c_2(y)$. In this case, the local secondary code is correlated with the N_{c_2} pilot in-phase correlator outputs. The performance study of the acquisition method based on the in-phase correlator output is given Table 7.5.

Normalized acquisition detector	$\frac{1}{K}\sum_{k=1}^{K}\frac{I_{c_2}(k)}{\sqrt{\sigma_\eta^2/N_{c_2}}}$
Output noise distribution	$\mathcal{N}\left(0,\frac{N_0}{4KT_C}\right)$
Probability of false alarm	$P_{FA}=1-F_{\mathcal{N}(0,1)}(\gamma)$
Probability of detection	$P_D=1-F_{\mathcal{N}\left(\frac{A_p}{\sqrt{N_0}}\sqrt{KT_CN_{c_2}}\mathrm{sinc}(\pi\varepsilon_{f_D}T_C)\widetilde{R_{c_2}}(0),1\right)}(\gamma)$

Table 7.5 Performance study for the acquisition of the secondary based on the pilot in-phase correlator output

Some variants can be envisaged. For example, the local secondary code is multiplied by the sign of the normalized pilot in-phase correlator outputs $I_p(k,y)$. When the signal is strong enough, the sign of $I_p(k,y)$ is the sign of the secondary code.

7.2.3 Simulation results

The goal of the simulations is to confirm that at the desired sensitivity (27 dB-Hz, equivalent to 24 dB-Hz for the Galileo E1 OS pilot component), the secondary code of the pilot component is acquired with a high probability. The simulation scheme consists in generating the in-phase and quadrature-phase correlator outputs as modelled in (7.14) with a random noise following a centered Gaussian distribution.

The desired probability of false alarm does not need to be very low because there can only be a maximum of $N_{c_2}-1$ false alarms (then in the order of 2 or 3 tens or one hundred depending on the considered signal).

7.2.3.1 Secondary code autocorrelation function property when bit sign are badly estimated

Both secondary code acquisition techniques are based on an estimation of the sign of the received secondary code bits. But due to noise and residual errors, the sign of the in-phase correlator output can be the opposite of the sign of the secondary code bit. In this section, the isolation of the main peak of the secondary code autocorrelation function is studied as a function of the number of wrong estimations of the secondary code bits. This permits to give an overview of potential acquisition of the secondary code as a function of the received C/N_0.

Simulations to study the isolation of the main peak (regarding the amplitude of the highest secondary peak) are only run for short secondary codes. All the combinations on the position of wrong secondary code bit sign are computed and only the worst case (potentially obtained for several combinations) is presented in Table 7.6.

		Number of wrong secondary code bits						
		0	1	2	3	4	5	6
Galileo E1 OS	Main peak	25	23	21	19	17	15	13
	Max sec. peaks	3	5	7	9	11	13	13
GPS L5	Main peak	20	18	16	14	12		
	Max sec. peaks	4	6	8	10	12		

Table 7.6 Galileo E1 OS and GPS L5 secondary code autocorrelation function (not normalized by Nc_2) properties in presence of wrong secondary code bit sign estimation

If the number of wrong GPS L5 secondary code bit sign estimation exceeds 3 (that means less than 85% of correct estimation), the secondary code autocorrelation function peaks can be equal or higher than the main peak, leading to correct peak detection fail. For Galileo E1 OS, this occurs when 5 or more secondary code bits are wrong estimated, that means 80% of correct estimation is needed.

Knowing the properties of the autocorrelation function in presence of wrong secondary code bit estimations, it can be interesting to evaluate for which C/N_0 the sign of the in-phase correlator output is mainly driven by the sign of the secondary code. This is represented in Figure 7.37. The probability of correct sign estimation is higher for Galileo E1 OS compared to signals in the L5 band since the noise variance is lower for Galileo E1 OS (coherent integration duration of 4 ms instead of 1 ms).

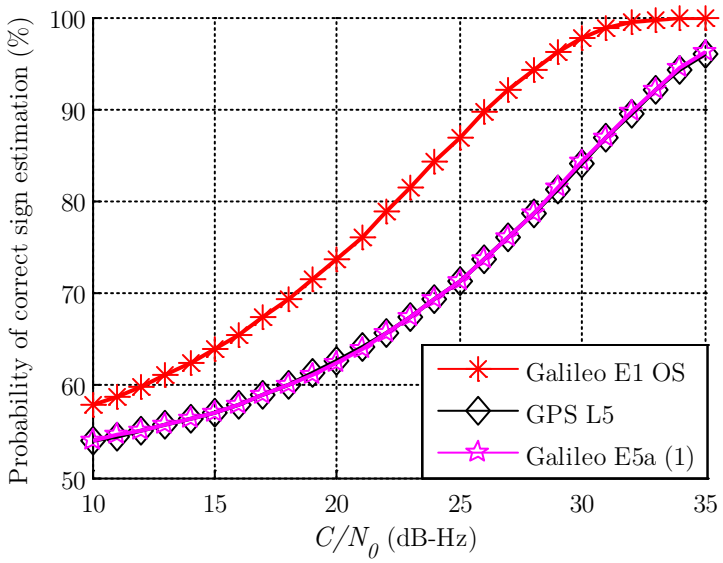

Figure 7.37 Probability that the sign of the in-phase correlator output is the sign of the secondary code (all secondary code bits)

For Galileo E1 OS, the limit of number of wrong secondary code bit estimation is 5 (Table 7.6), equivalent to say that at least 20 secondary code bits should be correctly estimated. Regarding Figure 7.37, the limit 80% of correct secondary code bit sign estimation is in average for a C/N_0 of 23 dB-Hz (total signal power).

For GPS L5, to clearly observe the main peak of the secondary code autocorrelation function, not more than 3 bit signs can be badly estimated, this corresponds to a percentage of good estimation of 85%. To reach this percentage, the signal should be strong enough (above 30 dB-Hz).

7.2.3.2 Simulation results considering no Doppler frequency and phase errors

Firstly, the simulations are run assuming that the carrier phase tracking is perfect, that means that in (7.14) and (7.15), the cos term of the in-phase correlation output is equal to 1 because the phase ε_ϕ is null. Figure 7.38 illustrates the adequacy of the performance study (probability of detection determined by the CDF) with the experimental results (comparison of the detector amplitude with the predefined threshold), for Galileo E1 OS as an example. The cyan dashed line represents the probability of detection given by the performance study for both methods and the marked lines represent the experimental probability. The probability of false alarm was set to 10^{-3}, assuming no Doppler frequency error and no initial phase error.

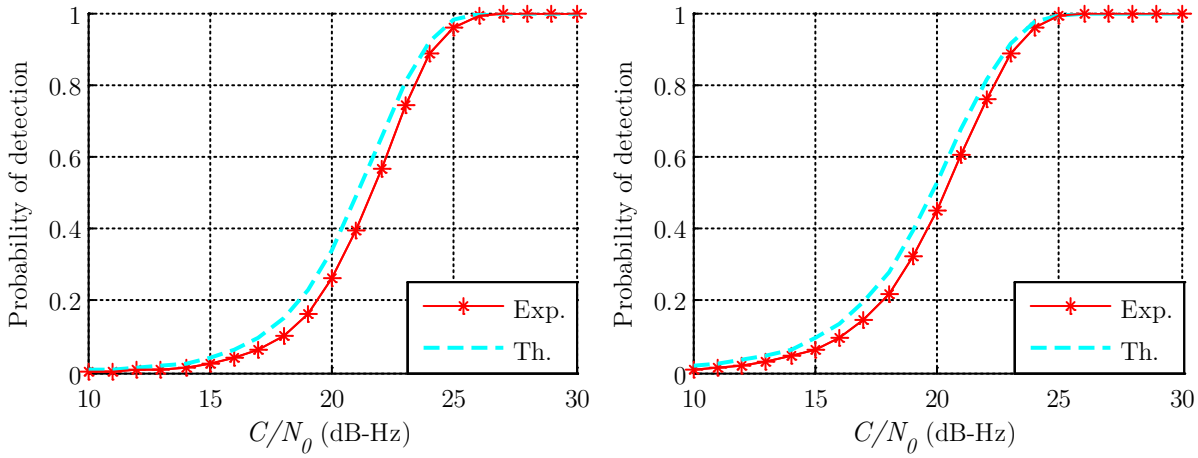

(a) Technique 1 (both components) (b) Technique 2 (only I_p)

Figure 7.38 Probability of correct main peak secondary code autocorrelation function detection for both techniques (applied to Galileo E1 OS for $K = 1$)

To compare the acquisition performance between both secondary code acquisition methods, Figure 7.39 can be used. The probability of the secondary code delay estimation is presented for a probability of false alarm equal to $P_{FA} = \frac{1}{10N_{c_2}}$, which means that one time over 10 secondary code acquisitions, a false alarm can be present. It corresponds to $P_{FA} = 10^{-3}$ for Galileo E5 a/b, $P_{FA} = 4 \times 10^{-3}$ for Galileo E1 OS and $P_{FA} = 5 \times 10^{-3}$ for GPS L5.

In Figure 7.39, the solid lines represent the probabilities of detection using only the in-phase correlator output whereas the marked and dashed lines represent the probabilities of detection when considering the correlator output pair. As it can be observed, even if the probabilities of detection obtained by both methods are close, the acquisition method

considering only the in-phase correlator output outperforms the acquisition method considering the correlator output pair, since under the assumptions (null phase error), the quadrature-phase correlator output is only noise.

Already reflected in Figure 7.37, for a given C/N_0, the correct estimation of the secondary code delay of the GPS L5 occurs less often than this of Galileo E1 OS for example. For a total received C/N_0 of 27 dB-Hz, the acquisition of the secondary code is a success for Galileo E1 OS and E5a signals based on the use of one secondary code period. For the GPS L5 pilot secondary code, it requires the use of two spreading code periods (which corresponds to 40 ms, still shorter than the 100-ms Galileo pilot secondary codes).

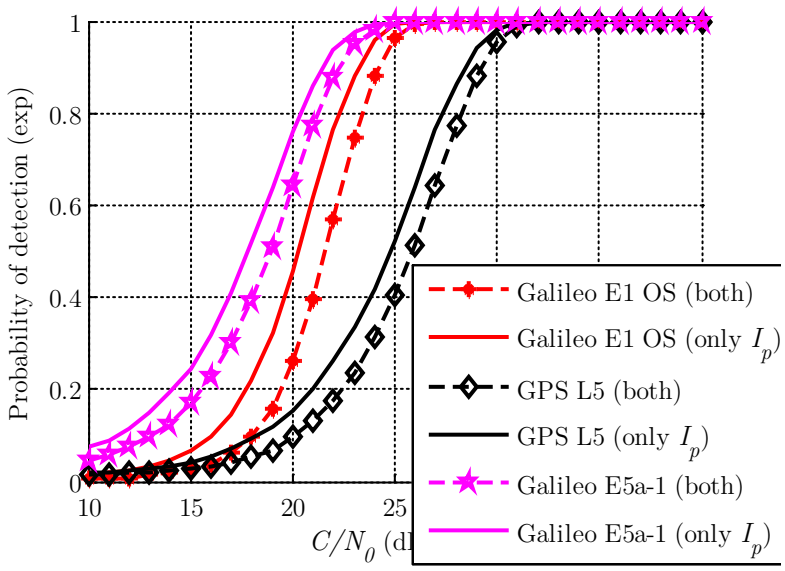

Figure 7.39 Comparison of the secondary code acquisition methods for three signals ($K = 1$)

7.2.3.3 Simulation results considering Doppler frequency error

This section studies the acquisition of the secondary code when considering a non-null Doppler frequency error. This small perturbation implies degradations on the secondary code isolation. For GPS L5 secondary code, when there is no residual Doppler frequency error, the isolation between the main peak and the secondary peaks is -13.98 dB. But, as already presented in [Macabiau *et al.*, 2003], when there is a Doppler frequency error of 25 Hz, the isolation becomes only 6.63 dB and the loss on the main peak amplitude is 3.92 dB. These two characteristic values of correlation properties are given for different value of Doppler frequency errors in Figure 7.38 ((a) for the loss on the main peak and (b) for the isolation), in black for GPS L5.

They are compared to the pilot secondary properties of Galileo signals, in red and magenta, respectively for Galileo E1 OS and E5. Obviously, for Galileo signals, even if the pilot secondary code properties are better when there is no Doppler, they are rapidly degraded when the Doppler frequency error increases. As an example, for similar figures as GPS L5 previously described for a Doppler frequency error of 25 Hz, for Galileo signals, it is for a Doppler

frequency error around 5-6 Hz. The need for fine estimation of the frequency is especially true for Galileo signals to permit a correct secondary code acquisition.

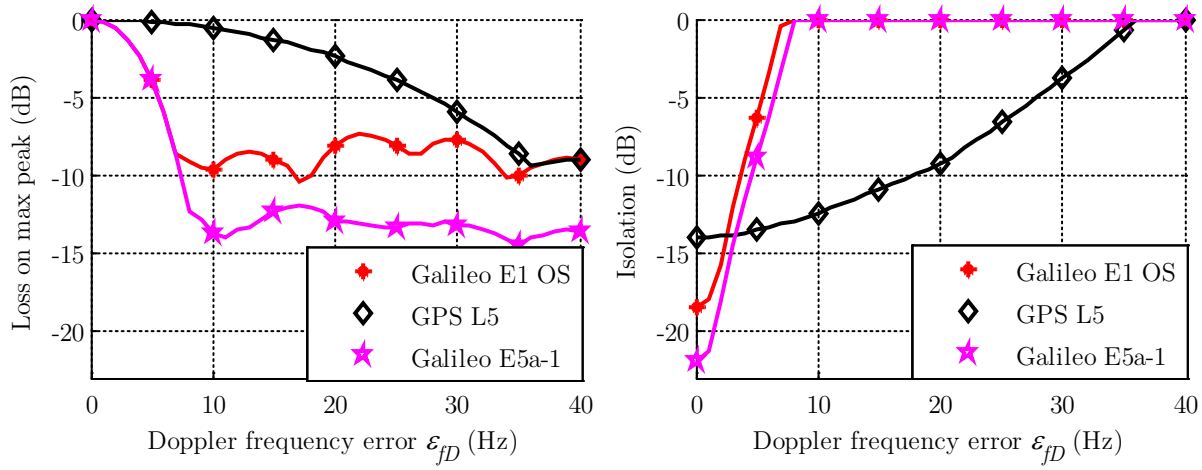

(a) Loss on the main peak amplitude (b) Isolation of the main peak

Figure 7.40 Pilot secondary code correlation properties in presence of residual Doppler frequency error

The simultaneous acquisition of the PRN and secondary codes does not seem an option for a received C/N_0 of 27 dB-Hz. Indeed, when assuming a perfect estimation of the code delay and Doppler frequency, the secondary code acquisition is a success, but if there is a small uncertainty on the Doppler frequency, the success is compromised. For example, if one wants to acquire the Galileo E1 OS signal, the coherent integration time is 100 ms. The width of an acquisition grid cell in the frequency domain is then 5 Hz which is not fine enough to permit the correct secondary code acquisition.

7.2.3.4 Simulation results considering realistic phase tracking

It has seen that to correctly acquire the secondary code, the incoming Doppler frequency should be perfectly estimated. However, to be realistic, the carrier phase tracking error should be considered. Then, the correlator outputs can be expressed as follows:

$$I_{c_2}(k) = \frac{A_p}{2N_{c_2}} \sum_{y=1}^{N_{c_2}} c_{2,p}(y-\Delta) c_{2,p}\left(y-\widehat{\Delta}\right) \cos\left(\eta_f(k,y)\right) + \eta_{I_{c_2}}\left(k,\widehat{\Delta}\right)$$
$$Q_{c_2}(k) = \frac{A_p}{2N_{c_2}} \sum_{y=1}^{N_{c_2}} c_{2,p}(y-\Delta) c_{2,p}\left(y-\widehat{\Delta}\right) \sin\left(\eta_f(k,y)\right) + \eta_{Q_{c_2}}\left(k,\widehat{\Delta}\right) \quad (7.19)$$

where $\eta_f(k,y)$ refers to as the frequency error noise at the instant $t = t_0 + T_C\left(kN_{c_2} + y\right)$.

For simulations, the noise is generated following a Gaussian distribution (7.12) and assumed not correlated between two consecutive instants. Figure 7.41 presents the probability of detection for the three considering cases as a function of the C/N_0. The ideal case, when assuming no frequency and phase errors, is represented in red. As previously explained, the probability of detection when considering residual Doppler frequency errors, in the cell

uncertainty range $\left[-\frac{1}{4T_C},\frac{1}{4T_C}\right]$, in green, is the lowest one and the secondary code acquisition at 27 dB-Hz occurs only 84% of the time. When considering a correct estimation of the Doppler frequency but a frequency error noise (carrier phase tracking error), the average probability of detection is relatively close to the one in an ideal case, in particular for the high C/N_0.

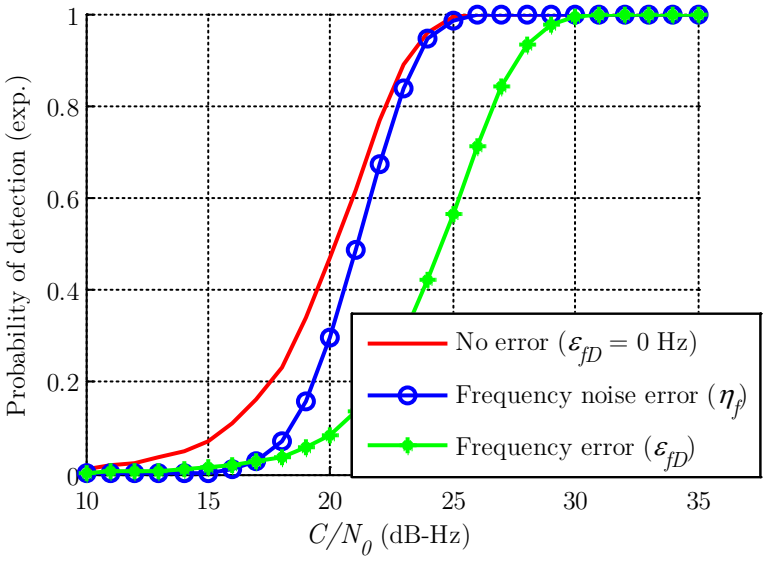

Figure 7.41 Probability of Galileo E1 OS secondary code acquisition when considering or not frequency and phase errors (Technique 1 – 5000 simulations)

7.3 Discussion

For GPS L1 C/A, the acquisition-to-tracking transition using a FLL is not a problem at 27 dB-Hz because the loop always converges using CP or Atan2 discriminators.

For the modernized GNSS signals, the acquisition-to-tracking success is subject to some conditions. Firstly, the frequency estimation should be refined to allow the demodulation of the pilot secondary code. To have a successful lock of the FLL, it is preferable to:

- Use both data and pilot components instead of using only one component,
- Update the frequency every 20 ms instead of every $2T_{c_1}$,
- Use the data sensitive discriminators (Atan2 is maybe better than CP discriminator and is self-normalized) considering partial correlations (half the spreading code period seems the best compromise).

Another point of interest is the convergence time. With another choice of loop bandwidth (higher than $B_L = 1$ Hz), it is possible to reduce the convergence time.

For all the considered modernized GNSS signals, the frequency refinement can be done with a high probability to success even when considering the realistic case of a carrier phase tracking error.

Chapter 8
Conclusions and Recommendations for Future Work

Nowadays, the satellite navigation is present in many fields: professional, sports, leisure... The variety of GNSS signals that will be available around 2020 implies to rethink the signal processing made in GNSS receivers. Indeed, the design of the modernized GNSS signals is different from the oldest signal, GPS L1 C/A signal.

In GNSS receivers, the acquisition plays a key and crucial role. In this thesis, a comprehensive study on the acquisition performance of the modernized GNSS signals and the development of an innovative acquisition method were proposed.

In this chapter, the main signal design differences between GPS L1 C/A and the modernized GNSS signals are recalled, with the associated impact on the acquisition performance. The research performed and presented in this thesis can be extended, then some recommendations for future work are presented.

8.1 Thesis achievements

As discussed in *Chapter 1*, the purpose of this thesis was to propose an acquisition strategy to acquire the Galileo E1 OS signal, at 27 dB-Hz with a success rate which is at least equal to 90%. A study of the receiver market over the years 2012-2014 on around 400 GNSS receivers showed that an acquisition sensitivity of 27 dB-Hz associated with a high acquisition probability was typical receivers, working outdoors and potentially in degraded environment.

To reach this objective, it appeared necessary to firstly evaluate the main sources of degradations and their impact on the acquisition performance in function of the GNSS signal features. As previously presented, the signal design of the modernized GNSS signals is different from the GPS L1 C/A signal design on many points.

- Pilot component

The modernized GNSS signals are mainly characterized by the presence of a pilot component together with a data component. The data component carries the navigation message while the pilot component is dataless, permitting a robust tracking. The structure of the pilot component is however similar to the data component, it contains a spreading code (different from the spreading code on the data component) and a secondary code playing the same role as the navigation message from the point of view of the acquisition, with the specificity that a secondary code bit only lasts for one PRN code repetition. The split of the transmitted signal into two components implies the split of the total signal power between both components. For most of the modernized GNSS signals, the share is equitable: 50% on each, except for the GPS L1C signal, which has 75% of the power on the pilot component.

Due to the presence of the pilot component, the acquisition methods must be adapted to the modernized GNSS signals. *Chapter 3* presented a state-of-the-art of the acquisition methods for composite GNSS signals. When the assumed received C/N_0 is low with a large acquisition search, as it is the case in this study, it seems much more difficult to only acquire the pilot component (except maybe for the GPS L1C signal). Indeed, the gain of acquiring only one component (in comparison with the acquisition of both components, the number of required operations is globally divided by 2) does not compensate for the loss of 3 dB, in terms of acquisition execution time.

Among the acquisition methods based on the acquisition of both components, the classical non-coherent combining seems the most appropriate and efficient. The coherent combining with sign recovery acquisition method is not reliable at 27 dB-Hz because 50% of the time, the chosen local sequence (data+pilot or data-pilot) does not correspond to the incoming one. The acquisition methods over multiple spreading code periods (exhaustive bit sign combinations and primary code acquisition based on multi-hypothesis secondary code) are more computationally expensive due to the test of all the bit sign combinations.

- Spreading code length

The modernized GNSS signals have spreading codes of 4092 and 10 230 chips, which is 4 and 10 times longer than the GPS L1 C/A codes, respectively.

This implies better correlation properties. For example, as presented in *Appendix C*, the isolation of Galileo E1 OS (-23.44 dB) is 4.2 dB higher than GPS L1 C/A (19.08 dB) when the Doppler frequency is in the range of $[-10,10]$ kHz. In the same way, the maximum of GPS L1 C/A codes cross-correlation is -19.08 dB whereas for Galileo E1 OS, considering the CBOC

modulation, the isolation of the cross-correlation of two codes, assigned to two different satellites is -22.82 dB. The cross-correlation of the data and pilot codes assigned to the same satellite (chosen as orthogonal as possible) is -25.16 dB.

Galileo satellites emit E1 OS signal containing the data and the pilot component. That means that the cross-correlation between the data and the pilot component is always present when acquiring the Galileo E1 OS signal. They are chosen as orthogonal as possible and the maximum of the cross-correlation is -25.16 dB, which corresponds to approximately a tenth of the amplitude of secondary peak of the autocorrelation function.

The counterpart of long spreading code is that the code delay uncertainty space is 4 or 10 times larger (for an identical modulation). From the point of view of the acquisition, this implies the processing of longer vectors and an acquisition grid which contains more cells in the time domain. The higher the number of cells in the acquisition grid is, the longer the acquisition process is and the higher the number of false alarms is for the same probability of detection. It thus seems important to reduce the probability of false alarm but this means that the associated probability of detection is also reduced, as discussed in *Chapter 6* and should be compensated by a higher acquisition dwell time.

- Modulation

The GPS L1 C/A signals are BPSK modulated. However, the modernized GPS and Galileo signals on the L1 band are based on the BOC modulation. The shape of the autocorrelation function of BOC-modulated codes is different from BPSK-modulated codes. The peak around 0 is sharper, which leads to a more precise estimation of the code delay and is an important advantage for tracking. However, the sharp peak induces a finer discretization of the code delay uncertainty space and thus a high number of cells in the time domain for the acquisition algorithm. Similarly, the sampling frequency should be higher than for a BPSK signal with the same chipping rate (at least $14f_0$ to correctly describe the CBOC and TMBOC-modulated signals). From the point of view of the acquisition, this results in the processing of bigger vectors and matrices. In addition, the BOC autocorrelation function presents secondary peaks. During the acquisition process, in weak conditions, the amplitude of the secondary peak can be higher than the amplitude of the main peak can lead to a missed-detection.

In addition, as presented in *Chapter 4*, the impact of the residual code Doppler not taken into account at the receiver level is detrimental on the acquisition performance since the correlation function shape becomes rounded leading to the disappearance of the secondary peaks. But, the detection of the main peak and the associated code delay becomes harder since the amplitude of the peak is reduced and its width is large and it is then difficult to correctly estimate the code delay. Indeed, since the main peak is rounded and if it exceeds the acquisition threshold, several cells detect the presence of the signal. An additional step is required to determine which cell corresponds to the correct estimation of the code delay. Moreover, because of the shift of the main peak, the code delay, for which the amplitude is maximum, does not correspond to the incoming code delay. A solution to counter this problem is to locally take into account the incoming Doppler frequency by compensating for the code Doppler. Unlike

the acquisition of the GPS L1 C/A signal for which this step is recommended but not indispensable, this step is absolutely required for the acquisition of the modernized GNSS signals. This implies the generation of several local replicas in function of the estimated incoming Doppler frequency.

- The chipping rate f_{c_1}

The chipping rate is 10 times higher for signals in the L5 band than for signals in the L1 band. One direct consequence is the important impact of the code Doppler. Indeed, the slip of 1 chip between the received sequence (affected by the code Doppler) and the local sequence (not Doppler code compensated) occurs quicker when the chipping rate is high: it occurs in 20 ms (*Chapter 4*) for L5 signals and an incoming Doppler frequency of 10 kHz. After the slip of 1 chip, the acquisition does not make sense and this implies that weak signals cannot be acquired with uncompensated code Doppler.

- Secondary code

The pilot component is dataless but contains a secondary code which should be acquired to permit to extend the coherent integration time during the tracking process. The simultaneous acquisition of the pilot spreading and secondary codes (coherent integration on the pilot secondary code period acquisition method) is not easily possible at 27 dB-Hz since it would require the use of extremely long coherent integration that would result in a very large number of Doppler cells. The presence of a secondary code on the pilot component is equivalent to the acquisition of the data component because bit sign transition occurs with the same rate, meaning that a specific data-insensitive acquisition technique should be used for the acquisition of the modernized GNSS signals. As discussed in *Chapter 7*, the Doppler frequency estimate should be fine enough to permit the correct demodulation of the secondary code.

- Data bit rate

A GPS L1 C/A data bit lasts 20 ms, which is equivalent to a data bit rate of 50 bit/s. The modernized GNSS signals are designed to have shorter data bits. In addition the data bit duration is generally equal to the spreading code period. This means that a bit sign transition can potentially occur at each spreading code period (for the GPS L5 signal, the pilot secondary code bit transition occurs at the same frequency as the secondary code on the data component, the data bit lasting 10 secondary code bits). For the GPS L1 C/A signal, one step of the acquisition is to find the beginning of the data bit duration over the 20 spreading code periods (bit synchronization). For the modernized GNSS signals, the data bit coincides in general with the spreading code period so this step is not required.

But, for the acquisition step, the presence of bit sign transition on both components potentially at each spreading code period poses a significant problem. *Chapter 4* focused on the development of the expression of the correlator output in presence of bit sign transition during

the correlation and its resulting impact on the average impact on the average probability of detection. For GPS L1 C/A, its intrinsic structure shows that it is preferable to use a coherent integration on 5 or 10 ms in weak signal conditions. But for the acquisition of the signal, it is preferable to coherent integrate over 5 or 10 ms in weak conditions. For the modernized GNSS signals, the presence of data bits was shown to be a significant drawback due to the occurrence of data transitions at each PRN code period. The degradation is equivalent on average to a loss of at least 2 dB on the received C/N_0 highlighting the need to use an acquisition technique immune to such events.

When comparing the average probabilities of detection for the acquisition on 20 ms of the modernized GNSS signals, it can be observed that the probability of detection for GPS L1C is higher, in particular for low C/N_0. For example, at 27 dB-Hz, the average probability of detection for the GPS L1C signal is around 0.3, it is equivalent on average to a loss of 1.5 dB for Galileo E1 OS and 4 dB for GPS L5 signals. For high C/N_0 (higher than 33 dB-Hz), the GPS L1C average probability of detection becomes flattened because the spreading code period is half the coherent integration time. The comparison of the average probabilities of detection of GPS L1 C/A and the modernized GNSS signals shows the impact of the number of bit sign transitions. Indeed, for GPS L1 C/A, on 20 ms, one bit sign transition occurs with a probability of 50% but for the modernized GNSS signals, there can be up to 20 bit sign transitions on both components (GPS L5 and Galileo E5). On the average probability of detection, this implies a loss between 2 dB (GPS L1C) and 3 dB (GPS L5).

Chapter 7 provides a comprehensive study on the impact of bit sign transition during the last step of the acquisition, for the refinement of the Doppler frequency estimate. Indeed, once again, the presence of bit sign transition, even if the code delay is well estimated can degrade the lock of the FLL. One solution is to resort to data insensitive frequency discriminators or to use data sensitive frequency discriminators such as the Cross-Product or Four-Quadrant Arctangent discriminators but with partial correlations. Indeed, for example, the FLL is always locked at 27 dB-Hz when using the Four-Quadrant Arctangent discriminator (which is self-normalized) on both components and with a frequency update every 20 ms (instead of every 2 spreading code periods and partial correlations on half the spreading code period. By this way, for the frequency discriminator computation, the sign of the data bit (or secondary code bit for the pilot component) of the couple of the partial correlator output is the same.

Based on this theoretical comprehensive study on the acquisition, *Chapter 5* proposed an innovative acquisition method, based on an acquisition method, the DBZP, well-known for its efficiency. The development of the expression of the DBZP outputs and the performance study permit to point out the strengths and the weaknesses of this method and open the way for the DBZPTI, a version of DBZP which is, among others, transition insensitive. One of the weaknesses of the DBZP is that the acquisition performance highly depends on the incoming Doppler frequency. In the worst case, the losses can reach 8 dB, some improvements are proposed, the use of zero-padding to oversample the FFT result and by considering the double of the Doppler frequency uncertainty space; this permits to reduce the losses to 1.1 dB. The

gain is then considerable on the probability of detection. Specifically to the modernized GNSS signals and in particular Galileo E1 OS, due to the presence of bit transition at each spreading code and potentially bit sign transition, a step of the DBZP is modified to permit the transition insensivity of the DBZPTI. When comparing the number of operations for the execution of the DBZPTI with the execution of the reference acquisition method for the same probability of detection, there is a gain of 15%, which proves the efficiency of the developed DBZPTI. It is possible to evaluate the impact of this work on the DBPZTI on the scientific community by listing the works which cite Publication *P1*. In addition of the author publications, at least 6 works deal with the DBPZTI: [Esteves *et al.*, 2013], [Wang *et al.*, 2014], [Leclère *et al.*, 2014], [Zhongliang *et al.*, 2014], [Boto, 2014] and [Marmet *et al.*, 2014].

After the development of an efficient acquisition method for the modernized GNSS signals, *Chapter 6* is dedicated to the choice of the acquisition parameters to success the acquisition of Galileo E1 OS at 27 dB-Hz with a probability of 90%.

8.2 Recommendations for future work

In line with the research results presented here, several questions are also raised for future work.

- Impact of bit sign transitions for other coherent integration times

In *Chapter 4* the probability of detection when considering bit sign transitions is studied. To do so, some assumptions were taken such as that only one bit sign transition can occur over the correlation interval. For the GPS L1 C/A signal, only coherent integration times which are integer divider of the data bit duration are considered. It is possible to lead a similar study for coherent integration times such as 3 or 7 ms for the GPS L1 CA signal. In the same way, it can be asked the performance of the acquisition when considering coherent integration time longer than the data bit duration (for the modernized GNSS signals that means longer than the spreading code period). This implies that 2 or more bit sign transitions can occur in the correlation interval. It appears hard to develop the theoretical models but the study can be based on simulations.

- Adaptation of the acquisition strategy to specific cases

The acquisition strategy proposed in this work is dedicated to the acquisition of the Galileo E1 OS signal with a received C/N_0 of 27 dB-Hz. For other applications, or cases of study, the acquisition strategy should be adapted. In addition, this can require the development of specific efficient code Doppler compensated acquisition methods. Indeed, as presented, the DBZPTI does not locally compensate for the code Doppler. Even if the uncertainty Doppler frequency search space is centered in 0, as showed, Doppler frequencies of a few kHz lead to degradation on the acquisition performance.

- Development of the global acquisition strategy

The presented acquisition strategy is defined for the acquisition of one satellite. In the view of the development of a GNSS receiver, the order of the satellites acquisition should be studied. In priority, the strongest signals (in general the highest) must be acquired. A practical scenario needs to be established to define the limit of "strong" signals and how to exploit the knowledge of the acquisition of one or several satellites to acquire the other satellites. In addition, for a multi-constellation GNSS receiver, it may be preferable to begin by the acquisition of some GPS L1 C/A signals and then with this knowledge, acquire the acquisition of the other GPS L1 C/A signals and the modernized GNSS signals.

- Test on simulated/real signals

Most of the results presented in this thesis are theoretical and it must be very interesting to compare the theoretical performance study with experimental results. Firstly, the global acquisition strategy can be used to acquire simulated signals, generated by a GNSS signal simulator software. In this way, different scenarios of test can be simulated, based on different set of simulation parameters, including receiver/satellite profiles and delay/noise error modeling. This permits to test the acquisition strategy on a Galileo full constellation. In addition, the post-processing (and re-run) allows understanding the joint effect of the choice of several parameters. It can be imagined that the acquisition parameters recalibration by processing on simulated signals, permits, in a second time, a successful acquisition of GNSS real signals.

- Development of tracking strategy

In GNSS receivers, the step after the acquisition is the tracking. So, in the aim of the development of the entire GNSS receiver, the tracking strategy should be developed. The modernized GNSS signals cannot be tracked like the GPS L1 C/A signal and then specific tracking methods should be considered, such as the Autocorrelation Side-Peak Correlation Technique (ASPeCT) technique [Julien, 2005]. For the BOC-modulated signals, the presence of secondary peaks in the autocorrelation function adds potential ambiguity and the ASPeCT technique provides fully reliable and unbiased code measurements.

- Development of the GNSS receiver software and performance comparison

Currently, the global acquisition strategy is developed in Matlab. In the context of the GNSS receiver software development, the acquisition should be developed on the targeted platform. Matlab manipulates matrix but algorithms should be adapted to be efficient for object-oriented language such as the C++ language. In addition, to optimize the execution time and be close to the real-time, the management of the threads (and cores for multi-core platform) in terms of synchronization and distribution should be studied. Then, it can be

interesting to compare its acquisition performance with developed hardware and software GNSS receivers.

The developed GNSS software receiver is addressing domains such as research and education. Some test scenarios can be developed in order to compare algorithm performance on specific points such as the execution time, the rate of objective reach… Unlike the hardware GNSS receiver, the software receiver can be easily manipulated and then it does not appear as a black blox. For the teaching of the signal processing done in GNSS receivers, this can be done by means of manipulations on the software receiver.

Bibliography

[Aalborg University, 2014] Aalborg University,. [Online]. Available: http://www.en.aau.dk/ [Accessed: August2014].

[Akopian, 2001] D. Akopian, *A Fast Satellite Acquisition Method*, in Proceedings of the 14th International Technical Meeting of the Satellite Division of The Institute of Navigation (ION GPS 2001). Salt Lake City, UT (USA), pp. 2871 – 2881, September 2001.

[Avila-Rodriguez, 2008] J.A. Avila-Rodriguez, *On Generalized Signal Waveforms for Satellite Navigation*. Ph.D. thesis, University FAF, Munich, Germany, June 2008.

[Avila-Rodriguez *et al.*, 2004] J.-A. Avila-Rodriguez, T. Pany and B. Eissfeller, *A Theoretical Analysis of Acquisition Algorithms for Indoor Positioning*, in Proceedings of the 2nd ESA Workshop on Satellite Navigation User Equipment Technologies NAVITEC. Noordwijk (The Netherlands), December 2004.

[Bastide *et al.*, 2002] F. Bastide, O. Julien, C. Macabiau and B. Roturier, *Analysis of L5/E5 Acquisition, Tracking and Data Demodulation Thresholds*, in Proceedings of the 15th International Technical Meeting of the Satellite Division of The Institute of Navigation (ION GPS 2002). Portland, OR (USA), pp. 2196 – 2207, September 2002.

[Betz, 2001] J.W. Betz, *Binary Offset Carrier Modulations for Radionavigation*. NAVIGATION, Journal of the Institute of Navigation , vol. 48, no. 4, pp. 227 – 246, Winter 2001.

[Borio, 2008] D. Borio, *A Statistical Theory for GNSS Signal Acquisition*. Ph.D. thesis, Politecnico di Torino, Torino (Italy), March 2008.

[Borio, 2011] D. Borio, *M-Sequence and Secondary Code Constraints for GNSS Signal Acquisition*. Aerospace and Electronic Systems, IEEE Transactions on , vol. 47, no. 2, pp. 928 – 945, 2011.

[Borio & Akos, 2009] D. Borio and D.M. Akos, *Noncoherent Integrations for GNSS Detection: Analysis and Comparisons*. IEEE Transactions on Aerospace and Electronic Systems , vol. 45, no. 1, pp. 360 – 375, January 2009.

[Borio *et al.*, 2009] D. Borio, C. O'Driscoll and G. Lachapelle, *Coherent, Noncoherent, and Differentially Coherent Combining Techniques for Acquisition of New Composite GNSS Signals*. IEEE Transactions on Aerospace and Electronic Systems , vol. 45, no. 3, pp. 1227–1240, July 2009.

[Borre *et al.*, 2007] K. Borre, D.M. Akos, N. Bertelsen, P.J. Rinder and S.H. Jensen, *A Software-Defined GPS and Galileo Receiver, A Single-Frequency Approach*. Birhäuser, December 2007.

[Boto, 2014] P. Boto, *Analysis and Development of Algorithms for Fast Acquisition of Modern GNSS Signals*. Master, Instituto Superior Tecnico, Lisboa (Portugal), December 2014.

[Carrasco-Martos *et al.*, 2010] S. Carrasco-Martos, G. López-Risueño, D. Jiménez-Baños and E.K.A. Gill, *Snapshot Software Receiver for GNSS in Weak Signal Environments: An Innovative Approach for Galileo E5*, in Proceedings of the 23rd International Technical Meeting of the Satellite Division of the Institute of Navigation (ION GNSS 2010). 435 - 447, September 2010.

[Chibout, 2008] B. Chibout, *Application of Indoor and Urban GNSS Localisation Techniques to Space Navigation*. Ph.D. thesis, Institut National Polytechnique de Toulouse (INP), Toulouse (France), December 2008.

[Coenen & Van Nee, 1992] A.J.R.M. Coenen and D. Van Nee, *Novel Fast GPS/GLONASS Code-Acquisition Technique using Low Update Rate FFT*. Electronics Letters , vol. 28, no. 9, pp. 863 – 865, April 1992.

[Cooley & Tukey, 1965] J.W. Cooley and J.W. Tukey, *An Algorithm for the Machine Calculation Complex Fourier Series*. Mathematics of Computation , vol. 19, no. 90, pp. 297 – 301, April 1965.

[Corazza, 1996] G.E. Corazza, *On the MAX/TC Criterion for Code Acquisition and its Application to DS-SSMA Systems*. IEEE Transactions on Communications , vol. 44, no. 9, pp. 1173 – 1182, September 1996.

[Corazza *et al.*, 2004] G.E. Corazza, C. Caini and A. Vanelli-Coralli, *DS-CDMA Code Acquisition in the Presence of Correlated Fading - Part I: Theoretical Aspects*. IEEE Transactions on Communications , vol. 52, no. 7, pp. 1160 – 1168, June 2004.

[Corazza *et al.*, 2007] G.E. Corazza, C. Palestini, R. Pedone and M. Villanti, *Galileo Primary Code Acquisition Based on Multi-hypothesis Secondary Code Ambiguity Elimination*, in Proceedings of the 20th International Technical Meeting of the Satellite Division of The Institute of Navigation (ION GNSS 2007). Fort Worth, TX (USA), pp. 2459 – 2465, September 2007.

[Cornell University, 2014] Cornell University,. Available: http://www.cornell.edu/ [Accessed: August2014].

[Curran, 2010] J.T. Curran, *Weak Signal Digital GNSS Tracking Algorithms*. Ph.D. thesis, National University of Ireland, Cork (Ireland), November 2010.

[Curran *et al.*, 2012] J.T. Curran, G. Lachapelle and C.C. Murphy, *Improving the Design of Frequency Lock Loops for GNSS Receivers*. IEEE Transactions on Aerospace and Electronic Systems , vol. 48, no. 1, pp. 850–868, January 2012.

[Dicarlo & Weber, 1983] D.M. Dicarlo and C.L. Weber, *Multiple Dwell Serial Search: Performance and Application to Direct Sequence Code Acquisition*. IEEE Transactions on Communications , vol. 31, no. 5, pp. 650 – 659, May 1983.

[Esteves, 2014] P. Esteves, *High-sensitivity Adaptive GNSS Acquisition Schemes*. Ph.D. thesis, Institut Supérieur de l'Aéronautique et de l'Espace (ISAE), Toulouse (France), May 2014.

[Esteves *et al.*, 2013] P. Esteves, M. Sahmoudi, L. Ries and M.-L. Boucheret, *Accurate Doppler-Shift Estimation for Increased Sensitivity of Computationally Efficient GNSS Acquisition*, in Proceedings of the European Navigation Conference (ENC 2013). Vienna, Austria, April 2013.

[European Commission, 2015] European Commission,*Galileo: Satellite launches* [Online]. Available: http://ec.europa.eu/enterprise/policies/satnav/galileo/satellite-launches/index_en.htm

[European GNSS Service Centre, 2015] European GNSS Service Centre,*Constellation Information* [Online]. Available: http://www.gsc-europa.eu/system-status/Constellation-Information#

[European Union, 2014] European Union, *European GNSS (Galileo) Open Service Signal In Space Interface Control Document (OS SIS ICD) Issue 1.2*.

[Federal Space Agency, 2014] Federal Space Agency,*GLONASS constellation status* [Online]. Available: https://glonass-iac.ru/en/GLONASS/ [Accessed: November2014].

[Foucras *et al.*, 2012] M. Foucras, O. Julien, C. Macabiau and B. Ekambi, *A Novel Computationally Efficient Galileo E1 OS Acquisition Method for GNSS Software Receiver*, in Proceedings of the 25th International Technical Meeting of The Satellite Division of the Institute of Navigation (ION GNSS 2012). Nashville, TN (USA), pp. 365 – 383, September 2012.

[Foucras *et al.*, 2013a] M. Foucras, O. Julien, C. Macabiau and B. Ekambi, *An Efficient Strategy for the Acquisition of Weak Galileo E1 OS Signals*, in Proceedings of the European Navigation Conference 2013 (ENC 2013). Vienna (Austria), April 2013.

[Foucras *et al.*, 2013b] M. Foucras, O. Julien, C. Macabiau and B. Ekambi, *Probability of Secondary Code Acquisition for Multi-Component GNSS Signals*, in Proceedings of the 6th European Workshop on GNSS Signals and Signal Processing (SIGNALS 2013). Neubiberg (Germany), December 2013.

[Foucras *et al.*, 2014a] M. Foucras, O. Julien, C. Macabiau and B. Ekambi, *Detailed Analysis of the Impact of the Code Doppler on the Acquisition Performance of New GNSS Signals*, in Proceedings of the 2014 International Technical Meeting of The Institute of Navigation (ION ITM 2014). San Diego, CA (USA), pp. 513 – 524, January 2014.

[Foucras *et al.*, 2014b] M. Foucras, O. Julien, C. Macabiau, B. Ekambi and F. Bacard, *Optimal GNSS Acquisition Parameters when Considering Bit Transitions*, in

Proceedings of IEEE/ION PLANS 2014. Monterey, CA (USA), pp. 804 – 817, May 2014.

[Foucras *et al.*, 2014c] M. Foucras, O. Julien, C. Macabiau, B. Ekambi and F. Bacard, *Assessing the Performance of GNSS Signal Acquisition New Signals and GPS L1 C/A Code*. Inside GNSS , vol. 9, no. 4, pp. 68 – 79, August 2014.

[Foucras *et al.*, 2014d] M. Foucras, O. Julien, C. Macabiau, B. Ekambi and F. Bacard, *Probability of Detection for GNSS Signals with Sign Transitions*. IEEE Transactions on Aerospace and Electronic Systems, In 2nd revision, Submitted in August 2014.

[Foucras *et al.*, 2015] M. Foucras, J. Leclère, C. Botteron, O. Julien, C. Macabiau, P.-A. Farine and B. Ekambi, *Study on the cross-correlation of GNSS signals and usual approximations*. GPS Solutions July 2015.

[Foucras *et al.*, 2014e] M. Foucras, U. Ngayap, J.Y. Li, O. Julien, C. Macabiau and B. Ekambi, *Performance Study of FLL Schemes for a Successful Acquisition-to-Tracking Transition*, in Proceedings of IEEE/ION PLANS 2014. Monterey, CA (USA), pp. 529 – 540, May 2014.

[GNSS-SDR, 2014] GNSS-SDR,*An Open Source Global Navigation Satellite System Software Defined Receiver* [Online]. Available: http://gnss-sdr.org/ [Accessed: August2014].

[Gold, 1967] R. Gold, *Optimal Binary Sequences for Spread Spectrum Multiplexing (Corresp.)*. IEEE Transactions on Information Theory , vol. 13, no. 4, pp. 619 – 621, October 1967.

[Hamilton, 2011] J. Hamilton, *Receiver Survey 2011, sponsored by Novatel*. GPS World , vol. 22, no. 1, January 2011.

[Hamilton, 2012] J. Hamilton, *Receiver Survey 2012, sponsored by Novatel*. GPS World , vol. 23, no. 1, January 2012.

[Hamilton, 2013] J. Hamilton, *Receiver Survey 2013, sponsored by Novatel*. GPS World , vol. 24, no. 1, January 2013.

[Hamilton, 2014] J. Hamilton, *Receiver Survey 2014, sponsored by Novatel*. GPS World , vol. 25, no. 1, January 2014.

[Holmes, 2007] J.K. Holmes, *Spread Spectrum Systems for GNSS and Wireless Communications*, GNSS Technology and Applications Series. Artech House, May 2007.

[Hopkins, 1987] P.M. Hopkins, *A Unified Analysis of Pseudonoise Synchronization by Envelope Correlation*. IEEE Transactions on Communications , vol. 23, no. 4, pp. 425 – 437, September 1987.

[Humphreys *et al.*, 2009] T.E. Humphreys, J.A. Bhatti, T. Pany, B.M. Ledvina and B.W. O'Hanlon, *Exploiting Multicore Technology in Software-Defined GNSS Receivers*, in Proceedings of the 22nd International Technical Meeting of The Satellite Division of the Institute of Navigation (ION GNSS 2009). Savannah, GA (USA), pp. 326 – 338, September 2009.

[IFEN GmbH, 2007] IFEN GmbH, *NavX-NSR - GPS/Galileo Navigation Software Receiver.*

[IFEN GmbH, 2014] IFEN GmbH,*GNSS Simulator and Receiver Products and Services* [Online]. Available: http://www.ifen.com/ [Accessed: August2014].

[IFEN GmbH, 2013] G. IFEN GmbH,*SX-NSR GNSS Receiver* [Online]. Available: http://www.ifen.com/fileadmin/user_upload/product_flyer/Datasheet.SX-NSR-May2013_DINA4.pdf [Accessed: August2014].

[ISMB, 2014] ISMB,*Istituto Superiore Mario Boella* [Online]. Available: http://www.ismb.it/ [Accessed: August2014].

[Jiao *et al.*, 2012] X. Jiao, J. Wang and X. Li, *High Sensitivity GPS Acquisition Algorithm Based on Code Doppler Compensation*, in IEEE 11th International Conference on Signal Processing (ICSP 2012). Beijing (China), pp. 241 – 245, October 2012.

[Joseph & Petovello, 2010] A. Joseph and M.G. Petovello, *Measuring GNSS Signal Strength What is the Difference between SNR and C/N0?*. Inside GNSS , vol. 5, no. 8, pp. 20 – 25, December 2010.

[Julien, 2005] O. Julien, *Design of Galileo L1F Receiver Tracking Loops*. Ph.D. thesis, University of Calgary, Calgary (Canada), July 2005.

[Julien, 2008] O. Julien, *ENGO 638: GNSS Receiver Design.*

[Julien *et al.*, 2007] O. Julien, C. Macabiau, J. Issler and L. Ries, *Two for One Tracking Galileo CBOC Signal with TMBOC*. Inside GNSS , vol. 2, no. 3, pp. 50 –57, Spring 2007.

[Kaplan & Hegarty, 2005] E.D. Kaplan and C. Hegarty, *Understanding GPS: Principles and Applications*, 2nd. Artech House, November 2005.

[Knežević *et al.*, 2010] A. Knežević, C. O'Driscoll and G. Lachapelle, *Co-Processor Aiding for Real-Time Software GNSS Receiver*, in Proceedings of the 2010 International Technical Meeting of The Institute of Navigation (ION ITM 2010). San Diego, CA (USA), pp. 667 – 678, January 2010.

[Kubrak, 2007] D. Kubrak, *Hybridisation of a GPS Receiver with Low-Cost Sensors for Personal Positioning in Urban Environment*. PhD, Telecom Paris, Telecom Paris, May 2007.

[Leclère, 2014] J. Leclère, *Resource-efficient Parallel Acquisition Architectures for Modernized GNSS Signals*. Ph.D. thesis, École Polytechnique Fédérale de Lausanne (EPFL), Lausanne (Switzerland), June 2014.

[Leclère *et al.*, 2013] J. Leclère, C. Botteron and P.-A. Farine, *Modified Parallel Code-phase Search for Acquisition in Presence of Sign Transition*, in International Conference on Localization and GNSS (ICL-GNSS). 1 - 6, June 2013.

[Leclère *et al.*, 2014] J. Leclère, C. Botteron and P.-A. Farine, *Acquisition of Modern GNSS Signals using a Modified Parallel Code-phase Search Architecture*. Signal Processing , vol. 95, pp. 177 –191, February 2014.

[Lecoutre & Tassi, 1987] J.-P. Lecoutre and P. Tassi, *Statistique non-Paramétrique et Robustesse*. Economica Collection "Economie et statistiques avancées," January 1987.

[Ledvina *et al.*, 2003] B.M. Ledvina, S.P. Powell, P.M. Kintner and M.L. Psiaki, *A 12-Channel Real-Time GPS L1 Software Receiver*, in Proceedings of the 2003 National Technical Meeting of The Institute of Navigation (ION NTM 2003). Anaheim, CA (USA), pp. 767 – 782, January 2003.

[Lin *et al.*, 1999] D.M. Lin, J.B.Y. Tsui and D. Howell, *Direct P(Y)-Code Acquisition Algorithm for Software GPS Receivers*, in Proceedings of the 12th International Technical Meeting of the Satellite Division of The Institute of Navigation (ION GPS 1999). Nashville, TN (USA), pp. 363 – 368, September 1999.

[Lin & Tsui, 2000] D. Lin and J.B.Y. Tsui, *Comparison of Acquisition Methods for Software GPS Receiver*, in Proceedings of the 13th International Technical Meeting of the Satellite Division of The Institute of Navigation (ION GPS 2000). Salt Lake City, UT (USA), pp. 2385 – 2390, September 2000.

[Macabiau *et al.*, 2003] C. Macabiau, L. Ries, F. Bastide and J.L. Issler, *GPS L5 Receiver Implementation Issues*, in Proceedings of the 16th International Technical Meeting of the Satellite Division of The Institute of Navigation (ION GPS/GNSS 2003). Portland, OR (USA), pp. 153 – 164, September 2003.

[Marmet *et al.*, 2014] F.-X. Marmet, T. Calmettes, C. Dulery and L. Ries, *A Computationally Efficient GPS/Galileo Acquisition Technique for GNSS Use Beyond Low Earth Orbit*, in Proceedings of 7th ESA Workshop on Satellite Navigation Technologies NAVITEC 2014). Noorwijk (The Netherlands), December 2014.

[Mattos & Petovello, 2013] P.G. Mattos and M.G. Petovello, *Markets and Multi-Frequency GNSS What Will the Spread of Multi-Frequency GNSS Receivers into the Mass Market.* Inside GNSS , vol. 8, no. 1, February 2013.

[Motella *et al.*, 2010] B. Motella, L. Lo Presti and M.G. Petovello, *The Math of Ambiguity What is the Acquisition Ambiguity Function and How Is It Expressed Mathematically?.* Inside GNSS , vol. 5, no. 4, pp. 20 – 28, June 2010.

[Natali, 1984] F.D. Natali, *AFC Tracking Algorithms.* IEEE Transactions on Communications , vol. 32, no. 8, pp. 935 – 947, August 1984.

[Navstar, 2012a] Navstar, *GPS Space Segment/Navigation User Interfaces (IS-GPS-200G).*

[Navstar, 2012b] Navstar, *GPS Space Segment/User Segment L1C Interface (IS-GPS-800C).*

[Navstar, 2012c] Navstar, *GPS Space Segment/User Segment L5 Interfaces (IS-GPS-705C).*

[NAVSYS, 2014] NAVSYS,*GNSS and Inertial Systems, Receivers and Signal Processing* [Online]. Available: http://www.navsys.com/ [Accessed: August2014].

[NovAtel, 2006] NovAtel,*OEM4-G2L* [Online]. Available: http://www.novatel.com/assets/Documents/Papers/oem4g2l.pdf [Accessed: August2014].

[NSL, 2014] NSL,*Delivering Reliable and Robust GNSS* [Online]. Available: http://www.nsl.eu.com/ [Accessed: August2014].

[O'Driscoll, 2007] C. O'Driscoll, *Performance Analysis of the Parallel Acquisition of Weak GPS Signals*. Ph.D. thesis, National University of Ireland, Cork (Ireland), January 2007.

[Pan *et al.*, 1990] S.-M. Pan, D.E. Dodds and S. Kumar, *Acquisition Time Distribution for Spread-Spectrum Receivers*. IEEE Journal on Selected Areas in Communications , vol. 8, no. 5, pp. 800 – 808, June 1990.

[Pany, 2010] T. Pany, *Signal Detection*, in Navigation Signal Processing for GNSS Software Receivers. Artech House, pp. 129 – 162, January 2010.

[Pany *et al.*, 2009] T. Pany, B. Riedl, J. Winkel, T. Worz, R. Schweikert, H. Niedermeier, S. Lagrasta, G. Lopez-Risueno and D. Jimenez-Banos, *Coherent Integration Time The Longer, the Better*. Inside GNSS , vol. 4, no. 6, pp. 52 – 61, December 2009.

[Petovello *et al.*, 2009] M.G. Petovello, C. O'Driscoll, G. Lachapelle, D. Borio and H. Murtaza, *Architecture and Benefits of an Advanced GNSS Software Receiver*. Journal of Global Positioning Systems , vol. 7, no. 2, pp. 156 – 168, 2009.

[Polydoros & Weber, 1984] A. Polydoros and C.L. Weber, *A Unified Approach to Serial Search Spread-Spectrum Code Acquisition - Part II: A Matched-Filter Receiver*. IEEE Transactions on Communications , vol. 32, no. 5, pp. 550 – 560, May 1984.

[Proakis, 2007] J.G. Proakis, *Digital Communications*, 5th. McGraw-Hill Series in Electrical and Computer Engineering, November 2007.

[Psiaki, 2001] M.L. Psiaki, *Block Acquisition of Weak GPS Signals in a Software Receiver*, in Proceedings of the 14th International Technical Meeting of the Satellite Division of The Institute of Navigation (ION GPS 2001). Salt Lake City, UT (USA), pp. 2838 – 2850, September 2001.

[Pulikkoonattu & Antweiler, 2004] R. Pulikkoonattu and M. Antweiler, *Analysis of Differential Non-Coherent Detection Scheme for CDMA Pseudo Random (PN) Code Acquisition*, in IEEE Eighth International Symposium on Spread Spectrum Techniques and Applications. Bologna (Italy), pp. 212 – 217, September 2004.

[Qaisar & Dempster, 2007] S.U. Qaisar and A.G. Dempster, *An Analysis of L1-C/A Cross Correlation & Acquisition Effort in Weak Signal Environments*, in Proceedings of International Global Navigation Satellite Systems Society, IGNSS Symposium. Sydney, Australia, December 2007.

[Ramachandran *et al.*, 2011] G.K. Ramachandran, D. Akopian, G.W. Heckler and L.B. Winternitz, *Performance Evaluation of Block Acquisition and Tracking Algorithms using an Open Source GPS Receiver Platform*, in Proceedings of the 2011 International Technical Meeting of The Institute of Navigation (ION ITM 2011). San Diego, CA (USA), pp. 759 – 766, January 2011.

[RTCA, Inc, 2008] RTCA, Inc, *Assessment of Radio Frequency Interference Relevant to the GNSS L1 Frequency Band RTCA/DO-235B.*

[Rushanan, 2007] J.J. Rushanan, *The spreading and Overlay Codes for the L1C Signal.* DTIC Document, March 2007. DTIC Document, March 2007.

[SpaceFlight, 2014] SpaceFlight,. Available: http://www.spaceflightnow.com/tracking/launchlog.html

[Spilker, 1996] J.J. Spilker, *GPS Signal Structure and Theoretical Performance*, in Global Positioning System: Theory and Applications. American Institute of Aeronautics and Astronautics, August 1996.

[Spirit DSP, 2014] Spirit DSP,*TeamSpirit* [Online]. Available: http://www.spiritdsp.com/contact/ [Accessed: August2014].

[Stanford University, 2014] Stanford University,. Available: http://www.stanford.edu/ [Accessed: August2014].

[Stansell *et al.*, 2010] T.A. Stansell, K.W. Hudnut and R. Keegan, *GPS L1C: Enhanced Performance, Receiver Design Suggestions, and Key Contributions*, in 23rd International Technical Meeting of The Satellite Division of the Institute of Navigation (ION GNSS 2010). Portland, OR, September 2010.

[Starzyk & Zhu, 2001] J.A. Starzyk and Z. Zhu, *Averaging Correlation for C/A Code Acquisition and Tracking in Frequency Domain*, in Proceedings of the 44th IEEE Midwest Symposium on Circuits and Systems (MWSCAS 2001). Dayton, OH (USA), pp. 905 – 908, August 2001.

[Sun & Lo Presti, 2010] K. Sun and L. Lo Presti, *Channels Combining Techniques for a Novel Two Steps Acquisition of New Composite GNSS Signals in Presence of Bit Sign Transitions*, in Proceedings of IEEE/ION PLANS 2010. Indian Wells, CA, USA, pp. 443 – 457, May 2010.

[Tawk *et al.*, 2011] Y. Tawk, A. Jovanovic, J. Leclère, C. Botteron and P.-A. Farine, *A New FFT-Based Algorithm for Secondary Code Acquisition for Galileo Signals*, in IEEE Vehicular Technology Conference (VTC Fall). San Francisco, CA (USA), pp. 1 – 6, September 2011.

[Thales Group, 2014] Thales Group,. Available: https://www.thalesgroup.com/fr [Accessed: August2014].

[Tsinghua University, 2014] Tsinghua University,: 清华大学 [Online]. Available: http://www.tsinghua.edu.cn/publish/newthuen/index.html [Accessed: August2014].

[Tsui, 2005] J.B.-Y. Tsui, *Fundamentals of Global Positioning System Receivers: A Software Approach*, 2nd. Wiley Series in Microwave and Optical Engineering, January 2005.

[u-blox, 2014a] u-blox,*Leading Provider of GPS/GNSS Receiver Modules* [Online]. Available: http://www.u-blox.com/en/ [Accessed: August2014].

[u-blox, 2014b] u-blox,*LEA-M8F: u-blox M8 Time & Frequency Reference GNSS Module* [Online]. Available: http://www.u-blox.com/en/gps-modules/u-blox-6-timing-module/lea-m8f-precision-timing-gnss-module.html [Accessed: August2014].

[University of Calgary, 2014] University of Calgary,. Available: http://ucalgary.ca/ [Accessed: August2014].

[University of Colorado Boulder, 2014] University of Colorado Boulder,. Available: http://www.colorado.edu/ [Accessed: August2014].

[University of Texas, 2014] University of Texas,*The University of Texas at Austin* [Online]. Available: http://www.utexas.edu/ [Accessed: August2014].

[University of Westminster, 2014] University of Westminster,*: Shaping the Future* [Online]. Available: http://www.westminster.ac.uk/ [Accessed: August2014].

[UNSW, 2014] UNSW,. Available: http://www.unsw.edu.au/ [Accessed: August2014].

[U.S. Naval Observatory, 2014] U.S. Naval Observatory,*Current GPS Constellation* [Online]. Available: http://tycho.usno.navy.mil/gpscurr.html [Accessed: November2014].

[Van Dierendonck, 1996] A.J. Van Dierendonck, *GPS receivers*, in Global Positioning System: Theory and Applications. American Institute of Aeronautics and Astronautics, pp. 329 – 407, August 1996.

[Van Dierendonck, 2014] A.J. Van Dierendonck, *New GNSS Signals Will Modern Also Be Better?*. Inside GNSS , vol. 9, no. 2, pp. 42 – 43, April 2014.

[Van Dierendonck & Spilker, 1999] A.J. Van Dierendonck and J.J. Spilker, *Proposed Civil GPS Signal at 1176.45 MHz: In-Phase/Quadrature Codes at 10.23 MHz Chip Rate*, in Proceedings of the 55th Annual Meeting of The Institute of Navigation. Cambridge, MA (USA), pp. 761 – 770, June 1999.

[Van Diggelen, 2014] F. Van Diggelen, *Who's Your Daddy? Why GPS Will Continue to Dominate Consumer GNSS?*. Inside GNSS , vol. 9, no. 2, pp. 30 – 41, April 2014.

[Van Diggelen, 2009] F.S.T. Van Diggelen, *A-GPS: Assisted GPS, GNSS, and SBAS*, GNSS Technology and Applications Series. Artech House, March 2009.

[Wallner *et al.*, 2007] S. Wallner, J.-A. Avila-Rodriguez, G.W. Hein and J.J. Rushanan, *Galileo E1 OS and GPS L1C Pseudo Random Noise Codes - Requirements, Generation, Optimization and Comparison* -, in Proceedings of the 20th International Technical Meeting of the Satellite Division of The Institute of Navigation (ION GNSS 2007). Fort Worth, TX, USA, pp. 1549 – 1563, September 2007.

[Wang *et al.*, 2014] Y. Wang, J. Tian, J. Leclère, C. Botteron, V. Capuano and P.-A. Farine, *An Efficient Time-frequency Algorithm for the Weak Signal Acquisition of Modernized GNSS Signals*, in Proceedings of the 27th International Technical Meeting of The Satellite Division of the Institute of Navigation (ION GNSS+ 2014). Tampa, Florida (USA), pp. 2767 – 2775, September 2014.

[Ward *et al.*, 2005a] P. Ward, J.W. Betz and C. Hegarty, *GPS Satellite Signal Charactristics*, in Understanding GPS: Principles and Applications. Artech House, November 2005.

[Ward *et al.*, 2005b] P. Ward, J.W. Betz and C.J. Hegarty, *Satellite Signal Acquisition, Tracking, and Data Demodulation*, in Understanding GPS: Principles and Applications. Artech House, November 2005.

[Ward, 1996] P.W. Ward, *GPS Receiver Search Techniques*, in IEEE Position Location and Navigation Symposium. Atlanta, GA (USA), pp. 604 – 611, April 1996.

[Weill & Petovello, 2011] L.R. Weill and M.G. Petovello, *Difference Between Signal Acquisition and Tracking*. Inside GNSS , vol. 6, no. 1, pp. 22 – 27, February 2011.

[Yang *et al.*, 2004] C. Yang, C. Hegarty and M. Tran, *Acquisition of the GPS L5 Signal Using Coherent Combining of I5 and Q5*, in Proceedings of the 17th International Technical Meeting of the Satellite Division of The Institute of Navigation (ION GNSS 2004). Long Beach, CA (USA), pp. 2184 – 2195, September 2004.

[Zarrabizadeh & Sousa, 1997] R.H. Zarrabizadeh and E.S. Sousa, *A Differentially Coherent PN Code Acquisition Receiver for CDMA Systems*. IEEE Transactions on Communications , vol. 45, no. 11, pp. 1456 – 1465, November 1997.

[Zhang & Ghogho, 2010] W. Zhang and M. Ghogho, *Improved Fast Modified Double-Block Zero-Padding (FMDBZP) Algorithm for Weak GPS Signal Acquisition*, in Proceedings of 18th European Signal Processing Conference (EUSIPCO 2010). Aalborg (Denmark), August 2010.

[Zhongliang *et al.*, 2014] D. Zhongliang, X. Jue, J. Jichao and Y. Lu, *Unambiguous Acquisition for Galileo E1 OS Signal Based on Delay and Multiply*. TELKOMNIKA Indonesian Journal of Electrical Engineering , vol. 12, no. 4, pp. 950 – 962, December 2014.

[Ziedan, 2006] N.I. Ziedan, *GNSS Receivers for Weak Signals*. Artech House, July 2006.

Appendix A
Receiver Survey

The study of the characteristics of GNSS receivers sold over the last years permits to highlight the current trends. Based on the receiver studies published in GPS World each year [Hamilton, 2011], [Hamilton, 2012], [Hamilton, 2013] and [Hamilton, 2014], some statistics are given here. Note that the receiver study published in 2011 concerns the GNSS receivers available in 2010 and so on. It is worth some discussion to present the radical changes in tracked GNSS signals in 4 years.

Firstly, let us focus on the number of available GNSS receivers (presented in second column of Table A.1). It can be seen that it fluctuate between 366 and 514. In 4 years, the number of manufacturers decreased from 61 to 48. This can be explained in part by the fusion of several companies. The GNSS receivers market is dominated (by the number of proposed receiver models) by the manufacturers Trimble (50 receivers in 2013), JAVAD GNSS (37 receivers) and NovAtel, ftech Radio Frequency System Corporation, Hemisphere GNSS and Septentrio (16 or 17 receivers), which represents around 40% of the market. Except for these 6 companies, the average number of available GNSS receivers per manufacturer is around 5 or 6.

From Table A.1, it can be observed that an half of the receivers on the market in 2013 can track GLONASS signals and only 32% can track Galileo signals. It confirms the trend already present in 2010 but in other proportions 28%/18%.

Table A.2 presents also the multi-constellation GNSS receivers deployment. In 2010, half of the developed GNSS receivers, tracked only GPS L1 C/A and there was no GNSS receiver tracking more than 3 constellations. 4 years later, the repartition of GPS L1 C/A only becomes a quarter and then more than an half tracks at least 2 constellations. As it can be observed, around 1/5 of the developed GNSS receivers in 2013 tracks the 5 constellations (GPS, GLONASS, Galileo, QZSS and BeiDou). For Galileo, QZSS and BeiDou, this configuration represents clearly the higher percentage between the multi-constellation repartition (Table A.5 and Table A.6).

It is interesting to figure out the use of each constellation. Table A.3 and Table A.4 can help. The bi-constellation GNSS receivers market is dominated by the association of GPS with GLONASS (16% in 2013); the GPS/Galileo represents only 2%; this represents respectively 1/3 of the GNSS receivers able to track GLONASS and only 5% of the GNSS receivers able to track Galileo (Table A.5 and Table A.6). QZSS and BeiDou signals start to be tracked in 2013 and are mainly tracked when 4 or 5 constellations are considered.

Year	Number of GNSS receivers	Only GPS	Galileo	GLONASS	QZSS	BeiDou
2010	434	*64%*	*18%*	*28%*	0%	0%
2011	469	61%	21%	31%	7%	9%
2012	514	47%	31%	45%	13%	17%
2013	366	40%	*32%*	*52%*	28%	26%

Table A.1 Repartition of the GNSS constellations

Table A.1 should be read as:

- *18% of the 434 GNSS receivers, in 2010, can track at least one Galileo signal*
- *64% of the 434 GNSS receivers, in 2010 track only GPS signals (that means GPS L1 C/A and GPS L5 or GPS L1 C/A and GPS L2) (the 3rd column corresponds to the 4th column of* Table A.2*)*

Year	Number of GNSS receivers	Only GPS L1 C/A	Only GPS	2 const.	3 const.	4 const.	5 const.
2010	434	*52%*	64%	*25%*	11%	*0%*	*0%*
2011	469	53%	61%	23%	7%	4%	5%
2012	514	38%	47%	24%	13%	9%	7%
2013	366	*27%*	40%	*23%*	*10%*	*7%*	*17%*

Table A.2 Repartition of the multi-constellation GNSS receivers

Table A.2 should be read as:

- *52% of the 434 GNSS receivers, in 2010 track only GPS L1 C/A*
- *25% of the 434 GNSS receivers, in 2010 track signals of 2 constellations (for example, GPS/Galileo or GPS/ GLONASS)*

Year	GPS				Galileo				GLONASS			
	2	3	4	5	2	3	4	5	2	3	4	5
2010	*25%*	11%	0%	0%	*7%*	11%	0%	0%	18%	11%	0%	0%
2011	23%	7%	4%	5%	5%	7%	4%	5%	18%	7%	1%	5%
2012	24%	13%	9%	7%	6%	9%	9%	7%	16%	13%	9%	7%
2013	23%	10%	7%	*17%*	*2%*	6%	6%	*17%*	*16%*	9%	7%	*17%*

Table A.3 Absolute repartition of each constellation (GPS, Galileo, GLONASS)

Year	QZSS				BeiDou			
	2	3	4	5	2	3	4	5
2010	0%	0%	0%	0%	0%	0%	0%	0%
2011	0%	0%	2%	5%	0%	0%	4%	5%
2012	1%	4%	0%	7%	0%	1%	9%	7%
2013	4%	3%	2%	*17%*	1%	1%	6%	*17%*

Table A.4 Absolute repartition of each constellation (QZSS, BeiDou)

Table A.3 and Table A.4 should be read as:

- *7% of the GNSS receivers, in 2010, is a bi-constellation GPS/Galileo*
- *25% of the GNSS receivers, in 2010, is a bi-constellation with GPS (as observed GPS/Galileo and GPS/GLONASS)*
- *17% of the GNSS receivers, on the market in 2013, is a 5-constellation*

Year	GPS					Galileo					GLONASS				
	only	2	3	4	5	only	2	3	4	5	only	2	3	4	5
2010	64%	*25%*	11%	0%	0%	0%	41%	59%	0%	0%	0%	63%	37%	0%	0%
2011	61%	23%	7%	4%	5%	0%	25%	34%	18%	22%	0%	56%	24%	5%	15%
2012	47%	24%	13%	9%	7%	0%	20%	28%	30%	22%	0%	35%	29%	20%	15%
2013	40%	24%	10%	8%	18%	1%	*5%*	20%	19%	*55%*	4%	*31%*	17%	14%	34%

Table A.5 For each constellation, relative repartition of the association with 1, 2, 3 or 4 GNSS (GPS, Galileo, GLONASS)

Year	QZSS					BeiDou				
	only	2	3	4	5	only	2	3	4	5
2010	0%	100%	0%	0%	0%	100%	0%	0%	0%	0%
2011	0%	0%	3%	32%	65%	2%	0%	0%	44%	56%
2012	0%	11%	34%	2%	54%	1%	0%	4%	54%	41%
2013	5%	15%	10%	9%	*62%*	1%	3%	5%	24%	*67%*

Table A.6 For each constellation, relative repartition of the association with 1, 2, 3 or 4 GNSS (QZSS, BeiDou)

Table A.5 and Table A.6 should be read as:

- *25% of the GNSS receivers, in 2010 which can track at least one GPS signal is a bi-constellation GNSS receiver,*
- *55% of the GNSS receivers, in 2013, which can track at least one Galileo signal, can track signals from the 5 constellations.*

The number of GNSS receivers which can track at least one Galileo signal, for example, can be found with Table A.1.

The augmentations such as SBAS, EGNOS are not considered in this study.

Appendix B
Mathematical identities

Some identities, which are used in mathematical developments, are reminded. In the following:, $\alpha, \beta \in \mathbb{R}$, $N, L \in \mathbb{N}$.

B.1 Trigonometric identities

Firstly, the addition and subtraction formulae are presented:

$$\begin{aligned}
\cos(\alpha) \times \cos(\beta) &= \tfrac{1}{2}(\cos(\alpha-\beta)+\cos(\alpha+\beta)) \\
\sin(\alpha)+\sin(\beta) &= 2\sin\left(\frac{\alpha+\beta}{2}\right)\cos\left(\frac{\alpha-\beta}{2}\right) \\
\sin(\alpha)-\sin(\beta) &= 2\cos\left(\frac{\alpha+\beta}{2}\right)\sin\left(\frac{\alpha-\beta}{2}\right) \\
\cos(\alpha)+\cos(\beta) &= 2\cos\left(\frac{\alpha+\beta}{2}\right)\cos\left(\frac{\alpha-\beta}{2}\right) \\
\cos(\alpha)-\cos(\beta) &= -2\sin\left(\frac{\alpha+\beta}{2}\right)\sin\left(\frac{\alpha-\beta}{2}\right) \\
\cos(\alpha+\beta) &= \cos(\alpha)\cos(\beta)-\sin(\alpha)\sin(\beta) \\
\sin(\alpha+\beta) &= \cos(\alpha)\sin(\beta)+\cos(\beta)\sin(\alpha) \\
\cos^2(\alpha)+\sin^2(\alpha) &= 1
\end{aligned} \tag{B.1}$$

B.2 Complex identities

Let us note:

$$\begin{aligned} z &= a+ib \\ Z &= A+iB \end{aligned}$$

Then,

$$\begin{aligned}
aA+bB &= \mathrm{Re}\big((a+ib)(A-iB)\big) = \mathrm{Re}(zZ^*) \\
&= \left(\left(\frac{a+A}{2}\right)^2+\left(\frac{b+B}{2}\right)^2\right)-\left(\left(\frac{a-A}{2}\right)^2+\left(\frac{b-B}{2}\right)^2\right) \\
&= \left|\frac{z+Z}{2}\right|^2-\left|\frac{z-Z}{2}\right|^2
\end{aligned} \tag{B.2}$$

B.3 Summations identities

The sum of the first N first integer numbers is:

$$\sum_{n=1}^{N} n = \frac{N(N+1)}{2} \tag{B.3}$$

The sum of the first N terms of a geometric series of common ratio $\beta \neq 1$ is:

$$\sum_{n=0}^{N-1} \beta^n = \frac{1-\beta^N}{1-\beta} \tag{B.4}$$

which is a special case ($L = 0$) of:

$$\sum_{n=L}^{N-1} \beta^n = \frac{\beta^L - \beta^N}{1-\beta} \tag{B.5}$$

In the case that the common ratio is an exponential term ($\beta = e^{2i\pi\alpha}$):

$$\begin{aligned}\sum_{n=0}^{N-1} e^{2i\pi\alpha n} &= \sum_{n=0}^{N-1} \left(e^{2i\pi\alpha}\right)^n = \frac{1-e^{2i\pi\alpha N}}{1-e^{2i\pi\alpha}} \\ &= \frac{e^{i\pi\alpha N}\left(e^{-i\pi\alpha N} - e^{i\pi\alpha N}\right)}{e^{i\pi\alpha}\left(e^{-i\pi\alpha} - e^{i\pi\alpha}\right)} = e^{i\pi\alpha(N-1)}\frac{\sin(\pi\alpha N)}{\sin(\pi\alpha)} \\ &= N e^{i\pi\alpha(N-1)}\frac{\operatorname{sinc}(\pi\alpha N)}{\operatorname{sinc}(\pi\alpha)}\end{aligned} \tag{B.6}$$

In addition,

$$\sum_{n=0}^{N-1} e^{i\alpha\frac{n}{N}} = N \text{ only if } \alpha = 0 \text{ or multiple of } 2\pi \tag{B.7}$$

If the first term of the sum is for $n = L \neq 0$, the sum becomes:

$$\sum_{n=L}^{N-1} e^{2i\pi\alpha n} = \sum_{n=L}^{N-1} \left(e^{2i\pi\alpha}\right)^n = \frac{e^{2i\pi\alpha L} - e^{2i\pi\alpha N}}{1-e^{2i\pi\alpha}} \tag{B.8}$$

Appendix C

GPS L1 C/A and Galileo E1 OS code correlation properties

As previously mentioned, the spreading codes are carefully chosen to have very good pseudo-randomness properties to spread the signal bandwidth effectively. This property is reflected in the autocorrelation function. In this section, significant values of autocorrelation and cross-correlation values of the GPS L1 C/A and Galileo E1 OS spreading codes are presented, resulting of exhaustive simulations. These results are provided for a null Doppler frequency and for several Doppler frequency ranges (for which the Doppler frequency is considered constant). A Doppler frequency range contains all the Doppler frequencies between 0 and the frequency range limit, with a frequency step of 10 Hz. Simulations are run on only positive Doppler frequencies due to symmetry. When it is not specified, the correlation integration time is the spreading code period, that means 1 ms for GPS L1 C/A and 4 ms for Galileo E1 OS. For the Galileo E1 OS, some more simulations were run mimicking a realistic case with a local and a received CBOC modulation.

The simulation scenario is the following. Two spreading codes are generated $c_{1,k}$ and $c_{1,l}$ and their correlation is computed by means of Fourier transforms, taking into account potential Doppler frequency.

$$R(\tau) = 20\log_{10}\left(\left|\frac{1}{N_{c_1}}\mathcal{F}^{-1}\left(\mathcal{F}\left(c_{1,k}\right)\times \mathrm{e}^{2i\pi f_D t}\times\overline{\mathcal{F}\left(c_{1,l}\right)}\right)\right|\right) \tag{C.1}$$

This is done for all spreading code couples, for each code delay and for each Doppler frequency in the Doppler frequency range.

C.1 Autocorrelation

C.1.1 GPS L1 C/A

Without any Doppler and except at the correct alignment, the autocorrelation of the GPS L1 C/A codes can take only three possible values as presented in Table C.1. The associated average probability of occurrence, based on [Spilker, 1996] is also provided. It is worth noting that depending on the C/A code and because 12.5% of 1022 does not provide an integer number, the worst case (-23.94 dB) can occur between 10% and 16% of the time. [Qaisar & Dempster, 2007] provided partial numerical values and the figure of Table C.1 provides the experimental PDF and the experimental CDF. The value at 0.5 of the experimental CDF shows that the worst case occurs more than 12.5% of the time.

Real value	$\frac{1}{1023}$	$\frac{63}{1023}$	$-\frac{65}{1023}$
Decibel value (dB)	-60.20	-24.21	-23.94
Probability of occurrence	75%	12.5%	12.5%

(a) Theoretical C/A code autocorrelation

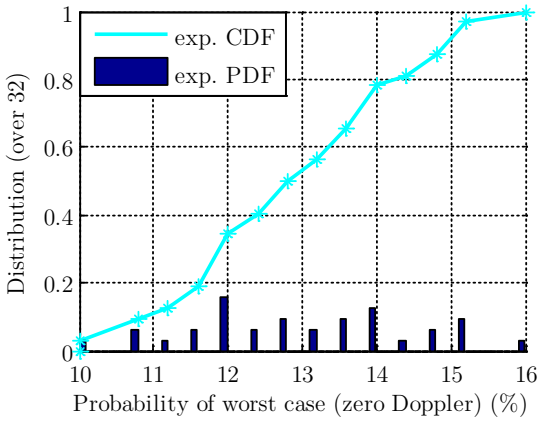

(b) Experimental PDF and CDF of the probability of occurrence of -23.94 dB

Table C.1 Theoretical and experimental C/A code autocorrelation properties (no Doppler)

However, the characteristic values of the C/A code autocorrelation properties radically change when considering a not null Doppler frequency. As an example for 3 PRN C/A codes, in Figure C.1 the maximum of the autocorrelation function per Doppler frequency is represented for a Doppler frequency between 0 and 10 kHz.

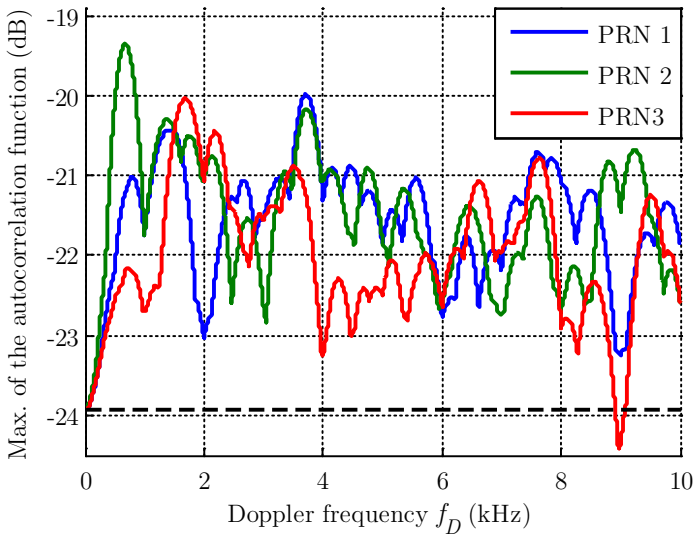

Figure C.1 Maximum of the autocorrelation function versus the Doppler frequency (excluding the correct code delay alignment)

In this case, to obtain the most precise values, simulations are run for each hertz. Then, it can be observed that the maximum of the autocorrelation function per PRN code on the considered Doppler frequency range $[0, 10]$ kHz, is at least 4 dB higher than the symbolic value of -23.94 dB at 0 Hz (materialized by a black dashed line). In addition, this figure shows that the maximum per C/A code is not for the same Doppler frequency. Indeed, for the PRN C/A code 2, the maximum is -19.36 dB obtained for a Doppler frequency of 677 Hz whereas the maximum of the PRN C/A code 1 is -19.98 dB for 3719 Hz. For each PRN C/A code, Figure C.2 presents the amplitude (Figure(a)) and the Doppler frequency (Figure(b)) of the maximum.

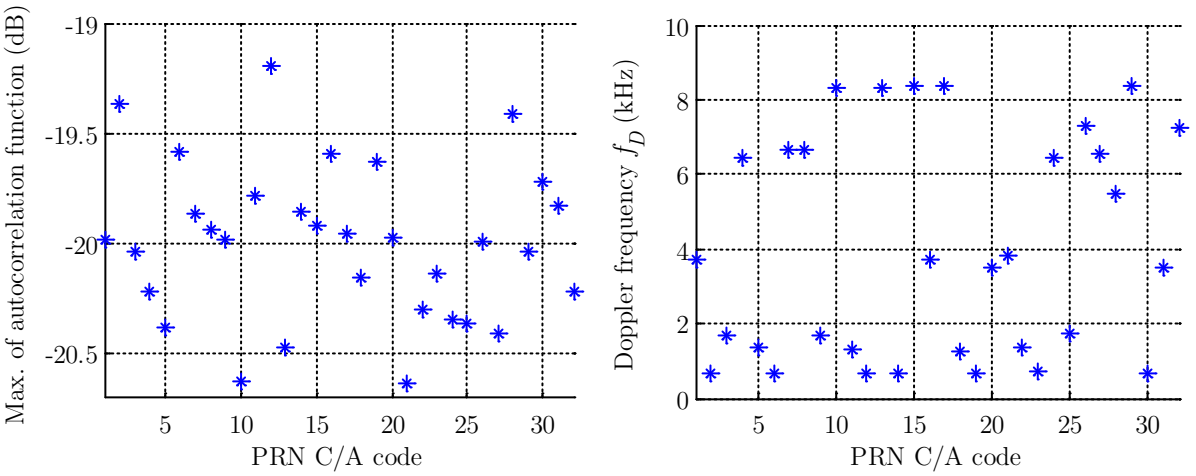

(a) Maximum of the autocorrelation function per PRN C/A code

(b) Doppler frequency providing the maximum per PRN C/A code

Figure C.2 Maximum per C/A code of the autocorrelation function (excluding the correct code delay alignment)

It is important to note that for Doppler frequencies multiple of 1 kHz, the autocorrelation function does not take a discrete value (maximum or minimum). So as presented in this work (and rarely in literature), to be exhaustive, the autocorrelation function should be studied over a range and not some punctual Doppler frequencies such as integer kHz multiples.

The distribution of all autocorrelation function values (excluding the correct code delay alignment) for all the PRN C/A codes and for different Doppler frequency ranges is computed and the significant percentiles are presented in Table C.2. The numerical values of the maximum for all the Doppler frequency ranges are provided in the table.

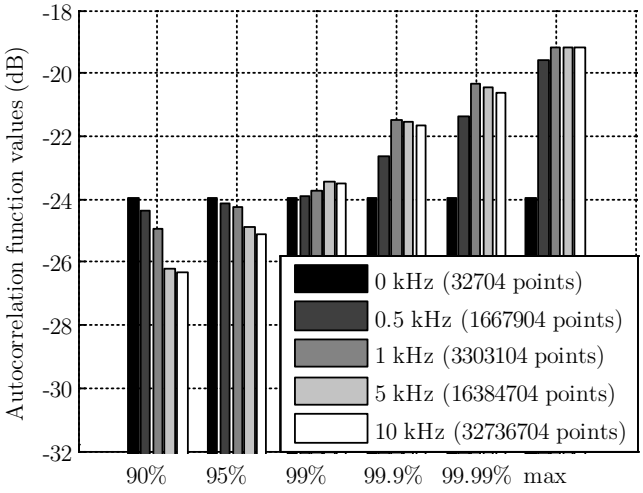

Doppler frequency	Maximum
$f_D = 0$ Hz	-23.94 dB
$f_D \in [0, 0.5]$ kHz	-19.58 dB
$f_D \in [0, 1]$ kHz	-19.18 dB
$f_D \in [0, 5]$ kHz	-19.18 dB
$f_D \in [0, 10]$ kHz	-19.18 dB

Table C.2 Distribution of the GPS L1 C/A codes autocorrelation function values (excluding the correct code delay alignment and all Doppler)

The black bars represent the distribution of the autocorrelation function values for a null Doppler frequency. Since there are only three possible values, all percentiles higher than 90% (and even higher than around 87.5%) correspond to the worst case (-23.94 dB). It is computed on the 32 704 points, which are the 1022 values taken per the autocorrelation function for all the 32 PRN C/A codes. The interpretation of the bars is for example: for a Doppler frequency in the range $[-5, 5]$ kHz, 90% of the values are below -26.2 dB and thus there is only one point over 10 that has a higher value.

Obviously, when the Doppler frequency range increases, the maximum of the autocorrelation function (bars on the right of the figure) increases. At the contrary, the lowest considered percentiles decreases because there are more values. It should be retained that the maximum autocorrelation function values is -19.18 dB when considering Doppler frequency in the range $[-10,10]$ kHz.

To have an order of idea of the behavior of the maximum per Doppler frequency when the coherent integration time is extended to several spreading code periods, Figure C.3 shows the behavior for a Doppler frequency around 1 kHz. As it can be observed, the distribution of the maximum per Doppler frequency drastically changes, the higher the coherent integration time is, the narrower the main lobe is.

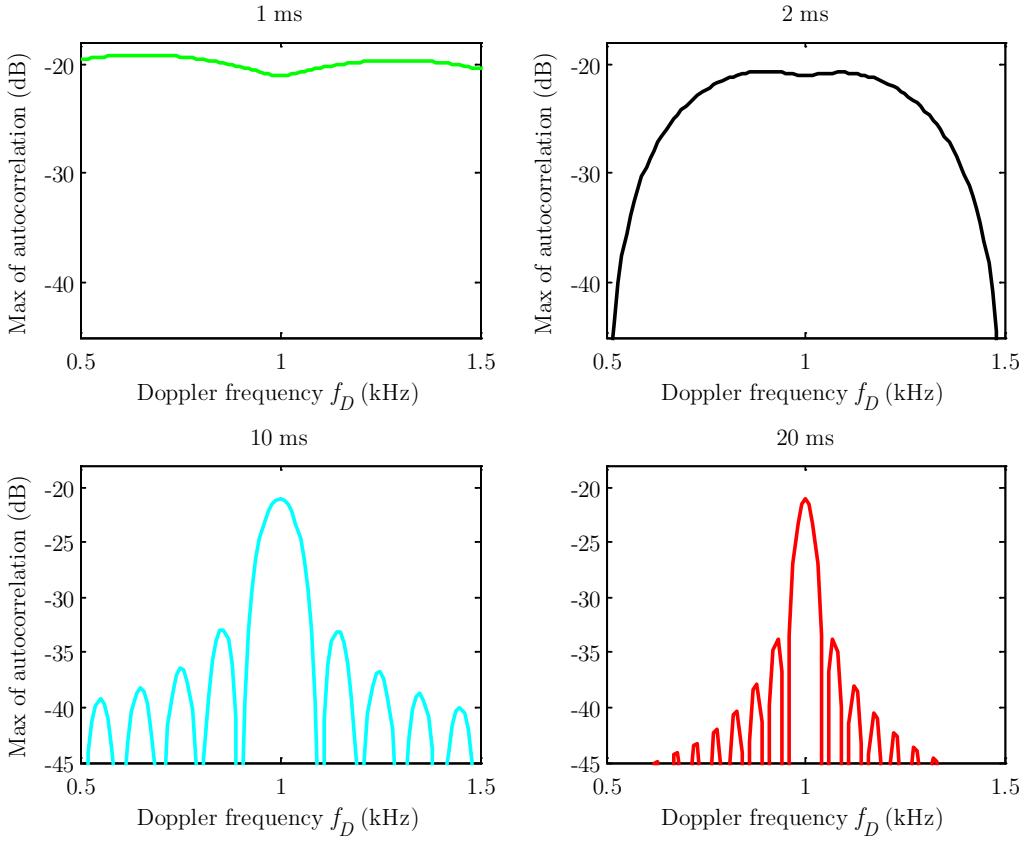

Figure C.3 Maximum of the autocorrelation function per Doppler frequency for different coherent integration times (excluding the correct code delay alignments)

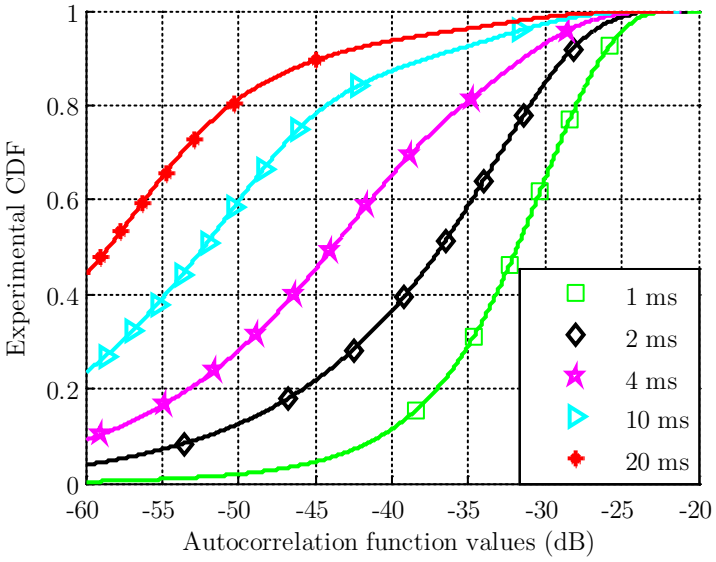

Figure C.4 Experimental CDF of the autocorrelation function values for different coherent integration times (for a Doppler frequency between 0 and 10 kHz)

To complete the observation, Figure C.4 provides the experimental CDF of the distribution of all values taken by the autocorrelation function for a Doppler frequency between 0 and 10 kHz. When the coherent integration time is equal to 20 ms, 90% of the autocorrelation function values are below -44.5 dB whereas for a coherent integration time of 1ms, only 5% of the values are below – 44.5 dB.

C.1.2 Galileo E1 OS

As previously done for GPS L1 C/A codes, the same study is lead for the memory codes chosen as the PRN codes on the data and pilot components of the Galileo E1 OS signal. There is no distinction between the Galileo E1B and Galileo E1C codes when presenting results. Unlike the GPS L1 C/A signal, for the Galileo E1 OS signal, when not considering Doppler frequency, the number of possible autocorrelation values tends to be very high, as depicted in Figure C.5. Let us note that when considering CBOC modulation (both received and local), the maximum (-25.39 dB) is unchanged.

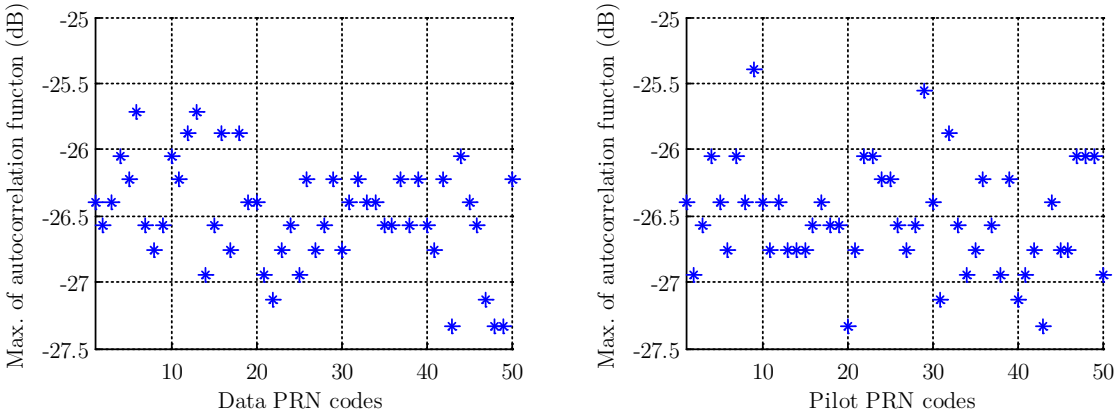

(a) Maximum of data code autocorrelation (b)Maximum of pilot code autocorrelation

Figure C.5 Maximum of the autocorrelation function per PRN code (excluding the correct code delay alignment and no Doppler)

In the same way, the autocorrelation function is studied when considering Doppler frequency, as introduced in [Wallner *et al.*, 2007].

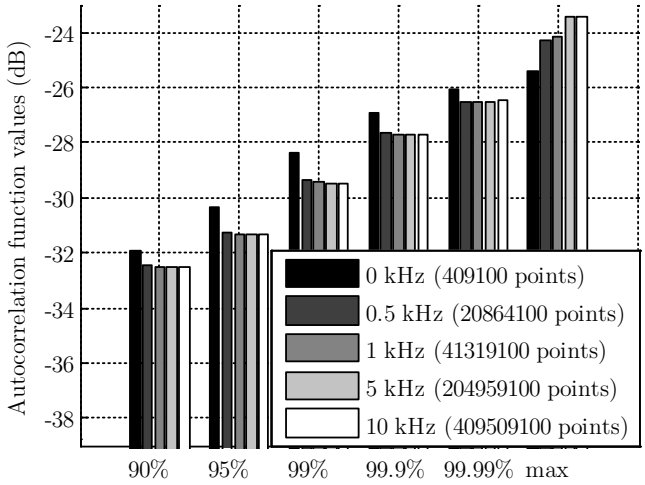

Doppler frequency	Maximum
$f_D = 0$ Hz	-25.39 dB
$f_D \in [0, 0.5]$ kHz	-24.26 dB
$f_D \in [0, 1]$ kHz	-24.17 dB
$f_D \in [0, 5]$ kHz	-23.44 dB
$f_D \in [0, 10]$ kHz	-23.44 dB

Table C.3 Distribution of the Galileo PRN codes autocorrelation function values (excluding the correct code delay alignment)

When the Doppler frequency is between 0 and 10 kHz, the maximum of the autocorrelation function is -23.44 dB. But that does not mean that for all the codes, the maximum of the autocorrelation function per code is -23.44 dB. Indeed, as represented in Figure C.6, 50% of the maximum of the autocorrelation function per Galileo PRN code (data and pilot) are below -25.04 dB.

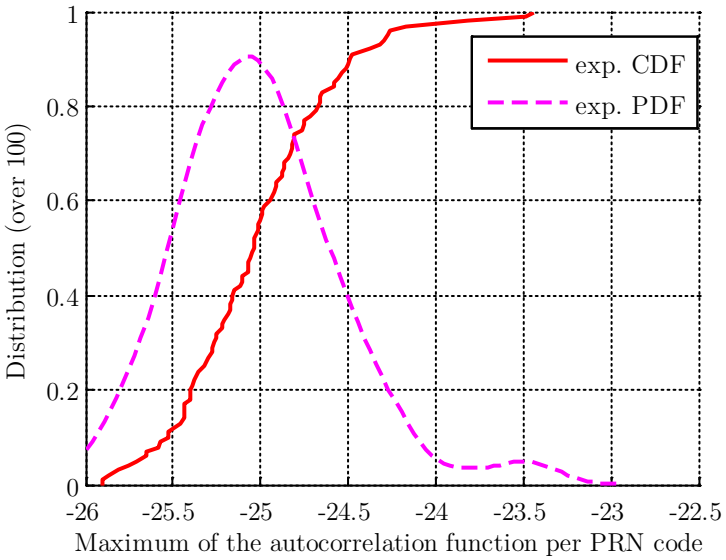

Figure C.6 Distribution of the maximum Galileo PRN codes autocorrelation function per PRN code (excluding the correct code delay alignment)

C.2 Cross-correlation

The second point of interest of the correlation properties of the PRN codes is the cross-correlation isolation, which means the correlation values when two different codes are correlated.

C.2.1 GPS L1 C/A

When there is no Doppler, the cross-correlation function can only take only 3 values, the same as the autocorrelation function with the same theoretical distribution, as presented in Table C.1. In the case of the cross-correlation, the average occurrence of the worst case (-23.94 dB) is 11.73% as presented in Table C.4, whereas it was 12.78% for the autocorrelation. It is worth noting that for all the C/A code couples, the cross-correlation value with no delay and no Doppler is always equal to -1/1023, which is the best isolation.

Real value	$\frac{1}{1023}$	$\frac{63}{1023}$	$-\frac{65}{1023}$
Decibel value (dB)	-60.20	-24.21	-23.94
Probability of occurrence	75%	12.5%	12.5%

(a) Theoretical C/A code cross-correlation

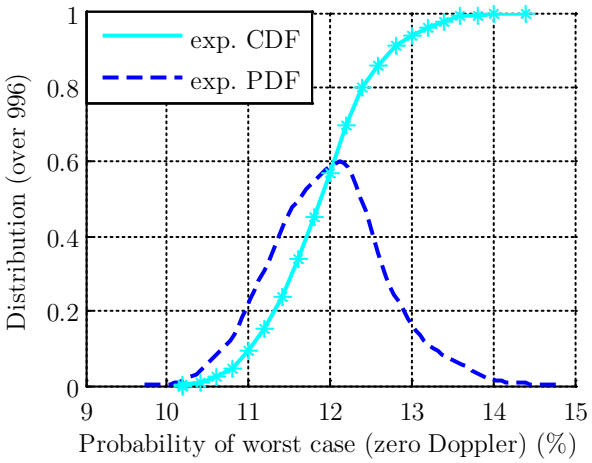

(b) Experimental PDF and CDF of the probability of occurrence of -23.94 dB

Table C.4 Theoretical and experimental C/A code cross-correlation properties (no Doppler)

Once again, when there is a not null Doppler frequency, the distribution and characteristic values of the cross-correlation function of the C/A codes change and it is important to understand that the worst cases are not for the kHz Doppler frequency. For example, in [Ward *et al.*, 2005a], the cumulative probability of occurrence is given for all the kHz Doppler frequencies between 1 kHz and 5 kHz.

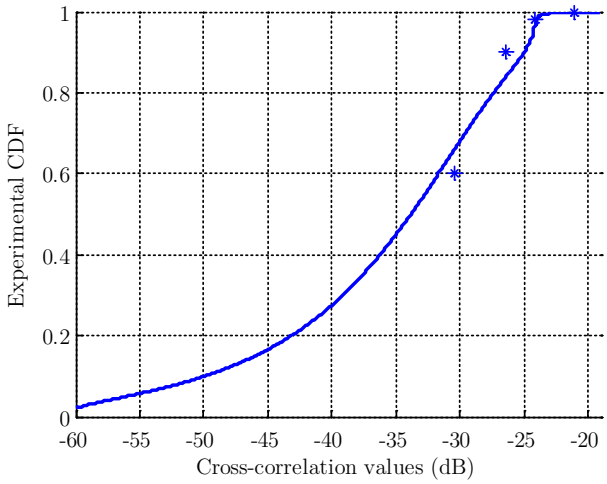

Figure C.7 Distribution of the GPS C/A codes cross-correlation function values per C/A code (Doppler frequency between 0 and 1 kHz)

However, as represented in Figure C.7, the high percentiles at 1 kHz are higher than those on a range of 1 kHz; the curve represents the experimental CDF computed for all the couples of C/A codes, for all codes delays and for all Doppler frequencies between 0 and 1 kHz with a step of 10 Hz, and the stars represent the values given in the reference.

Due to the high number of points when considering all C/A code couples, all code delays and all Doppler frequency (more than 5×10^8), it is difficult to compute the exact value of the percentiles for the ranges of Doppler 0 to 5 and 10 kHz. In Table C.5 provides the maximum per Doppler frequency range.

Doppler frequency	Maximum
$f_D = 0$ Hz	-23.94 dB
$f_D \in [0, 0.5]$ kHz	-19.44 dB
$f_D \in [0, 1]$ kHz	-19.05 dB
$f_D \in [0, 5]$ kHz	-19.05 dB
$f_D \in [0, 10]$ kHz	-19.05 dB

Table C.5 Maximum of the GPS L1 C/A code couples cross-correlation function

In Figure C.8, the distribution of the maximum, per C/A code couple, of the cross-correlation function is represented by the experimental CDF and PDF, for a Doppler frequency between 0 and 10 kHz. The maximum value taken by the cross-correlation function is -19.05 dB and 90% of the maximums per C/A code couple, are below -19.58 dB.

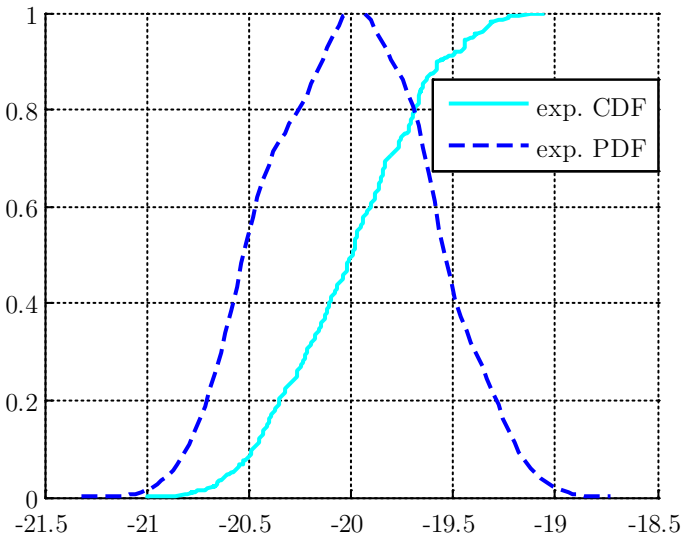

Figure C.8 Distribution of the maximum of the cross-correlation function per GPS C/A codes couple (Doppler frequency between 0 and 10 kHz)

C.2.2 Galileo E1 OS

For the Galileo E1 OS signal, two cross-correlations should be considered. The first one concerns the cross-correlation of the codes for the same satellite, which means the correlation of the data and the pilot codes. If, for example, locally, only the data component is generated, when computing the autocorrelation of the data PRN codes, the cross-correlation between the received pilot and the local data PRN codes is present. As it can be read with Table C.6, the isolation is -23.42 dB when considering a Doppler frequency in the range $[-10, 10]$ kHz.

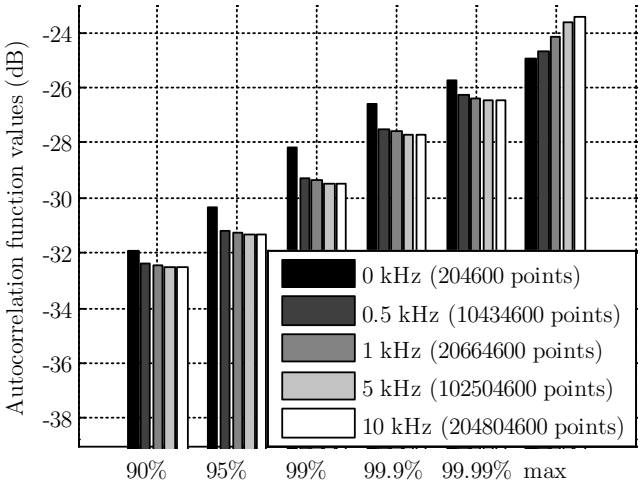

Doppler frequency	Maximum
$f_D = 0$ Hz	-24.93 dB
$f_D \in [0, 0.5]$ kHz	-24.69 dB
$f_D \in [0, 1]$ kHz	-24.16 dB
$f_D \in [0, 5]$ kHz	-23.62 dB
$f_D \in [0, 10]$ kHz	-23.42 dB

Table C.6 Distribution of the Galileo PRN codes cross-correlation function values (data and pilot codes for the same satellite)

The second kind of Galileo E1 OS PRN code cross-correlation results in the correlation of two codes of two different satellites. There are, then, 3 possibilities:

- Correlation of two data codes,
- Correlation of two pilot codes,
- Correlation of a data and a pilot codes from two different satellites.

Figure C.9 provides the maximum value of the cross-correlation function computed for all couples. Due to the high number of points, the percentiles are not computed for a Doppler frequency higher than 1 kHz.

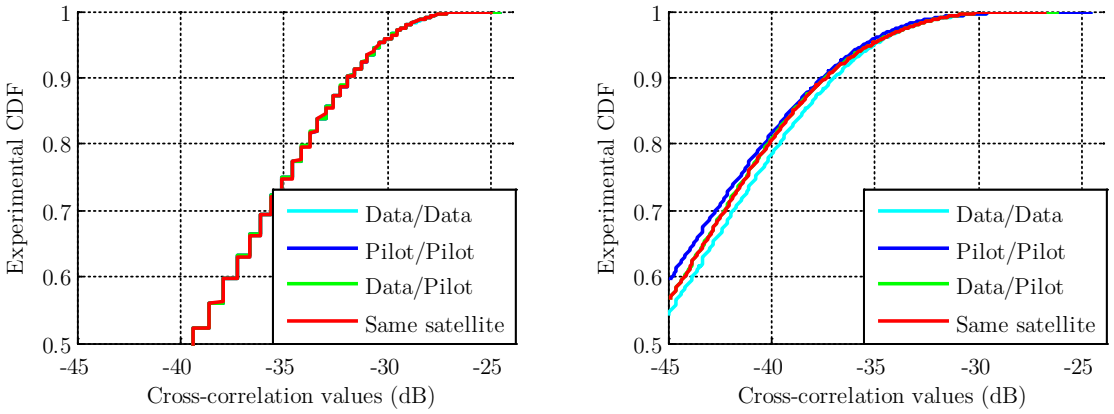

(a) code/code (b) CBOC/CBOC

Figure C.9 Experimental CDF of the Galileo E1 OS PRN codes cross-correlation (no Doppler)

As it can be observed with Figure C.9 the difference of the cross-correlation between two codes, from or not, the same satellites is very slight when only the codes are correlated (Figure C.9(a)) or when the spreading code sequences (code and CBOC subcarrier) are correlated (Figure C.9(b))). However, the CBOC modulation permits a better isolation (Table C.7) when a data and a pilot codes are correlated (from the same satellite or not). When considering the CBOC modulation, the isolation for the cross-correlation of both data and pilot satellite is - 26.66 dB whereas it is -24.49 dB for two data or two pilot codes.

		Same satellite	Different satellite		
			Data/Data	Pilot/Pilot	Data/Pilot
$f_D = 0$ Hz	Code/code	-24.93 dB	-24.49 dB	*-24.49 dB*	-24.09 dB
	CBOC/CBOC	*-26.66 dB*			-26.13 dB
$f_D \in [0, 10]$ kHz	Code/code	-23.42 dB	-22.59 dB	-23.00 dB	22.82 dB
	CBOC/CBOC	-25.16 dB			-24.57 dB

Table C.7 Maximum of the Galileo PRN codes cross-correlation function values

C.2.3 Discussion on the correlation properties of the GPS L1 C/A and Galileo E1 OS PRN codes

The Galileo E1 OS codes have better autocorrelation properties than GPS L1 C/A codes. Indeed, when not considering Doppler frequency, the difference is 1.45 dB. However, when considering Doppler frequency, the difference of the maximum values taken by the autocorrelation functions on $[-10,\ 10]$ kHz is 4.23 dB in favor of Galileo E1 OS. As it can be observed in Figure C.10(a), the average value on the Doppler range $[-10,\ 10]$ kHz is -20.54 dB for GPS L1 C/A (with a standard deviation of 0.73 dB) whereas the average value is -24.88 dB (with a standard deviation of 0.41 dB) for Galileo E1 OS.

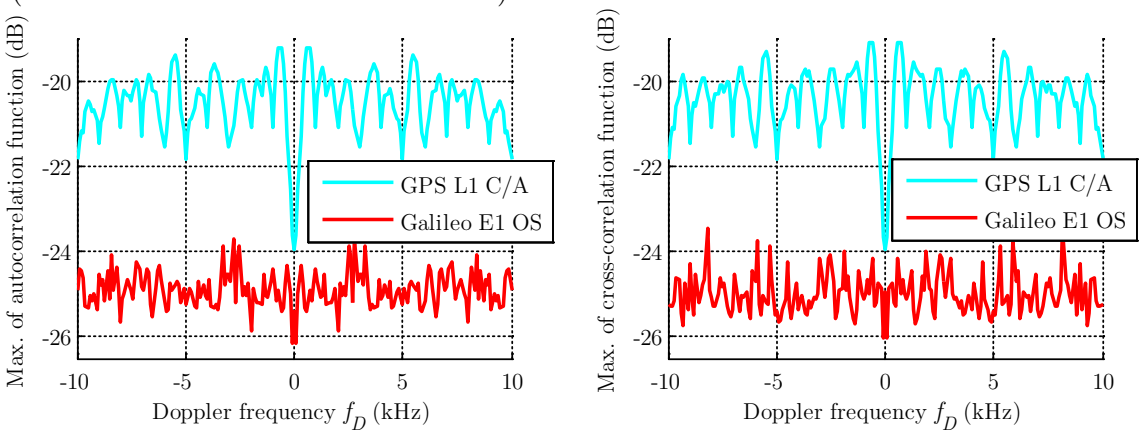

(a) Autocorrelation (b) Cross-correlation

Figure C.10 Maximum of the autocorrelation and cross-correlation functions per Doppler frequency for all codes and couples of codes

The same trend is observable for the cross-correlation between the GPS L1 C/A codes on one side and the Galileo E1 OS codes from the same satellite on the other side (Figure C.10(b)). The characteristic figures of the correlation properties of both signals are reminded in Table C.8.

	Autocorrelation		Cross-correlation		
	GPS L1 C/A	Galileo E1 OS	GPS L1 C/A	Galileo E1 OS	
				Same satellite	Diff. satellite
$f_D = 0$ Hz	-23.94 dB	-25.39 dB	-23.94 dB	-26.66 dB	-24.49 dB
$f_D \in [0, 10]$ kHz	-19.18 dB	-23.44 dB	-19.08 dB	-25.16 dB	-22.82 dB

Table C.8 Characteristic figures of the correlation for the GPS L1 C/A and Galileo E1 OS signals (considering CBOC modulation)

C.2.4 GPS and Galileo E1 OS codes cross-correlation

Due to the high number of constellations sharing the same frequency bands, the cross-correlation between signals from two systems should also be taken into account. For GPS and Galileo, two cases should be considered:

- Locally a Galileo E1 OS signal is generated and correlated with a received slice of signal of 4 ms which can contain 4 repetitions of GPS L1 C/A codes,
- Locally a GPS L1 C/A signal is generated and correlated with a received slice of signal of 1 ms which can contain a portion of Galileo E1 OS codes.

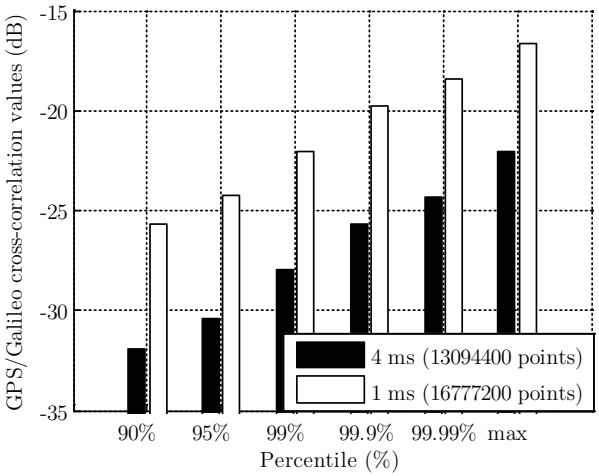

		Code	CBOC
Correlations on...	4 ms	-22.03 dB	-25.19 dB
	1 ms	-19.14 dB	

Table C.9 Distribution of the GPS and Galileo PRN codes (no Doppler)

Table C.9 provides the main percentiles of the cross-correlation between GPS L1 C/A codes and Galileo codes (no modulation). When the coherent integration time is 4 ms, the 100 Galileo codes (data and pilot) are correlated with 4 repetitions of the 32 GPS C/A codes. The maximum cross-correlation value is -22.03 dB. When considering the Galileo CBOC modulation, that means that 12 samples are used to describe the respective data and pilot subcarriers of the Galileo codes and the GPS C/A code chips are repeated 12 times, the maximum cross-correlation becomes -25.19 dB. When the coherent integration time is 1 ms, the GPS L1 C/A codes are correlated of one of the 4092 slices of 1023 chips of the Galileo E1 OS codes but due to the high number of potential combinations, only partial results are presented.

The conclusion of this section is that the Galileo E1 OS codes have better correlation properties than the GPS L1 C/A codes. For a Doppler frequency in $[-10, 10]$ kHz and considering CBOC modulation, the autocorrelation isolation is -23.44 dB, the cross-correlation of two codes not for the same satellite is -22.82 dB and for to codes for the same satellite, it is -25.16 dB which is equivalent to the cross-correlation on 4 ms of GPS and Galileo E1 OS.

Appendix D
Correlator output expression

The correlation interval is $[T_0 + (k-1)T_C;\ T_0 + kT_C]$. It is assumed that the local estimates of the Doppler frequency and code delay are constant; but the incoming signal parameters values depend on the correlation interval. Let us denote by $\phi_0(k)$ the phase at the beginning of the correlation interval of the incoming signal (that means at $(T_0 + (k-1)T_C)$).

Firstly, the received signal is multiplied by a local carrier $\cos\left(2\pi\left(f_{IF} + \hat{f}_D\right)t + \hat{\phi}_0\right)$ depending on an estimate of the Doppler frequency $\hat{f}_D$ and potentially a local initial phase $\hat{\phi}_0$ and knowing that the product of the carriers is equal to:

$$\begin{aligned}&\cos\left(2\pi\left(f_{IF} + \hat{f}_D\right)t + \hat{\phi}_0\right) \times \cos\left(2\pi\left(f_{IF} + f_D(k)\right)t + \phi_0(k)\right)\\ &= \frac{1}{2}\cos\left(2\pi\left(f_D(k) - \hat{f}_D\right)t + \left(\phi_0(k) - \hat{\phi}_0\right)\right) = \frac{1}{2}\cos\left(2\pi\varepsilon_{f_D}(k)t + \varepsilon_{\phi_0}(k)\right)\end{aligned} \tag{D.1}$$

Assuming that the low-pass filter eliminates the terms at double frequency:

$$\frac{1}{2}\cos\left(2\pi\left(2f_{IF} + f_D(k) + \hat{f}_D\right)t + \phi_0(k) + \hat{\phi}_0\right) \tag{D.2}$$

Secondly, the signal is multiplied by a local replica of the spreading code with an estimation of the code delay $c_1(t - \hat{\tau})$.

Then, the resulting signal is accumulated on T_C and provides the in-phase correlator output:

$$\begin{aligned}&I(k)\\ &= \frac{A}{2T_C}\int_{T_0+(k-1)T_C}^{T_0+kT_C} d(k)c_1\left(t - \tau(k)\right)c_1(t - \hat{\tau})\cos\left(2\pi\varepsilon_{f_D}(k)t + \varepsilon_{\phi_0}(k)\right)dt + \eta_I(k)\end{aligned} \tag{D.3}$$

where the noise at the correlator output is denoted $\eta_I\,(k)$.

As said in [Holmes, 2007], since the Doppler frequency error is small compared to the chipping rate, the autocorrelation function R_{c_1} can be factored out of the integral and then I becomes:

$$\begin{aligned} I(k) &= \frac{A}{2T_C} d(k) \int_{T_0+(k-1)T_C}^{T_0+kT_C} c_1\big(t-\tau(k)\big) c_1(t-\hat{\tau}) dt \int_{T_0+(k-1)T_C}^{T_0+kT_C} \cos\Big(2\pi\varepsilon_{f_D}(k)t + \varepsilon_{\phi_0}(k)\Big) dt \\ &\quad + \eta_I(k) \\ &= \frac{A}{2T_C} d(k) R_{c_1}(\tau(k)-\hat{\tau}) \times \frac{1}{2\pi\varepsilon_{f_D}} \Big[\sin\Big(2\pi\varepsilon_{f_D}(k)t + \varepsilon_{\phi_0}(k)\Big)\Big]_{T_0+(k-1)T_C}^{T_0+kT_C} + \eta_I(k) \\ &= \frac{A}{2} d(k) R_{c_1}\big(\varepsilon_\tau(k)\big) \cos\Big(\pi\varepsilon_{f_D}(k)T_C + \varepsilon_{\phi_0}(k)\Big) \operatorname{sinc}\big(\pi\varepsilon_{f_D}(k)T_C\big) + \eta_I(k) \end{aligned} \tag{D.4}$$

In the same way, the quadrature–phase correlator output is:

$$Q(k) = \frac{A}{2} d(k) R_{c_1}\big(\varepsilon_\tau(k)\big) \sin\Big(\pi\varepsilon_{f_D}(k)T_C + \varepsilon_{\phi_0}(k)\Big) \operatorname{sinc}\big(\pi\varepsilon_{f_D}(k)T_C\big) + \eta_Q(k) \tag{D.5}$$

Appendix E
Signals Effects on the Acquisition

E.1 Effect of the code Doppler

E.1.1 Main formulas of Doppler frequency shift

The expressions of the received chipping rate $f_{c_1,D}$ (affected by a code Doppler shift $\delta_{f_{c_1,D}}$) and thus the received spreading code chip duration $t_{c_1,D}$ (and the chip durations difference) are:

$$\begin{aligned} f_{c_1,D} &= f_{c_1}\left(1+\frac{f_D}{f_L}\right) \\ t_{c_1,D} &= t_{c_1}\left(\frac{f_L}{f_D+f_L}\right) \\ \delta_{f_{c_1,D}} &= f_{c_1,D} - f_{c_1} = f_{c_1}\times\frac{f_D}{f_L} \\ \delta_{t_{c_1,D}} = t_{c_1} - t_{c_1,D} &= t_{c_1}\left(1-\left(\frac{f_L}{f_D+f_L}\right)\right) = \frac{1}{f_{c_1}}\frac{f_D}{f_D+f_L} \end{aligned} \tag{E.1}$$

Let us note n the number of chips (or in the same way, t the number of seconds) after the shift of 1 chip (it is assumed that $f_D > 0$ and then $t_{c_1,D} < t_{c_1}$)

$$\begin{aligned} n &> \frac{f_D+f_L}{f_D} \text{ chips} \\ t &> \frac{f_D+f_L}{f_D f_{c_1}} \text{ seconds} \end{aligned} \tag{E.2}$$

The amount of change after t seconds is:

$$\left| t f_{c_1} \frac{f_D}{f_L} \right| \text{ chips} \tag{E.3}$$

E.1.2 Mathematical model of distorted autocorrelation function

The product of two rectangular functions can be seen as an indicator function:

$$\begin{aligned}\operatorname{rect}\left(\frac{t}{t_{c_1}}-u\right)\operatorname{rect}\left(\frac{t}{t_{c_1,D}}-v\right) &= \begin{cases}1, \begin{cases}(u-1)t_{c_1} \le t \le ut_{c_1}\\ (v-1)t_{c_1,D} \le t \le vt_{c_1,D}\end{cases}\\ 0, \text{otherwise}\end{cases}\\ &= \begin{cases}1, \begin{cases}\max\left((u-1)t_{c_1};\ (v-1)t_{c_1,D}\right) \le t\\ t \le \min\left(ut_{c_1}; vt_{c_1}\right)\end{cases}\\ 0, \text{otherwise}\end{cases}\\ &= \mathbf{1}_{\left[\max\left((u-1)t_{c_1};(v-1)t_{c_1,D}\right);\min\left(ut_{c_1};vt_{c_1,D}\right)\right]}(t)\end{aligned} \tag{E.4}$$

The autocorrelation function depends on the term:

$$c(u)\sum_{v=1}^{N_{c_1}} c(v)\,\mathbf{1}_{\left[\max\left((u-1)t_{c_1};(v-1)t_{c_1,D}\right);\min\left(ut_{c_1};vt_{c_1,D}\right)\right]}(t)$$

On the first integration and assuming no initial code delay, two cases are possible: the first one assumes an expansion of the received spreading code and the second one a shrinking as illustrated in Figure E.1. Since the incoming Doppler frequency is assumed to be less than 10 kHz, in one spreading code period, there is no an entire chip slip and then the chip "u" of the local code is the chip "u" of the received spreading code and the closest neighborhoods ("$u-1$" and "$u+1$").

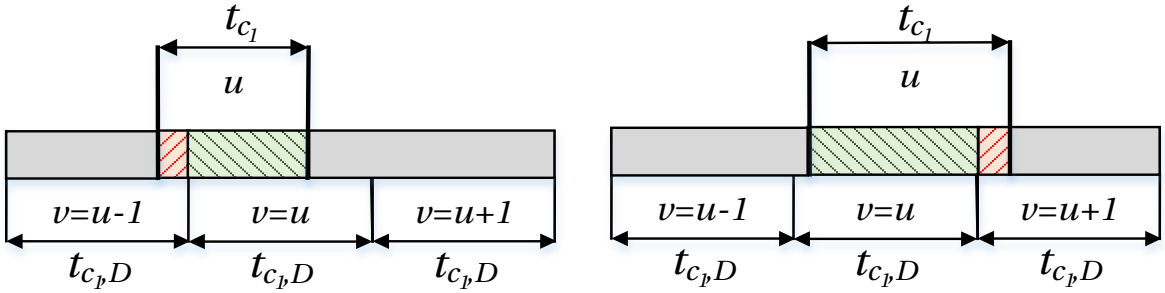

$$c(u)\times\begin{pmatrix}c(u-1)\mathbf{1}_{[(u-1)t_{c_1};(u-1)t_{c_1,D}]}(t)\\ +c(u)\mathbf{1}_{[(u-1)t_{c_1,D};ut_{c_1}]}(t)\end{pmatrix}$$
$$= c(u)c(u-1)(u-1)\delta_{t_{c_1,D}} - u\delta_{t_{c_1,D}} + t_{c_1,D}$$

(a) $\delta_{t_{c_1,D}} = t_{c_1,D} - t_{c_1} \ge 0$

$$c(u)\times\begin{pmatrix}c(u)\mathbf{1}_{[(u-1)t_{c_1};ut_{c_1,D}]}(t)\\ +c(u+1)\mathbf{1}_{[ut_{c_1,D};ut_{c_1}]}(t)\end{pmatrix}$$
$$= u\delta_{t_{c_1,D}} + t_{c_1} - c(u)c(u+1)u\delta_{t_{c_1,D}}$$

(b) $\delta_{t_{c_1,D}} = t_{c_1,D} - t_{c_1} \le 0$

Figure E.1 Product of the chip "u" of the local spreading code by the received spreading code

Then, the autocorrelation function in both cases can be developed:

- Case(a) : $t_{c_1,D} \geq t_{c_1}$

$$\begin{aligned} R_{c_1}(f_D,0) &= \frac{1}{T_C}\sum_{u=1}^{N_{c_1}} \int_{(u-1)t_{c_1}}^{ut_{c_1}} c(u) \sum_{v=1}^{N_{c_1}} c(v)\, \mathbf{1}_{\left[max\left((u-1)t_{c_1};(v-1)t_{c_1,D}\right);min(ut_{c_1};vt_{c_1,D})\right]}(t)dt \\ &= \frac{1}{T_C}\left(\left(-\delta_{t_{c_1},D}+t_{c_1,D}\right)+\sum_{u=2}^{N_{c_1}}\left(c(u)c(u-1)(u-1)\delta_{t_{c_1},D}+u\delta_{t_{c_1},D}+t_{c_1,D}\right)\right) \\ &= \frac{1}{T_C}\left(N_{c_1}t_{c_1,D}\delta_{t_{c_1},D}\Delta\sum_{u=1}^{N_{c_1}}u+\delta_{t_{c_1},D}\sum_{u=2}^{N_{c_1}}c(u)c(u-1)(u-1)\right) \\ &= \frac{1}{T_C}\left(N_{c_1}t_{c_1,D}-\delta_{t_{c_1},D}\frac{N_{c_1}\left(N_{c_1}+1\right)}{2}+\delta_{t_{c_1},D}\sum_{u=1}^{N_{c_1}-1}c(u+1)c(u)u\right) \end{aligned} \tag{E.5}$$

- Case(b) : $t_{c_1} \leq t_{c_1,D}$

$$\begin{aligned} R_{c_1}(f_D,0) &= \frac{1}{T_C}\sum_{u=1}^{N_{c_1}} \int_{(u-1)t_{c_1}}^{ut_{c_1}} c(u) \sum_{v=1}^{N_{c_1}} c(v)\, \mathbf{1}_{\left[max\left((u-1)t_{c_1};(v-1)t_{c_1,D}\right);min(ut_{c_1};vt_{c_1,D})\right]}(t)dt \\ &= \frac{1}{T_C}\left(\sum_{u=1}^{N_{c_1}}\left(u\delta_{t_{c_1},D}+t_{c_1}\right)-\delta_{t_{c_1},D}\left(\sum_{u=1}^{N_{c_1}-1}c(u)c(u+1)u+c\left(N_{c_1}\right)c(1)N_{c_1}\right)\right) \\ &= \frac{1}{T_C}\left(\delta_{t_{c_1},D}\frac{N_{c_1}\left(N_{c_1}+1\right)}{2}+N_{c_1}t_{c_1}-\delta_{t_{c_1},D}\sum_{u=1}^{N_{c_1}-1}c(u)c(u+1)u-\delta_{t_{c_1},D}c\left(N_{c_1}\right)c(1)N_{c_1}\right) \end{aligned} \tag{E.6}$$

In the end,

$$\begin{aligned} R_{c_1}(f_D,0) &= \frac{1}{T_C}\left(N_{c_1}\max\left(t_{c_1};t_{c_1,D}\right)-\left|\delta_{t_{c_1},D}\right|\frac{N_{c_1}\left(N_{c_1}+1\right)}{2}\right. \\ &\qquad \left.+\left|\delta_{t_{c_1},D}\right|\left(\sum_{u=1}^{N_{c_1}-1}uc(u)c(u+1)+N_{c_1}c(1)c\left(N_{c_1}\right)\mathbf{1}_{\left[t_{c_1,D}\leq t_{c_1}\right]}\right)\right) \\ &= \frac{1}{t_{c_1}}\left(\max\left(t_{c_1};t_{c_1,D}\right)-\left|\delta_{t_{c_1},D}\right|\frac{\left(N_{c_1}+1\right)}{2}\right. \\ &\qquad \left.+\frac{\left|\delta_{t_{c_1},D}\right|}{N_{c_1}}\left(\sum_{u=1}^{N_{c_1}-1}uc(u)c(u+1)+N_{c_1}c(1)c\left(N_{c_1}\right)\mathbf{1}_{\left[t_{c_1,D}\leq t_{c_1}\right]}\right)\right) \end{aligned} \tag{E.7}$$

E.2 Correlator output in presence of data modulation

E.2.1 Correlator output in presence of data modulation

In an ideal case, the data bit is assumed to be constant during the correlation process. Here, the more realistic case is envisaged, a bit sign transition occurs at $t_0 \in [0; T_C]$. Then, the integration of the resulting carrier term is equivalent to the integration of two carrier terms with opposite sign. The in-phase correlator output $I(t_0)$ is based on (E.8). In the same way, the quadrature phase correlator output $Q(t_0)$ is based on (E.8).

$$\begin{aligned}
&\frac{1}{T_C}\left(\int_{T_0+(k-1)T_C}^{T_0+t_0}(1)\cos\left(2\pi\varepsilon_{f_D}(k)t+\phi_0\right)dt+\int_{T_0+t_0}^{T_0+kT_C}(-1)\cos\left(2\pi\varepsilon_{f_D}t+\varepsilon_{\phi_0}(k)\right)dt\right)\\
&=\frac{\left[\sin\left(2\pi\varepsilon_{f_D}(k)t+\varepsilon_{\phi_0}(k)\right)\right]_{T_0+(k-1)T_C}^{T_0+t_0}-\left[\sin\left(2\pi\varepsilon_{f_D}(k)t+\varepsilon_{\phi_0}(k)\right)\right]_{T_0+t_0}^{T_0+kT_C}}{2T_C\pi\varepsilon_{f_D}(k)}\\
&=\frac{\sin\left(2\pi\varepsilon_{f_D}(k)t_0+\varepsilon_{\phi_0}(k)\right)-\sin\left(\pi\varepsilon_{f_D}(k)T_C+\varepsilon_{\phi_0}(k)\right)\cos\left(\pi\varepsilon_{f_D}(k)T_C\right)}{\pi\varepsilon_{f_D}(k)T_C}\\
&=\frac{\sin\left(2\pi\varepsilon_{f_D}(k)t_0+\varepsilon_{\phi_0}(k)\right)}{\pi\varepsilon_{f_D}(k)T_C}-\sin\left(\pi\varepsilon_{f_D}(k)T_C+\varepsilon_{\phi_0}(k)\right)\frac{\cos\left(\pi\varepsilon_{f_D}(k)T_C\right)}{\pi\varepsilon_{f_D}(k)T_C}
\end{aligned} \tag{E.8}$$

$$\begin{aligned}
&\frac{1}{T_C}\left(\int_{T_0+(k-1)T_C}^{T_0+t_0}(1)\sin\left(2\pi\varepsilon_{f_D}(k)t+\phi_0\right)dt+\int_{T_0+t_0}^{T_0+kT_C}(-1)\sin\left(2\pi\varepsilon_{f_D}t+\varepsilon_{\phi_0}(k)\right)dt\right)\\
&=\frac{-\left[\cos\left(2\pi\varepsilon_{f_D}(k)t+\varepsilon_{\phi_0}(k)\right)\right]_{T_0+(k-1)T_C}^{T_0+t_0}+\left[\cos\left(2\pi\varepsilon_{f_D}(k)t+\varepsilon_{\phi_0}(k)\right)\right]_{T_0+t_0}^{T_0+kT_C}}{2T_C\pi\varepsilon_{f_D}(k)}\\
&=\frac{\cos\left(2\pi\varepsilon_{f_D}(k)t_0+\varepsilon_{\phi_0}(k)\right)-\cos\left(\pi\varepsilon_{f_D}(k)T_C+\varepsilon_{\phi_0}(k)\right)\cos\left(\pi\varepsilon_{f_D}(k)T_C\right)}{\pi\varepsilon_{f_D}(k)T_C}\\
&=\frac{\cos\left(2\pi\varepsilon_{f_D}(k)t_0+\varepsilon_{\phi_0}(k)\right)}{\pi\varepsilon_{f_D}(k)T_C}-\cos\left(\pi\varepsilon_{f_D}(k)T_C+\varepsilon_{\phi_0}(k)\right)\frac{\cos\left(\pi\varepsilon_{f_D}(k)T_C\right)}{\pi\varepsilon_{f_D}(k)T_C}
\end{aligned} \tag{E.9}$$

E.2.2 Non-centrality parameter expression

The non-centrality parameter results in the sum of the squared expectation values of $I(t_0,k)$ and $Q(t_0,k)$.

$$(t_0) = \left(\frac{E\big(I(t_0,k)\big)}{\sigma_\eta}\right)^2 + \left(\frac{E\big(Q(t_0,k)\big)}{\sigma_\eta}\right)^2 = \frac{1}{\sigma_\eta^2}\left(\frac{A}{2}R(\varepsilon_\tau)\right)^2 \times \Lambda \tag{E.10}$$

where

$$\begin{aligned}\Lambda = &\left(\frac{\sin\left(2\pi\varepsilon_{f_D}t_0 + \varepsilon_{\phi_0}(k)\right)}{\pi\varepsilon_{f_D}T_C} - \sin\left(\pi\varepsilon_{f_D}T_C + \varepsilon_{\phi_0}(k)\right)\frac{\cos\left(\pi\varepsilon_{f_D}T_C\right)}{\pi\varepsilon_{f_D}T_C}\right)^2 \\ &+\left(-\frac{\cos\left(2\pi\varepsilon_{f_D}t_0 + \varepsilon_{\phi_0}(k)\right)}{\pi\varepsilon_{f_D}T_C} + \cos\left(\pi\varepsilon_{f_D}T_C + \varepsilon_{\phi_0}(k)\right)\frac{\cos\left(\pi\varepsilon_{f_D}T_C\right)}{\pi\varepsilon_{f_D}T_C}\right)^2\end{aligned} \tag{E.11}$$

Let us replace $u = \pi\varepsilon_{f_D}T_C$:

$$\begin{aligned}&\sin\left(2\pi\varepsilon_{f_D}t_0 + \varepsilon_{\phi_0}(k)\right)\sin\left(u + \varepsilon_{\phi_0}(k)\right) + \cos\left(2\pi\varepsilon_{f_D}t_0 + \varepsilon_{\phi_0}(k)\right)\cos\left(u + \varepsilon_{\phi_0}(k)\right) \\ &= \cos\left(\pi\varepsilon_{f_D}(T_C - 2t_0)\right)\end{aligned} \tag{E.12}$$

The non-centrality parameter becomes:

$$\begin{aligned}\Lambda &= \frac{1}{u^2}\left(1 + \cos^2(u) - 2\cos(u)\cos\left(\pi\varepsilon_{f_D}(T_C - 2t_0)\right)\right) \\ &= \frac{1}{u^2}\left(\frac{1+\cos(2u)}{2} + 1 - 2\cos(u)\cos\left(u\left(1 - \frac{2t_0}{T_C}\right)\right)\right)\end{aligned} \tag{E.13}$$

At the end, the non-centrality parameter is then:

$$\lambda(t_0) = \frac{A^2}{4\sigma_\eta^2}\frac{{R_{c_1}}^2(\varepsilon_\tau)}{\left(\pi\varepsilon_{f_D}T_C\right)^2}\left(1 + \cos^2\left(\pi\varepsilon_{f_D}T_C\right) - 2\cos\left(\pi\varepsilon_{f_D}T_C\right)\cos\left(\pi\varepsilon_{f_D}T_C\left(1 - \frac{2t_0}{T_C}\right)\right)\right) \tag{E.14}$$

Attention should be taken when ε_{f_D} is close to 0. In the neighborhood of $u \approx 0$, $\cos(u)$ can be approximated by $\left(1 - \frac{u^2}{2}\right)$:

$$\begin{aligned}\Lambda &\approx_{u\approx 0} \frac{1}{u^2}\left(\frac{1}{2}\left(1+\left(1-\frac{(2u)^2}{2}\right)\right)+1-2\left(1-\frac{u^2}{2}\right)\left(1-\frac{u^2}{2}\left(1-\frac{2t_0}{T_C}\right)^2\right)\right)\\ &\approx_{u\approx 0} \frac{1}{u^2}\left(2\left(1-\frac{u^2}{2}\right)-2\left(1-\frac{u^2}{2}\right)+2\left(1-\frac{u^2}{2}\right)\frac{u^2}{2}\left(1-\frac{2t_0}{T_C}\right)^2\right)\\ &\approx_{u\approx 0} \frac{1}{u^2}\left(\left(1-\frac{u^2}{2}\right)u^2\left(1-\frac{2t_0}{T_C}\right)^2\right)\\ &\approx_{u\approx 0} \left(1-\frac{u^2}{2}\right)\left(1+4\frac{t_0^2}{T_C^2}-4\frac{t_0}{T_C}\right)\end{aligned} \tag{E.15}$$

When there is no error on the Doppler frequency, the non-centrality parameter is approximated by:

$$\lambda\left(t_0, \varepsilon_{f_D}=0\right) \approx \frac{A^2}{4\sigma_\eta^2} {R_{c_1}}^2(\varepsilon_\tau)\left(1+4\frac{t_0^2}{T_C^2}-4\frac{t_0}{T_C}\right) \tag{E.16}$$

E.2.3 Probability of detection for any number of non-coherent summations

Some explanations are provided in this section on the probability of detection, more precisely on the probability of occurrence.

For Galileo E1 OS signal, it seems clear that is corresponds to the probability for a binomial random variable. Indeed, for K non-coherent summations, there are $2K$ bit transitions and for each one, it can be a bit sign transition with a probability of 50%.

In the case of GPS L1 C/A, it is not as simple as for Galileo E1 OS because the spreading code period is shorter than the data bit period. In addition, since the data bit beginning is not known, several cases should be considered depending on the integration time and on the position of the integration interval regarding the data bit beginning. Two examples are firstly presented and then the general case can be developed.

On the example of $T_I = KT_C = 15$ ms ,there is a bit sign transition if the integration interval overlaps two data bit. The issue is to determine the probability of occurrence.

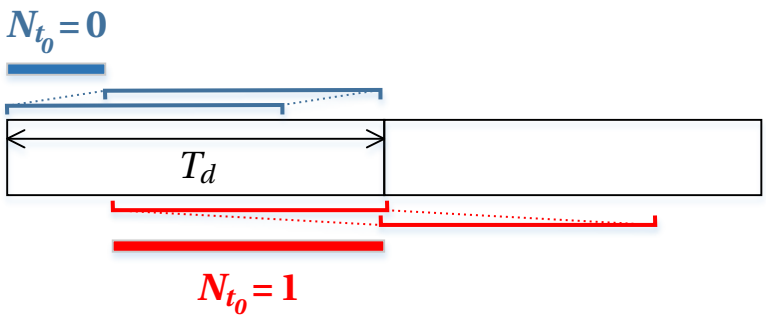

Figure E.2 Illustration of the potential integration intervals (GPS L1 C/A)

For an integration time of 15 ms, $N_d = 1$ and then $N_{t_0} \in \{0,1\}$. As illustrated with Figure E.2 :

- There is no bit transition ($N_{t_0} = 0$) with a probability of $\frac{T_I}{T_d} = \frac{15}{20} = \frac{3}{4}$,
- There is one bit transition ($N_{t_0} = 1$) with a probability of $\frac{T_d - T_I}{T_d} = \frac{5}{20} = \frac{1}{4}$ and there can be a bit sign transition with a probability of 50%.

At the end, the probability of one bit transition can be expressed as :

$$\begin{aligned} P_D(t_0) &= \frac{15}{20} \times P_{D_0} + \frac{5}{20} \times \left(\frac{1}{2} P_{D_0} + \frac{1}{2} P_{D_1}\right) \\ &= \left(\frac{15}{20} + \frac{5}{20} \times \frac{1}{2}\right) P_{D_0} + \frac{5}{20} \times \frac{1}{2} P_{D_1} \end{aligned} \tag{E.17}$$

In the same way, on the example of $T_I = KT_C = 35$ ms :

- There is 1 bit transition ($N_{t_0} = 1$) with a probability of $\frac{2T_d - T_I}{T_d} = \frac{40-35}{20} = \frac{1}{4}$,
- There is 2 bit transitions ($N_{t_0} = 2$) with a probability of $\frac{T_I - T_d}{T_d} = \frac{35-20}{20} = \frac{3}{4}$.

The probability of detection of two bit transitions is :

$$\begin{aligned} P_D(t_0) &= \frac{5}{20} \times \left(\frac{1}{2} P_{D_0} + \frac{1}{2} P_{D_1}\right) + \frac{15}{20} \times \left(\frac{1}{4} P_{D_0} + \frac{2}{4} P_{D_1} + \frac{1}{4} P_{D_2}\right) \\ &= \left(\frac{5}{20} \times \frac{1}{2} + \frac{15}{20} \times \frac{1}{4}\right) P_{D_0} + \left(\frac{5}{20} \times \frac{1}{2} + \frac{15}{20} \times \frac{2}{4}\right) P_{D_1} + \frac{15}{20} \times \frac{1}{4} P_{D_2} \end{aligned} \tag{E.18}$$

The result can be then generalized on T_I ms :

- There is $N_d - 1$ bits transitions with a probability of $\frac{N_d T_d - T_I}{T_d}$,
- There is N_d bit transitions with a probability of $\frac{T_I - (N_d - 1) T_d}{T_d}$

The sum of the probabilities is checked to be equal to 1.

$$\frac{N_d T_d - T_I}{T_d} + \frac{T_I - (N_d - 1) T_d}{T_d} = 1 \tag{E.19}$$

Knowing that

$$\begin{aligned} (N_d - 1) T_d \leq T_I \leq N_d T_d \\ N_d - 1 \leq \frac{T_I}{T_d} \leq N_d \\ (N_d - 1) - \frac{T_I}{T_d} \leq 0 \leq N_d - \frac{T_I}{T_d} \end{aligned} \tag{E.20}$$

It can be shown that in both cases, the probability is equal to $1 - \left| N_{t_0} - \frac{T_I}{T_d} \right|$.

- If $N_{t_0} = N_d - 1$:

$$\frac{N_d T_d - T_I}{T_d} = N_d - \frac{T_I}{T_d} = N_{t_0} + 1 - \frac{T_I}{T_d} = 1 + N_{t_0} - \frac{T_I}{T_d} = 1 - \left| N_{t_0} - \frac{T_I}{T_d} \right| \tag{E.21}$$

If $N_{t_0} = N_d - 1$ then $N_{t_0} - \frac{T_I}{T_d} \leq 0$ and then $N_{t_0} - \frac{T_I}{T_d} = -\left|N_{t_0} - \frac{T_I}{T_d}\right|$

- If $N_{t_0} = N_d$:

$$\frac{T_I - (N_d - 1)T_d}{T_d} = \frac{T_I}{T_d} - (N_d - 1) = \frac{T_I}{T_d} - \left(N_{t_0} - 1\right) = \frac{T_I}{T_d} - N_{t_0} + 1 = 1 - \left(N_{t_0} - \frac{T_I}{T_d}\right) = 1 - \left|N_{t_0} - \frac{T_I}{T_d}\right| \quad \text{(E.22)}$$

The probability of occurrence of j bit transitions can be easily deduced:

$$P_{j/N_{t_0}} = \frac{1}{2^{N_{t_0}}}\left(1 - \left|N_{t_0} - \frac{T_I}{T_d}\right|\right)\binom{N_{t_0}}{j} \quad \text{(E.23)}$$

Appendix F

Double-Block Zero-Padding

F.1 DBZP outputs

The partial correlator outputs can be expressed as follows:

$$\begin{aligned}\widetilde{I_l}(k) &= \frac{A}{2}\tilde{R}_{c_1}\left(\varepsilon_\tau(k,l)\right)\cos\left(\pi f_D t_b + \varepsilon_{\phi_0}(k,l)\right)\mathrm{sinc}(\pi f_D t_b) + \eta_{\widetilde{I_l}}(k)\\ \tilde{Q}_l(k) &= \frac{A}{2}\tilde{R}_{c_1}\left(\varepsilon_\tau(k,l)\right)\sin\left(\pi f_D t_b + \varepsilon_{\phi_0}(k,l)\right)\mathrm{sinc}(\pi f_D t_b) + \eta_{\widetilde{Q_l}}(k)\end{aligned} \tag{F.1}$$

The objective is then to compute the DBZP output after the application of the FFT. For a better reading, the notation $\tilde{\phi}_0(k)$ is defined as:

$$\pi f_D t_b + \varepsilon_{\phi_0}(k,l) = \tilde{\phi}_0(k) + 2\pi f_D l t_b \tag{F.2}$$

The vector on which the FFT is applied represents the partial correlator outputs for the same code delay shift.

$$\begin{bmatrix}\tilde{I}_0(k)\\ \tilde{I}_1(k)\\ \vdots\\ \tilde{I}_{N_b-1}(k)\end{bmatrix} = \begin{bmatrix}\frac{A}{2}\tilde{R}_{c_1}\left(\varepsilon_\tau(k,0)\right)\cos\left(\tilde{\phi}_0(k)\right)\mathrm{sinc}(\pi f_D t_b) + \eta_{\tilde{I}_0}(k)\\ \frac{A}{2}\tilde{R}_{c_1}\left(\varepsilon_\tau(k,1)\right)\cos\left(2\pi f_D t_b + \tilde{\phi}_0(k)\right)\mathrm{sinc}(\pi f_D t_b) + \eta_{\tilde{I}_1}(k)\\ \vdots\\ \frac{A}{2}\tilde{R}_{c_1}\left(\varepsilon_\tau(k,N_b-1)\right)\cos\left(2\pi f_D (N_b-1) t_b + \tilde{\phi}_0(k)\right)\mathrm{sinc}(\pi f_D t_b) + \eta_{\tilde{I}_{N_b-1}}(k)\end{bmatrix} \tag{F.3}$$

Even if they are computed with different blocks of incoming signal, it is assumed that $\widetilde{R_{c_1}}\left(\varepsilon_\tau(l)\right)$ is constant and furthermore:

$$\forall k, \forall l = 0, 1, \dots, N_b - 1, \tilde{R}_{c_1}\left(\varepsilon_\tau(k,l)\right) \approx R_{c_1}(\varepsilon_\tau) \tag{F.4}$$

The computation of the FFT on the in-phase correlator output is equivalent to compute the FFT on the cos term series:

$$\begin{aligned}&\mathcal{F}\left(\widetilde{I_l}(k)\right)\left(m_{m=0,\dots,N_b-1}\right)\\ &= \frac{A}{2}\tilde{R}_{c_1}\left(\varepsilon_\tau(N_b-1)\right) \times \mathcal{F}\left(\cos\left(2\pi f_D l t_b + \tilde{\phi}_0(k)\right)\right)\left(m_{m=0,\dots,N_b-1}\right) + \eta_\iota(k)\end{aligned} \tag{F.5}$$

where η_ι is the in-phase DBZP output noise, developed in (F.9).

The in-phase DBZP output is based on:

$$\begin{aligned}
&\mathcal{F}\left(\cos\left(2\pi f_D l t_b + \tilde{\phi}_0(k)\right)\right)\left(m_{m=0,\dots,N_b-1}\right) \\
&= \sum_{l=0}^{N_b-1} \cos\left(2\pi f_D l t_b + \tilde{\phi}_0(k)\right) e^{-2i\pi\frac{ml}{N_b}} \\
&= \mathrm{Re}\left(\sum_{l=0}^{N_b-1} e^{i\left(2\pi f_D l t_b + \tilde{\phi}_0(k)\right)} e^{-2i\pi\frac{ml}{N_b}}\right) \\
&= \mathrm{Re}\left(e^{i\tilde{\phi}_0(k)} \sum_{l=0}^{N_b-1} e^{2i\pi l\left(f_D t_b - \frac{m}{N_b}\right)}\right) = \mathcal{R}_e\left(e^{i\tilde{\phi}_0(k)} \sum_{l=0}^{N_b-1} e^{2i\pi l\left(\frac{f_D T_C - m}{N_b}\right)}\right) \\
&= \mathrm{Re}\left(e^{i\tilde{\phi}_0(k)} \times N_b e^{i\pi\frac{(N_b-1)}{N_b}(f_D T_C - m)} \frac{\mathrm{sinc}\left(\pi(f_D T_C - m)\right)}{\mathrm{sinc}\left(\pi\frac{f_D T_C - m}{N_b}\right)}\right) \\
&= N_b \frac{\mathrm{sinc}\left(\pi(m - f_D T_C)\right)}{\mathrm{sinc}\left(\pi\frac{m - f_D T_C}{N_b}\right)} \cos\left(\tilde{\phi}_0(k) + \pi\frac{(N_b-1)}{N_b}(f_D T_C - m)\right)
\end{aligned} \tag{F.6}$$

At the end, the FFT of the in-phase and quadrature-phase partial correlator outputs depend on:

$$\begin{aligned}
\mathcal{F}\left(\cos\left(2\pi f_D l t_b + \tilde{\phi}_0(k)\right)\right)(m) &= N_b \frac{\mathrm{sinc}\left(\pi(m - f_D T_C)\right)}{\mathrm{sinc}\left(\pi\frac{m - f_D T_C}{N_b}\right)} \cos\left(\phi(k)\right) \\
\mathcal{F}\left(\sin\left(2\pi f_D l t_b + \tilde{\phi}_0(k)\right)\right)(m) &= N_b \frac{\mathrm{sinc}\left(\pi(m - f_D T_C)\right)}{\mathrm{sinc}\left(\pi\frac{m - f_D T_C}{N_b}\right)} \sin\left(\phi(k)\right)
\end{aligned} \tag{F.7}$$

with

$$\begin{aligned}
\phi(k) &= \tilde{\phi}_0(k) + \pi\frac{(N_b-1)}{N_b}(f_D T_C - m) \\
&= \pi f_D t_b + 2\pi f_D(T_0 + (k-1)T_C) + \pi\frac{(N_b-1)}{N_b}(f_D T_C - m)
\end{aligned} \tag{F.8}$$

The DBZP output noises are defined by:

$$\begin{aligned}
\eta_\iota(k) &= \mathcal{F}\left(n_{\tilde{I}_l}(k)\right) = \sum_{m=0}^{N_b-1} n_{\tilde{I}_l}(k) e^{-2i\pi\frac{ml}{N_b}} \\
\eta_\rho(k) &= \mathcal{F}\left(n_{\tilde{Q}_l}(k)\right) = \sum_{m=0}^{N_b-1} n_{\tilde{Q}_l}(k) e^{-2i\pi\frac{ml}{N_b}}
\end{aligned} \tag{F.9}$$

Their variances are:

$$\begin{aligned}\sigma^2_{\eta_{DBZP}} = var(\eta_\iota) = E\left[\eta_\iota(k)\overline{\eta_\iota(k)}\right] &= E\left[\sum_{l=0}^{N_b-1} n_{\tilde{l}_l}(k)e^{-2\iota\pi\frac{ml}{N_b}} \times \overline{\sum_{l=0}^{N_b-1} n_{\tilde{l}_l}(k)e^{-2\iota\pi\frac{ml}{N_b}}}\right] \\ &= E\left[\sum_{l=0}^{N_b-1}\sum_{l'=0}^{N_b-1} n_{\tilde{l}_l}(k)n_{\tilde{l}_{l'}}(k)e^{2i\pi\frac{m(l'-l)}{N_b}}\right] \\ &= \sum_{l=0}^{N_b-1}\sum_{l'=0}^{N_b-1} E\left[n_{\tilde{l}_l}(k)n_{\tilde{l}_{l'}}(k)\right]e^{2i\pi\frac{m(l'-l)}{N_b}} \\ &= N_b\sigma^2_{\tilde{l}_l}\end{aligned} \tag{F.10}$$

In conclusion, the variance of the DBZP output noises is N_b times the variance of the partial correlator output noise:

$$\sigma^2_{\eta_{DBZP}} = var(\eta_\iota) = N_b\sigma^2_{\tilde{l}_l} = N_b\frac{N_0}{4t_b} = \frac{N_b^2N_0}{4T_C} \tag{F.11}$$

F.2 DBZP output with zero-padding (Step 4')

An improvement of the DBZP has been proposed, it consists in zero-padding the vector on which the FFT is applied to refine the frequency resolution output. From the mathematical point of view, it is:

$$\begin{aligned}&\mathcal{F}\left(\cos\left(2\pi f_D l t_b + \tilde{\phi}_0(k)\right)\right)\left(m_{m=0,\dots,N_b+\beta N_b-1}\right) \\ &= \mathrm{Re}\left(\sum_{l=0}^{N_b-1} e^{i\left(2\pi f_D l t_b+\tilde{\phi}_0(k)\right)}e^{-2i\pi\frac{ml}{(1+\beta)N_b}}\right) \\ &= N_b\frac{\mathrm{sinc}\left(\pi\frac{m-(1+\beta)f_DT_C}{(1+\beta)}\right)}{\mathrm{sinc}\left(\pi\frac{m-(1+\beta)f_DT_C}{(1+\beta)N_b}\right)}\cos\left(\tilde{\phi}_0(k)+\pi\frac{(N_b-1)}{(1+\beta)N_b}\left((1+\beta)f_DT_C-m\right)\right)\end{aligned} \tag{F.12}$$

In the end, the FFT of the cos and sin term series, in presence of zero-padding, are:

$$\begin{aligned}\mathcal{F}\left(\cos\left(\tilde{\phi}_0(k)+2\pi f_D l t_b\right)\right)(m) &= N_b\frac{\mathrm{sinc}\left(\pi\frac{m-(1+\beta)f_DT_C}{(1+\beta)}\right)}{\mathrm{sinc}\left(\pi\frac{m-(1+\beta)f_DT_C}{(1+\beta)N_b}\right)}\cos\left(\phi(k)\right) \\ \mathcal{F}\left(\sin\left(\widetilde{\phi_0}(k)+2\pi f_D l t_b\right)\right)(m) &= N_b\frac{\mathrm{sinc}\left(\pi\frac{m-(1+\beta)f_DT_C}{(1+\beta)}\right)}{\mathrm{sinc}\left(\pi\frac{m-(1+\beta)f_DT_C}{(1+\beta)N_b}\right)}\sin\left(\phi(k)\right)\end{aligned} \tag{F.13}$$

Résumé

Depuis le développement du GPS, les systèmes de navigation par satellites (GNSS) se sont largement diversifiés : maintenance, modernisation et déploiement de nouveaux systèmes, comme l'européen Galileo. De plus, le nombre d'applications basées sur l'utilisation de signaux GNSS ne cesse d'augmenter. Pour répondre à ces nouveaux challenges et besoins, les récepteurs GNSS ne cessent d'évoluer. Un nouvel axe est le développement du récepteur logiciel qui présente la particularité d'un traitement logiciel des signaux contrairement au récepteur matériel, équipant nos véhicules, smartphones par exemple. Cette thèse de doctorat s'inscrit dans le projet commun d'un laboratoire et d'une PME consistant au développement d'un récepteur logiciel poursuivant les signaux GPS L1 C/A et Galileo E1 OS. L'objectif plus spécifique de la thèse est d'étudier l'acquisition, première étape du traitement du signal GNSS qui doit fournir une estimation grossière des paramètres du signal entrant. Ce travail vise particulièrement les signaux à faible puissance, un seuil d'acquisition est fixé à 27 dB-Hz pouvant s'apparenter à l'acquisition en milieu urbain ou dégradé. Il est important de noter qu'une des contraintes est de réussir l'acquisition de tels signaux au moins 9 fois sur 10, sans aucune aide extérieure ou connaissance des almanachs ou éphémérides. Dans un premier temps, une solide étude théorique portant sur les performances de l'acquisition et les sources de dégradations est menée. Parmi elles, peuvent être citées, les transitions de bits dues à la présence du message de navigation et du code secondaire sur la voie pilote des nouveaux signaux. Est ainsi mis en lumière la nécessité d'avoir recours à une méthode d'acquisition insensible aux inversions de signe du message de navigation. Dans un deuxième temps, une méthode innovante, le Double-Block Zero-Padding Transition-Insensitive (DBZPTI), est donc développée pour permettre l'acquisition du signal Galileo E1 OS de façon efficiente. Elle prend part au développement de la stratégie globale d'acquisition dont l'objectif est d'avoir en sortie une estimation de la fréquence Doppler et du retard de code du signal entrant, assez fine et fiable pour une satisfaisante poursuite du signal.

Mots-clés: Acquisition – Galileo – GPS – Analyse de performance – Transition de signe

Abstract

Since the development of the GPS, the global navigation satellite systems (GNSS) have been widely diversified: maintenance, modernization and deployment of new systems such as the European Galileo. In addition, the number of GNSS signals applications, based on the use of GNSS signals, is increasing. To meet these new challenges and requirements, GNSS receivers are constantly evolving. A new trend is the development of software receiver which processes the GNSS signal in a software way unlike hardware receiver, equipping our vehicles, smartphones, for example. This thesis is part of a common project between a laboratory and a company, consisting of the development of a software receiver tracking GPS L1 C/A and Galileo E1 OS. The more specific aim of the thesis is to study the acquisition, first signal processing which provides a rough estimation of the incoming signal parameters. This work focuses particularly the low power signals, an acquisition threshold is set at 27 dB-Hz considered as a representative of urban or degraded environments. It is important to note that the success of the acquisition of such signals should be at least 9 times out of 10, without any aid or knowledge of almanac or ephemeris. Initially, a solid theoretical study of the acquisition performance and sources of degradation is conducted. One of them is the bit transitions due to the presence of the navigation message and the secondary code on pilot component of the new signals. It is thus highlighted the need to use a Transition-Insensitive acquisition method. Secondly, an innovative method, the Double-Block Zero-Padding Transition-Insensitive (DBZPTI) is developed to permit efficiently the acquisition of Galileo E1 OS signal. It takes part in the development of the global acquisition strategy, which should provide an estimate of the Doppler frequency and code delay, fine and reliable, for a satisfactory signal tracking.

Keywords: Acquisition – Galileo – GPS – Performance analysis – Bit sign transition